ETIOPATHOGENESIS OF SYSTEMIC SCLEROSIS: AN UPDATE

EDITED BY: Raffaele De Palma and Giuseppina Stifano
PUBLISHED IN: Frontiers in Immunology

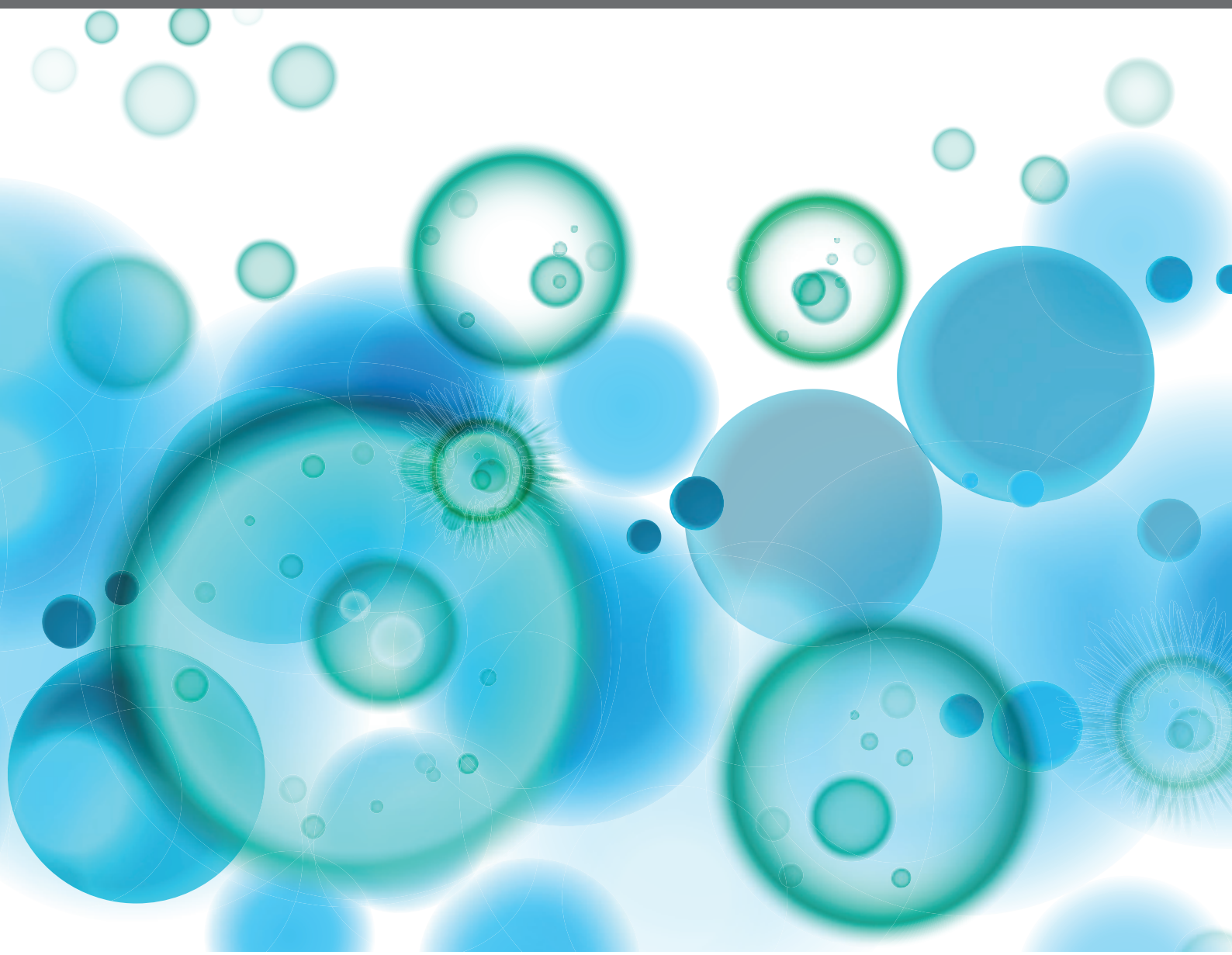

frontiers Research Topics

ISSN 1664-8714
ISBN 978-2-88966-773-4
DOI 10.3389/978-2-88966-773-4

About Frontiers

Frontiers is more than just an open-access publisher of scholarly articles: it is a pioneering approach to the world of academia, radically improving the way scholarly research is managed. The grand vision of Frontiers is a world where all people have an equal opportunity to seek, share and generate knowledge. Frontiers provides immediate and permanent online open access to all its publications, but this alone is not enough to realize our grand goals.

Frontiers Journal Series

The Frontiers Journal Series is a multi-tier and interdisciplinary set of open-access, online journals, promising a paradigm shift from the current review, selection and dissemination processes in academic publishing. All Frontiers journals are driven by researchers for researchers; therefore, they constitute a service to the scholarly community. At the same time, the Frontiers Journal Series operates on a revolutionary invention, the tiered publishing system, initially addressing specific communities of scholars, and gradually climbing up to broader public understanding, thus serving the interests of the lay society, too.

Dedication to Quality

Each Frontiers article is a landmark of the highest quality, thanks to genuinely collaborative interactions between authors and review editors, who include some of the world's best academicians. Research must be certified by peers before entering a stream of knowledge that may eventually reach the public - and shape society; therefore, Frontiers only applies the most rigorous and unbiased reviews.
Frontiers revolutionizes research publishing by freely delivering the most outstanding research, evaluated with no bias from both the academic and social point of view. By applying the most advanced information technologies, Frontiers is catapulting scholarly publishing into a new generation.

What are Frontiers Research Topics?

Frontiers Research Topics are very popular trademarks of the Frontiers Journals Series: they are collections of at least ten articles, all centered on a particular subject. With their unique mix of varied contributions from Original Research to Review Articles, Frontiers Research Topics unify the most influential researchers, the latest key findings and historical advances in a hot research area! Find out more on how to host your own Frontiers Research Topic or contribute to one as an author by contacting the Frontiers Editorial Office: frontiersin.org/about/contact

ETIOPATHOGENESIS OF SYSTEMIC SCLEROSIS: AN UPDATE

Topic Editors:
Raffaele De Palma, Università degli Studi di Genova, Italy
Giuseppina Stifano, Boston University, United States

Citation: De Palma, R., Stifano, G., eds. (2021). Etiopathogenesis of Systemic Sclerosis: An Update. Lausanne: Frontiers Media SA.
doi: 10.3389/978-2-88966-773-4

Table of Contents

frontiers in Immunology

EDITORIAL
published: 22 March 2021
doi: 10.3389/fimmu.2021.663381

Editorial: Etiopathogenesis of Systemic Sclerosis: An Update

Giuseppina Stifano[1] *and Raffaele De Palma*[2,3]*

[1] Arthritis Center, Boston University School of Medicine, Boston, MA, United States, [2] Dipartimento di Medicina Interna e Specialità Mediche (DIMI), University of Genova, Genova, Italy, [3] Clinical Immunology, IRCCS Ospedale Policlinico San Martino-IST-Genova, Genova, Italy

Keywords: systemic sclerosis (scleroderma), autoimmunity, vascular injury, fibrosis, immune response

Editorial on the Research Topic

Etiopathogenesis of Systemic Sclerosis: An Update

Systemic Sclerosis (SSc) or Scleroderma is a complex and puzzling disease having an incidence of 1–2 cases per 100,000. In SSc, inflammation leads to organ failure due to severe fibrosis of the skin and internal organs. At late stages, this disease is characterized by a profound decline in the quality of life and premature death (1). The Research Topic "Etiopathogenesis of Systemic Sclerosis: An Update" is aiming to explore three major features of SSc: vascular injury, fibrosis, and immune dysregulation. Here, we summarize the novel insights reported in this Topic with a list of references to further exploit the given issues. Apostolidis et al. identify genes linked to vascular injury in SSc by scRNA-seq. Among several genes, they found Apelin Receptor (APLNR) and Heparan Sulfate Proteoglycan 2 (HSPG2), not yet associated to SSc pathogenesis but of great interest as they have been reported to sustain vascular dysfunction and fibrosis in different settings (2). These data provide the ground to characterize new biomarkers of vascular injury and, possibly, therapeutic targets. Svegliati et al. define the role of the Anti- platelet- derived growth factor (PDGF) autoantibodies in vascular injury. The authors analyze the expression of distinct functional markers of smooth muscle cells (SMC) from human pulmonary arteries (HPASMC) exposed *in vitro* to anti-PDGFR autoantibodies from SSc patients. They show that PDGFR autoantibodies activate SMC and may contribute to the development of SSc vascular lesions, therefore suggesting that a downregulation of B cell response could modify disease development (3). Napolitano et al. show that *N*-formyl peptide receptors (FPRs) can induce Reactive Oxygen Species (ROS) generation in fibroblasts through the interaction with the urokinase-type plasminogen activator/uPA receptor (uPA/uPAR) system, activation of the nicotinamide adenine dinucleotide phosphate (NADPH) oxidase and alteration of the redox state observed in SSc. Napolitano's data indicate novel therapeutic strategies in SSc, through the use of small molecules to impair FPRs functional interaction with uPAR and their signal (4). Dolcino et al. suggest the presence of modulated genes and miRNAs playing a predisposing role in the development of malignancies in SSc. Genetic and epigenetic features shared by SSc and cancer shed new light on the pathogenesis of the disease and support the idea that immune activation against a tumor may have a central role in the initiation and progression of SSc, as also indicated by the presence or development of malignancies associated with particular autoantibodies (5). Xiong et al. show that in a murine model of SSc, Sclerodermatous Graft Versus Host Disease (sclGvHD), daily stretching produced a measurable beneficial on reducing skin thickness and improved mobility during the fibrotic phase of the model. Of note, stretching reduced mRNA expression of C-C Motif

OPEN ACCESS

Edited and Reviewed by:
Fabio Candotti,
Centre Hospitalier Universitaire Vaudois (CHUV), Switzerland

***Correspondence:**
Raffaele De Palma
depalma_raffaele@libero.it

Specialty section:
This article was submitted to Primary Immunodeficiencies, a section of the journal Frontiers in Immunology

Received: *02 February 2021*
Accepted: *08 March 2021*
Published: *22 March 2021*

Citation:
Stifano G and De Palma R (2021) Editorial: Etiopathogenesis of Systemic Sclerosis: An Update . Front. Immunol. 12:663381. doi: 10.3389/fimmu.2021.663381

Chemokine Ligand-2 (CCL2) and a disintegrin and metalloproteinase domain-8 (ADAM8) which are important inflammatory mediators associated with the sclGvHD model and upregulated in SSc skin. B cells appear to have an important role in SSc pathophysiology beyond the classical production of autoantibodies. Data on B cells subsets distribution and functional properties in animal models of SSc are scarce. Moreover, no study has ever considered a possible variation in B cell involvement during the course of SSc. This is of peculiar importance since several works have suggested that B cell-targeted therapeutic strategies may have different effects whether they are started at an early or late stage of the disease. To address these issues (6), Sanges et al. use a novel murine model of SSc in which daily intradermal injections of hypochlorous acid (HOCl) induce a systemic fibrosis. The authors study the modifications in B cell homeostasis. Phenotypic analyses show an early expansion of the mature naïve subset, decrease in plasmablasts, and memory B cells. Functional analyses reveal B-cell overproduction of pro-inflammatory cytokines (Interleukin 6 and CCL3) and an impairment of their anti-inflammatory capacities (decreased production of IL-10 and Transforming growth factor-β and reduced levels of B-regs) at the early inflammatory stage, followed by an overproduction of pro-fibrotic cytokines (TGF-β and IL-6) at the late fibrotic stage. This work reports, for the first time in an SSc animal model, the existence of B cell dysfunctions similar to those observed in SSc patients. It is of note that these anomalies vary over the course of the disease and may contribute to the inflammatory and fibrotic events observed in SSc. This makes the HOCl mouse a relevant experimental model for the study of B cells, and especially B cell- targeted therapies, in SSc (7). SSc is also characterized by alterations of the normal function of T cell, in particular an unbalanced ratio between the effector and regulatory arms of the immune system. Negrini et al. report that CD8+ T-regulatory (T-reg) subsets display functional defects in SSc patients (8), suggesting an impairment of maturation processes affecting CD8+ T-reg cells in SSc patients. This impairment of maturation involves phenotypic alterations that are mainly characterized by a deficient CD39 upregulation and a lack of down-modulation of the CD127 molecule. These data may shed a new light in the dysfunction of immune response underlying SSc. Vettori et al. investigate the dynamics and the function of T cell–fibroblast interaction in SSc, using an experimental co-culture setting, highlighting the role of IL-17A. IL-17 has been proposed to have a central role in SSc (9). The authors show that T cell–fibroblast co-cultures overexpress IL17A and IL17RA, co-cultured fibroblasts also upregulate IL-17A targets while two key effectors of the TGF-β signaling, *TGFBR2* and *SMAD3*, are downregulated. Simultaneous α-IL-17RA mAb treatment restore ProCollagen I levels and reduce fibroblast apoptosis in IL-17A-stimulated co-cultures. Long et al. review the mechanisms regulating ubiquitination in SSc and explore potential anti-fibrosis drugs (10). Considering the central role of TGF-β signaling WNT/β-catenin signaling and STAT3 in SSc, the use of ubiquitin–proteasome system (UPS) inhibitors to selectively disrupt the formation of receptor or co-receptor complexes or block intracellular signaling may yield advances in the development of urgently needed treatments.

AUTHOR CONTRIBUTIONS

The two authors share the supervision of the papers included in the Research Topics and the expressed view. All authors contributed to the article and approved the submitted version.

ACKNOWLEDGMENTS

We thank our coworkers for the exciting discussion on this topic.

REFERENCES

1. Gabrielli A, Avvedimento EV, Krieg T. Scleroderma. *N Engl J Med* (2009) 360 (19):1989–2003. doi: 10.1056/NEJMra0806188
2. Schäfer MKE, Tegeder I. NG2/CSPG4 and progranulin in the posttraumatic glial scar. *Matrix Biol* (2018) 68-69:571–88. doi: 10.1016/j.matbio.2017.10.002
3. Murakami K, Mimori T. Recent Advances in Research Regarding Autoantibodies in Connective Tissue Diseases and Related Disorders. *Intern Med* (2019) 58(1):5–14. doi: 10.2169/internalmedicine.1423-18
4. Morry J, Ngamcherdtrakul W, Yantasee W. Oxidative stress in cancer and fibrosis: opportunity for therapeutic intervention with antioxidant compounds, enzymes, and nanoparticles. *Redox Biol* (2017) 11:240–53. doi: 10.1016/j.redox.2016.12.011
5. Shah, AmiA, Rosen A. Cancer and systemic sclerosis: novel insights into pathogenesis and clinical implications. *Curr Opin Rheumatol* (2011) 23 (6):530–5. doi: 10.1097/BOR.0b013e32834a5081
6. Barnas JL, RJ L, Anolik JH. B cell targeted therapies in autoimmune disease. *Curr Opin Immunol* (2019) 61:92–9. doi: 10.1016/j.coi.2019.09.004
7. Meng M, Tan J, Chen W, Du Q, Xie B, Wang N, et al. The Fibrosis and Immunological Features of Hypochlorous Acid Induced Mouse Model of Systemic Sclerosis. *Front Immunol* (2019) 10:1861. doi: 10.3389/fimmu.2019.01861
8. Frantz C, Auffray C, Avouac J, Allanore Y. Regulatory T Cells in Systemic Sclerosis. *Front Immunol* (2018) 9:2356. doi: 10.3389/fimmu.2018.02356
9. Servaas NH, Zaaraoui-Boutahar F, Wichers CGK, Ottria A, Chouri E, Affandi AJ, et al. Longitudinal analysis of T-cell receptor repertoires reveals persistence of antigen-driven $CD4^+$ and $CD8^+$ T-cell clusters in systemic sclerosis. *J Autoimmun* (2021) 117:102574. doi: 10.1016/j.jaut.2020.102574
10. Tang Y, Zha L, Zeng X, Yu Z. Identification of Biomarkers Related to Systemic Sclerosis With or Without Pulmonary Hypertension Using Co-expression Analysis. *J Comput Biol* (2020) 27(10):1519–31. doi: 10.1089/cmb.2019.0492

Conflict of Interest: The authors declare that the research was conducted in the absence of any commercial or financial relationships that could be construed as a potential conflict of interest.

frontiers in Immunology

ORIGINAL RESEARCH
published: 19 January 2017
doi: 10.3389/fimmu.2017.00018

Phenotypic Alterations Involved in CD8+ Treg Impairment in Systemic Sclerosis

*Simone Negrini[1,2], Daniela Fenoglio[1,2], Alessia Parodi[1], Francesca Kalli[1], Florinda Battaglia[1], Giorgia Nasi[1], Monica Curto[1], Samuele Tardito[1], Francesca Ferrera[1] and Gilberto Filaci[1,2]**

[1] Center of Excellence for Biomedical Research, University of Genoa, Genoa, Italy, [2] Department of Internal Medicine, Clinical Immunology Unit, University of Genoa, Genoa, Italy

Systemic sclerosis (SSc) is a connective tissue disease characterized by tissue fibrosis, vasculopathy, and autoimmunity. Although the exact pathogenetic mechanisms behind SSc remain to be fully elucidated, a great deal of evidence suggests the existence of an unbalanced ratio between the effector and regulatory arms of the immune system. With regard to the T regulatory (Treg) compartment, we observed that CD8+ Treg subsets display functional defects in SSc-affected patients. Since CD127 down-modulation and CD39 upregulation have been observed on Treg subsets, the phenotypic expression of these molecules was analyzed on the CD8+CD28− Treg precursors and on CD8+ Treg cells generated *in vitro* through interleukin-10 commitment. Immunophenotypic data from SSc patients were compared to those obtained from healthy subjects. The analyses performed on *ex vivo*-isolated CD8+CD28− Treg precursors did not show any significant differences in CD39 or CD127 expression as compared to values obtained from healthy donors. On the contrary, *in vitro*-generated CD8+ Tregs obtained from SSc patients displayed reduced expression of the CD39 molecule as compared to controls. Moreover, the percentage of CD127+ cells was significantly higher in *in vitro*-generated CD8+ Tregs from SSc patients compared to CD8+ Tregs obtained from healthy donors. Taken together, these findings may indicate an impairment of maturation processes affecting CD8+ Treg cells in SSc patients. This impairment of maturation involves phenotypic alterations that are mainly characterized by a deficient CD39 upregulation and a lack of down-modulation of the CD127 molecule.

Keywords: systemic sclerosis, scleroderma, CD8+ T regulatory cells, CD127, CD39

OPEN ACCESS

Edited by:
Raffaele De Palma, Seconda Università degli Studi di Napoli, Italy

Reviewed by:
Ciriaco A. Piccirillo, McGill University, Canada
Giuseppe Matarese, University of Naples Federico II, Italy

***Correspondence:**
Gilberto Filaci
gfilaci@unige.it

Specialty section:
This article was submitted to Primary Immunodeficiencies, a section of the journal Frontiers in Immunology

Received: *19 September 2016*
Accepted: *05 January 2017*
Published: *19 January 2017*

Citation:
Negrini S, Fenoglio D, Parodi A, Kalli F, Battaglia F, Nasi G, Curto M, Tardito S, Ferrera F and Filaci G (2017) Phenotypic Alterations Involved in CD8+ Treg Impairment in Systemic Sclerosis. Front. Immunol. 8:18. doi: 10.3389/fimmu.2017.00018

INTRODUCTION

Several subsets of T regulatory (Treg) lymphocytes with distinct phenotypes and mechanisms of action have been described among CD8+ T cells. As the CD4+ Treg counterpart, these cells play an important role in physiological and pathological conditions such as autoimmune, infectious, or neoplastic diseases (1, 2). In particular, our group has characterized a subset of CD8+ Treg lymphocytes that mediate suppression without antigen restriction. These CD8+ Treg cells originate from circulating CD8+CD28−CD127+CD39− T lymphocytes through *in vitro* conditioning with interleukin (IL)-2 and IL-10; therefore, they belong to the "peripherally induced" CD8+ Treg subpopulations (1, 3, 4). From a functional point of view, these non-antigen-specific CD8+ Tregs

inhibit both T cell proliferation and cellular cytotoxicity through the secretion of cytokines, mostly IL-10, and do not require direct cell-to-cell contact to mediate their inhibitory functions (1, 5, 6). Furthermore, we recently identified an additional regulatory mechanism involving the activity of CD39 ecto-nucleotidase (4), as already described for CD4+ Tregs. Finally, these cells share with CD4+ Treg the down-modulation of the CD127 molecule, so that their exact phenotype is CD8+CD28−CD127loCD39+ (3, 4, 7).

Systemic sclerosis (SSc) is a systemic connective tissue disease characterized by small vessel vasculopathy, immune alterations, and fibroblast dysfunction leading to diffuse tissue fibrosis (8). Even though SSc pathogenesis is still largely elusive, autoimmunity seems to be implicated in disease development as suggested by the presence of several abnormalities in humoral and cellular immunity (9). Concerning this latter point, alterations of the normal functional balance between pro-inflammatory subpopulations, in particular Th17, and Treg subpopulations have been demonstrated in patients affected by SSc (10–15).

With regard to the Treg compartment, we observed that both CD4+ and CD8+ Treg subsets show quantitative and functional defects in SSc patients (16). This is reminiscent of what we recently found studying CD8+ Tregs in primary biliary cirrhosis (PBC), an organ-specific, fibrotic autoimmune disease that share with SSc several pathogenetic mechanisms (17). In PBC, CD8+ Treg abnormalities seem to correlate with increased CD127 antigen expression and reduced CD39 molecule expression. This observation is not surprising since CD127, the α-chain of the IL-7 receptor, is mainly expressed on effector cells and is physiologically down-modulated on Treg lymphocytes (18), while CD39 is a membrane-bound nucleosidase whose activity has been correlated with Treg function (4, 7, 19).

Therefore, we decided to analyze CD127 and CD39 molecule expression in CD8+ Tregs derived from SSc patients in order to determine whether alterations affecting these two pathways could explain the functional impairment observed in the CD8+ Treg subpopulation.

MATERIALS AND METHODS

Patients and Controls

Twenty-eight patients affected with SSc (mean age 64 ± 14 years, female/male ratio 3/1) were enrolled at the Division of Internal Medicine and Clinical Immunology of the Department of Internal Medicine, University of Genoa, after providing informed consent.

Diagnosis of SSc was made according to the American College of Rheumatology criteria (20). Enrolled patients were being treated with vasoactive (e.g., iloprost or dihydropyridine calcium channel blockers) but not with immunosuppressive drugs. Ten healthy subjects, age and sex matched with the SSc patients, were enrolled as controls.

The study was carried out in compliance with the Helsinki Declaration and was approved by the Ethics Committee of the San Martino Hospital in Genoa, Italy.

Monoclonal Antibodies (mAbs)

The following mAbs were used for immunostaining and analysis by flow cytometry (FACS): allophycocyanin (APC)-cyanin 7 (Cy7) conjugated anti-CD4 (Clone RPA-T4), APC-conjugated anti-CD39 (Clone TU66), phycoerythrin-conjugated anti-CD127 (Clone M21), PeCy7 conjugated anti-CD25 (Clone M-A251), fluorescein isothiocyanate-conjugated anti CD45RA (Clone HI100), Brilliant Violet 421-conjugated anti-CD8 (Clone RPA-T8), and Horizon V500-conjugated anti-CD3 (Clone UCHT1) [Becton Dickinson (BD) Biosciences]; PerCP-cyanin 5-conjugated anti-CD28 (Clone CD28.2) (Biolegend). CD8+ T cells (1×10^6) were incubated with a mAb cocktail for 30 min at 4°C in the dark. After staining procedures, the samples were washed with PBS and stored at 4°C. The samples were acquired and analyzed by a FACSCanto flow cytometer II equipped with three lasers (BD Biosciences, San Josè, CA, USA) using the FACSDIVA software (BD Biosciences). Fluorescence minus one was used to properly interpret flow cytometry data.

Purification of CD8+ T Lymphocytes

Peripheral blood mononuclear cells (PBMCs) were purified from the venous heparinized blood samples of healthy controls and SSc patients by centrifugation on Ficoll-Hypaque gradient (Biochrom AG, Berlin, Germany) for 30 min at 1,800 rpm. CD8+ T lymphocytes were isolated by sequential cycles of cell sorting on magnetic beads using microbeads conjugated with a mAb specific for the CD8 antigen (Dynal CD8 positive isolation kit, Invitrogen by Life Technologies Ltd., Paisley, UK) following the manufacturer's instructions.

In Vitro Generation of CD8 Tregs from the Peripheral Blood Precursors

CD8+ Tregs were generated as previously described (21). Briefly, purified CD8+ T lymphocytes (2×10^5 cells/well) resuspended in culture medium consisting of RPMI 1640 culture medium (Gibco by Life Technologies Ltd., Paisley, UK) added with 10% fetal calf serum (Invitrogen by Life Technologies Ltd., Paisley, UK) were incubated with 20 U/ml of IL-2 (Proleukin, Eurocetus, Amsterdam, The Netherlands) and 10 ng/ml of IL-10 (PeproTech, Rocky Hill, NJ, USA) in 96-well flat bottomed plates (Sardsted) at 37°C for 7 days. The regulatory activity and the membrane antigen study were performed on both freshly *ex vivo*-purified CD8+ T cells and on *in vitro*-generated CD8+ Tregs.

Proliferation Suppression Assay

The suppressive activity of Treg was evaluated by monitoring the inhibition of dye dilution in PBMC stained with carboxyfluorescein diacetate succinimidyl ester (CFDA-SE, 5 μM, Molecular Probes, Invitrogen).

Briefly, the PBMC-CFDA-SE+ were pulsed with the anti-CD3 UCTH-1 mAb (5 μg/ml, BD Bioscience) and cultured for 5 days in a 96-well U bottomed plate (1×10^5 cells/well) in the presence (or not) of *ex vivo*- or *in vitro*-generated CD8+ T lymphocytes (1×10^5 cells/well). Then, the samples were harvested, washed in PBS, and analyzed by flow cytometry. The dead cells were excluded from analysis by adding 7-aminoactinomycin D

(7-AAD) (BD Bioscience) prior to analysis. Suppression activity was expressed as the percentage reduction of the proliferation in the presence of CD8+ Treg lymphocytes compared to the levels of proliferation observed in control cultures of PBMCs cultured in the absence of Treg cells. A suppression activity ≥25% was considered significant. This threshold was chosen based on the results achieved in a large historical cohort of more than 50 healthy subjects of both sexes with age ranging from 18 to 87 years. In healthy donors, CD8+ Treg suppression activity never fell below 25%.

Statistical Analyses

Statistically significant differences between frequencies were analyzed by Fisher's exact test. Statistically significant differences between mean values were analyzed by the Mann–Whitney test for non-parametric values. Differences were considered statistically significant when $p < 0.05$. Statistical analyses were performed using GraphPad Prism version 6.03 for Windows (GraphPad Software, San Diego, CA, USA).

RESULTS

Altered Generation of CD8 Tregs in SSc Patients

The suppressive activity of *in vitro*-generated CD8+ Tregs obtained from SSc patients was analyzed in comparison with that of healthy donors. *In vitro* generation of CD8+ Tregs led to the differentiation of circulating CD8+ T cells into CD8+CD28−CD127−CD39+ T lymphocytes mediating a suppressive activity ≥25% in suppression assays in 10 out of 10 (100%) healthy donors. In contrast, impaired *in vitro* generation of CD8+ Tregs was observed in 1/3 of SSc patients since *in vitro*-generated CD8+ Tregs from 10 out of 28 SSc patients failed to exert a suppressive activity above the 25% threshold. The differences between the frequencies of subjects showing ≥25% suppressive activity by their CD8+ Treg in healthy controls and SSc patients was statistically significant ($p = 0.04$) as assessed by Fisher's exact test (**Figure 1**; Tables S1 and S2 in Supplementary Material).

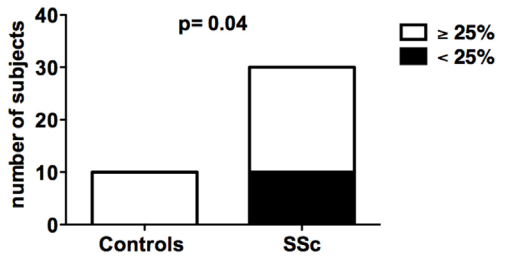

FIGURE 1 | *In vitro* generation of CD8+ T regulatory (Treg) cell in healthy donors and systemic sclerosis (SSc) patients. The bars indicate the frequency of healthy donors (left bar) and SSc patients (right bar) showing normal (suppression activity ≥25%, white bars) or impaired (suppression activity <25%, black bars) CD8+ Treg function. Statistical analyses were performed by Fisher's exact test.

CD39 Expression on CD8+ Treg Cells

Given that the expression of CD39 is related to the suppressive activity of both CD4 and CD8 Treg cells (4, 7), its expression was analyzed on freshly isolated CD8+CD28− (formally CD8+ Treg precursors) and on *in vitro*-generated CD8+ Treg cells from both SSc patients and healthy donors.

CD39 molecule was undetectable (with values below 0.01% among the CD3+ T cell population) on freshly isolated CD8+CD28− lymphocytes obtained from both SSc patients and healthy controls at T0 (**Figure 2A**). Interestingly, while CD39 expression was strongly upregulated in CD8+ Tregs generated from healthy subjects with respect to their circulating precursor CD8+CD28− T cells, this increase was not observed in SSc patients. Indeed, CD39 expression was significantly lower in *in vitro*-generated CD8+ Tregs from SSc patients with respect to *in vitro*-generated CD8+ Tregs from healthy donors, as assessed by Mann–Whitney test ($p = 0.0032$; **Figures 2A,B**).

CD127 Expression in CD8 Treg Subpopulation

We previously observed that CD127 antigen down-modulation is strictly related to the correct functional maturation/generation of CD8+ Tregs: thus, we explored its expression on freshly isolated CD8+CD28− and on *in vitro*-generated CD8+ Tregs from SSc patients and healthy donors.

No differences in CD127 expression were observed on CD8+CD28− cells from the peripheral blood of SSc patients and healthy controls at T0 (**Figures 3A,B**). However, CD127 expression diminished on CD8+CD28− after IL10 commitment for Treg generation in healthy donors ($p = 0.04$), while it increased on the corresponding cells from SSc patients ($p = 0.029$) with respect to their circulating precursors (**Figures 3A,B**, analyses performed by Mann–Whitney test). Accordingly, the percentage of CD127+ T cells on CD8+CD28− T lymphocytes after *in vitro* CD8+ Treg generation was significantly higher in cells from SSc patients as compared to healthy subjects ($p = 0.02$, **Figure 3A**).

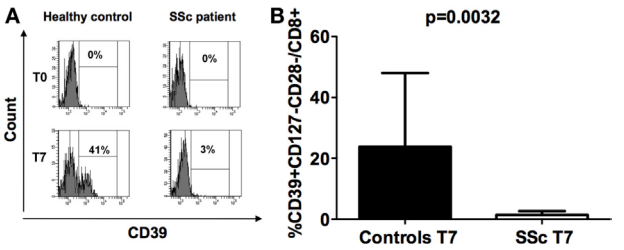

FIGURE 2 | CD39 expression on freshly isolated CD8+CD28− lymphocytes and *in vitro*-generated CD8+ T regulatory (Treg) cell. **(A)** Histograms showing the percentages of expression of the CD39 molecule on freshly isolated CD8+CD28− lymphocytes (T0) and on interleukin-10-committed CD8+CD28−CD127− T cells (T7) from a representative healthy donor (left) and a representative systemic sclerosis (SSc) patient (right). **(B)** Mean percentages of CD39+CD8+CD28− Treg cells in healthy donors (black bar) and SSc patients (white bar). Statistical analyses were performed by Mann–Whitney test.

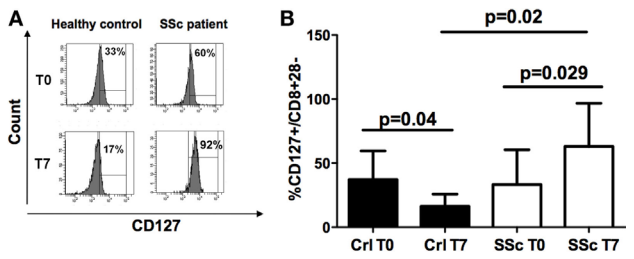

FIGURE 3 | CD127 expression on freshly isolated CD8+CD28− lymphocytes and *in vitro*-generated CD8+ T regulatory (Treg) cell. **(A)** Mean percentages of CD127+ cells in freshly isolated CD8+CD28− lymphocytes (T0) and *in vitro*-generated CD8+ Treg (T7) in healthy donors (black bar) and systemic sclerosis (SSc) patients (white bar). **(B)** Histograms showing the percentages of expression of the CD127 molecule on freshly isolated CD8+CD28− lymphocytes (T0) and on interleukin-10-committed CD8+CD28− T cells (T7) from a representative healthy donor (left) and a representative SSc patient (right). Statistical analyses were performed by Mann–Whitney test.

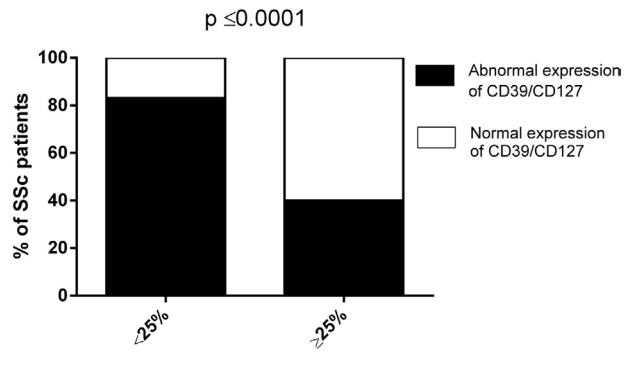

FIGURE 4 | Analysis of the suppression activity of CD8+ T regulatory (Treg) cell generated from systemic sclerosis (SSc) patients in relation to the expression patterns of CD39/CD127. The bars display the frequencies of SSc patients showing impaired (suppression activity <25%, left bar) or normal (suppression activity ≥25%, right bar) CD8+ Treg function in relation to the expression patterns of CD39/CD127 molecules (normal—white bars, abnormal—black bars). Statistical analyses were performed by Fisher's exact test.

Collectively, our data envisage the dependence of abnormal CD8+ Treg function in SSc patients on their altered expression of CD39 and/or CD127 molecules. In order to find support to this pathogenic mechanism, the frequencies of SSc patients showing impaired (suppression activity <25%) or normal (suppression activity ≥25%) CD8+ Treg function were related, by Fisher's exact test analysis, to the existence, in the CD8+ Treg of each single patient, of an abnormal expression of CD39 and/or CD127 molecules (considering as altered expression the downregulation of CD39 and the upregulation of CD127 with respect to the relative CD8+CD28− T cell precursors, respectively). **Figure 4** and **Table 1** show that the frequency of SSc patients showing abnormal expression of CD39 and/or CD127 molecules within patients with altered CD8+ Treg function was more than twice that observed in patients with normal CD8+ Treg activity. This observation highlights the strict relationship between altered CD39 and/or Cd127 expression and CD8+ Treg function.

DISCUSSION

The results of our work show that (1) *in vitro* generation of CD8 Treg lymphocytes may be altered in SSc patients, thus leading to impaired suppressor activity; (2) CD8 Tregs generated from SSc patients display reduced CD39 expression and increased CD127 expression compared to CD8+ Tregs generated from healthy donors.

Systemic sclerosis is a chronic connective tissue disease characterized by diffuse tissue fibrosis, microangiopathy, and immune abnormalities. Although the cause of SSc is unknown, autoimmunity seems to play an important role in the pathogenesis of the disease. Support for this hypothesis includes the presence of autoantibodies, evidence of abnormalities in B and T cell compartments in both the circulation and the affected organs, altered levels of growth factors, chemokines and cytokines, and the potential clinical overlap with other clearly recognized autoimmune diseases such as systemic lupus erythematosus and rheumatoid arthritis (8, 17, 22, 23). Our group recently described the existence of an imbalance between effector and regulatory responses in SSc patients. In particular, we observed that an increased Th17 effector response is associated with defective T cell regulation involving quantitative and functional alterations in both CD4+CD25+ and CD8+ Treg subpopulations (16). Furthermore, we recently described the qualitative defects affecting CD8+ Tregs in PBC, an organ-specific, fibrotic autoimmune disease. In this disease, CD8+ Treg functional abnormalities correlate with the defective expression of the CD39 molecule and the increased expression of the CD127 antigen (17).

CD39 is a cell surface ecto-nucleotidase that hydrolyzes extracellular ATP or ADP to AMP. Additionally, in concert with CD73, another ecto-nucleotidase which dephosphorylates AMP, its activity leads to the production of adenosine. Furthermore, there is increasing evidence indicating that CD39 and purinergic signaling alterations may be implicated in pathological conditions such as neoplastic and inflammatory diseases (24). Although the role of CD39 has been less investigated in CD8+ Tregs, our group recently reported that CD39 is expressed and involved in the activity of non-antigen-specific CD8+ Treg cells (4). Furthermore, we correlated the defective expression of CD39 molecules with the functional impairment of CD8+ Tregs generated from patients affected by PBC (17). Based on this, we explored the role of CD39 in SSc. Interestingly, CD8+ Tregs generated from healthy subjects exhibit a significant upregulation of CD39 expression with respect to their precursor CD8+CD28− T cells, while this phenomenon was not observed in CD8+ Tregs generated from SSc patients. Considering the important role of CD39 for Treg regulatory activity, CD39 expression defects could explain, at least in part, the functional impairment observed in CD8+ Tregs generated from SSc patients.

TABLE 1 | Percentage of CD127 and CD39 expression on CD8+CD28− T cells before and after *in vitro* CD8+ Treg generation.

Patient No.	CD8+ Treg suppression (< or ≥25%)	CD127+/CD8+CD28− T cells at T0[a] (%)	CD127+/CD8+CD28− T cells at T7[b] (%)	CD39+/CD8+CD28− T cells at T0[a] (%)	CD39+/CD8+CD28− T cells at T7[b] (%)
1	≥	13	93	1	1.7
2	<	17	81	2	1.5
3	<	12	11	1	1.2
4	<	19	89	1.5	0.3
5	≥	33	29	0.6	0.8
6	≥	20	35	2.2	4.6
7	≥	40	36	2.2	2.4
10	≥	9.4	25	1.3	3
11	≥	27	2	0	0.5
12	≥	83	80	0.3	1
13	≥	80	85	0.3	1
14	≥	60	55	0	1
15	<	30	35	0.5	0
16	<	58	64	0.5	0
17	≥	60	50	1	1.4
18	≥	19	26	2	0.1
19	<	33	30	0.1	0.5
20	≥	82	78	0.1	1
21	≥	40	99	0	1
22	≥	15	10	0.1	1
23	≥	20	30	1	0.5
24	≥	40	30	0.5	1
25	≥	15	10	0	0.5
26	≥	20	15	0.5	1
27	<	15	35	0.5	0.1
28	<	19	22	1.6	0
29	<	27	25	1	0
30	<	25	20	0.7	0

[a]*Baseline.*

[b]*At the end of 7 days in vitro generation of CD8+ Treg.*

To further define if additional phenotypic abnormalities could be involved in functional alterations found in CD8+ Tregs generated from SSc patients, we analyzed the role of CD127. CD127, the IL-7 receptor α chain, is reportedly a useful marker for identifying memory and effector T cells, while its expression is down-modulated on CD4+CD25+ Treg cells (18, 25, 26).

Similarly to what we observed for CD4+CD25+ Tregs, we previously demonstrated that maturation of circulating CD8+CD28− T cells to CD8+ Tregs is associated with CD127 down-modulation (3). CD127 expression on CD8+CD28− cells from the peripheral blood of SSc patients was similar to what was observed in healthy controls. As expected, CD8+ Tregs generated from healthy donors displayed a down-modulation of CD127 expression with respect to their circulating precursors. On the contrary, CD127 expression increased in CD8+ Tregs generated from SSc patients. Our observation is consistent with recent literature data indicating that IL-7 may play a significant role in numerous T cell-driven chronic inflammatory autoimmune diseases, and that this cytokine likely regulates the proliferation of autoreactive T cells (27).

Our data show for the first time that CD8+ Treg lymphocytes derived from SSc patients display a maturation defect that is characterized by reduced CD39 expression associated with abnormal CD127 overexpression. Alterations of CD39 and CD127 expression could explain, at least partly, the functional defects observed in the CD8+ Tregs generated from patients affected by SSc.

AUTHOR CONTRIBUTIONS

All the authors listed have made substantial, direct, and intellectual contribution to the work and approved it for publication.

FUNDING

This work was supported by Grants from Mediolanum Farmaceutici spa and Gruppo Italiano Lotta alla Sclerodermia (GILS). The sponsors had no role in study design, in the collection, analysis and interpretation of data, in the writing of the report, and in the decision to submit the article for publication.

SUPPLEMENTARY MATERIAL

The Supplementary Material for this article can be found online at http://journal.frontiersin.org/article/10.3389/fimmu.2017.00018/full#supplementary-material.

TABLE S1 | Raw data of percent suppression activity by CD8+ Treg generated from 10 healthy donors.

TABLE S2 | Raw data of percent suppression activity by CD8+ Treg generated from 28 SSc patients.

FIGURE S1 | Percentage expression of CD39 (A) and CD127 (B) molecules on CD8+CD28+ T cells. Panel **(A)** also shows CD39 percentage expression on freshly isolated CD4+ Treg. T0: analyses performed on freshly purified cells; T7: analyses performed after 7 days incubation with IL2 and IL10 for CD8+ Treg generation. HC, healthy controls; SSc, systemic sclerosis patients.

REFERENCES

1. Filaci G, Fenoglio D, Indiveri F. CD8(+) T regulatory/suppressor cells and their relationships with autoreactivity and autoimmunity. *Autoimmunity* (2011) 44(1):51–7. doi:10.3109/08916931003782171
2. Suzuki M, Konya C, Goronzy JJ, Weyand CM. Inhibitory CD8+ T cells in autoimmune disease. *Hum Immunol* (2008) 69(11):781–9. doi:10.1016/j.humimm.2008.08.283
3. Fenoglio D, Ferrera F, Fravega M, Balestra P, Battaglia F, Proietti M, et al. Advancements on phenotypic and functional characterization of non-antigen-specific CD8+CD28- regulatory T cells. *Hum Immunol* (2008) 69(11):745–50. doi:10.1016/j.humimm.2008.08.282
4. Parodi A, Battaglia F, Kalli F, Ferrera F, Conteduca G, Tardito S, et al. CD39 is highly involved in mediating the suppression activity of tumor-infiltrating CD8+ T regulatory lymphocytes. *Cancer Immunol Immunother* (2013) 62(5):851–62. doi:10.1007/s00262-013-1392-z
5. Filaci G, Suciu-Foca N. CD8+ T suppressor cells are back to the game: are they players in autoimmunity? *Autoimmun Rev* (2002) 1(5):279–83. doi:10.1016/S1568-9972(02)00065-4
6. Filaci G, Fravega M, Fenoglio D, Rizzi M, Negrini S, Viggiani R, et al. Non-antigen specific CD8+ T suppressor lymphocytes. *Clin Exp Med* (2004) 4(2):86–92. doi:10.1007/s10238-004-0042-3
7. Borsellino G, Kleinewietfeld M, Di Mitri D, Sternjak A, Diamantini A, Giometto R, et al. Expression of ectonucleotidase CD39 by Foxp3+ Treg cells: hydrolysis of extracellular ATP and immune suppression. *Blood* (2007) 110(4):1225–32. doi:10.1182/blood-2006-12-064527
8. Gabrielli A, Avvedimento EV, Krieg T. Scleroderma. *N Engl J Med* (2009) 360(19):1989–2003. doi:10.1056/NEJMra0806188
9. Gu YS, Kong J, Cheema GS, Keen CL, Wick G, Gershwin ME. The immunobiology of systemic sclerosis. *Semin Arthritis Rheum* (2008) 38(2):132–60. doi:10.1016/j.semarthrit.2007.10.010
10. Fenoglio D, Bernuzzi F, Battaglia F, Parodi A, Kalli F, Negrini S, et al. Th17 and regulatory T lymphocytes in primary biliary cirrhosis and systemic sclerosis as models of autoimmune fibrotic diseases. *Autoimmun Rev* (2012) 12(2):300–4. doi:10.1016/j.autrev.2012.05.004
11. Radstake TR, van Bon L, Broen J, Hussiani A, Hesselstrand R, Wuttge DM, et al. The pronounced Th17 profile in systemic sclerosis (SSc) together with intracellular expression of TGFbeta and IFNgamma distinguishes SSc phenotypes. *PLoS One* (2009) 4(6):e5903. doi:10.1371/journal.pone.0005903
12. Rodriguez-Reyna TS, Furuzawa-Carballeda J, Cabiedes J, Fajardo-Hermosillo LD, Martinez-Reyes C, Diaz-Zamudio M, et al. Th17 peripheral cells are increased in diffuse cutaneous systemic sclerosis compared with limited illness: a cross-sectional study. *Rheumatol Int* (2012) 32(9):2653–60. doi:10.1007/s00296-011-2056-y
13. Papp G, Horvath IF, Barath S, Gyimesi E, Sipka S, Szodoray P, et al. Altered T-cell and regulatory cell repertoire in patients with diffuse cutaneous systemic sclerosis. *Scand J Rheumatol* (2011) 40(3):205–10. doi:10.3109/03009742.2010.528021
14. Murata M, Fujimoto M, Matsushita T, Hamaguchi Y, Hasegawa M, Takehara K, et al. Clinical association of serum interleukin-17 levels in systemic sclerosis: is systemic sclerosis a Th17 disease? *J Dermatol Sci* (2008) 50(3):240–2. doi:10.1016/j.jdermsci.2008.01.001
15. Kurasawa K, Hirose K, Sano H, Endo H, Shinkai H, Nawata Y, et al. Increased interleukin-17 production in patients with systemic sclerosis. *Arthritis Rheum* (2000) 43(11):2455–63. doi:10.1002/1529-0131(200011)43:11<2455:AID-ANR12>3.0.CO;2-K
16. Fenoglio D, Battaglia F, Parodi A, Stringara S, Negrini S, Panico N, et al. Alteration of Th17 and Treg cell subpopulations co-exist in patients affected with systemic sclerosis. *Clin Immunol* (2011) 139(3):249–57. doi:10.1016/j.clim.2011.01.013
17. Bernuzzi F, Fenoglio D, Battaglia F, Fravega M, Gershwin ME, Indiveri F, et al. Phenotypical and functional alterations of CD8 regulatory T cells in primary biliary cirrhosis. *J Autoimmun* (2010) 35(3):176–80. doi:10.1016/j.jaut.2010.06.004
18. Liu W, Putnam AL, Xu-Yu Z, Szot GL, Lee MR, Zhu S, et al. CD127 expression inversely correlates with FoxP3 and suppressive function of human CD4+ T reg cells. *J Exp Med* (2006) 203(7):1701–11. doi:10.1084/jem.20060772
19. Antonioli L, Pacher P, Vizi ES, Hasko G. CD39 and CD73 in immunity and inflammation. *Trends Mol Med* (2013) 19(6):355–67. doi:10.1016/j.molmed.2013.03.005
20. van den Hoogen F, Khanna D, Fransen J, Johnson SR, Baron M, Tyndall A, et al. 2013 classification criteria for systemic sclerosis: an American College of Rheumatology/European League against Rheumatism collaborative initiative. *Arthritis Rheum* (2013) 65(11):2737–47. doi:10.1002/art.38098
21. Filaci G, Fravega M, Negrini S, Procopio F, Fenoglio D, Rizzi M, et al. Nonantigen specific CD8+ T suppressor lymphocytes originate from CD8+CD28- T cells and inhibit both T-cell proliferation and CTL function. *Hum Immunol* (2004) 65(2):142–56. doi:10.1016/j.humimm.2003.12.001
22. Chizzolini C. T cells, B cells, and polarized immune response in the pathogenesis of fibrosis and systemic sclerosis. *Curr Opin Rheumatol* (2008) 20(6):707–12. doi:10.1097/BOR.0b013e32830c45ae
23. Abraham DJ, Krieg T, Distler J, Distler O. Overview of pathogenesis of systemic sclerosis. *Rheumatology* (2009) 48(Suppl 3):iii3–7. doi:10.1093/rheumatology/ken481
24. Longhi MS, Robson SC, Bernstein SH, Serra S, Deaglio S. Biological functions of ecto-enzymes in regulating extracellular adenosine levels in neoplastic and inflammatory disease states. *J Mol Med* (2013) 91(2):165–72. doi:10.1007/s00109-012-0991-z
25. Kaech SM, Tan JT, Wherry EJ, Konieczny BT, Surh CD, Ahmed R. Selective expression of the interleukin 7 receptor identifies effector CD8 T cells that give rise to long-lived memory cells. *Nat Immunol* (2003) 4(12):1191–8. doi:10.1038/ni1009
26. Seddiki N, Santner-Nanan B, Martinson J, Zaunders J, Sasson S, Landay A, et al. Expression of interleukin (IL)-2 and IL-7 receptors discriminates between human regulatory and activated T cells. *J Exp Med* (2006) 203(7):1693–700. doi:10.1084/jem.20060468
27. Bikker A, Hack CE, Lafeber FP, van Roon JA. Interleukin-7: a key mediator in T cell-driven autoimmunity, inflammation, and tissue destruction. *Curr Pharm Des* (2012) 18(16):2347–56. doi:10.2174/138161212800165979

Conflict of Interest Statement: The authors declare that the research was conducted in the absence of any commercial or financial relationships that could be construed as a potential conflict of interest.

frontiers in Immunology

ORIGINAL RESEARCH
published: 07 February 2017
doi: 10.3389/fimmu.2017.00053

B Cell Homeostasis and Functional Properties Are Altered in an Hypochlorous Acid-Induced Murine Model of Systemic Sclerosis

*Sébastien Sanges[1,2,3,4], Manel Jendoubi[1,2], Niloufar Kavian[5], Carine Hauspie[1,2,6], Silvia Speca[1,2], Jean-Charles Crave[7], Thomas Guerrier[1,2], Guillaume Lefèvre[1,2,3,4,6], Vincent Sobanski[1,2,3,4], Ariel Savina[8], Eric Hachulla[1,2,3,4], Pierre-Yves Hatron[1,2,3,4], Myriam Labalette[1,2,6], Frédéric Batteux[5], Sylvain Dubucquoi[1,2,6] and David Launay[1,2,3,4]**

[1] U995, LIRIC – Lille Inflammation Research International Center, Université de Lille, Lille, France, [2] INSERM, U995, Lille, France, [3] Département de Médecine Interne et Immunologie Clinique, CHU Lille, Lille, France, [4] Centre National de Référence Maladies Systémiques et Auto-immunes Rares (Sclérodermie Systémique), Lille, France, [5] Faculté de Médecine, Institut Cochin INSERM U1016 et Laboratoire d'immunologie biologique, AP-HP Hôpital Cochin, Université Paris Descartes, Sorbonne Paris-Cité, Paris, France, [6] Institut d'Immunologie, CHU Lille, Lille, France, [7] Octapharma France SAS, Medical Department, Boulogne-Billancourt, France, [8] Institut Roche, Boulogne-Billancourt, France

OPEN ACCESS

Edited by:
Giuseppina Stifano,
Boston University, USA

Reviewed by:
Elham Hossny,
Ain Shams University, Egypt
Hans Dooms,
Boston University, USA

***Correspondence:**
David Launay
david.launay@univ-lille2.fr

Specialty section:
This article was submitted to Primary Immunodeficiencies, a section of the journal Frontiers in Immunology

Received: 30 September 2016
Accepted: 12 January 2017
Published: 07 February 2017

Citation:
Sanges S, Jendoubi M, Kavian N, Hauspie C, Speca S, Crave J-C, Guerrier T, Lefèvre G, Sobanski V, Savina A, Hachulla E, Hatron P-Y, Labalette M, Batteux F, Dubucquoi S and Launay D (2017) B Cell Homeostasis and Functional Properties Are Altered in an Hypochlorous Acid-Induced Murine Model of Systemic Sclerosis. Front. Immunol. 8:53. doi: 10.3389/fimmu.2017.00053

Introduction: During systemic sclerosis (SSc), peripheral B cells display alterations in subset homeostasis and functional properties and are a promising therapeutic target. However, there is only few data regarding whether these anomalies are accurately reproduced in animal models of SSc.

Objective: In this work, we assessed the B cell homeostasis modifications in an experimental model of SSc [hypochlorous acid (HOCl)-induced mouse], both at a phenotypic and functional level, during the course of the disease.

Methods: Balb/c mice underwent daily intradermal injections of HOCl (or phosphate-buffered saline) and were then sacrificed at day 21 (early inflammatory stage) or day 42 (late fibrotic stage). For phenotypic studies, the distribution of the main spleen cell subsets (B cells, T CD4 and CD8 cells, NK cells, macrophages) and splenic B cell subsets (immature, mature naïve, germinal center, antibody-secreting, memory, B1) was assessed by flow cytometry. For functional studies, splenic B cells were immediately MACS-sorted. Production of interleukin (IL)-6, CCL3, IL-10, and transforming growth factor (TGF)-β was assessed *ex vivo* by RT-PCR and after 48 h of culture by ELISA. Regulatory B cell (Breg) counts were quantified by flow cytometry.

Results: Phenotypic analyses showed an early expansion of transitional B cells, followed by a late expansion of the mature naive subset and decrease in plasmablasts and memory B cells. These anomalies are similar to those encountered in SSc patients. Functional analyses revealed a B-cell overproduction of pro-inflammatory cytokines (IL-6 and CCL3) and an impairment of their anti-inflammatory capacities (decreased production of IL-10 and TGF-β, reduced levels of Bregs) at the early inflammatory stage; and an overproduction of pro-fibrotic cytokines (TGF-β and IL-6) at the late fibrotic stage. These results approximate the anomalies observed in human SSc.

Conclusion: This work reports the existence of anomalies in B cell homeostasis and functional properties in an animal model of SSc that approximate those displayed by SSc patients. These anomalies vary over the course of the disease, which pleads for their participation in inflammatory and fibrotic events. This makes the HOCl mouse a relevant experimental model for the study of B cells, and therefore, B-cell-targeted therapies in SSc.

Keywords: systemic sclerosis, B cell, regulatory B cells, interleukin-6, interleukin-10, animal model

INTRODUCTION

Systemic sclerosis (SSc) is a rare and severe condition classified within the connective tissue diseases. It is characterized by the progressive development of fibrosis in the skin and/or the internal organs such as lungs, digestive tract, and heart (1), impacting on vital and functional prognoses (2–5).

Systemic sclerosis pathophysiology is complex and only partially elucidated (6). It combines, to different degrees, a fibrotic (excessive synthesis of collagen fibers by activated fibroblasts), vascular (microangiopathy), and immunological (dysregulation of cellular and humoral immune systems) components. Among the different immunity actors involved in SSc, the almost-constant presence of autoantibodies and hypergammaglobulinemia has long suggested a potential implication of B cells in the pathogenesis of the disease (7).

Recent data reinforce this hypothesis. Several works have shown alterations in B cell homeostasis and function in SSc patients. For example, there is a decrease in circulating memory B cell counts and an increase in naive B cell counts (8–12). Other teams have documented an enhanced secretion of pro-inflammatory cytokines [such as interleukin (IL)-6], a reduced production of anti-inflammatory cytokines (such as IL-10), and a decrease in circulating regulatory B cell (Breg) counts (9–11, 13–15). In SSc patients, B cells have also been shown to induce pro-fibrotic characteristics in dermal fibroblasts (16). Finally, B cell-targeted therapeutic strategies like anti-CD20 antibodies have been suggested to be effective in this disease (13).

Overall, B cells appear to have an important role in SSc pathophysiology beyond the classical production of autoantibodies. A better description of B cell alterations in this disease, as well as animal models successfully recapitulating them, are therefore mandatory to further understand their pathogenic role and develop new therapeutic approaches. However, data on the modifications in B cell subset distribution and functional properties in animal models of SSc are scarce. Moreover, no study has ever considered a possible variation in B cell involvement during the course of SSc. This is of peculiar importance since several works have suggested that B cell-targeted therapeutic strategies may have different effects whether they are started at an early or late stage of the disease (17–20).

To address these issues, we used a novel murine model of SSc in which daily intradermal injections of hypochlorous acid (HOCl) induce a systemic fibrosis (21). We studied the modifications in B cell homeostasis, both at a phenotypic (B cell subsets distribution) and functional (cytokine production and interaction with fibroblasts) level, at different time points during the course of the experimental disease.

ANIMALS AND METHODS

Induction of the Experimental Disease

Animals

Six-week-old female BALB/c mice (*Janvier Labs*) were used in all experiments. Animals were housed in a specific pathogen-free facility, within autoclaved ventilated cages with sterile food and water *ad libitum*, under constant room temperature and with 12-h day–night cycles. This study was carried out in accordance with the local and national guidelines (directive #68/609 CEE). The protocol was approved by the Regional Ethics Committee on Animal Experimentation.

Experimental Procedure

Experimental SSc was induced by daily intradermal injections of 300 µl of an HOCl-generating solution into the shaved backs of mice, using a 27-gauge needle and a 1-ml syringe, as previously described (21). The HOCl-generating solution was extemporaneously prepared by adding NaClO solution (9.6% as active chlorine) to a 100 mM KH_2PO_4 solution (pH 6.2). The NaClO amount was determined by measuring the optical density (OD) of the solution at 280 nm, and then adjusted to obtain an OD between 0.7 and 0.9. Control mice received injections of 300 µl of sterilized phosphate-buffered saline (PBS).

Sample Collection

Mice were sacrificed by cervical dislocation under deep CO_2 anesthesia at either day 21 (early stage) or day 42 (late stage) after the first injection. All samples were collected at the time of euthanasia. Skin samples were collected near the injection site, and either immediately frozen and stored at −80°C (for biomolecular analyses), or fixed in a fresh 4% paraformaldehyde/PBS solution and embedded in paraffin (for histological and immunohistochemical analyses). Whole spleens were immediately dissected to create a spleen cell suspension, filtered on a 70-µm nylon mesh and depleted in erythrocytes using an appropriate lysing buffer (*Red Blood Cell Lysing Buffer Hybri-Max*, cat. #R7757, Sigma-Aldrich). Blood samples were collected by retro-orbital puncture, set aside for clotting for 30 min, then centrifuged, and stored at −80°C.

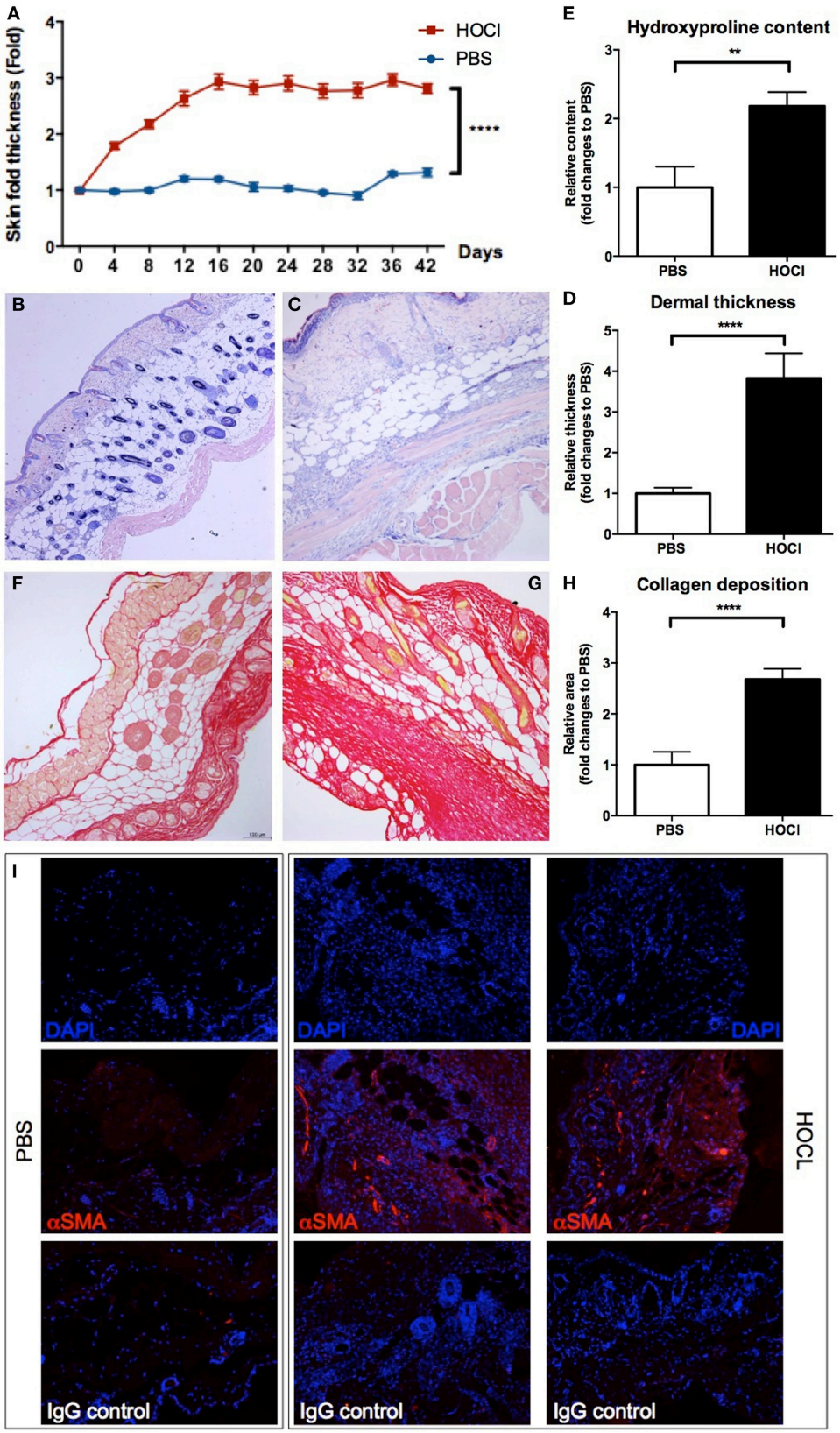

FIGURE 1 | **Continued**

FIGURE 1 | Continued

Evaluation of skin fibrosis in phosphate-buffered saline (PBS) and HOCl mice. To confirm the proper induction of the experimental disease, skin fibrosis was assessed by different methods in PBS and HOCl mice at day 42 after the beginning of the protocol. **(A)** Skin fold thickness (mm) measured sequentially by caliper (n = 20–26 per group). **(B,C)** Representative images of skin sections stained with May-Grünwald–Giemsa coloration from PBS [**(B)**; 10×] and HOCl [**(C)**; 10×] mice, showing dermal thickening in the HOCl mouse. **(D)** Dermal thickness measured on skin sections (n = 10–12 per group). Results are expressed as fold changes compared to the PBS group. **(E)** Hydroxyproline content in 6-mm skin punch biopsies (n = 7–8 per group). Results are expressed as fold changes compared to the PBS group. **(F,G)** Representative images of skin sections stained with picrosirius-red coloration from PBS [**(F)**; 10×] and HOCl [**(G)**; 10×] mice, showing collagen deposition in the HOCl mouse. **(H)** Collagen deposition total surface measured on skin sections (n = 10–12 per group). Results are expressed as fold changes compared to the PBS group. **(I)** Representative images of skin sections immunostained with DAPI alone (top row), DAPI and anti-α-smooth muscle actin (α-SMA) antibody (middle row), or DAPI and isotype control (bottom row) from PBS (left column) and HOCl (center and right columns) mice, showing expression of α-SMA in the HOCl mouse.

Evaluation of the Experimental Disease

Measurement of Skin Fold Thickness

Skin fold thickness was assessed with a caliper by averaging the measure of two different locations near the injection site, twice a week until sacrifice.

Histological Evaluation

Skin samples embedded in paraffin were sliced into serial 4-µm sections. Dermal thickness at the injection site was assessed by performing a May-Grünwald–Giemsa (MGG) staining and measuring the distance between the epidermal–dermal junction and the dermal–subcutaneous fat junction at a 40-fold magnification using the ImageJ morphometic software (*U.S. National Institute of Health*) (22). Ten random measurements per section were performed by two blinded investigators and averaged for each section. Collagen deposition in the skin was evaluated by performing a picrosirius-red staining and delineating the stained area using a color deconvolution method (23). This allowed a precise quantification of the total area occupied by collagen deposits in each section. Expression of α-smooth muscle actin (α-SMA) in the skin was assessed by immunofluorescence with a specific anti-α-SMA antibody (clone 1A4, cat. #ab7817, Abcam) coupled with DAPI (1:1,000-fold dilution, Thermo Fischer Scientific). Non-specific binding was appreciated using an isotype control antibody. Protein visualization was performed by using a specific Alexa Fluor 488 goat anti-rabbit antibody.

Measurement of Hydroxyproline Content

Collagen content was assessed by using a colorimetric *Hydroxyprolin Kit Assay* (Sigma-Aldrich) according to the manufacturer's protocol. Briefly, approximately 10 mg of skin were homogenized in 100 ml of water and hydrolyzed at 120°C for 3 h in an equal volume of concentrated hydrochloric acid (HCl, 12 M). Then, a colorimetric product, visualized at 560 nm and proportional to the hydroxyproline content, was generated by reaction of oxidized hydroxyproline in each sample with 4-(Dimethylamino)benzaldehyde.

Quantification of Fibrosis, Inflammation, and Proliferation Markers RNA Expression in Skin Samples

Approximately 0.5 cm of frozen skin samples were minced and mechanically homogenized. Then, total RNA was extracted with a *Nucleospin RNA kit* (Macherey-Nagel, Hoerdt, France) and eluted in RNAse-free water. The purity of RNA was evaluated by UV spectroscopy on a Nanodrop system from 220 to 350 nm. Then, 1 µg of total RNA was used to obtain single-stranded cDNA by using a specific *Reverse Transcription Kit* (Thermo Fisher Scientific) according to the manufacturer's protocol. Quantitative RT-PCR was performed by using *LightCycler FastStart DNA Master SYBR Green I* (Thermo Fisher Scientific), according to the manufacturer's protocol. Primers sets include TGFB for transforming growth factor (TGF)-β1, Acta2 for α-SMA, Fn1 for Fibronectin, COL1a1 for Collagen I-1III, Il-6 for IL-6, Il-1b for IL-1β, tnfa for tumor necrosis factor (TNF)-α, and Pcna for proliferating cell nuclear antigen (PCNA). Sequences and relative NCBI references for each gene are listed in Table S1 in Supplementary Material. All samples were amplified in duplicate. DNA quantification was expressed as critical threshold cycle (Ct) value, or rather the cycle number at which the DNA amplification was first detected. Relative gene expression value was calculated as $E = 2^{-\Delta Ct}$, where ΔCt is the difference in crossing points between GAPDH and each gene.

Phenotypic Evaluation of B Cells

Flow Cytometry

Immediately after collection, spleen cells were counted using an automated method (*Flow-Count Fluorospheres*, cat. #7547053, Beckman Coulter); and their viability was assessed with propidium iodide staining. Approximately 1 million spleen cells were incubated with mouse anti-Fc receptor antibody (*FcBlock*, clone 2.4G2; cat. #553142, BD Biosciences) for 15 min at 4°C protected from light to limit non-specific antibody binding. They were next incubated with different antibody mixes for membrane staining (Table S2 in Supplementary Material) for 20 min at 4°C protected from light. Data were then acquired on a 3-laser cytometer (*Navios*, Beckman Coulter) and analyzed with a dedicated software (*Kaluza*, Beckman Coulter).

Quantification of Serum B Cell-Activating Factor (BAFF) Levels

B cell-activating factor levels were assessed on serum samples in duplicate at a 1:3-dilution using an ELISA assay (*Quantikine ELISA Mouse BAFF*, cat. #MBLYS0, R&D systems), according to the manufacturer's protocol.

Quantification of CD19 Expression in Skin Samples

CD19 expression in skin samples was assessed by immunofluorescence using a specific anti-CD19 antibody (0.5 µg/ml, BioLegend) overnight at 4°C, coupled with DAPI (1:1,000-fold dilution, Thermo Fischer Scientific). Protein visualization was performed by using a specific Alexa Fluor 566 goat anti-mouse antibody incubated for 1 h at room temperature.

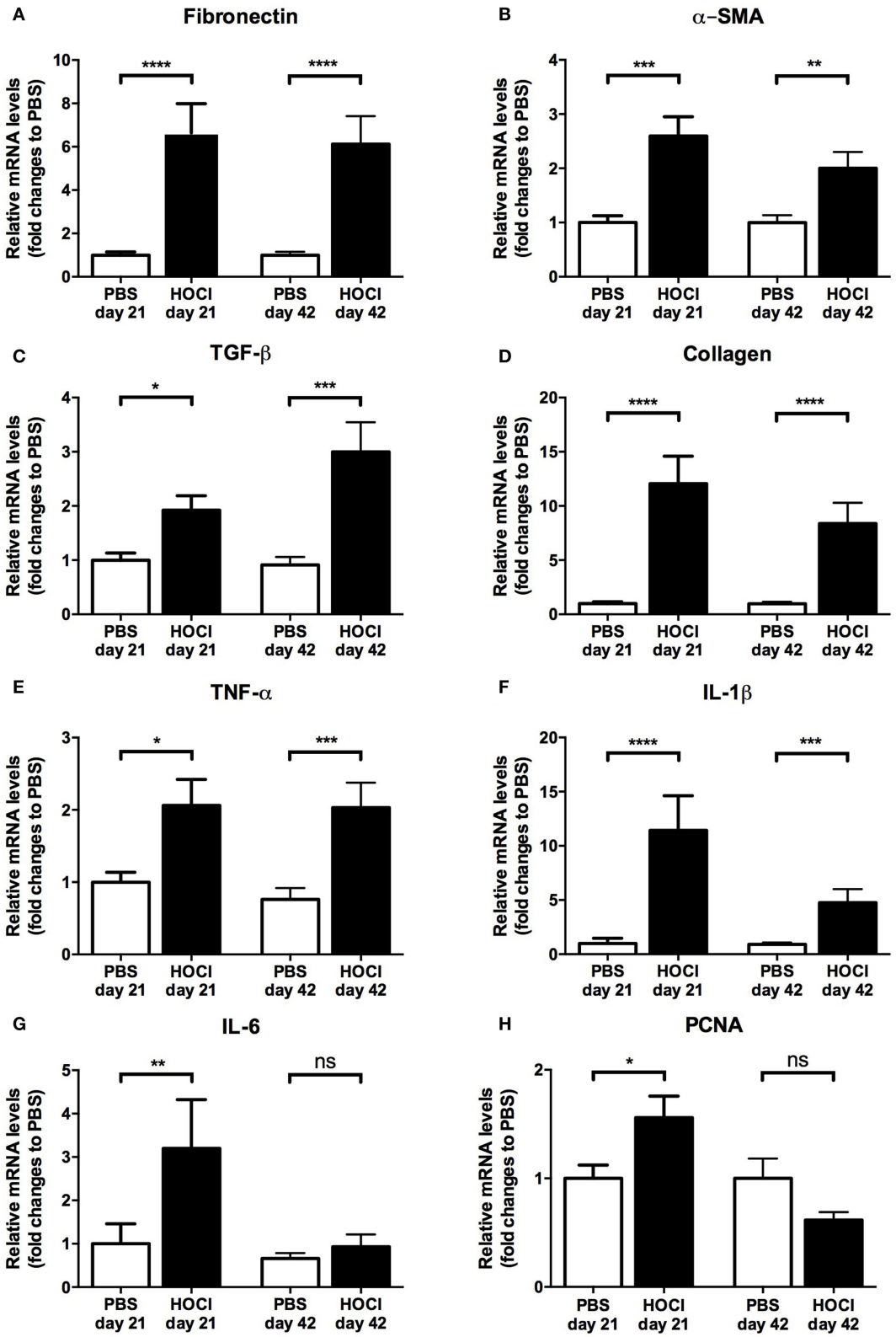

FIGURE 2 | Expression of fibrosis, inflammation, and proliferation markers in the skin of phosphate-buffered saline (PBS) and HOCl mice at day 21 and day 42 of the protocol. mRNA levels of various markers of fibrosis [fibronectin **(A)**, α-smooth muscle actin (α-SMA) **(B)**, transforming growth factor (TGF)-β **(C)**, collagen **(D)**], inflammation [tumor necrosis factor (TNF)-α **(E)**, interleukin (IL)-1β **(F)**, IL-6 **(G)**], and proliferation [proliferating cell nuclear antigen (PCNA) **(H)**], normalized to GAPDH and expressed as fold changes to PBS day 21 (for day-21 groups) or to PBS day 42 (for day-42 groups) (n = 15–24 per group).

Functional Evaluation of B Cells

B Cell Sorting

Immediately after collection, B cells were isolated from splenocytes using a negative magnetic bead-assisted sorting assay (*EasySep Mouse Pan-B Cell Isolation Kit*, cat. #19844, StemCell), according to the manufacturer's protocol. B cell purity was always above 95% as assessed by flow cytometry.

Quantification of IL-6, CCL3, IL-10, and TGF-β RNA Expression in B Cells

Immediately after sorting, purified B cells were ultra-centrifuged, treated with lysis buffer (*NucleoSpin RNA kit*, Macherey-Nagel), and stored at −80°C. Quantification of IL-6, chemokine ligand (CCL) 3, IL-10, and TGF-β RNA expression in B cells was performed as detailed in Section "Quantification of Fibrosis, Inflammation, and Proliferation Markers RNA Expression in Skin Samples" (except that levels were normalized to GUSB).

Quantification of IL-6, IL-10, and CCL3 Protein Levels in B Cells

Immediately after sorting, purified B cells were seeded on a 96-well plate (400,000 B cells per well) within complete medium [Roswell Park Memorial Institute (RPMI) 1640 medium containing 10% heat-inactivated fetal calf serum (FCS), 20 UI/ml penicillin, 20 µg/ml streptomycin, 2 mM L-glutamin, 1 mM pyruvate, 50 µM 2-mercaptoethanol, and 1% non-essential amino acids]. They were cultured during 48 h at 37°C in humidified atmosphere with 5% CO_2 and stimulated either with lipopolysaccharide (LPS) (*Escherichia coli* serotype O127:B8, 10 µg/ml; cat. #L4516, Sigma-Aldrich), with LPS and anti-CD40 antibody (clone HM40/3, 2.5 µg/ml; cat. #553721, BD Biosciences), or without immunostimulation. After culture, supernatants were collected and immediately stored at −80°C.

Interleukin-6, IL-10, and CCL3 protein levels in supernatant samples were assessed in duplicate using ELISA assays (*Quantikine ELISA Mouse IL-6*, cat. #M6000B; *Quantikine ELISA Mouse IL-10*, cat. #M1000B; *Quantikine ELISA Mouse CCL3*, cat. #MMA00; R&D systems), at appropriate dilutions (1:10 for IL-6; 1:1 for IL-10; 1:100 for CCL3). All experiments were conducted according to the manufacturer's protocols.

IL-10 Intracellular Staining

Immediately after sorting, purified B cells were seeded on a 48-well plate (2 million B cells per well) within complete

TABLE 1 | Phenotypic definitions of spleen cell and B cell subsets.

Cell subsets	Abbreviation	Phenotypic definition
Spleen cell subsets		
B cell	/	$CD19^+$
T cell	/	$CD3^+$
T $CD4^+$ cell	/	$CD3^+$ $CD4^+$
T $CD8^+$ cell	/	$CD3^+$ $CD8^+$
NK cell	/	$CD335^+$
Monocyte–macrophage	MM	$CD11b^+$ FSC^{hi}
B cell subsets		
B2 cell	B2	$CD19^+$ $B220^{hi}$
Immature B cells		
=Transitional B cell	TR	$CD19^+$ $B220^{hi}$ $CD93^+$
Type 1 transitional B cell	T1	$CD19^+$ $B220^{hi}$ $CD93^+$ $CD23^-$ IgM^{hi}
Type 2 transitional B cell	T2	$CD19^+$ $B220^{hi}$ $CD93^+$ $CD23^+$ IgM^{hi}
Type 3 transitional B cell	T3	$CD19^+$ $B220^{hi}$ $CD93^+$ $CD23^+$ IgM^{lo}
Marginal zone precursor B cell	MZP	$CD19^+$ $B220^{hi}$ $CD93^{-/+}$ $CD23^{hi}$ IgM^{hi} $CD21^{hi}$
Mature naive B cells		$CD19^+$ $B220^{hi}$ $CD93^-$
Follicular B cell	FO	$CD19^+$ $B220^{hi}$ $CD93^-$ $CD23^+$ $CD21^{lo/med}$
Follicular type I B cell	FO-I	$CD19^+$ $B220^{hi}$ $CD93^-$ $CD23^+$ $CD21^{lo/med}$ IgM^{lo}
Follicular type II B cell	FO-II	$CD19^+$ $B220^{hi}$ $CD93^-$ $CD23^+$ $CD21^{lo/med}$ IgM^{hi}
Marginal zone B cell	MZ	$CD19^+$ $B220^{hi}$ $CD93^-$ $CD23^-$ $CD21^{hi}$ IgM^{hi}
Nature non-naïve B cells		
Germinal center B cells	GC	$CD19^+$ $CD38^-$ $GL7^+$
Centroblasts	CB	$CD19^+$ $CD38^-$ $GL7^+$ $CXCR4^+$
Centrocytes	CC	$CD19^+$ $CD38^-$ $GL7^+$ $CXCR4^-$
Antibody-secreting cells	ASC	$CD138^{hi}$ $CD19^{lo/-}$
Plasmablasts	PB	$CD138^{hi}$ $CD19^{lo}$ $CD22^+$
Plasma cells	PC	$CD138^{hi}$ $CD19^{lo/-}$ $CD22^-$
Memory B cells	MemB	$CD19^+$ $CD93^-$ $CD38^+$ IgM^-
B1 cells	B1	$CD19^+$ $B220^{lo}$ $CD23^-$ $CD43^+$ IgM^{hi}
B1a B cells	B1a	$CD19^+$ $B220^{lo}$ $CD23^-$ $CD43^+$ IgM^{hi} $CD5^+$
B1b B cells	B1b	$CD19^+$ $B220^{lo}$ $CD23^-$ $CD43^+$ IgM^{hi} $CD5^-$
Regulatory B cells		
$CD5^+$ $CD1d^{hi}$ B cells	/	$CD19^+$ $CD5^+$ $CD1d^{hi}$
$IL\text{-}10^+$ B cells	B10	$CD19^+$ $IL\text{-}10^+$

CXCR, CXC-chemokine receptor; FSC, forward scatter; Ig, immunoglobulin; IL, interleukin.

medium (RPMI 1640 medium containing 10% heat-inactivated FCS, 20 UI/ml penicillin, 20 µg/ml streptomycin, 2 mM L-glutamin, 1 mM pyruvate, 50 µM 2-mercaptoethanol, and 1% non-essential amino-acids). As previously described (24), they were cultured during 48 h at 37°C in humidified atmosphere with 5% CO_2 and stimulated by anti-CD40 antibody (clone HM40/3, 1 µg/ml; cat. #553721, BD Biosciences). During the last 5 h of culture, LPS (*E. coli* serotype O111:B4, 10 µg/ml; cat. #L4391, Sigma-Aldrich), PMA (50 ng/ml, cat. #P8139, Sigma-Aldrich), ionomycin (500 ng/ml, cat. #I0634, Sigma-Aldrich), and monensin (2 mM, cat. #00-4505-51, eBiosciences) were added to the culture medium to induce IL-10 expression and block exocytosis (24).

Interleukin-10 intracellular detection was performed as previously described (24). First, B cells were stained with a viability dye (*Live/Dead Fixable Far Red Dead Cell Stain Kit*, 1:3,200-dilution, cat. #L10120, Life Technologies), saturated with an anti-Fc receptor antibody (*FcBlock*, clone 2.4G2; cat.

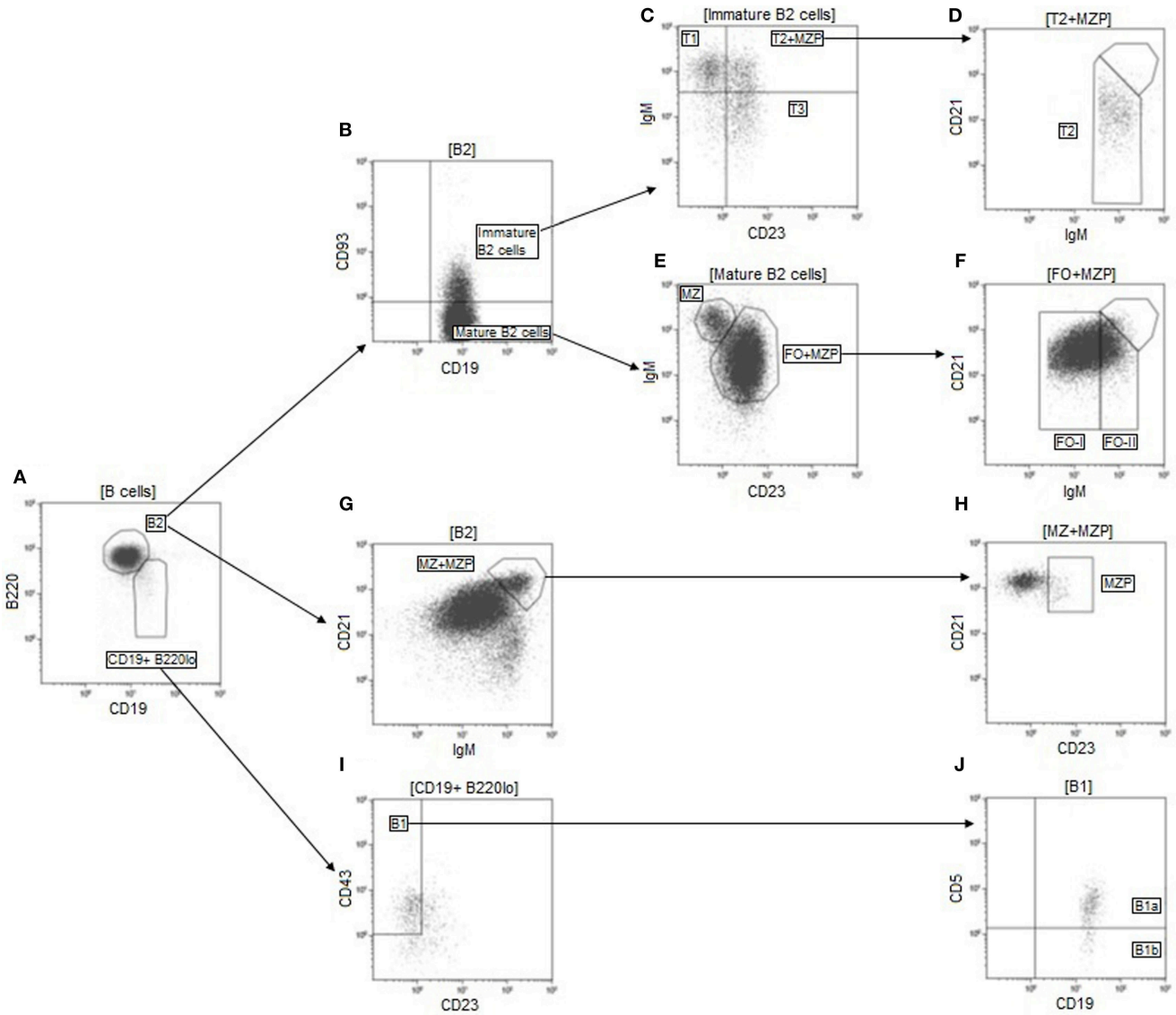

FIGURE 3 | **Gating strategy used for identification of the main B cell subsets**. Doublets were first excluded on an FSC-area/FSC-height dot-plot (not shown). Lymphocytes were then selected based on their size and internal complexity on a FSC/SSC dot-plot (not shown). B cells were next delimited on a CD19/open channel dot-plot and defined as $CD19^+$ non-autofluorescent cells (not shown). B2 cells were identified as $CD19^+$ $B220^{hi}$ cells on a CD19/B220 dot-plot gated on B cells **(A)**. Transitional B cells were then selected as $CD93^+$ cells **(B)** and divided into their three main subsets based on their expression of CD23 and IgM **(C,D)**. Among mature B2 cells, defined as $CD93^-$ cells **(B)**, follicular (FO) and marginal zone (MZ) B cells were separated based on their membrane levels of CD23 and IgM **(E)**. FO B cells were further divided into follicular type I (FO-I) and follicular type II (FO-II) depending on their expression levels of IgM **(F)**. MZP B cells were identified as $CD23^{hi}$ cells within a gate containing $CD21^{hi}$ IgM^{hi} B2 cells **(G,H)**. MZP cells were then backgated out of the T2 and FO populations **(D,F)**. B1 cells were identified as $CD23^-$ $CD43^+$ cells among $CD19^+$ $B220^{hi}$ cells **(A,I)**. B1a cells were then separated from B1b cells based on their membrane expression of CD5 **(J)**. FSC, forward scatter; Ig, immunoglobulin; SSC, side scatter.

#553142, BD Biosciences) to prevent non-specific binding, and stained with an anti-CD19 antibody (*Brillant Violet 510 Rat Anti-Mouse CD19*, clone 1D3; cat. # 562956, BD Biosciences). Next they were fixed and permeabilized with the *Cytofix/Cytoperm* kit (cat. #554722, BD Biosciences) according to the manufacturer's protocol. Permeabilized cells were then stained with an anti-IL-10 antibody (*PE Rat Anti-Mouse IL-10*, clone JES5-16E3; cat. #554467, BD Biosciences). Data were acquired on a 3-laser cytometer (*Navios*, Beckman Coulter) and analyzed with a dedicated software (*Kaluza*, Beckman Coulter).

Fibroblasts–B Cells Coculture Experiments

Mouse embryonic fibroblast cells (BALB/c 3T3, ATCC clone A31) were purchased from American Type Culture Collection (ATCC; MD, USA). B cells were sorted as described in Section "B Cell Sorting." Cells were cultured in complete medium (RPMI 1640 medium containing 10% heat-inactivated FCS, 20 UI/ml penicillin, 20 μg/ml streptomycin). 3T3 fibroblasts (10^5 cells) alone, B cells (5×10^5 cells) alone, or cocultures were seeded in 12-well plates for 72 h.

Quantification of fibrosis and proliferation markers RNA expression in fibroblasts was performed as detailed in Section

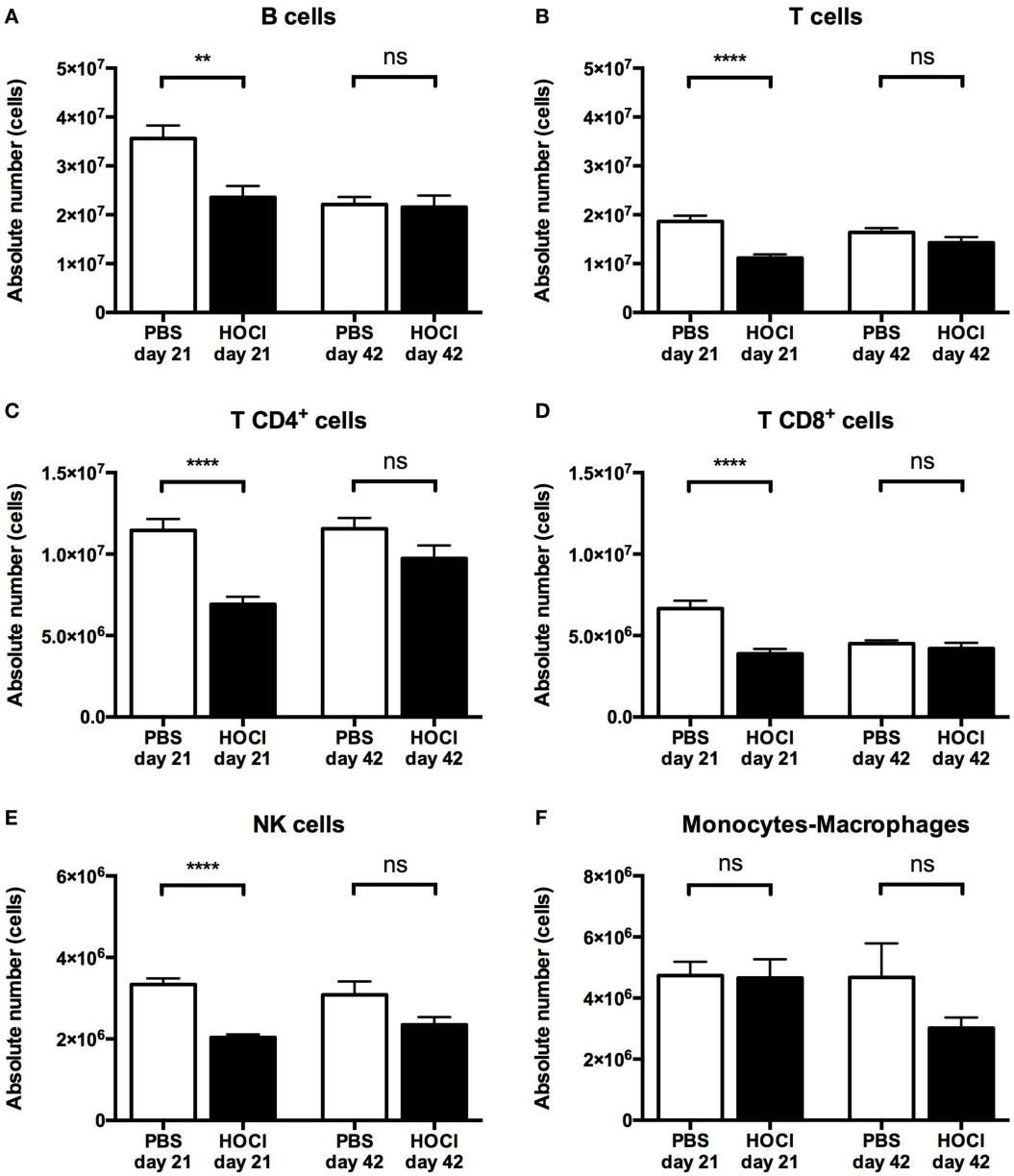

FIGURE 4 | Distribution of the main spleen cell subsets in phosphate-buffered saline (PBS) and HOCl mice at day 21 and day 42. Distribution of B cells **(A)**, T cells **(B)**, T CD4+ cells **(C)**, T CD8+ cells **(D)**, NK cells **(E)**, and monocytes–macrophages **(F)** in absolute values expressed in cells (n = 12–17 per group).

"Quantification of Fibrosis, Inflammation, and Proliferation Markers RNA Expression in Skin Samples."

Statistical Analysis

Multi-group comparisons were performed using Kruskall and Wallis non-parametric test. Whenever a significant difference was detected, Mann–Whitney test was used to compare each group by pair. All statistical analyses were performed on SPSS v22 (IBM) and GraphPad Prism v6 (GraphPad Software). Quantitative data were expressed as mean ± SEM. Significance was set at $p < 0.05$. In figures, levels of significance were pictured as follows: $^{****}p \leq 0.0001$; $^{***}p \leq 0.001$, $^{**}p \leq 0.01$, $^{*}p \leq 0.05$, $^{\circ}p \leq 0.20$; and ns for $p \geq 0.20$.

RESULTS

HOCl Injections Induce an Experimental Disease Whose Characteristics and Course Resemble Human SSc

HOCl Intradermal Injections Induce Skin Fibrosis in Mice

In a first step, we wanted to confirm the validity of the experimental disease. Induction of skin fibrosis in HOCl mice was assessed through clinical, protein, and histological evaluations (**Figure 1**). Thus, we observed a significant increase in the macroscopic skin fold in HOCl mice compared to PBS mice ($p < 0.0001$) (**Figure 1A**). Dermal thickness, measured on MGG-stained skin sections, was also significantly higher in the HOCl group than in the control group ($p < 0.0001$) (**Figures 1B–D**). A higher amount of collagen fibers in skin sections of HOCl mice, compared to PBS mice, was observed by histological picrosirius-red staining ($p < 0.0001$) and confirmed by evaluation of the hydroxyproline content, which was significantly increased in HOCl mice ($p < 0.05$) (**Figures 1E–H**). Finally, a consistent amount of α-SMA-positive cells on skin from HOCl mice was qualitatively appreciated by immunofluorescence, whereas PBS mice showed a very low number of α-SMA-expressing cells (**Figure 1I**). Overall, these results indicated the validity of the experimental disease, as previously described (21).

The Early Stage of the HOCl Model Displays More Inflammatory Features than the Late Stage

As human SSc usually evolves through an early inflammatory stage and a late fibrotic stage, we wondered whether a similar phenomenon occurred during the course of the HOCl experimental disease. An evaluation of mRNA

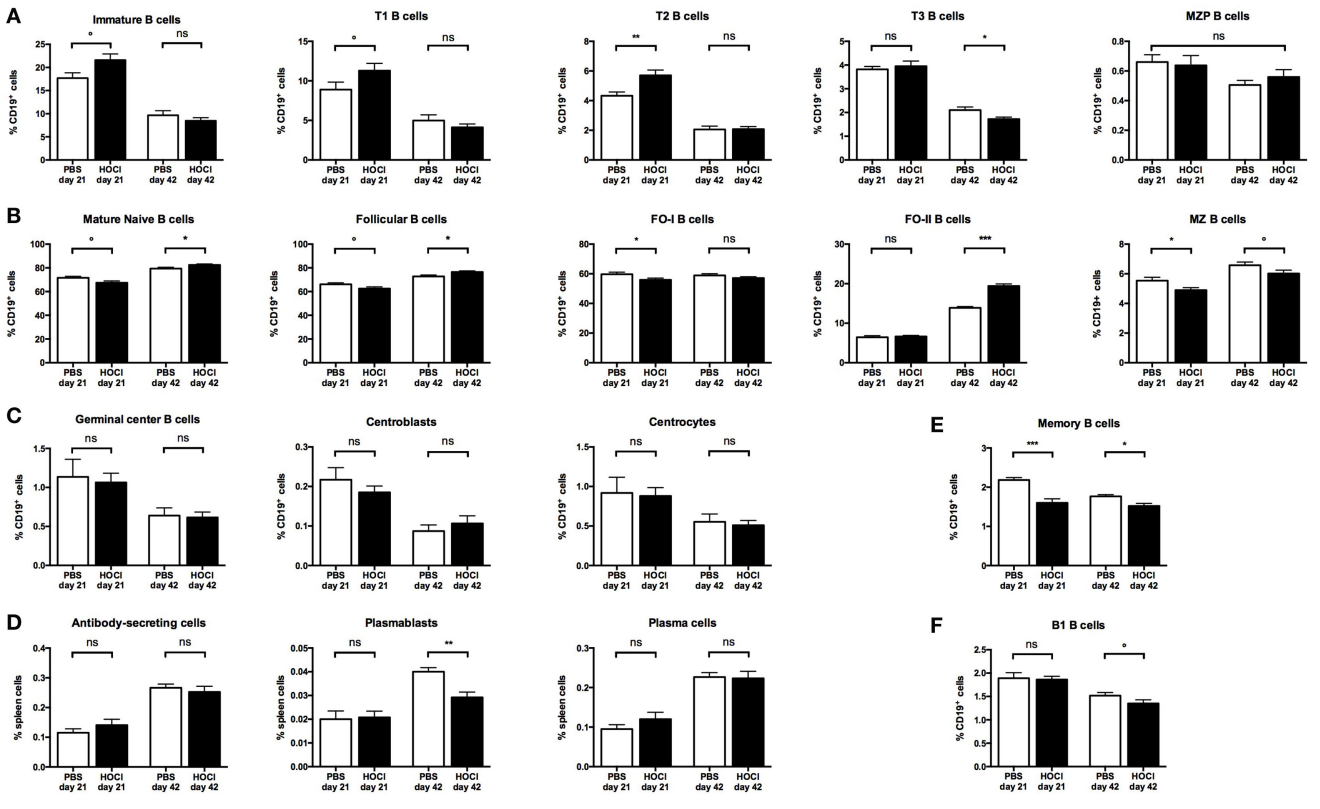

FIGURE 5 | Distribution of the main B cell subsets in phosphate-buffered saline (PBS) and HOCl mice at day 21 and day 42. Distribution of immature B cells and its main subsets **(A)**, mature naive B cells and its main subsets **(B)**, germinal center B cells and its main subsets **(C)**, antibody-secreting cells and its main subsets **(D)**, memory B cells **(E)**, and B1 cells **(F)** in relative values expressed in percentages of CD19+ cells (except for ASC, PB, and PC expressed in percentages of total spleen cells) (n = 7–8 per group).

expression profile of various fibrosis (fibronectin, α-SMA, collagen, TGF-β), inflammatory (TNF-α, IL-1β, IL-6), and proliferation (PCNA) markers in the skin of PBS and HOCl mice was thus performed at two different time points from the beginning of the protocol (day 21: early stage; day 42: late stage).

At day 21, we observed a significant increase in the mRNA expression of fibrotic, inflammatory, and proliferation markers in the HOCl mice compared to PBS mice (fibronectin: $p < 0.0001$; α-SMA: $p = 0.0004$; collagen: $p < 0.0001$; TGF-β: $p = 0.01$; TNF-α: $p = 0.02$; IL-1β: $p < 0.0001$; IL-6: $p = 0.004$; PCNA: $p = 0.04$) (**Figure 2**). At day 42, a significant increase in the mRNA levels of all pro-fibrotic proteins was still observed (fibronectin: $p < 0.0001$; α-SMA: $p = 0.001$; collagen: $p < 0.0001$; TGF-β: $p = 0.0001$). However, among inflammatory and proliferation markers, only TNF-α and IL-1β were differentially expressed ($p = 0.0006$ and $p = 0.0005$, respectively); there was no longer a significant difference in the production of IL-6 ($p = 0.67$) and PCNA ($p = 0.31$) (**Figure 2**). Overall, these results suggested that the early stage of the experimental disease displays more inflammatory and proliferative features than the late stage, which mimics to some extent the natural course of human SSc.

Splenic B Cell Homeostasis Is Altered in HOCl Mice

Splenic B Cell Subset Distribution Is Modified in HOCl Mice and Varies over Time

Several works have reported disturbances in B cell homeostasis in SSc, especially in B cell subset distribution. We wondered if

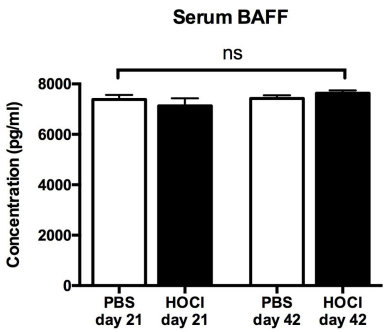

FIGURE 7 | Serum B cell-activating factor (BAFF) levels in phosphate-buffered saline (PBS) and HOCl mice at day 21 and day 42. Results expressed in picograms per milliliter (n = 6–7 per group).

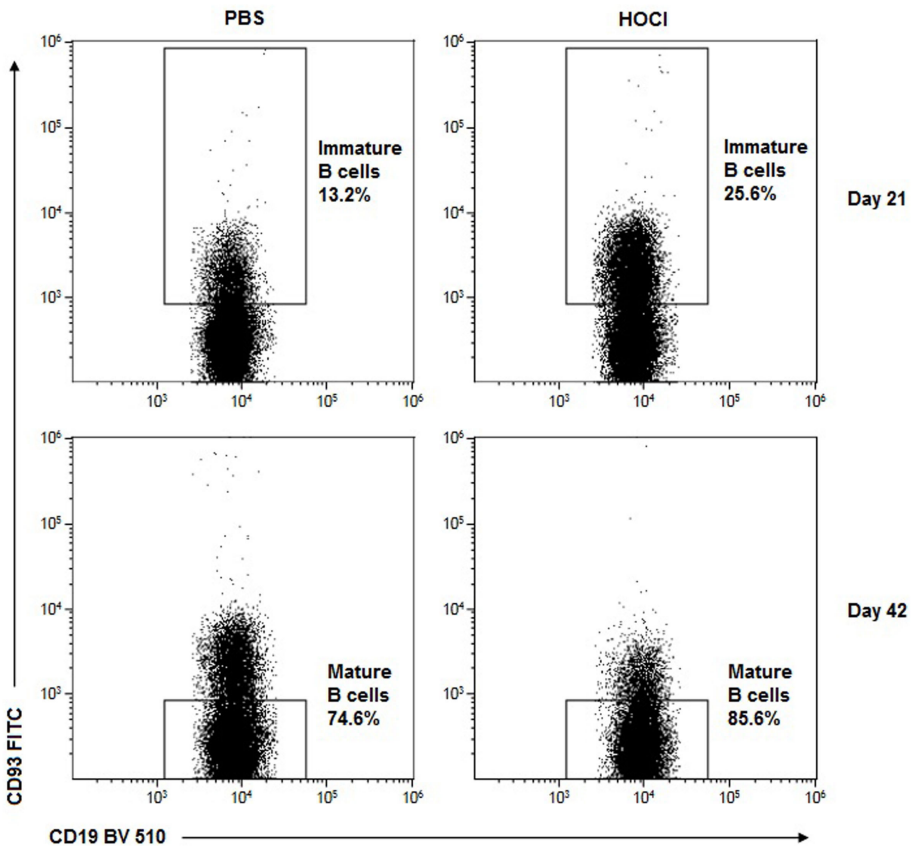

FIGURE 6 | Representative dot-plots of immature and mature B2 cells in phosphate-buffered saline (PBS) and HOCl mice at day 21 and day 42. Representative CD19/CD93 dot-plots gated on B cells from PBS (left column) and HOCl (right column) mice at day 21 (top row) and day 42 (bottom row), showing early expansion of the transitional subset and late expansion of the mature naïve cells in the HOCl mouse.

such anomalies existed in the HOCl model, and if so, how they would evolve during the course of the experimental disease. We compared the main leukocyte and B cell subsets in the spleens of HOCl and PBS mice, at the early and late stages of the disease. The phenotypic definitions and gating strategy used for their identification are detailed in **Table 1** and **Figure 3**, respectively.

Regarding total splenic B cell counts, we observed a significant decrease in HOCl mice at day 21 ($p = 0.007$), but no difference between the two groups at day 42 ($p = 0.53$) (**Figure 4A**). A similar trend was noted for the other splenic lymphocyte subsets, with a significant reduction in T $CD4^+$, T $CD8^+$, and NK cells at the early stage, and no difference at the late stage (**Figures 4B–E**). Monocyte and macrophage counts were equivalent at both stages of the disease (**Figure 4F**).

Regarding immature B cell subsets (**Figures 5A** and **6**), there was a trend for an increase in transitional forms at day 21 ($p = 0.07$) and a non-significant decrease at day 42 ($p = 0.33$) in HOCl mice. These anomalies reached statistical significance for transitional type 2 (T2) B cells at the early stage ($p = 0.009$) and transitional type 3 (T3) B cells at the late stage ($p = 0.03$).

Regarding mature naive subsets (**Figures 5B** and **6**), the opposite phenomenon was noted, with a trend for a decrease at day 21 ($p = 0.07$) and a significant increase ($p = 0.04$) at day 42. These anomalies were mainly carried by the major mature naive subset, called follicular (FO) B cells ($p = 0.07$ at day 21; $p = 0.02$ at day 42). Interestingly though, the early FO decrease was essentially explained by the follicular type I B cells ($p = 0.05$) whereas the late FO increase was mostly supported by the follicular type II B cells ($p = 0.0003$). Conversely, the minor mature naive subset, named marginal zone B cells, was non-significantly decreased at both stages of the disease ($p = 0.05$ at day 21; $p = 0.10$ at day 42).

Regarding non-naive B cell subsets, germinal center B cell counts were similar in both groups at both time points, even when considering the centroblast and centrocyte subsets (**Figure 5C**). Although there was no difference in antibody-secreting cell and plasma cell counts between the two groups, a significant decrease in the plasmablast subset was noted at day 42 ($p = 0.003$) (**Figure 5D**). Switched memory B cells were also decreased in HOCl mice at both stages of the disease ($p = 0.0007$ at day 21; $p = 0.001$ at day 42) (**Figure 5E**).

Regarding B1 B cells (**Figure 5F**), we observed a trend for a decrease in HOCl mice at day 42 ($p = 0.09$) that reached significance for the B1a subset ($p = 0.04$).

Overall, these results confirmed that the HOCl model displays alterations in splenic B cell subset distribution (early expansion of transitional B cells; late expansion of the mature naive subset; and decrease in plasmablasts and memory B cells).

Alterations in B Cell Subset Homeostasis Are Independent of BAFF

B cell homeostasis and maturation are regulated by a large number of factors among which survival signals (such as BAFF) play a critical role. Since serum BAFF levels are increased in SSc patients, we wondered if it could contribute to the alterations in B cell subset distribution observed in the HOCl model. However, serum BAFF levels were identical in both groups at both time points (**Figure 7**), suggesting that this cytokine does not participate in these anomalies.

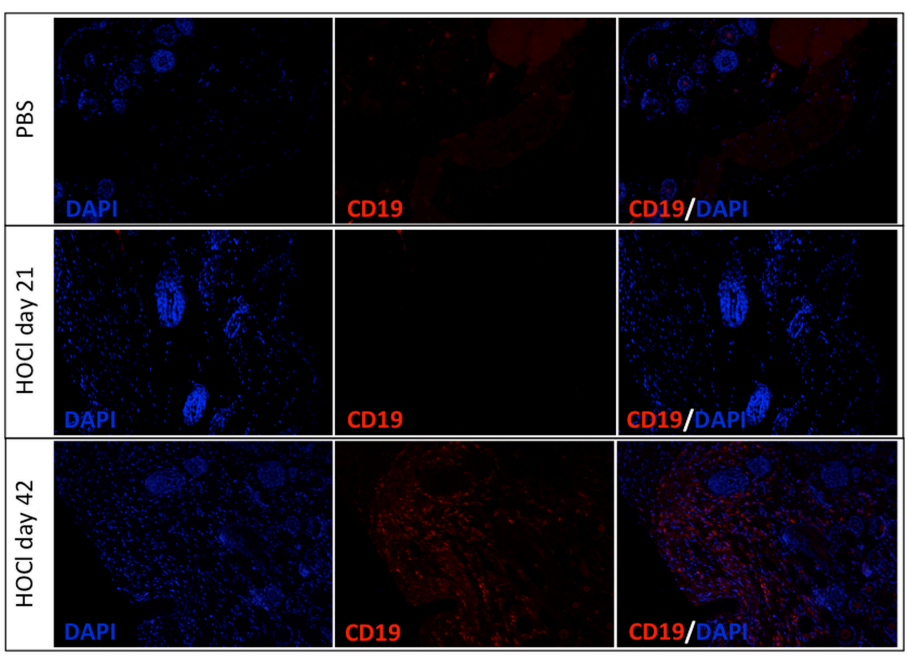

FIGURE 8 | Representative images of skin sections immunostained for CD19 in phosphate-buffered saline (PBS) and HOCl mice at day 21 and day 42. Representative images of PBS skin (top row), HOCl skin at day 21 (middle row), and HOCl skin at day 42 (bottom row) immunostained with DAPI (left column), with anti-CD19 antibody (middle column), and with both (right column) ($n = 5$ per group).

HOCl Skin Is Infiltrated by B Cells at the Late Stage

Next we wondered if anomalies in B cell homeostasis were also observed outside the spleen and within disease-targeted organs. To do so, we assessed CD19 expression in skin samples from the two groups and found a significant B cell infiltration in HOCl skin at day 42, but no difference with PBS mice at day 21 (**Figure 8**).

Taken together with our previous results, these findings might indicate that B cells could be recruited from the spleen to infiltrate the skin.

Splenic B Cell Functional Properties Are Altered in HOCl Mice

As human SSc B cells display functional anomalies that contribute to the pathogenesis of the disease, we next wondered whether the same holds true for HOCl splenic B cells. Therefore, we sought to investigate their pro-inflammatory, anti-inflammatory, and pro-fibrotic properties by studying their production of various cytokines.

Splenic B Cell Production of Pro-inflammatory Cytokines Is Increased in HOCl Mice

Based on data from a preliminary work (not shown), we selected two candidate proteins, IL-6 and CCL3, to assess the pro-inflammatory properties of B cells in the HOCl model.

First we measured IL-6 and CCL3 mRNA levels in splenic B cells *ex vivo* (just after collection and sorting). IL-6 mRNA levels did not differ at day 21 ($p = 0.83$); but there was a trend for a significant increase in the HOCl group at day 42 ($p = 0.06$) (**Figure 9A**). CCL3 production was significantly higher in HOCl mice at both time points ($p = 0.02$ in both cases) (**Figure 10A**).

As to further explore these anomalies, we then studied the secretion of IL-6 and CCL3 in splenic B cells cultured with various stimulation conditions. Without immunostimulation, there was only negligible basal secretion of both cytokines at both time points. When stimulated by LPS alone or with anti-CD40 antibody, HOCl B cells produced more IL-6 and CCL3 than the control group at both time points (**Figures 9B** and **10B**). This

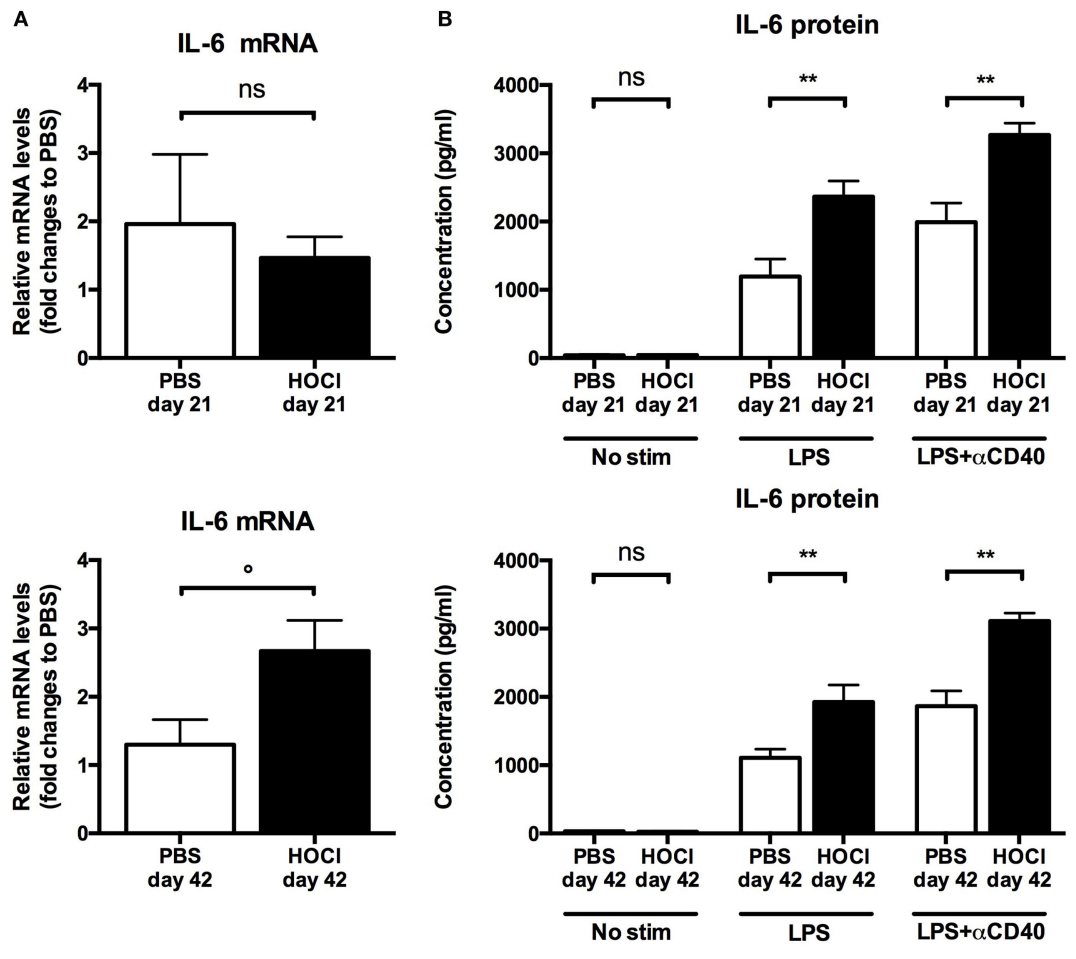

FIGURE 9 | **Interleukin (IL)-6 production by splenic B cells in phosphate-buffered saline (PBS) and HOCl mice at day 21 and day 42. (A)** IL-6 mRNA levels in splenic B cells after collection and sorting, normalized to GUSB and expressed as fold changes to PBS day 21 for day-21 groups (top row), and to PBS day 42 for day-42 groups (bottom row) (n = 4–6 per group). **(B)** IL-6 supernatant levels after culture of splenic B cells for 48 h with various stimulation conditions [none, lipopolysaccharide (LPS), LPS + anti-CD40 antibody] at day 21 (top row) and day 42 (bottom row), expressed in picograms per milliliter (n = 6–8 per group).

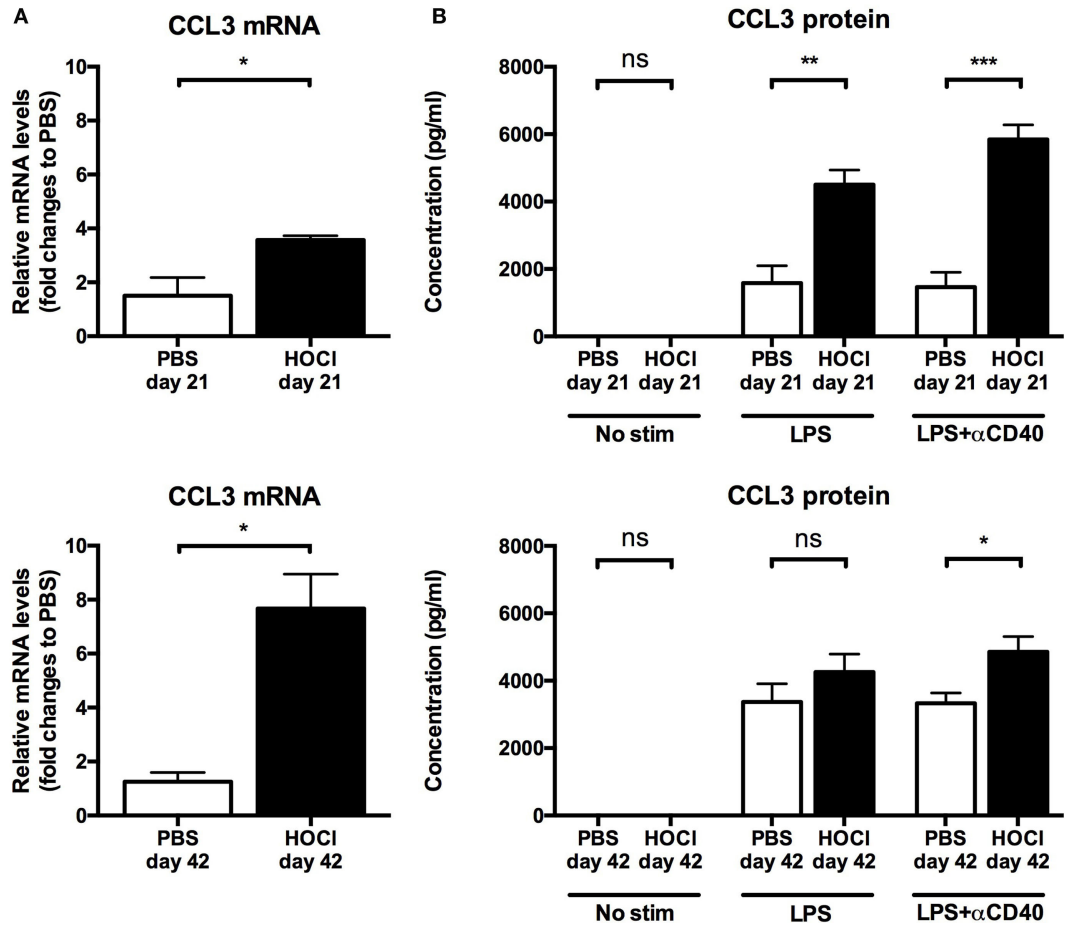

FIGURE 10 | CCL3 production by splenic B cells in phosphate-buffered saline (PBS) and HOCl mice at day 21 and day 42. (A) CCL3 mRNA levels in splenic B cells after collection and sorting, normalized to GUSB and expressed as fold changes to PBS day 21 for day-21 groups (top row), and to PBS day 42 for day-42 groups (bottom row) (n = 4–6 per group). **(B)** CCL3 supernatant levels after culture of splenic B cells for 48 h with various stimulation conditions [none, lipopolysaccharide (LPS), LPS + anti-CD40 antibody] at day 21 (top row) and day 42 (bottom row), expressed in picograms per milliliter (n = 6–8 per group).

increase always reached statistical significance, except for CCL3 at day 42 with LPS stimulation ($p = 0.18$) (**Figures 9B** and **10B**). IL-6 and CCL3 levels in HOCl B cells did not differ between day 21 and day 42 in both stimulation conditions.

Overall, these results suggested that splenic B cells display pro-inflammatory features in HOCl mice.

B Cell Production of IL-10 and Breg Levels Are Reduced in HOCl Mice

As there is a growing body of evidence implicating B cells in immune response suppression and regulatory processes in autoimmune diseases (25), we next studied the anti-inflammatory properties of B cells in the HOCl model. We first assessed the production of IL-10, a potent anti-inflammatory cytokine, by splenic B cells. When measured *ex vivo*, IL-10 mRNA levels were significantly lower in HOCl B cells at day 21 ($p = 0.01$) but identical at day 42 ($p = 0.82$) (**Figure 11A**). After culture and stimulation by LPS alone or with anti-CD40 antibody, similar results were found: a significant decrease in IL-10 secretion by HOCl B cells at day 21 ($p = 0.002$ with both stimulations) and identical levels at day 42 ($p = 0.51$ with LPS and $p = 0.47$ with LPS + anti-CD40 antibody) (**Figure 11B**). Of note, without immunostimulation, IL-10 production by HOCl B cells was significantly higher than PBS mice but at negligible levels.

Within the B cell compartment, the main source of IL-10 production is Bregs, a recently identified subset endowed with anti-inflammatory properties (25). In mice, Bregs are formally identified as $CD19^+$ $IL\text{-}10^+$ cells ("B10" cells) and mostly contained within the $CD19^+$ $CD5^+$ $CD1d^{hi}$ subset (24). To confirm our previous results, we next measured splenic Breg counts using both phenotypic definitions. Here again, we made similar observations: a significant decrease in B10 cells ($p = 0.004$) and in $CD5^+$ $CD1d^{hi}$ B cells ($p = 0.006$) in HOCl mice at day 21; but no difference at day 42 ($p = 0.39$ and $p = 0.24$, respectively) (**Figures 11C,D** and **12**).

Overall, these results suggested that B cell anti-inflammatory properties are impaired at the early inflammatory stage of the experimental disease.

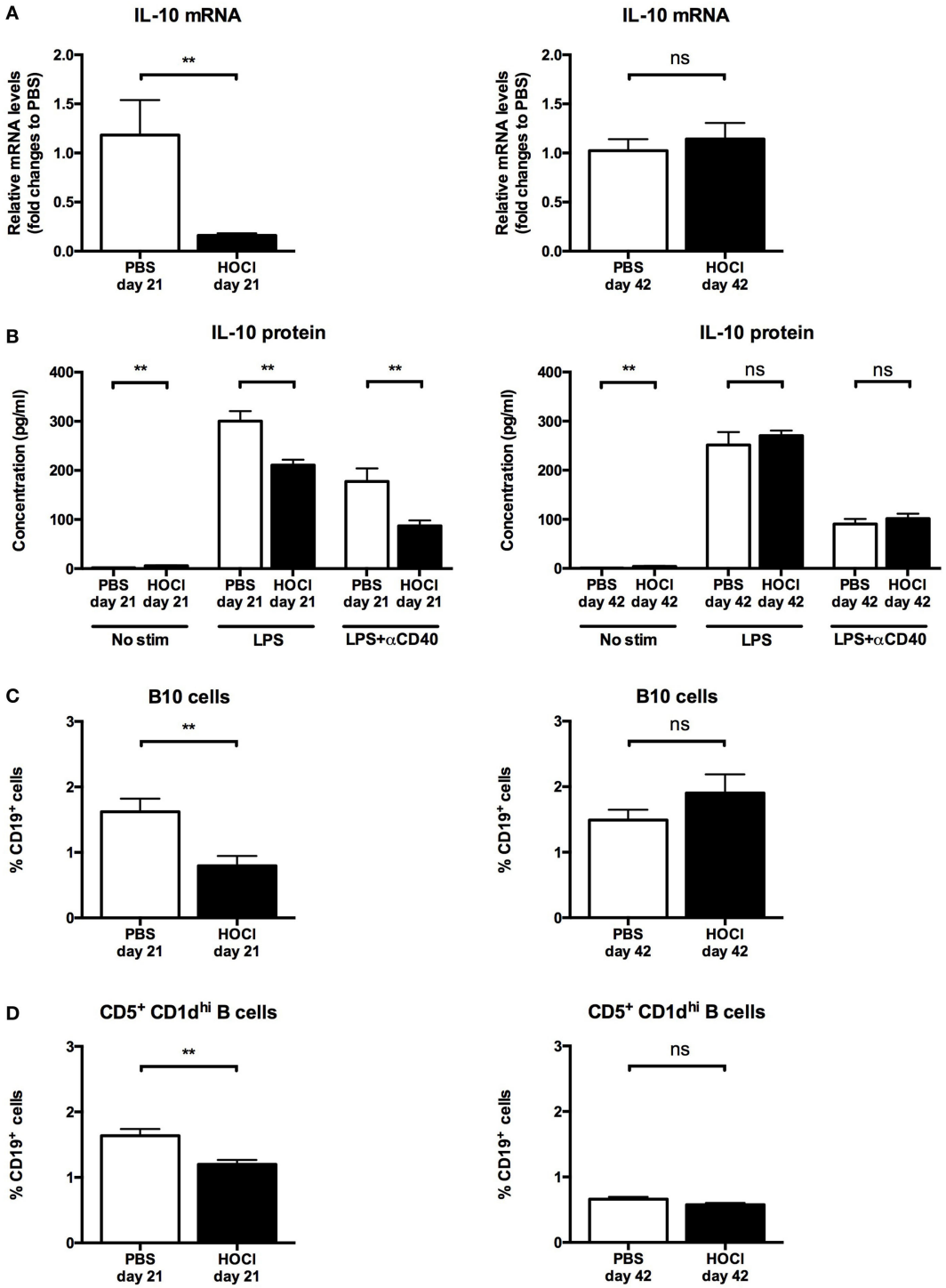

FIGURE 11 | Interleukin (IL)-10 production and regulatory B cell levels in phosphate-buffered saline (PBS) and HOCl mice at day 21 and day 42. **(A)** IL-10 mRNA levels in splenic B cells after collection and sorting, normalized to GUSB and expressed as fold changes to PBS day 21 for day-21 groups (left column), and to PBS day 42 for day-42 groups (right column) (n = 4–6 per group). **(B)** IL-10 supernatant levels after culture of splenic B cells for 48 h with various stimulation conditions [none, lipopolysaccharide (LPS), LPS + anti-CD40 antibody] at day 21 (left column) and day 42 (right column), expressed in picograms per milliliter (n = 6–8 per group). **(C)** Proportion of B10 cells identified by intracellular IL-10 detection at day 21 (left column) and day 42 (right column), expressed as percentages of $CD19^+$ cells (n = 10 per group). **(D)** Proportion of $CD5^+$ $CD1d^{hi}$ B cells identified by conventional membrane staining at day 21 (left column) and day 42 (right column), expressed as percentages of $CD19^+$ cells (n = 7–8 per group).

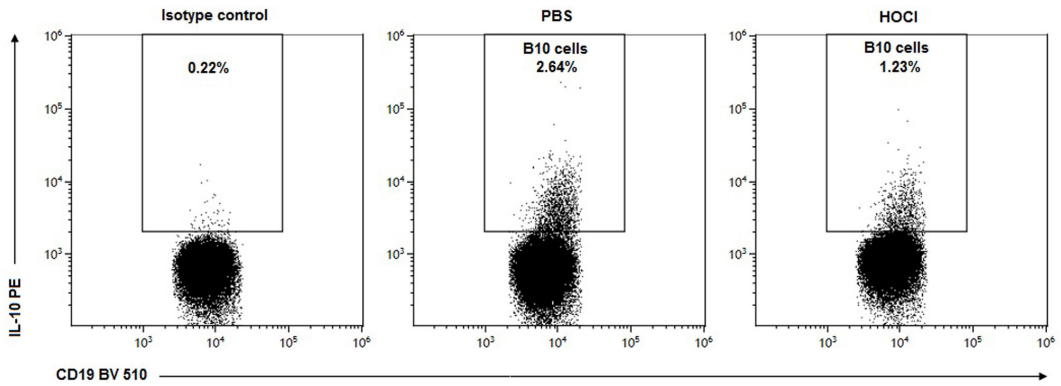

FIGURE 12 | Representative dot-plots of B10 cells in phosphate-buffered saline (PBS) and HOCl mice at day 21. Representative CD19/interleukin (IL)-10 dot-plots gated on B cells from PBS (middle column) and HOCl (left column) mice at day 21, showing a decreased proportion of B10 cells in the HOCl mouse.

Splenic B Cells Display Pro-Fibrotic Properties in HOCl Mice

As B cells have been shown to contribute to fibrogenesis in patients with SSc (16), we then wondered if similar findings could be made in our experimental model. We measured mRNA levels of TGF-β, a major pro-fibrotic cytokine, in HOCl and PBS splenic B cells at both time points. TGF-β production by HOCl B cells was found decreased at day 21 ($p = 0.03$) but increased at day 42 ($p = 0.02$) when compared to the control group (**Figure 13A**).

Finally, we next studied if B cells could directly induce a pro-fibrotic phenotype in fibroblasts. We found that fibroblasts cocultured with HOCl B cells produced higher levels of α-SMA ($p = 0.007$), collagen ($p = 0.0008$), and fibronectin ($p = 0.009$) than when cultured alone (**Figures 13B–D**). Coculture with HOCl B cells also triggered fibroblast proliferation as we observed a significant increase in PCNA ($p = 0.006$) (**Figure 13E**). These mRNA levels tended to be higher in fibroblasts cocultured with HOCl B cells than with PBS B cells ($p = 0.08$ for α-SMA, $p = 0.09$ for collagen, $p = 0.15$ for fibronectin, $p = 0.06$ for PCNA) (**Figures 13B–E**). Further studies are warranted to confirm these results.

Overall, these observations suggest that B cells also display pro-fibrotic properties in HOCl mice.

DISCUSSION

To our knowledge, this is the first study to focus on a thorough examination of B cells in an animal model of SSc. Our results can be summarized as follows: (1) HOCl mice exhibit alterations in B cell subset distribution (early expansion of transitional B cells; late expansion of the mature naive subset; and decrease in plasmablasts and memory B cells); (2) HOCl splenic B cells display enhanced pro-inflammatory features (increased production of IL-6 and CCL3); (3) HOCl splenic B cell anti-inflammatory properties are impaired at the early inflammatory stage of the experimental disease (decreased IL-10 production and Breg counts); (4) HOCl splenic B cells may contribute to fibrogenesis by producing TGF-β and inducing a pro-fibrotic phenotype in fibroblasts; and (5) these anomalies are dynamic and vary over the course of the experimental disease.

Perturbations in B cell homeostasis are well documented in human SSc (8–12) but have been rarely assessed in animal models. Aside from the present study, splenic B cell counts and subset distribution have only been examined in tight-skin (Tsk) mice, where they were found similar to controls (26). This makes our work the first to identify alterations in B cell subset homeostasis in an experimental model of SSc. More importantly, the anomalies found in HOCl mice are close to those reported in human SSc. Just as splenic B cell counts are decreased during the early active stage of the experimental protocol, circulating B cell lymphopenia is associated with disease activity and severity in SSc patients (27, 28). Characteristic B cell subset modifications in human SSc consist in an expansion of mature naive B cells and a depletion in memory B cells and plasmablasts (8–12), all of which were observed in HOCl mice in our study. Overall, it appears that the HOCl model correctly approximates the perturbations in B cell homeostasis observed in human SSc. These splenic anomalies could also bear a pathophysiological relevance, as they are associated with a B cell infiltration in the skin at the late stage.

B cell functional anomalies, and especially abnormal cytokine production, have been reported in SSc patients and experimental models (9–12, 14, 16, 26, 29–31). In both contexts, B cells display enhanced pro-inflammatory and pro-fibrotic properties, as well as impaired immune suppression capabilities, which pleads for a significant role in the pathogenesis of the disease and makes them a relevant therapeutic target. HOCl splenic B cells were found to produce higher levels of IL-6 than PBS mice. This confirms results from previous works that also documented an increased B cell secretion of IL-6 in this model (32), in the Tsk and bleomycin-induced SSc models (26, 29–31) and in human SSc (14). B cell overproduction of IL-6 is a significant feature of SSc pathogenesis, since treatment by rituximab induces a decrease in both IL-6 serum levels and skin fibrosis in SSc patients (13). Our study confirms that the HOCl model replicates this important characteristic of SSc B cells. Besides IL-6, we observe in our study a B cell overproduction of CCL3, a chemokine that promotes macrophage

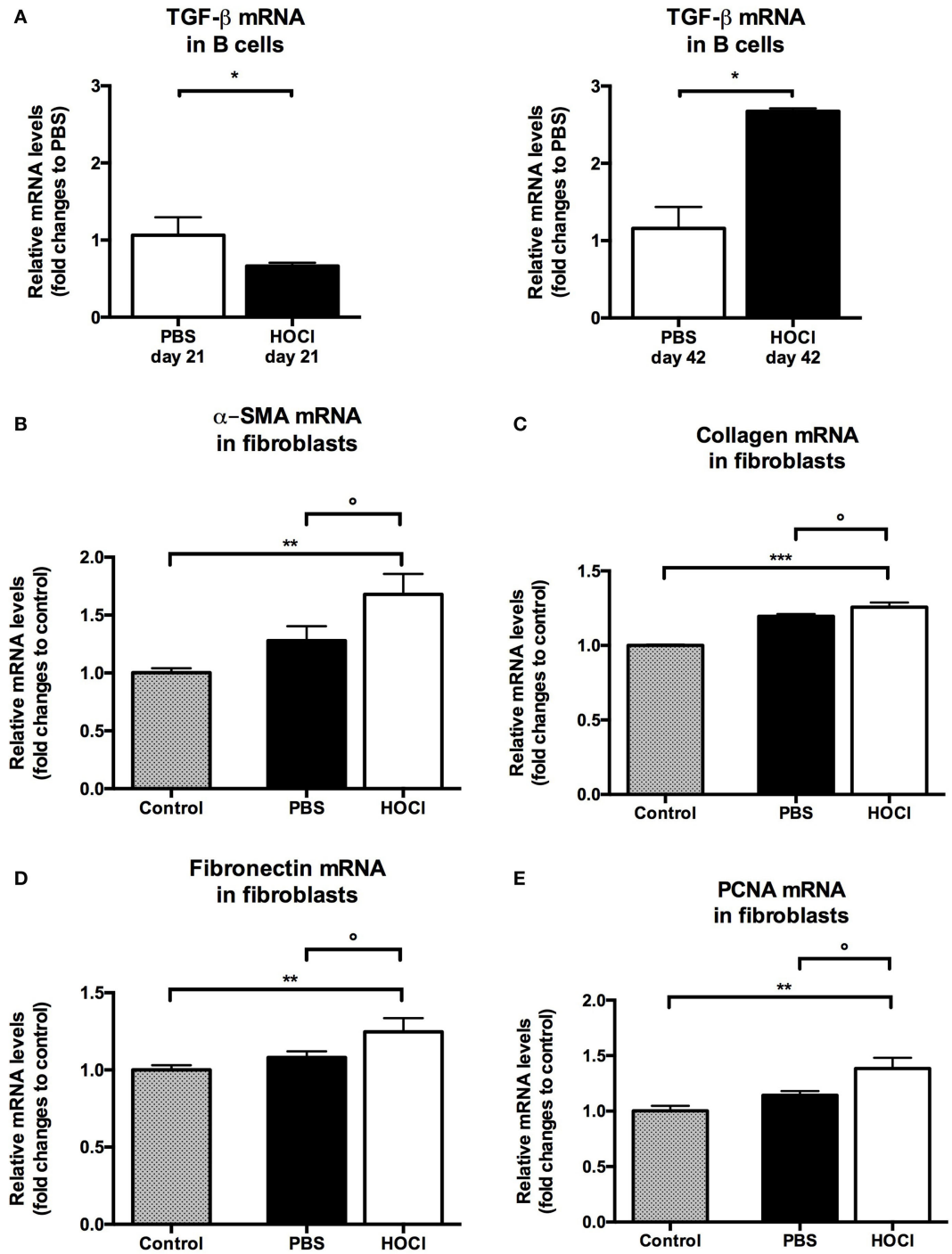

FIGURE 13 | Evaluation of pro-fibrotic properties of splenic B cells in phosphate-buffered saline (PBS) and HOCl mice at day 21 and day 42. (A) Transforming growth factor (TGF)-β mRNA levels in splenic B cells after collection and sorting, normalized to GUSB and expressed as fold changes to PBS day 21 for day-21 groups (left column), and to PBS day 42 for day-42 groups (right column) (n = 4–6 per group). **(B–E)** mRNA levels of markers of fibrosis [α-smooth muscle actin (α-SMA) **(B)**, collagen **(C)**, and fibronectin **(D)**] and proliferation [proliferating cell nuclear antigen (PCNA) **(E)**] in 3T3 fibroblasts cultured alone (control; gray bars), with day-42 PBS B cells (white bars) or with day-42 HOCl B cells (black bars). Results normalized to GAPDH and expressed as fold changes to control (n = 5–8 per group).

migration within inflammatory sites, which has never been described either in SSc models or patients. Interestingly, CCL3 levels are increased in the serum and bronchoalveolar fluid of SSc patients and associated with alveolitis and interstitial lung disease (33–35). As activated CD11b$^+$ macrophages are present in the skin of HOCl mice (36), one could hypothesize that production

of CCL3 by B cells may participate to their recruitment and activation in lesioned sites. Interestingly, B cell overproduction of IL-6 and CCL3 is documented not only at the early inflammatory stage, but also at the late fibrotic stage of the experimental disease. As sustained inflammation ultimately leads to fibrogenesis, this could indicate a dual role of these cytokines over time (initially pro-inflammatory and eventually pro-fibrotic).

A crucial result of our work is the documentation of impaired anti-inflammatory properties in HOCl B cells at the early stage of the protocol. Using multiple methods, we found a decrease in B cell production of IL-10 and a reduction in Breg counts in HOCl spleens. Similar observations were made in human SSc (9–11), which makes it yet another feature of SSc B cells adequately reproduced in this model. Interestingly, circulating Breg counts are inversely correlated with C-reactive protein serum levels, suggesting that, just like in HOCl mice, reduction in Breg counts occurs during the inflammatory stage of the disease (11). Bregs are currently the subject of intense research, as their therapeutic administration in several animal models of autoimmune diseases yielded promising results (25). Their potential as a treatment option in SSc remains, however, to be explored.

Aside from their role in inflammation, several studies suggested that B cells also participate in fibrogenesis during SSc. In this work, we found an increased B cell production of TGF-β at the late stage, confirming previous results in this model (32) and in others (30, 31). In SSc patients, B cells are able to induce production of extracellular matrix components by dermal fibroblasts (16). Preliminary data presented in this work tend to suggest that a similar phenomenon occurs in HOCl mice, but further studies are warranted to confirm this observation. Interestingly, we also observed a decreased TGF-β production by B cells at the early stage. Aside from its potent pro-fibrotic effect, TGF-β is also involved in immune response regulation (37). This result could suggest pleiotropic effects for TGF-β in this model, depending on the stage of the experimental disease.

Overall, our results suggest that B cells could participate in the early inflammatory events of the experimental protocol through an overproduction of pro-inflammatory cytokines (IL-6 and CCL3) and an impairment of their anti-inflammatory capabilities (decreased production of IL-10 and TGF-β, reduced levels of Bregs); and in the late fibrotic events through a cytokine overproduction (TGF-β and IL-6) which may induce a pro-fibrotic phenotype in fibroblasts. These functional anomalies are close to those encountered in human SSc.

Our work has some limitations. Most of our results are descriptive in nature, which does not allow for a definitive assessment of their relevance in the pathogenesis of the experimental disease. Further studies, either functional and/or mechanistical in design (such as complete B cell or specific subset depletions), are warranted to draw definitive conclusions.

In conclusion, this work reports, for the first time in an SSc model, the existence of anomalies in B cell homeostasis and functional properties that approximate those displayed by SSc patients. Furthermore, it suggests that these anomalies vary over the course of the disease, which has never been considered before and may contribute to the inflammatory and fibrotic events observed in SSc. This makes the HOCl mouse a relevant experimental model for the study of B cells, and especially B cell-targeted therapies, in SSc.

AUTHOR CONTRIBUTIONS

The authors confirm that all individuals listed as authors met all the required criteria for authorship (substantial contributions to the conception or design of the work; or the acquisition, analysis, or interpretation of data for the work; drafting the work or revising it critically for important intellectual content; final approval of the version to be published; and agreement to be accountable for all aspects of the work in ensuring that questions related to the accuracy or integrity of any part of the work are appropriately investigated and resolved).

ACKNOWLEDGMENTS

The authors wish to thank Sandrine Poizot (Institut d'Immunologie, Centre de Biologie-Pathologie-Génétique, CHRU Lille, France), Caroline Thuillier, Sébastien d'Aix (Plateau Commun de Biologie Moléculaire, Centre de Biologie-Pathologie-Génétique, CHRU Lille, France), Caroline Dubucquoy (Intestinal Biotech Development, Lille, France), Carole Nicco, Florence Morin, Christiane Chéreau (Université Paris Descartes, EA 1833, Hôpital Cochin, Paris, France), Alexandra Maria, Philippe Guilpain (Université de Montpellier, U1183 INSERM, Hôpital Saint-Eloi, Montpellier, France), Christelle Faveew (Université de Lille, Unité 547, Institut Pasteur, Lille, France), Simon Le Gallou and Sandra Weller (Université Paris Descartes, U1151 INSERM, Paris, France) for their valuable contribution to this work. The authors would also like to thank the DigestScience Foundation for its support.

FUNDING

This work was supported by grants from OctaPharma, Roche and the Association des Sclérodermiques de France (ASF).

SUPPLEMENTARY MATERIAL

The Supplementary Material for this article can be found online at http://journal.frontiersin.org/article/10.3389/fimmu.2017.00053/full#supplementary-material.

REFERENCES

1. Hachulla E, Launay D. Diagnosis and classification of systemic sclerosis. *Clin Rev Allergy Immunol* (2011) 40:78–83. doi:10.1007/s12016-010-8198-y
2. Lefèvre G, Dauchet L, Hachulla E, Montani D, Sobanski V, Lambert M, et al. Survival and prognostic factors in systemic sclerosis-associated pulmonary hypertension: a systematic review and meta-analysis: survival and prognosis in SSc-associated pulmonary hypertension. *Arthritis Rheum* (2013) 65:2412–23. doi:10.1002/art.38029
3. Launay D, Sitbon O, Hachulla E, Mouthon L, Gressin V, Rottat L, et al. Survival in systemic sclerosis-associated pulmonary arterial hypertension in the modern management era. *Ann Rheum Dis* (2013) 72:1940–6. doi:10.1136/annrheumdis-2012-202489

4. Launay D, Humbert M, Berezne A, Cottin V, Allanore Y, Couderc L-J, et al. Clinical characteristics and survival in systemic sclerosis-related pulmonary hypertension associated with interstitial lung disease. *Chest* (2011) 140:1016–24. doi:10.1378/chest.10-2473
5. Morell-Dubois S, Condette-Wojtasik G, Clerson P, Berezné A, Launay D, Lambert M, et al. [Complaints, needs of patients with systemic sclerosis: a better understanding for a better care]. *Rev Médecine Interne* (2011) 32:537–43. doi:10.1016/j.revmed.2011.02.004
6. Servettaz A, Agard C, Tamby MC, Guilpain P, Guillevin L, Mouthon L. Physiopathologie de la sclérodermie systémique: état des lieux sur une affection aux multiples facettes. *Presse Médicale* (2006) 35:1903–15. doi:10.1016/S0755-4982(06)74924-7
7. Sanges S, Guerrier T, Launay D, Lefèvre G, Labalette M, Forestier A, et al. Role of B cells in the pathogenesis of systemic sclerosis. *Rev Médecine Interne* (2016). doi:10.1016/j.revmed.2016.02.016
8. Sato S, Fujimoto M, Hasegawa M, Takehara K. Altered blood B lymphocyte homeostasis in systemic sclerosis: expanded naive B cells and diminished but activated memory B cells. *Arthritis Rheum* (2004) 50:1918–27. doi:10.1002/art.20274
9. Soto L, Ferrier A, Aravena O, Fonseca E, Berendsen J, Biere A, et al. Systemic sclerosis patients present alterations in the expression of molecules involved in B-cell regulation. *Front Immunol* (2015) 6:496. doi:10.3389/fimmu.2015.00496
10. Mavropoulos A, Simopoulou T, Varna A, Liaskos C, Katsiari CG, Bogdanos DP, et al. Breg cells are numerically decreased and functionally impaired in patients with systemic sclerosis. *Arthritis Rheumatol* (2016) 68:494–504. doi:10.1002/art.39437
11. Matsushita T, Hamaguchi Y, Hasegawa M, Takehara K, Fujimoto M. Decreased levels of regulatory B cells in patients with systemic sclerosis: association with autoantibody production and disease activity. *Rheumatology (Oxford)* (2016) 55:263–7. doi:10.1093/rheumatology/kev331
12. Simon D, Balogh P, Bognár A, Kellermayer Z, Engelmann P, Németh P, et al. Reduced non-switched memory B cell subsets cause imbalance in B cell repertoire in systemic sclerosis. *Clin Exp Rheumatol* (2016) 34(Suppl 100):30–6.
13. Bosello S, De Santis M, Lama G, Spanò C, Angelucci C, Tolusso B, et al. B cell depletion in diffuse progressive systemic sclerosis: safety, skin score modification and IL-6 modulation in an up to thirty-six months follow-up open-label trial. *Arthritis Res Ther* (2010) 12:R54. doi:10.1186/ar2965
14. Matsushita T, Hasegawa M, Yanaba K, Kodera M, Takehara K, Sato S. Elevated serum BAFF levels in patients with systemic sclerosis: enhanced BAFF signaling in systemic sclerosis B lymphocytes. *Arthritis Rheum* (2006) 54:192–201. doi:10.1002/art.21526
15. Giuggioli D, Lumetti F, Colaci M, Fallahi P, Antonelli A, Ferri C. Rituximab in the treatment of patients with systemic sclerosis. Our experience and review of the literature. *Autoimmun Rev* (2015) 14:1072–8. doi:10.1016/j.autrev.2015.07.008
16. François A, Chatelus E, Wachsmann D, Sibilia J, Bahram S, Alsaleh G, et al. B lymphocytes and B-cell activating factor promote collagen and profibrotic markers expression by dermal fibroblasts in systemic sclerosis. *Arthritis Res Ther* (2013) 15:R168. doi:10.1186/ar4352
17. Lafyatis R, Kissin E, York M, Farina G, Viger K, Fritzler MJ, et al. B cell depletion with rituximab in patients with diffuse cutaneous systemic sclerosis. *Arthritis Rheum* (2009) 60:578–83. doi:10.1002/art.24249
18. Smith V, Van Praet JT, Vandooren B, Van der Cruyssen B, Naeyaert J-M, Decuman S, et al. Rituximab in diffuse cutaneous systemic sclerosis: an open-label clinical and histopathological study. *Ann Rheum Dis* (2010) 69:193–7. doi:10.1136/ard.2008.095463
19. Le Huu D, Matsushita T, Jin G, Hamaguchi Y, Hasegawa M, Takehara K, et al. Donor-derived regulatory B cells are important for suppression of murine sclerodermatous chronic graft-versus-host disease. *Blood* (2013) 121:3274–83. doi:10.1182/blood-2012-11-465658
20. Hasegawa M, Hamaguchi Y, Yanaba K, Bouaziz J-D, Uchida J, Fujimoto M, et al. B-lymphocyte depletion reduces skin fibrosis and autoimmunity in the tight-skin mouse model for systemic sclerosis. *Am J Pathol* (2006) 169:954–66. doi:10.2353/ajpath.2006.060205
21. Servettaz A, Goulvestre C, Kavian N, Nicco C, Guilpain P, Chéreau C, et al. Selective oxidation of DNA topoisomerase 1 induces systemic sclerosis in the mouse. *J Immunol* (2009) 182:5855–64. doi:10.4049/jimmunol.0803705
22. Rasband WS. *ImageJ*. (1997). Available from: https://imagej.nih.gov/ij/
23. Ruifrok AC, Johnston DA. Quantification of histochemical staining by color deconvolution. *Anal Quant Cytol Histol* (2001) 23:291–9.
24. Matsushita T, Tedder TF. Identifying regulatory B cells (B10 cells) that produce IL-10 in mice. *Methods Mol Biol* (2011) 677:99–111. doi:10.1007/978-1-60761-869-0_7
25. Yang M, Rui K, Wang S, Lu L. Regulatory B cells in autoimmune diseases. *Cell Mol Immunol* (2013) 10:122–32. doi:10.1038/cmi.2012.60
26. Matsushita T, Fujimoto M, Hasegawa M, Matsushita Y, Komura K, Ogawa F, et al. BAFF antagonist attenuates the development of skin fibrosis in tight-skin mice. *J Invest Dermatol* (2007) 127:2772–80. doi:10.1038/sj.jid.5700919
27. Gambichler T, Tigges C, Burkert B, Höxtermann S, Altmeyer P, Kreuter A. Absolute count of T and B lymphocyte subsets is decreased in systemic sclerosis. *Eur J Med Res* (2010) 15:44–6. doi:10.1186/2047-783X-15-1-44
28. López-Cacho JM, Gallardo S, Posada M, Aguerri M, Calzada D, Mayayo T, et al. Association of immunological cell profiles with specific clinical phenotypes of scleroderma disease. *Biomed Res Int* (2014) 2014:148293. doi:10.1155/2014/148293
29. Saito E, Fujimoto M, Hasegawa M, Komura K, Hamaguchi Y, Kaburagi Y, et al. CD19-dependent B lymphocyte signaling thresholds influence skin fibrosis and autoimmunity in the tight-skin mouse. *J Clin Invest* (2002) 109:1453–62. doi:10.1172/JCI15078
30. Takahashi T, Asano Y, Ichimura Y, Toyama T, Taniguchi T, Noda S, et al. Amelioration of tissue fibrosis by toll-like receptor 4 knockout in murine models of systemic sclerosis. *Arthritis Rheumatol* (2015) 67:254–65. doi:10.1002/art.38901
31. Yoshizaki A, Iwata Y, Komura K, Ogawa F, Hara T, Muroi E, et al. CD19 regulates skin and lung fibrosis via toll-like receptor signaling in a model of bleomycin-induced scleroderma. *Am J Pathol* (2008) 172:1650–63. doi:10.2353/ajpath.2008.071049
32. Kavian N, Servettaz A, Marut W, Nicco C, Chéreau C, Weill B, et al. Sunitinib inhibits the phosphorylation of platelet-derived growth factor receptor β in the skin of mice with scleroderma-like features and prevents the development of the disease. *Arthritis Rheum* (2012) 64:1990–2000. doi:10.1002/art.34354
33. Bolster MB, Ludwicka A, Sutherland SE, Strange C, Silver RM. Cytokine concentrations in bronchoalveolar lavage fluid of patients with systemic sclerosis. *Arthritis Rheum* (1997) 40:743–51. doi:10.1002/art.1780400422
34. Hasegawa M, Sato S, Takehara K. Augmented production of chemokines (monocyte chemotactic protein-1 (MCP-1), macrophage inflammatory protein-1alpha (MIP-1alpha) and MIP-1beta) in patients with systemic sclerosis: MCP-1 and MIP-1alpha may be involved in the development of pulmonary fibrosis. *Clin Exp Immunol* (1999) 117:159–65.
35. Bandinelli F, Del Rosso A, Gabrielli A, Giacomelli R, Bartoli F, Guiducci S, et al. CCL2, CCL3 and CCL5 chemokines in systemic sclerosis: the correlation with SSc clinical features and the effect of prostaglandin E1 treatment. *Clin Exp Rheumatol* (2012) 30(2 Suppl 71):S44–9.
36. Raker VK, Yong Ook K, Haub J, Lorenz N, Schmidt T, Stegemann A, et al. Myeloid cell populations and fibrogenic parameters in bleomycin- and HOCl-induced fibrosis. *Exp Dermatol* (2016) 25(11):887–94. doi:10.1111/exd.13124
37. Li MO, Wan YY, Sanjabi S, Robertson A-KL, Flavell RA. Transforming growth factor-beta regulation of immune responses. *Annu Rev Immunol* (2006) 24:99–146. doi:10.1146/annurev.immunol.24.021605.090737

Conflict of Interest Statement: The authors declare that the research was conducted in the absence of any commercial or financial relationships that could be construed as a potential conflict of interest.

The reviewer HD and handling Editor declared their shared affiliation, and the handling Editor states that the process nevertheless met the standards of a fair and objective review.

frontiers in Immunology

ORIGINAL RESEARCH
published: 08 February 2017
doi: 10.3389/fimmu.2017.00075

Agonistic Anti-PDGF Receptor Autoantibodies from Patients with Systemic Sclerosis Impact Human Pulmonary Artery Smooth Muscle Cells Function *In Vitro*

*Silvia Svegliati[1†], Donatella Amico[1†], Tatiana Spadoni[1†], Colomba Fischetti[1], Doreen Finke[1], Gianluca Moroncini[1], Chiara Paolini[1], Cecilia Tonnini[1], Antonella Grieco[1], Marina Rovinelli[1], Ada Funaro[2] and Armando Gabrielli[1]**

[1] Clinica Medica, Dipartimento di Scienze Cliniche e Molecolari, Università Politecnica delle Marche, Ancona, Italy, [2] Dipartimento di Scienze Mediche, Università di Torino, Torino, Italy

One of the earliest events in the pathogenesis of systemic sclerosis (SSc) is microvasculature damage with intimal hyperplasia and accumulation of cells expressing PDGF receptor. Stimulatory autoantibodies targeting PDGF receptor have been detected in SSc patients and demonstrated to induce fibrosis *in vivo* and convert *in vitro* normal fibroblasts into SSc-like cells. Since there is no evidence of the role of anti-PDGF receptor autoantibodies in the pathogenesis of SSc vascular lesions, we investigated the biologic effect of agonistic anti-PDGF receptor autoantibodies from SSc patients on human pulmonary artery smooth muscle cells and the signaling pathways involved. The synthetic (proliferation, migration, and type I collagen gene α1 chain expression) and contractile (smooth muscle-myosin heavy chain and smooth muscle-calponin expression) profiles of human pulmonary artery smooth muscle cells were assessed *in vitro* after incubation with SSc anti-PDGF receptors stimulatory autoantibodies. The role of reactive oxygen species, NOX isoforms, and mammalian target of rapamycin (mTOR) was investigated. Human pulmonary artery smooth muscle cells acquired a synthetic phenotype characterized by higher growth rate, migratory activity, gene expression of type I collagen α1 chain, and less expression of markers characteristic of the contractile phenotype such as smooth muscle-myosin heavy chain and smooth muscle-calponin when stimulated with PDGF and autoantibodies against PDGF receptor, but not with normal IgG. This phenotypic profile is mediated by increased generation of reactive oxygen species and expression of NOX4 and mTORC1. Our data indicate that agonistic anti-PDGF receptor autoantibodies may contribute to the pathogenesis of SSc intimal hyperplasia.

Keywords: systemic sclerosis, autoantibodies, vascular smooth muscle cells, platelet-derived growth factor, synthetic phenotype

OPEN ACCESS

Edited by:
Raffaele De Palma, Seconda Università degli Studi di Napoli, Italy

Reviewed by:
Marta Rizzi, University Medical Center Freiburg, Germany
Piergiuseppe De Berardinis, Institute of Protein Biochemistry (CNR), Italy

***Correspondence:**
Armando Gabrielli
a.gabrielli@univpm.it

†These authors have contributed equally to this work.

Specialty section:
This article was submitted to Primary Immunodeficiencies, a section of the journal Frontiers in Immunology

Received: *28 October 2016*
Accepted: *17 January 2017*
Published: *08 February 2017*

Citation:
Svegliati S, Amico D, Spadoni T, Fischetti C, Finke D, Moroncini G, Paolini C, Tonnini C, Grieco A, Rovinelli M, Funaro A and Gabrielli A (2017) Agonistic Anti-PDGF Receptor Autoantibodies from Patients with Systemic Sclerosis Impact Human Pulmonary Artery Smooth Muscle Cells Function In Vitro. Front. Immunol. 8:75. doi: 10.3389/fimmu.2017.00075

INTRODUCTION

Systemic sclerosis (SSc; scleroderma) is a multiorgan disorder characterized by microvasculature damage, circulating autoantibodies, and fibroblast activation leading to fibrosis of the skin and visceral organs (1–3).

Vascular involvement is an early and very likely primary event in the pathogenesis of scleroderma, precedes fibrosis, and is characterized by endothelial cell (EC) injury and dysfunction, altered capillary permeability, increased expression of adhesion molecules, abnormal secretion of vasoactive mediators, and activation of platelets and fibrinolytic pathways (4–7). Microvascular injury and damage lead to vascular remodeling with striking intimal hyperplasia (also called neointima) due to increase in cell number and extracellular matrix and marked luminal narrowing (7, 8). The process culminates in rarefaction of blood vessels on nailfold capillaroscopy of SSc patients with late-stage disease (9). Loss of microvasculature is associated with tissue hypoxia, which induces strong expression of VEGF and its receptors (10–12).

The source of the intimal cells in scleroderma vasculopathy is a matter of debate. Medial smooth muscle cells, pericytes, circulating fibrocytes, ECs, adventitial fibroblasts, and adventitial stem cells have all been held responsible (13). Furthermore, the exact cause of vascular injury in SSc is unknown, and it may include reactive oxygen species (ROS)-mediated damage, viral agents, anti-EC antibodies, ischemia–reperfusion events, cytotoxic T-lymphocytes, and antibody-dependent cellular cytotoxicity [see for review Ref. (14)]. A further mechanisms has been reported by Riemekasten et al. who detected serum autoantibodies against angiotensin II type I receptor and endothelin-1 type 1 receptor, which induced extracellular signal-regulated kinase 1/2 (ERK 1/2) phosphorylation and increased TGF-β gene expression in ECs and were associated with severe disease manifestations (15).

While over the years much attention has been devoted to EC injury in scleroderma, oddly enough no *in vitro* studies focused on smooth muscle cells that are rich in PDGF receptors (PDGFR) (16), a key signaling molecule in the pathogenesis of SSc fibrosis. High levels of PDGF and PDGF receptor β (PDGFR β) have been found in skin lesions from patients with scleroderma (17, 18) and may contribute to the differentiation of perivascular pericytes into vascular smooth muscle cells, fibroblasts, and myofibroblasts (19). The beneficial effects of selective inhibitors of PDGF signaling on dermal fibrosis (20, 21) and lung fibrosis (22) further indicate the importance of PDGF in scleroderma. Finally, the relevance of PDGFR has been further emphasized by the high prevalence of anti-PDGFRα autoantibodies in SSc sera (23, 24).

Anti-PDGFRα autoantibodies play a role in the pathogenesis of scleroderma since they convert *in vitro* normal fibroblasts into SSc-like cells *via* the ROS, RAS, and ERK 1/2 pathway (23–26) and are capable to induce fibrosis *in vivo* (27). No report has, however, described their effect on human smooth muscle cells, and since a better understanding of the molecular mechanisms involved in scleroderma vascular events could help to prevent severe complications such as digital ulcers, pulmonary hypertension, and renal crisis, which are responsible for a substantially reduced survival and impaired quality of life (28–30), we decided to investigate the biological effects of SSc agonistic anti-PDGFR autoantibodies on human pulmonary artery smooth muscle cells (HPASMC) *in vitro*.

MATERIALS AND METHODS

Patients and Biological Samples

Serum samples were obtained from 11 SSc patients (2 were male and 9 were female) with median age of 56 years (range, 43–73 years), and median disease duration (defined as the time from the onset of the first non-Raynaud's phenomenon clinical manifestation) was 7 years (2–21). Diagnosis was made following the ACR/EULAR preliminary criteria for the classification of SSc (31). Five patients had limited cutaneous SSc and six diffuse cutaneous SSc according to LeRoy et al. (32). Six patients were antitopoisomerase I positive; two patients were anticentromere positive, and three were ANA positive but lacked specific SSc autoantibodies. In the whole group, median PAPs detected by echocardiography was 30 mmHg (range, 28.5–36.5 mmHg) (**Table 1**). The study was approved by the local ethic committee. A written informed consent was obtained from all patients. At the time of the investigation, patients who had never been on immunosuppressive therapy had not received any treatment for the previous 6 weeks. Control sera were obtained from 10 age-, sex-, and race-matched normal, non-smoking, healthy volunteers. All subjects provided informed consent and the study protocol was approved by the Institutional Ethics Committee of Università Politecnica delle Marche.

Antibody Purification

Immunoglobulins were purified from serum using gravity flow column packed with protein A/G agarose following manufacturer instruction (Pierce). Concentrations of all samples were calculated based on absorbance at 280 nm. The eluted IgG fractions that contain the highest absorbance were subjected to buffer exchange with PBS using desalting column, a size-exclusion chromatography with an average molecular weight exclusion limit of 5 KDa (Pierce). Purity of IgG preparations was checked by Coomassie blue staining, and PDGF and TGF-β contaminations were ruled out by immunoblotting with biotinylated anti-human PDGF-BB and anti-human TGF-β antibodies (Abcam), respectively, with detection limit of 0.1 ng cytokine/200 μg IgG.

TABLE 1 | Clinical characteristics of systemic sclerosis patients (n = 11).

Male/female	2/9
Mean age, years (range)	56 (43–73)
Mean modified Rodnan skin score (range)	11 (4–30)
Subset lSSc/dSSc	5/6
Median disease duration, years (range)	7 (2–21)
Antitopoisomerase I-positive patients	6
Anticentromere-positive patients	2
ANA-positive patients	3

Human Monoclonal Anti-PDGFRα Autoantibodies

Agonistic (V_HPAM-$V_κ$16F4) and non-agonistic (V_HPAM-$V_κ$13B8) human monoclonal autoantibodies targeting PDGFRα were generated from SSc memory B cells as already described (24).

Cell Cultures

Human pulmonary artery smooth muscle cells (HPASMC) were purchased from Lonza and maintained in Medium 231 supplemented with smooth muscle growth medium (SMGM) and 100 U/ml penicillin/streptomycin (all from Life Technologies). Cells between passages 3 and 9 were used in all experiments performed after 24 h of starvation (0.1% SMGM).

Total IgGs were isolated from each patient and control and were singly tested in triplicate. The same conditions were applied to human monoclonal antibodies. Each experiment was performed at least three times. Means of all experiments are shown.

ROS Detection

Relative changes in intracellular ROS were monitored using the fluorescent probe 2′, 7′-dichlorfluorescein-diacetate (DCFH-DA; Life Technologies). Cells were plated at 2.5×10^5/ml and then incubated with scleroderma (SSc IgG) or normal subjects IgG (N IgG) (200 μg/ml), PDGF (15 ng/ml), or human monoclonal anti-PDGFRα autoantibodies (10 μg/ml) for 15 min and then stained with 10 μM DCFH-DA (Life Technologies) for 10 min at 37°C. Fluorescence was read using a plate reader fluorimeter (Victor 2, Perkin Elmer).

For confocal microscopy experiments, cells were seeded on coverslides and treated as described earlier. Cells were loaded with 10 μM DCFH-DA for 30 min, washed with PBS, and then visualized on a confocal microscope Eclipse C1 (Nikon). Data were analyzed by ImageJ software.

The intracellular content of ROS was also measured at a single-cell level by flow cytometry (FACS, Becton Dickinson). Briefly, cells were detached by trypsin, washed with PBS, and incubated with 5 μM DCFH-DA for 20 min at 37°C. Cells were then washed and resuspended in 1 ml PBS. For each sample, 10,000 events were collected, and intracellular ROS formation was detected as a result of oxidation of DCFH-DA at a wavelength of 520 nm. Data analysis was carried out using the WinMDI software.

Where indicated, the inhibitor of flavoprotein-dependent oxidases diphenyleneiodonium (DPI; 10 μM, Calbiochem), a general ROS inhibitor *N*-acetyl-cysteine (NAC; 10 mM, Sigma), and the PDGFR chemical inhibitor AG1296 (2 μM, Calbiochem) were added 1 h before stimulation.

Proliferation Assay

Cell proliferation was determined by 5-bromo-2′-deoxyuridine (BrdU) incorporation assay (Roche). Briefly, HPASMC were seeded in 96-well pates at a density of 2.5×10^5 cells/ml and then treated with SSc IgG or N IgG (200 μg/ml), PDGF (15 ng/ml), or human monoclonal anti-PDGFRα autoantibodies (10 μg/ml) for 48 h. Cells were pulsed for 6 h with BrdU, and plates were analyzed in a plate reader at 450 nm (Victor 2, PerkinElmer).

Migration Assay

Migration was studied by the wound scratch assay (33). Briefly, the cell monolayer was scraped by a straight line to create a "scratch" with a pipette tip. Cells were incubated for 24 h with SSc IgG, N IgG (200 μg/ml), PDGF (15 ng/ml), or human monoclonal anti-PDGFRα autoantibodies (10 μg/ml) in the presence or absence of inhibitors. Mitomycin was added to inhibit cell proliferation. Unstimulated cells were used as negative controls. The percentage of cells repopulating the scratch wound was assessed after 24 h.

Reverse Transcriptase Polymerase Chain Reaction

Total RNA was isolated from HPASMC with Pure Link RNA Minikit (Life Technologies) and reverse transcribed using IScript cDNA Synthesis Kit (Bio-Rad Laboratories) according to the instructions of the manufacturer. Gene expression was quantified by SYBR Green real-time PCR in a iCycler iQ™ real-time PCR Detection System (Bio-Rad). Specific primer pairs for each gene were designed with the Universal ProbeLibrary Assay Design Centre by Roche Applied Science and were as follows: NOX1 5′-CTGTTTGTGGATGCCTTCCT-3′ (forward), 5′-TGTGGAAGGTGAGG-TTGTGA-3′ (reverse); NOX2 5′-TCACTTCCTCCACCAAAACC-3′ (forward), 5′GGGATTGGGCATTCCTTTAT-3′ (reverse); NOX4 5′-CTTCCGTTGGTTTGCAGATT-3′ (forward), 5′-GAATTGGGCCACAACAGA-3′ (reverse); type I collagen α1 chain (COL1A1) 5′-AGGGCCAAGACGAAGACATC-3′ (forward), 5′-AGATCACGTCATCGCACAACA-3′ (reverse); smooth muscle-myosin heavy chain (SM-MHC) 5′-CAGGCGTTCCGCCAACGCTA-3′ (forward), 5′-TCCCGTCCATGAAGCCTTTGG-3′ (reverse); smooth muscle-calponin (sm-calponin) 5′-TTTTGAGGCCAACGACCTGT-3′ (forward), 5′-TCCTTTCGTCTTCGCCATG-3′ (reverse); and GAPDH 5′-TGCACCACCAACTGCTTAGC-3′ (forward), 5′-TGGGATTTCCATTGATGA-CAAGC-3′ (reverse).

GAPDH was used to test the quality of cDNA and as a house keeping gene in real-time PCR. The threshold cycle (Ct) was used to detect the increase in the signal associated with an exponential growth of PCR product during the log-linear phase. The relative expression was calculated using the following formula: $2^{-\Delta\Delta}$Ct. The ΔCt validation experiments showed similar amplification efficiency for all templates used (difference between linear slopes for all templates less than 0.1).

Immunoblotting

Cells were lysed in RIPA buffer [1× PBS, 1% non-idet P-40, 0.5% sodium deoxycholate, 0.1% sodium dodecyl sulfate (SDS), 2 mM sodium orthovanadate] supplemented with a cocktail of protease inhibitors (Sigma). Proteins were separated on 4–12% gradient SDS–polyacrylamide gels, transferred onto nitrocellulose membranes, and immunoblotted with antibodies against NOX4, β-actin (Santa Cruz Biotechnology), and phospho mTOR and mTOR (Cell Signalling). Signals were detected by chemiluminescence (Pierce). Densitometric analysis was performed with Quantity One software (BioRad). Where indicated rapamycin (10 nM) was added 48 h before stimulation.

NOX4 Intracellular Expression

For intracellular staining assay, HPASMC were treated with SSc IgG or N IgG (200 μg/ml) and PDGF (15 ng/ml) for 24 h and then permeabilized with Cyto Fix/Perm (Becton Dickinson). Cells were detached by trypsin, washed with PBS, and incubated with antibody against NOX4 (AbCam) for 24 h at 37°C. Cells were then washed and incubated with FITC-conjugated secondary antibody and resuspended in 1 ml PBS. For each sample, 10,000 events were collected. Data analysis was carried out using the WinMDI software.

Small Interfering RNA (siRNA) Experiments

Nox4 was silenced using siRNA oligoribonucleotides (Qiagen) using Lipofectamine™ 2000 reagent (Life Technologies) following the manufacturer's instructions. Briefly, 10 μM NOX4 siRNA or scrambled oligos and Lipofectamine 2000 were mixed in serum-free Medium 231 without antibiotics and then added to the cells. Medium was changed after 4 h. Gene silencing and ROS production were monitored 72 h after transfection.

Statistical Analysis

Statistical analysis was performed using GraphPad Prism version 4.0 by two-tailed Student's *t*-test. *P* values less than 0.05 were considered significant.

RESULTS

Agonistic Anti-PDGFRα Receptor Autoantibodies from SSc Patients Induce Increased ROS Generation in HPASMC

Since the pathogenesis of scleroderma is characterized by an abnormal generation of ROS [for review, see Ref. (34)] and several lines of evidence implicate oxidative stress in the pathogenesis of PAH (35), we exploited our previous demonstration that agonistic anti-PDGFRα autoantibodies isolated from SSc sera induce an abnormal generation of ROS in normal fibroblasts *via* NOX (23, 24, 36). Hence, HPASMC were stimulated *in vitro* with IgG isolated from serum of distinct scleroderma patients (SSc IgG; $n = 11$) or distinct normal controls (N IgG; $n = 10$) (200 μg/ml, 15 min) and then incubated with the peroxide-sensitive fluorophore DCHF-DA. Confocal microscopy (**Figure 1A**), plate reader fluorimeter (**Figure 1B**), or FACS analysis (**Figure 1C**) showed that the levels of ROS, induced by PDGF and SSc IgG, were higher than the levels obtained in unstimulated cells ($p < 0.05$) and were inhibited by preincubating cells with PDGFR tyrosine kinase inhibitor AG 1296 (2 μM, 1 h) ($p < 0.05$), indicating that ROS production occurred through PDGFRα. The amount of ROS generated by N IgG was not significantly different from that obtained in unstimulated cells (**Figures 1A–C**).

Systemic sclerosis IgGs contain a multitude of SSc disease-specific and non-specific antibodies, including agonistic autoantibodies against angiotensin II receptor type 1 and the endothelin receptor type A (37). Thus, to demonstrate that the findings reported above are related to stimulatory antibodies targeting PDGFRα, HPASMC were exposed to combinatorial human monoclonal anti-PDGFRα autoantibody V_HPAM-$V_κ$16F4 (10 μg/ml), which binds and stimulate the PDGFRα *in vitro*, and to antibody V_HPAM-$V_κ$13B8 (10 μg/ml), which binds but does not stimulate the receptor *in vitro* (24). **Figure 1D** shows that the agonistic antibody V_HPAM-V_K16F4-stimulated cells produced significantly larger amount of ROS compared to unstimulated cells and V_HPAM-V_K13B8-treated HPASMC. No difference was observed between V_HPAM-V_K13B8-treated and unstimulated cells.

Enhanced Migration and Proliferation of HPASMC by SSc IgG through PDGFR

The *in vitro* scratch assay was used to study the effect of SSc IgG on HPASMC migration (33). Incubation with PDGF (15 ng/ml) or SSc IgG (200 μg/ml) for 24 h enhanced migratory ability of HPASMC compared to cells not stimulated used as controls (50 and 45%, respectively, over control cells, $p < 0.05$) (**Figure 2A**). Migration after N IgG was not statistically different from that of unstimulated HPSMC. The addition of AG1296 (2 μM, 1 h) significantly reduced PDGF- or SSc IgG-induced migration ($p < 0.05$). AG1296-treated cells did not differ from unstimulated or N IgG-treated cells ($p =$ n.s.) (**Figure 2A**).

Agonistic V_HPAM-V_K16F4 (10 μg/ml) significantly stimulated HPSMC migration when compared to unstimulated cells and V_HPAM-V_K13B8-treated cells (60 and 62%, respectively; $p < 0.05$) (**Figure 2A**). No difference was detected between unstimulated and V_HPAM-V_K13B8-treated cells ($p =$ n.s.) (**Figure 2A**).

HPASMC were incubated with PDGF (15 ng/ml) or IgG isolated from serum of distinct scleroderma patients (SSc IgG; $n = 11$) or normal controls (N IgG; $n = 10$) (200 μg/ml) for 48 h, and cell proliferation was determined by monitoring BrdU incorporation for 6 h. SSc IgG and PDGF significantly increased the number of BrdU-positive cells compared to unstimulated cells (1.8- and 1.58-fold, respectively; $p < 0.05$). This effect was reverted by incubating HPSMC with AG1296 (2 μM, 1 h) (**Figure 2B**). No difference was demonstrated between unstimulated cells and N IgG-treated cells. These findings were confirmed when cells were exposed to VH_{PAM}-V_K16F4 and proliferation compared to that obtained with VH_{PAM}-V_K13B8 (**Figure 2B**).

To determine whether SSc IgG contributed to establish a phenotypic modulation of HPASMC cells favoring a transition from contractile to synthetic state, we detected the expression of transcripts of COL1A1 and smooth muscle cell-specific contractile markers, SM-MHC, and SM-calponin mRNA (38). PDGF and SSc IgG increased COL1A1 gene expression (2.8 ± 0.7- and 2.4 ± 0.2-fold, respectively, when compared to unstimulated cells; $p < 0.05$) and decreased SM-MHC expression (0.46 ± 0.2- and 0.5 ± 0.1-fold, respectively, when compared to unstimulated cells; $p < 0.05$) and SM-calponin transcription (0.35 ± 016- and 0.4 ± 0.16-fold, respectively, when compared to unstimulated cells, respectively; $p < 0.05$) consistent with a synthetic phenotype (**Figure 2C**). Cells incubated with N IgG showed the same levels of transcripts of unstimulated cells. Experiments performed in the presence of AG1296 confirmed the role of PDGFR as a primary target of SSc IgG. All these findings are consistent with the

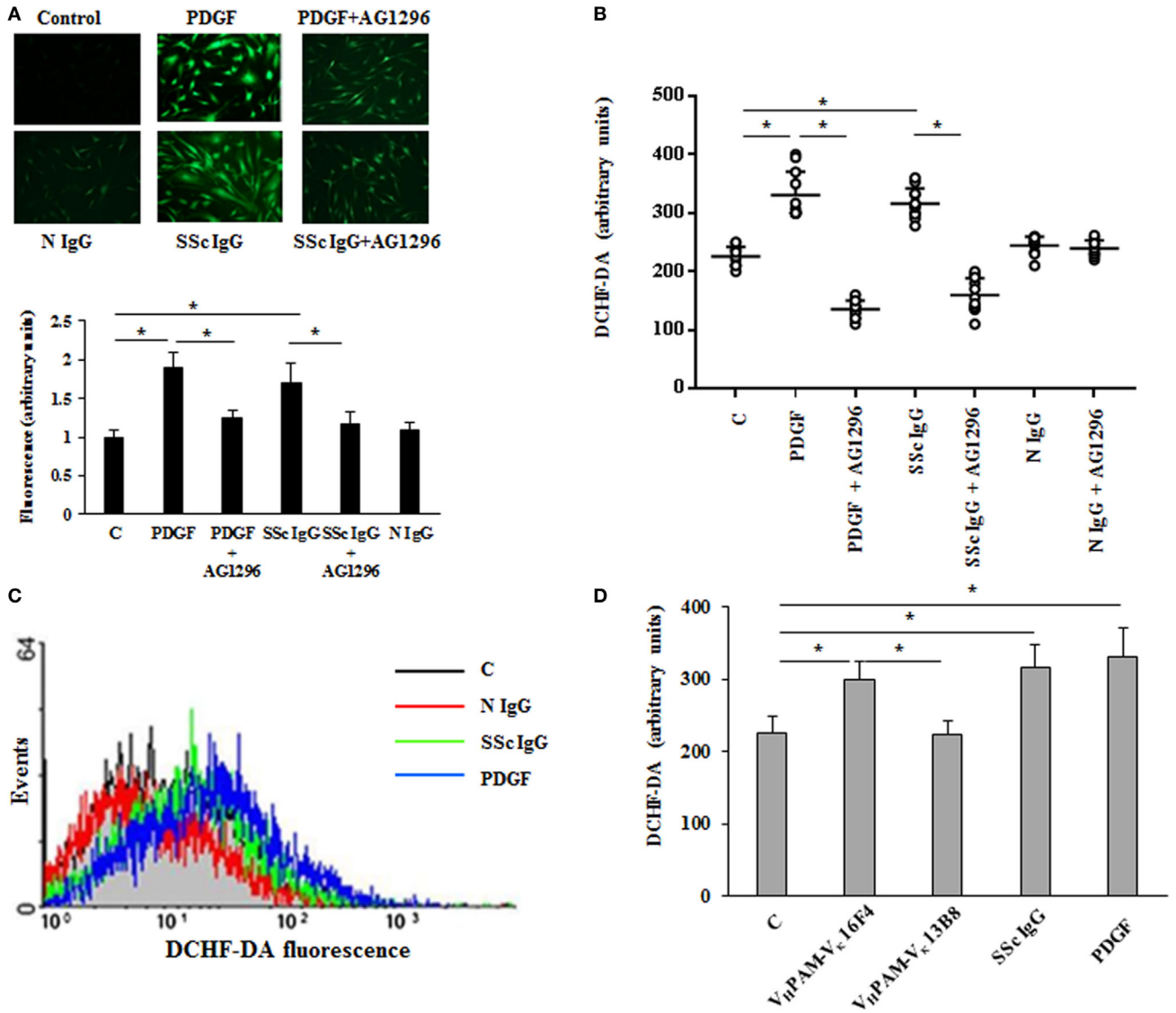

FIGURE 1 | Agonistic anti-PDGF receptor autoantibodies from systemic sclerosis (SSc) patients induce increased reactive oxygen species (ROS) generation in HPASMC. HPASMC were exposed to PDGF (15 ng/ml) or IgG isolated from each SSc patients (SSc IgG; $n = 11$; 200 μg/ml) or normal controls (N IgG; $n = 10$; 200 μg/ml) for 15 min in the presence or absence of AG1296 (2 μM) that was added 1 h before stimulation with Ig. Unstimulated cells were used as a control (C). **(A)** Generation of intracellular ROS was evaluated by fluorescence microscopy using DCHF-DA as a oxidative probe. Representative images of three independent experiments are shown (upper panel). Scale bar = 100 μm. The fluorescence was quantified by ImageJ software (lower panel). The IgG from each subject was tested. Data are presented as mean ± SD of three independent experiments. *$p < 0.05$. **(B)** Intracellular ROS production measured by plate reader fluorimeter. The IgG from each subject was tested in triplicate. Data are presented as mean ± SD of three independent experiments. *$p < 0.05$. **(C)** ROS production of untreated cells (C) (black line), SSc IgG-treated cells (green line), N IgG-treated cells (red line), and PDGF-treated cells (blue line) by FACS analysis. A representative histogram of three independent experiments is shown. **(D)** HPASMC were stimulated for 15 min with PDGF (15 ng/ml), SSc IgG (200 μg/ml), and the agonistic (V_HPAM-V_κ16F4) and non-agonistic (V_HPAM-V_κ13B8) human monoclonal anti-PDGFRα autoantibody (10 μg/ml each). Unstimulated cells were used as a control (C). ROS generation was evaluated by fluorometry. Data are presented as mean ± SD of three independent experiments. *$p < 0.05$.

induction of a synthetic phenotype in HPSMC by anti-PDGFRα autoantibodies.

The stimulation of HPASMC by single SSc IgG occurred through enhanced ROS generation, since the addition of the generic antioxidant NAC (10 mM) and the selective NADPH oxidase inhibitor DPI (10 μM) for 1 h before stimulation significantly prevented cell migration and proliferation induced by PDGF (15 ng/ml) and SSc IgG (200 μg/ml; $n = 11$) ($p < 0.05$) (**Figures 3A,B**). Moreover, the upregulation of COL1A1 and the reduction of mRNA transcript for SM-MHC and SM-calponin induced by PDGF and SSc IgG were reverted by the addition of NAC and DPI (**Figure 3C**).

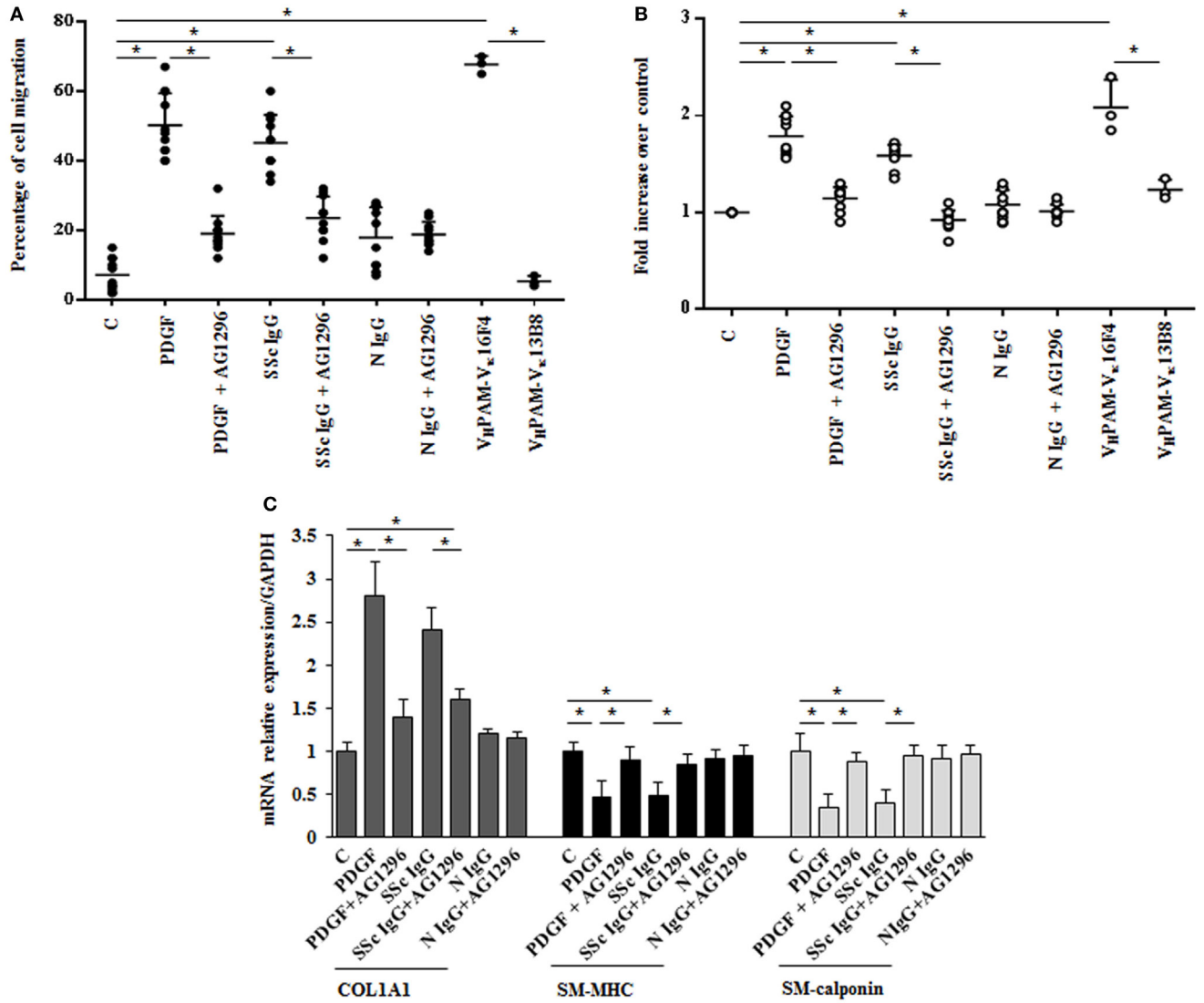

FIGURE 2 | Biological effects induced by systemic sclerosis (SSc) IgGs are mediated by PDGF receptor α (PDGFRα). **(A)** Migration was analyzed by the wound healing scratch test. Cells were scraped and stimulated with PDGF (15 ng/ml), distinct SSc IgG (200 μg/ml, $n = 11$), or distinct N IgG (200 μg/ml, $n = 10$) in the presence or absence of AG1296 or with agonistic (V_HPAM-$V_κ16F4$) and non-agonistic (V_HPAM-$V_κ13B8$) human monoclonal anti-PDGFRα autoantibody. After 24 h, the gap size was measured and expressed as a percentage of the original wound. The IgG from each subject was tested in triplicate. Data are presented as mean ± SD of three independent experiments. $^*p < 0.05$. **(B)** HPASMC treated with PDGF (15 ng/ml), single-tested SSc IgG (200 μg/ml; $n = 11$), or N IgG (200 μg/ml; $n = 10$) or with the human monoclonal anti-PDGFRα autoantibody V_HPAM-$V_κ16F4$ and V_HPAM-$V_κ13B8$ for 48 h in the presence or the absence of AG1296 (2 μM). Proliferation was determined by 5-bromo-2′-deoxyuridine assay and expressed as fold increase over controls. The IgG from each subject were tested in triplicate. Data are presented as mean ± SD of five independent experiments. $^*p < 0.05$. **(C)** HPASMC were treated with AG1296 (2 μM) for 1 h and then exposed to PDGF (15 ng/ml), SSc IgG (200 μg/ml; $n = 11$), or N IgG (200 μg/ml; $n = 10$) for 24 h. COL1A1, smooth muscle-myosin heavy chain, and SM-calponin mRNA levels were measured by real-time PCR. Data are presented as mean ± SD of three independent experiments. $^*p < 0.05$. The IgG from each subject was single tested.

These results indicate that SSc IgG induce phenotypic modulation and affect the rate of proliferation and migration of HPASMC through ROS produced by NOX activation.

Enhanced Expression of NOX4 by SSc IgG in HPASMC

To identify which NOX isoforms were upregulated in stimulated HPASMC, we treated HPASMC with PDGF (15 ng/ml) or single SSc IgG (200 μg/ml; $n = 11$) or IgG from normal subjects (N IgG; $n = 10$) (200 μg/ml) for 24 h, and the mRNA levels of the different NOX isoforms were assessed by real-time PCR. After stimulation, NOX4 mRNA levels were significantly upregulated compared to unstimulated cells (8.7 ± 1.5 and 8 ± 1.6 fold, respectively, $p < 0.05$), whereas NOX2, DUOX1, and DUOX2 were unaffected by the treatment (**Figure 4A**). PDGF, but not SSc IgG, increased NOX1 mRNA relative to control (2.9 ± 0.2-fold)

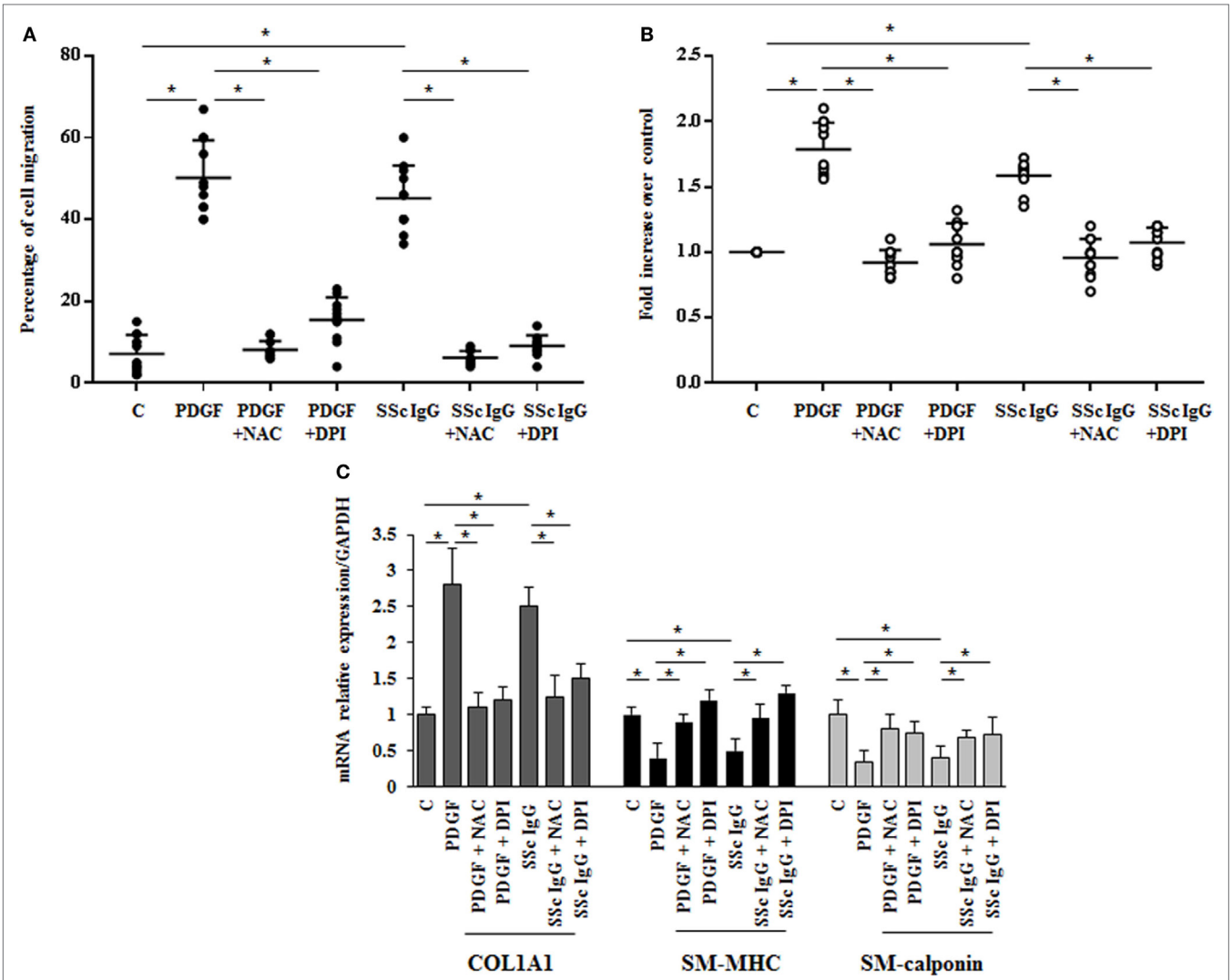

FIGURE 3 | **Biological effects induced by systemic sclerosis (SSc) IgG are mediated by reactive oxygen species**. **(A)** HPASMC were scraped and stimulated with PDGF (15 ng/ml) or IgG isolated from each SSc patient (200 μg/ml; $n = 11$) and single tested in the presence or absence of *N*-acetyl-cysteine (NAC) (10 mM) or diphenyleneiodonium (DPI) (10 μM). After 24 h, the gap size was measured and expressed as a percentage of the original wound. Data are presented as mean ± SD of five independent experiments. *$p < 0.05$. **(B)** HPASMC treated with PDGF (15 ng/ml) and SSc IgG (200 μg/ml) for 48 h in the presence or absence of NAC (10 mM) or DPI (10 μM) for 1 h. Proliferation was determined by 5-bromo-2′-deoxyuridine assay and expressed as fold increase over controls. Data are presented as mean ± SD of five independent experiments. *$p < 0.05$. The IgG from each subject was single tested. **(C)** HPASMC were treated with NAC (10 mM) or DPI (10 μM) for 1 h and then exposed to PDGF (15 ng/ml) and distinct SSc IgG (200 μg/ml, $n = 11$) for 24 h. COL1A1, smooth muscle-myosin heavy chain, and SM-calponin mRNA levels were measured by real-time PCR. Data are presented as mean ± SD of three independent experiments. *$p < 0.05$.

but, as demonstrated elsewhere (36), the silencing of NOX1 did not influence the ROS generation in these cells (data not shown).

A significant increase of NOX4 protein expression compared to basal conditions was observed by immunoblotting (**Figure 4B**; $p < 0.05$) and FACS analysis (**Figure 4C**; $p < 0.05$) after a 24-hour exposure to PDGF or SSc IgG, whereas no effect was observed after N IgG addition (200 μg/ml; $n = 10$).

To dissect the role of NOX4 in ROS generation after PDGF or SSc IgG stimulation, we silenced NOX4 using small interfering RNA (siRNA) ($p < 0.05$) (**Figure 5A**). The specific siRNA selectively prevented ROS generation in HPASMC stimulated with either 15 ng/ml PDGF or 200 μg/ml SSc IgG for 15 min (**Figure 5B**) and reverted the effects of PDGF or SSc IgG on migration and proliferation (**Figures 5C,D**) compared to unstimulated cells. Silencing of NOX4 inhibited PDGF, SSc IgG induction of COL1A1, and downregulation of SM-MHC and SM-calponin, indicating a regulatory role of NOX4 in the phenotypic modulation of HPASMC (**Figure 6**).

mTOR Modulated the Effects of SSc IgG

Mammalian target of rapamycin (mTOR) is a serine/threonine kinase that acts as a major activator of cell growth and proliferation. mTOR has also been shown to play a role in proliferation of vascular smooth muscle cells and when

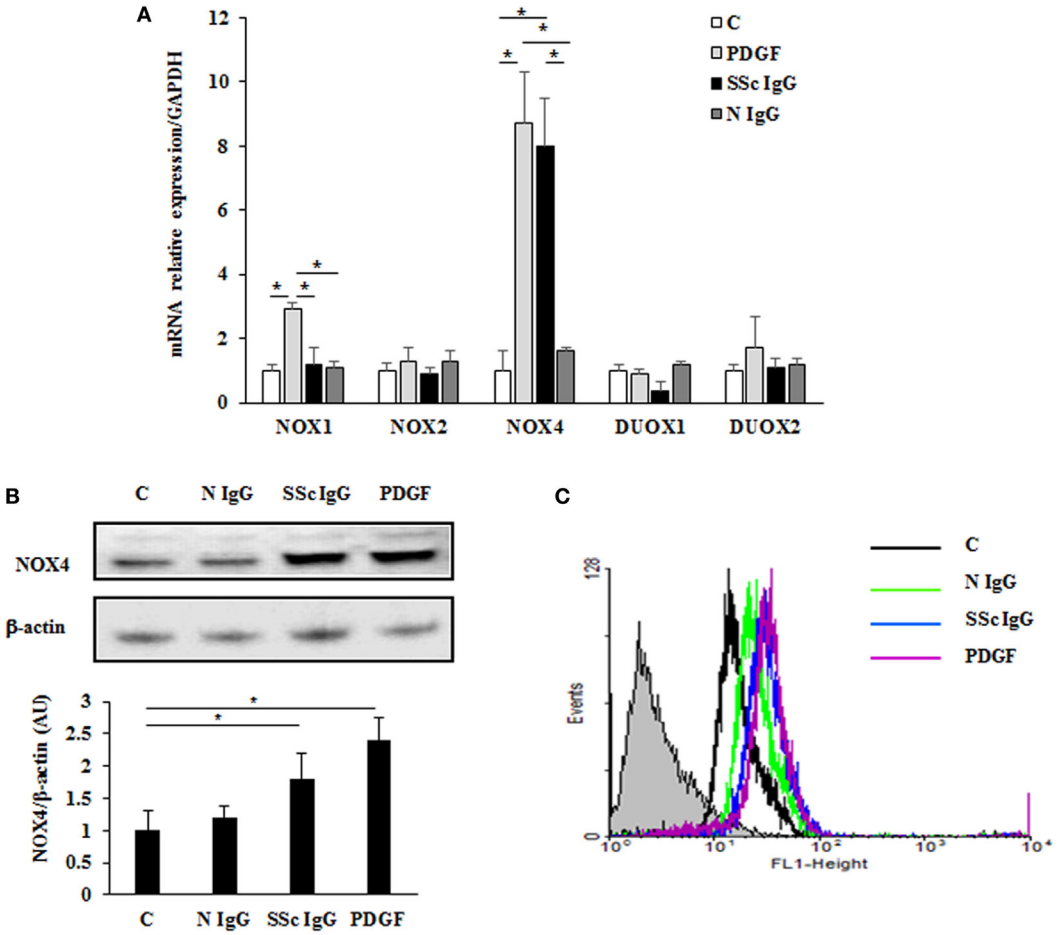

FIGURE 4 | Induction of NOX4 levels by systemic sclerosis (SSc) IgG. **(A)** Real-time PCR analysis of NOX isoforms in HPASMC treated with PDGF (15 ng/ml) or IgG isolated from distinct SSc patients (200 μg/ml; $n = 11$) or distinct N IgG (200 μg/ml; $n = 10$) and single tested for 24 h. Data are presented as mean ± SD of three independent experiments. *$p < 0.05$ compared to controls. **(B)** Total cell lysates from HPASMC stimulated with PDGF (15 ng/ml), single SSc IgG (200 μg/ml; $n = 5$), or single N IgG (200 μg/ml; $n = 5$) for 24 h were analyzed by immunoblotting with a specific antibody against NOX4. β-actin was used as a control for normalization. One representative experiment is shown in the upper panel. Densitometric analysis from three independent experiments is reported in the lower panel. Data are presented as mean ± SD from three independent experiments. *$p < 0.05$. **(C)** One representative FACS analysis of NOX4 expression is shown. Cells were stimulated with PDGF (15 ng/ml), distinct SSc IgG (200 μg/ml; $n = 11$), or N IgG (200 μg/ml; $n = 10$); permealized; and then labeled with anti-NOX4 and secondary FITC-conjugated antibody.

dysregulated has been implicated in vascular remodeling (39). To evaluate the role of mTOR as a possible downstream effector in stimulated HPASMC, we treated the cells with PDGF (15 ng/ml) or distinct SSc IgG (200 μg/ml; $n = 11$) for 24 h in the presence or absence of rapamycin (10 nM), a specific inhibitor of mTOR added 48 h before. Phosphorylation levels of mTOR were higher in samples incubated with PDGF or SSc IgG compared to unstimulated cells and were reverted by rapamycin (**Figure 7A**). Moreover, the treatment with rapamycin significantly decreased the migration rate (**Figure 7B**), proliferation (**Figure 7C**); and COL1A1 expression (**Figure 7D**) and restored the levels of SM-MHC, and SM-calponin (**Figure 7D**) in HPASMC incubated with PDGF or SSc IgG. These results demonstrated that mTOR is a crucial downstream signaling of SSc IgG effects *via* PDGFR.

DISCUSSION

Vascular smooth muscle cells are highly specialized cells whose principal functions are contraction and regulation of blood vessel tone. In the mature arterial wall, they exhibit a contractile phenotype characterized by low rate of proliferation and expression of specific markers such as α-SMA, SM-MHC, and SM-calponin. In response to vascular injury, they can dedifferentiate into a proliferative and synthetic phenotype. This phenotypic switching contributes to intimal hyperplasia and has been linked to the development and progression of several vascular disease (38). The functional state of smooth muscle cells is controlled by a complex combination of local environmental cues and epigenetic programs that influences synthetic or contractile, as well as intermediate phenotypes (40–44).

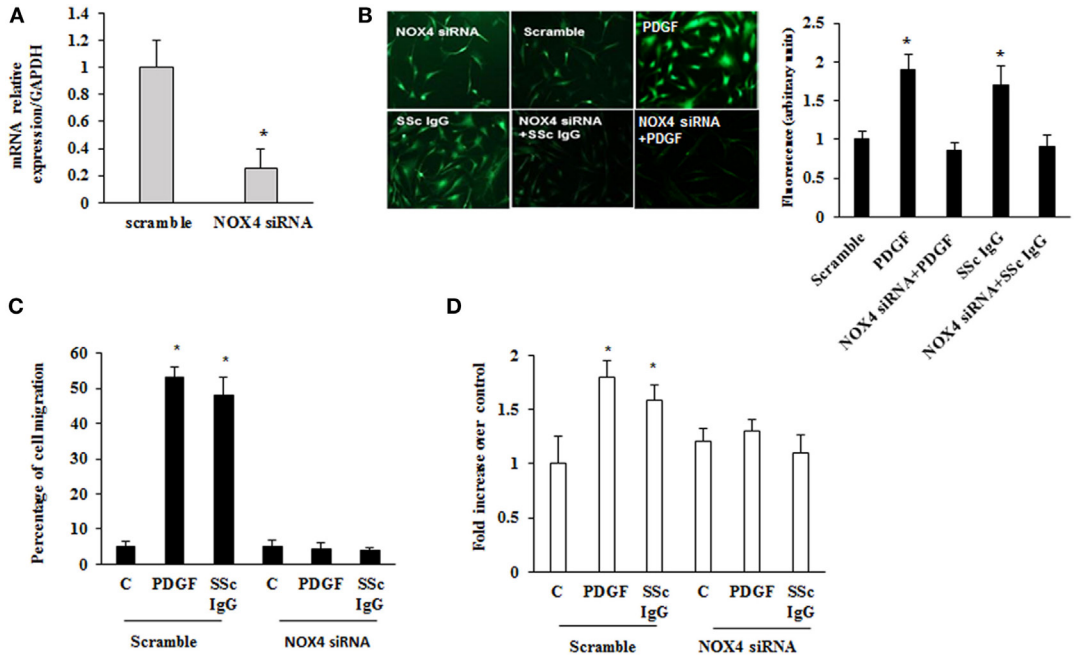

FIGURE 5 | Inhibition of systemic sclerosis (SSc) IgG biological effects by silencing NOX4. **(A)** HPASMC were transfected with NOX4 or scramble siRNA for 24 h, and NOX4 mRNA levels were analyzed by real-time PCR analysis. Data are presented as mean ± SD of three independent experiments. *$p < 0.05$ compared to cells transfected with scramble siRNA. **(B)** HPASMC were transfected with NOX4 siRNA or scramble siRNA for 24 h and then were stimulated with PDGF (15 ng/ml) or distinct SSc IgG (200 μg/ml; $n = 11$) for 15 min. Cells were incubated with DCHF-DA, and free radical production was evaluated by fluorescence microscopy. Representative images of three independent experiments are shown. The fluorescence was quantified using ImageJ software (right panel). **(C)** HPASMC were transfected with NOX4 or scramble siRNA for 24 h, scraped, and stimulated with PDGF (15 ng/ml) or single SSc IgG (200 μg/ml). After 24 h, the gap size was measured and expressed as a percentage of the original wound. Data are presented as mean ± SD of five independent experiments. *$p < 0.05$. **(D)** Transfected cells with NOX4 or scramble siRNA for 24 h were treated with PDGF (15 ng/ml) or single SSc IgG (200 μg/ml; $n = 11$) for 48 h. Proliferation was determined by 5-bromo-2′-deoxyuridine assay and expressed as fold increase over controls. Data are presented as mean ± SD of five independent experiments. *$p < 0.05$ compared to unstimulated cells.

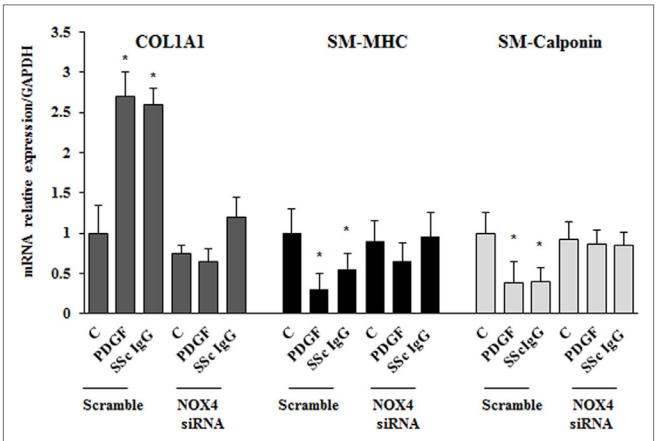

FIGURE 6 | NOX4 silencing drives a synthetic phenotype in HPASMC. Transfected cells with NOX4 siRNA or scramble siRNA for 24 h were treated with PDGF (15 ng/ml) or systemic sclerosis IgG (200 μg/ml; $n = 11$) for 24 h. COL1A1, smooth muscle-myosin heavy chain, and SM-calponin mRNA levels were measured by real-time PCR. Data are presented as mean ± SD of three independent experiments. *$p < 0.05$ compared to unstimulated cells.

In this study, we analyzed the expression of distinct functional markers of smooth muscle cells from human pulmonary arteries exposed *in vitro* to anti-PDGFR autoantibodies from SSc patients. In our experimental conditions, the data show that HPASMC acquire a synthetic phenotype characterized by higher growth rate, migratory activity, type I collagen gene expression, and minimal expression of markers characteristic of the contractile phenotype such as SM-MHC and smooth muscle-calponin. Thus, our findings indicate that anti-PDGFR autoantibodies may contribute not only to the development of SSc fibrotic lesions (23, 26) but also to the development of the vascular features. However, it is important to point out that our data do not allow to establish whether the new phenotype is due to the conversion of normal contractile vascular smooth muscle cells to a less differentiate state or to the expansion of medial-derived multipotent vascular stem cells (45).

Furthermore, since none of the SSc IgGs were from patients with pulmonary arterial hypertension, it seems that the impact of anti-PDGFRα autoantibodies on vascular smooth muscle cells reflects a general phenomenon, that is, scleroderma vasculopathy, and the association of their serum levels to specific clinical

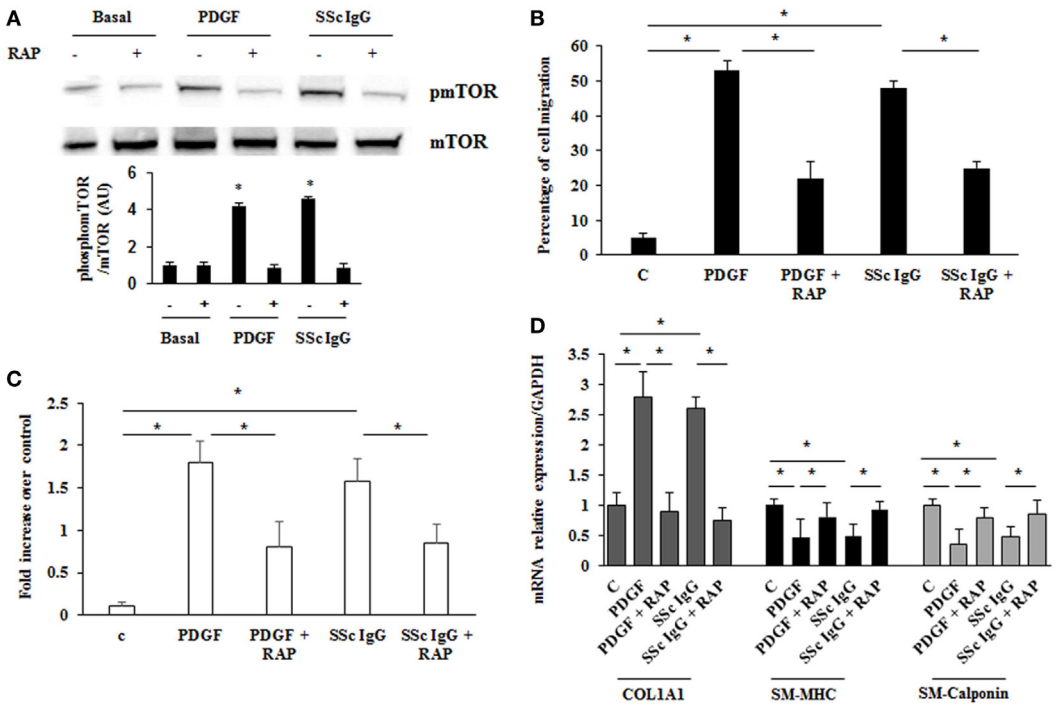

FIGURE 7 | **Modulation of systemic sclerosis (SSc) IgG effects by rapamycin**. **(A)** HPASMC were stimulated with PDGF (15 ng/ml) or SSc IgG (200 μg/ml; $n = 11$) for 24 h in the presence or absence of rapamycin (10 nM) added 48 h before. Phosphorylation of mTOR was detected by immunoblotting, and anti-total mTOR antibody was used as a control for normalization. One representative experiment is shown in the upper panel. Densitometric analysis from three independent experiments is reported in the lower panel. Data are presented as mean ± SD. *$p < 0.05$. **(B)** Migration was analyzed through wound healing scratch test. Cells were scraped and stimulated with PDGF (15 ng/ml) or single SSc IgG (200 μg/ml; $n = 11$) in the presence or absence of rapamycin (10 nM) added 48 h before. After 24 h, the gap size was measured and expressed as a percentage of the original wound. Data are presented as mean ± SD of five independent experiments. *$p < 0.05$. **(C)** HPASMC cells treated with PDGF (15 ng/ml) or single SSc IgG (200 μg/ml; $n = 11$) for 48 h in the presence or the absence of rapamycin (10 nM) added 48 h before. Proliferation was determined by 5-bromo-2′-deoxyuridine assay and expressed as fold increase over controls. Data are presented as mean ± SD of five independent experiments. *$p < 0.05$. **(D)** HPASMC were treated with rapamycin and then exposed to PDGF (15 ng/ml) or SSc IgG (200 μg/ml; $n = 11$) for 24 h. COL1A1, smooth muscle-myosin heavy chain, and SM-calponin mRNA levels were measured by real-time PCR. Data are presented as mean ± SD of three independent experiments. *$p < 0.05$. The IgG from each subject was single tested.

features (pulmonary arterial hypertension, digital ulcers, and scleroderma renal crisis) must be addressed in a larger cohort of SSc patients.

The activation of PDGFR by SSc IgG was both selective and ROS dependent since the presence of AG 1296 or NAC reduced the proliferation and migration of HPASMC and increased the expression of the differentiation markers. Our data are at variance with the findings reported by Arts et al. (46) who demonstrated that in smooth muscle cells SSc IgG engaged PDGFR leading to the activation of the epidermal growth factor receptor through a PDGFR-independent pathway. Furthermore, even if SSc IgG induced a profibrotic change in smooth muscle cells, collagen gene expression and cell proliferation were not influenced. Finally, some crucial experimental variables such as the source of the cells (aortic rat versus human pulmonary smooth muscle cells) and the timing of stimulation may explain the difference between their and our data.

Reactive oxygen species are known to mediate a variety of intracellular process, and the identification of the sources of these ROS has facilitated our understanding of a number of biological functions. Here, we demonstrated that the SSc IgG-induced abnormal oxidative stress through NOX4 activation facilitated the synthetic phenotype of human pulmonary artery smooth muscle cells. Interestingly and similar to what occurs in SSc fibroblasts (36), SSc IgG increased the expression of NOX4, while NOX1 was unaffected. These findings are the exact opposite of what reported by Lassègue et al. (47). If this discrepancy is to be ascribed to the different cell line and methodology used or indicates a different pathophysiological role of smooth muscle cells, NOX isoforms in response to distinct environmental cues remain to be established. Furthermore, at variance with what we found in normal fibroblasts (36), in HPSMC, SSc IgG did not induce NOX2, suggesting that individual NOX enzymes may play distinct roles between cell types. Thus, the precise interplay of NOX2 and NOX4 in HPSMC following SSc IgG stimulation needs further studies.

Cell proliferation and migration are thought to be a critical step in fibrogenesis, and since there is a strict interplay between mTOR and redox-based signaling (48, 49), we addressed the contribution of mTOR signaling to these phenotypes in cells exposed to ROS inducing stimuli.

mTOR is a serine/threonine kinase that consists of two distinct complexes mTORC1 and mTORC2. Growth factors, nutrients,

DNA damage, and hypoxia among others regulate mTOR, which, once activated, phosphorylates multiple downstream signals playing a key role in cellular protein synthesis, control of eukaryotic cell growth, and proliferation, including cell cycle progression, differentiation, protein degradation, apoptosis, and angiogenesis (50). The role of mTOR in the vasculature is subject to intense investigation, particularly in the field of pulmonary arterial hypertension, where evidence has been provided of its importance in the events leading to proliferation and survival of pulmonary vascular cells and its modulation by growth factors, vasoactive agents, vascular Ca^{2+} channels, and chronic hypoxia (50).

Interestingly, Eid et al. (51), in a different experimental system, have shown that the pharmacological inhibition of mTOR with rapamycin decreases NOX4 activity, ROS production, and podocytes apoptosis induced by high glucose, suggesting that rapamycin may represent a therapeutic modality of diabetic kidney disease (51). In line with their observations, we show that ROS-inducing SSc IgG activated mTOR, and its pharmacological inhibition with the antifungal macrolide rapamycin blocked PDGF and SSc IgG ability to promote crucial functions of vascular smooth muscle cells such as proliferation, migration, and collagen production, implying that mTORC1 mediated the phenotypic conversion.

These findings underscore the potential importance of mTOR in the pathogenesis of SSc, also in light of studies conducted on fibroblasts *in vitro* and in experimental models of fibrosis. mTOR activation contributes to type I collagen production by dermal fibroblasts (52, 53), and rapamycin improves skin fibrosis in two mouse models of fibrosis (54). Treatment of a small cohort of SSc patients with rapamycin was safe, but the efficacy was not impressive (55). However, the clinical benefit of a more efficient mTOR blockade should be explored exploiting the novel information regarding mTOR signaling targets.

In conclusion, our study demonstrates that stimulatory autoantibodies targeting PDGFR activate smooth muscle cells and may, thus, contribute to the development of SSc vascular lesions.

However, to better define their role in the pathogenesis of the individual SSc vascular manifestations, such as pulmonary arterial hypertension, digital ulcers, and SSc renal disease, it is necessary to study vascular smooth muscle cells of distinct organs, those isolated from tissues of SSc patients, and to establish whether there is indeed an association between the serum levels of anti-PDGFRα autoantibodies and particular vascular features. Nevertheless, the present findings and those already published (23, 24, 27) highlight the importance of an early treatment of scleroderma aimed at downregulating B cell immune response.

AUTHOR CONTRIBUTIONS

SS designed the experimental work analyzed results and wrote the first draft of the manuscript. DA, TS, and MR performed experimental work and analyzed results. CF and DF selected and provided samples and analyzed clinical data. GM, CP, CT, and AGR provided the monoclonal autoantibodies. AF contributed to write the final revised version of the manuscript. AGA designed, supervised, evaluated the experiments, and wrote the final version of the manuscript. All the authors read and approved the manuscript.

ACKNOWLEDGMENTS

This work was supported by Fondazione di Medicina Molecolare e Terapia Cellulare- Università Politecnica delle Marche and by grants from Ministero Italiano per l' Università e la Ricerca Scientifica and AILS (Associazione Italiana lotta alla Sclerodermia).

REFERENCES

1. Gabrielli A, Avvedimento EV, Krieg T. Scleroderma. *N Engl J Med* (2009) 360:1989–2003. doi:10.1056/NEJMra0806188
2. Varga J, Abraham D. Systemic sclerosis: a prototypic multisystem fibrotic disorder. *J Clin Invest* (2007) 117:557–67. doi:10.1172/JCI31139
3. Allanore Y, Simms R, Distler O, Trojanowska M, Pope J, Denton CP, et al. Systemic sclerosis. *Nat Rev Dis Primers* (2015) 1:15002. doi:10.1038/nrdp.2015.2
4. Prescott RJ, Freemont AJ, Jones CJ, Hoyland J, Fielding P. Sequential dermal microvascular and perivascular changes in the development of scleroderma. *J Pathol* (1992) 166:255–63. doi:10.1002/path.1711660307
5. Kahaleh B. Vascular disease in scleroderma: mechanisms of vascular injury. *Rheum Dis Clin North Am* (2008) 34:57–71. doi:10.1016/j.rdc.2007.12.004
6. Trojanowska M. Cellular and molecular aspects of vascular dysfunction in systemic sclerosis. *Nat Rev Rheumatol* (2010) 6:453–60. doi:10.1038/nrrheum.2010.102
7. Pattanaik D, Brown M, Postlethwaite AE. Vascular involvement in systemic sclerosis (scleroderma). *J Inflamm Res* (2011) 1:105–25. doi:10.2147/JIR.S18145
8. Rodnan GP, Myerowitz RL, Justh GO. Morphologic changes in the digital arteries of patients with progressive systemic sclerosis (scleroderma) and Raynaud phenomenon. *Medicine* (1980) 59:393–408. doi:10.1097/00005792-198011000-00001
9. Maricq HR, Downey JA, LeRoy EC. Standstill of nailfold capillary blood flow during cooling in scleroderma and Raynaud's syndrome. *Blood Vessels* (1976) 13:338–49.
10. Davies CA, Jeziorska M, Freemont AJ, Herrick AL. The differential expression of VEGF, VEGFR-2, and GLUT-1 proteins in disease subtypes of systemic sclerosis. *Hum Pathol* (2006) 37:190–7. doi:10.1016/j.humpath.2005.10.007
11. Distler O, Distler JH, Scheid A, Acker T, Hirth A, Rethage J, et al. Uncontrolled expression of vascular endothelial growth factor and its receptors leads to insufficient skin angiogenesis in patients with systemic sclerosis. *Circ Res* (2004) 95:109–16. doi:10.1161/01.RES.0000134644.89917.96
12. Mackiewicz Z, Sukura A, Povilenaité D, Ceponis A, Virtanen I, Hukkanen M, et al. Increased but imbalanced expression of VEGF and its receptors has no positive effect on angiogenesis in systemic sclerosis skin. *Clin Exp Rheumatol* (2002) 20:641–6.
13. Matucci-Cerinic M, Kahaleh B, Wigley FM. Evidence that systemic sclerosis is a vascular disease. *Arthritis Rheum* (2013) 65:1953–62. doi:10.1002/art.37988
14. Wigley FM. Vascular disease in scleroderma. *Clin Rev Allergy Immunol* (2009) 36:150–75. doi:10.1007/s12016-008-8106-x
15. Riemekasten G, Philippe A, Näther M, Slowinski T, Müller DN, Heidecke H, et al. Involvement of functional autoantibodies against vascular receptors in systemic sclerosis. *Ann Rheum Dis* (2011) 70:530–6. doi:10.1136/ard.2010.135772
16. Heldin CH, Westermark B. Mechanism of action and in vivo role of platelet-derived growth factor. *Physiol Rev* (1999) 79:1283–316.

17. Gay S, Jones RE Jr, Huang GQ, Gar RE. Immunohistologic demonstration of platelet-derived growth factor (PDGF) and sis-oncogene expression in scleroderma. *J Invest Dermatol* (1989) 92:301–3. doi:10.1111/1523-1747.ep12276895
18. Klareskog L, Gustafsson R, Scheynius A, Hallgren R. Increased expression of platelet-derived growth factor type B receptors in the skin of patients with systemic sclerosis. *Arthritis Rheum* (1990) 33:1534–41. doi:10.1002/art.1780331011
19. Rajkumar VS, Howell K, Csiszar K, Denton CP, Black CM, Abraham DJ. Shared expression of phenotypic markers in systemic sclerosis indicates a convergence of pericytes and fibroblasts to a myofibroblast lineage in fibrosis. *Arthritis Res Ther* (2005) 7:R1113–23. doi:10.1186/ar1790
20. Akhmetshina A, Dees C, Pileckyte M, Maurer B, Axmann R, Jüngel A, et al. Dual inhibition of c-abl and PDGF receptor signaling by dasatinib and nilotinib for the treatment of dermal fibrosis. *FASEB J* (2008) 22:2214–22. doi:10.1096/fj.07-105627
21. Olivieri A, Locatelli F, Zecca M, Sanna A, Cimminiello M, Raimondi R, et al. Imatinib for refractory chronic graft-versus-host disease with fibrotic features. *Blood* (2009) 114:700–18. doi:10.1182/blood-2009-02-204156
22. Fraticelli P, Gabrielli B, Pomponio G, Valentini G, Bosello S, Riboldi P, et al. Low-dose oral imatinib in the treatment of systemic sclerosis interstitial lung disease unresponsive to cyclophosphamide: a phase II pilot study. *Arthritis Res Ther* (2014) 16:R144. doi:10.1186/ar4606
23. Svegliati Baroni S, Santillo M, Bevilacqua F, Luchetti M, Spadoni T, Mancini M, et al. Stimulatory autoantibodies to the PDGF receptor in systemic sclerosis. *N Engl J Med* (2006) 354:2667–76. doi:10.1056/NEJMoa052955
24. Moroncini G, Grieco A, Nacci G, Paolini C, Tonnini C, Pozniak C, et al. Epitope specificity determines pathogenicity and detectability of anti-PDGFRα autoantibodies in systemic sclerosis. *Arthritis Rheumatol* (2015) 67:1891–903. doi:10.1002/art.39125
25. Svegliati S, Marrone G, Pezone A, Spadoni T, Grieco A, Moroncini M, et al. Oxidative DNA damage induces the ATM-mediated transcriptional suppression of the WNT inhibitor WIF-1 in systemic sclerosis and fibrosis. *Sci Signal* (2014) 7:ra84. doi:10.1126/scisignal.2004592
26. Svegliati S, Cancello R, Sambo P, Luchetti M, Paroncini P, Orlandini G, et al. Platelet-derived growth factor and reactive oxygen species (ROS) regulate Ras protein levels in primary human fibroblasts via ERK1/2. Amplification of ROS and Ras in systemic sclerosis fibroblasts. *J Biol Chem* (2005) 280:36474–82. doi:10.1074/jbc.M502851200
27. Luchetti MM, Moroncini G, Escamez MJ, Svegliati Baroni S, Spadoni T, Grieco A, et al. Induction of scleroderma fibrosis in skin-humanized mice by anti-platelet-derived growth factor receptor agonistic autoantibodies. *Arthritis Rheumatol* (2016) 68:2263–73. doi:10.1002/art.39728
28. Gelber AC, Manno RL, Shah AA, Woods A, Le EN, Boin F, et al. Race and association with disease manifestations and mortality in scleroderma: a 20-year experience at the Johns Hopkins Scleroderma Center and review of the literature. *Medicine* (2013) 92:191–205. doi:10.1097/MD.0b013e31829be125
29. Launay D, Sitbon O, Hachulla E, Mouthon L, Gressin V, Rottat L, et al. Survival in systemic sclerosis-associated pulmonary arterial hypertension in the modern management era. *Ann Rheum Dis* (2013) 72:1940–6. doi:10.1136/annrheumdis-2012-202489
30. Guillevin L, Hunsche E, Denton CP, Krieg T, Schwierin B, Rosenberg D, et al. Functional impairment of systemic scleroderma patients with digital ulcerations: results from the DUO Registry. *Clin Exp Rheumatol* (2013) 31(2 Supplement 76):71–80.
31. van den Hoogen F, Khanna D, Fransen J, Johnson SR, Baron M, Tyndall A, et al. 2013 classification criteria for systemic sclerosis: an American College of Rheumatology/European League against rheumatism collaborative initiative. *Arthritis Rheum* (2013) 65:2737–47. doi:10.1002/art.38098
32. LeRoy EC, Black CM, Fleischmajer R, Jablonska S, Krieg T, Medsger TA Jr, et al. Scleroderma (systemic sclerosis): classification, subsets and pathogenesis. *J Rheumatol* (1988) 12:217–23.
33. Liang CC, Park AY, Guan JL. In vitro scratch assay: a convenient and inexpensive method for analysis of cell migration in vitro. *Nat Protoc* (2007) 2:329–33. doi:10.1038/nprot.2007.30
34. Gabrielli A, Svegliati S, Moroncini G, Amico D. New insights into the role of oxidative stress in scleroderma fibrosis. *Open J Rheumatol* (2012) 6:87–95. doi:10.2174/1874312901206010087
35. Fessel JP, West JD. Redox biology in pulmonary arterial hypertension (2013 Grover Conference series). *Pulm Circ* (2015) 5:599–609. doi:10.1086/683814
36. Spadoni T, Svegliati Baroni S, Amico D, Albani L, Moroncini G, Avvedimento EV, et al. A reactive oxygen species–mediated loop maintains increased expression of NADPH oxidases 2 and 4 in skin fibroblasts from patients with systemic sclerosis. *Arthritis Rheumatol* (2015) 67:1611–22. doi:10.1002/art.39084
37. Riemekasten G, Cabral-Marques O. Vascular hypothesis revisited: role of stimulating antibodies against angiotensin and endothelin receptors in the pathogenesis of systemic sclerosis. *Autoimmun Rev* (2016) 15(7):690–4. doi:10.1016/j.autrev.2016.03.005
38. Rensen SS, Doevendans PA, Van Eys GJ. Regulation and characteristics of vascular smooth muscle cell phenotypic diversity. *Neth Heart J* (2007) 15:100–8. doi:10.1007/BF03085963
39. Montezano A, Touyz M. Mammalian target of rapamycin: a novel pathway in vascular calcification. *Can J Cardiol* (2014) 30:482–4. doi:10.1016/j.cjca.2014.03.001
40. Nguyen AT, Gomez D, Bell RD, Campbell JH, Clowes AW, Gabbiani G, et al. Smooth muscle cell plasticity: fact or fiction? *Circ Res* (2013) 112:17–22. doi:10.1161/CIRCRESAHA.112.281048
41. Owens GK, Kumar MS, Wamhoff BR. Molecular regulation of vascular smooth muscle cell differentiation in development and disease. *Physiol Rev* (2004) 84:767–801. doi:10.1152/physrev.00041.2003
42. Frid MG, Moiseeva EP, Stenmark KR. Multiple phenotypically distinct smooth muscle cell populations exist in the adult and developing bovine pulmonary arterial media in vivo. *Circ Res* (1994) 75:669–81. doi:10.1161/01.RES.75.4.669
43. Christen T, Verin V, Bochaton-Piallat M, Popowski Y, Ramaekers F, Debruyne P, et al. Mechanisms of neointima formation and remodeling in the porcine coronary artery. *Circulation* (2001) 103:882–8. doi:10.1161/01.CIR.103.6.882
44. Regan CP, Adam PJ, Madsen CS, Owens GK. Molecular mechanisms of decreased smooth muscle differentiation marker expression after vascular injury. *J Clin Invest* (2000) 106:1139–47. doi:10.1172/JCI10522
45. Majesky MW. Development basis of vascular smooth muscle diversity. *Arterioscler Tromb Vasc Biol* (2007) 27:1248–58. doi:10.1161/ATVBAHA.107.141069
46. Arts MR, Baron M, Chokr N, Fritzler MJ, Canadian Scleroderma Research Group (CSRG), Servant MJ. Systemic sclerosis immunoglobulin induces growth and pro-fibrotic state in vascular smooth muscle cells through the epidermal growth factor receptor. *PLoS One* (2014) 9:e100035. doi:10.1371/journal.pone.0100035
47. Lassègue B, Sorescu D, Szöcs K, Yin Q, Akers M, Zhang Y, et al. Novel gp91(phox) homologues in vascular smooth muscle cells: nox1 mediates angiotensin II-induced superoxide formation and redox-sensitive signaling pathways. *Circ Res* (2001) 88:888–94. doi:10.1161/hh0901.090299
48. Sarbassov DD, Sabatini DM. Redox regulation of the nutrient-sensitive raptor-mTOR pathway and complex. *J Biol Chem* (2005) 280(47):39505–9. doi:10.1074/jbc.M506096200
49. Yang Q, Guan KL. Expanding mTOR signaling. *Cell Res* (2007) 17:666–81. doi:10.1038/cr.2007.64
50. Goncharova EA. mTOR and vascular remodeling in lung diseases: current challenges and therapeutic prospects. *FASEB J* (2013) 27:1796–807. doi:10.1096/fj.12-222224
51. Eid A, Ford B, Bhandary B, De Cassia Cavaglieri R, Block K, Barnes J, et al. Mammalian target of rapamycin regulates NOX4-mediated podocyte depletion in diabetic renal injury. *Diabetes* (2013) 62:2935–47. doi:10.2337/db12-1504
52. Ponticos M, Papaioannou I, Xu S, Holmes AM, Khan K, Denton CP, et al. Failed degradation of JunB contributes to overproduction of type I collagen and development of dermal fibrosis in patients with systemic sclerosis. *Arthritis Rheumatol* (2015) 67:243–53. doi:10.1002/art.38897
53. Tamaki Z, Asano Y, Kubo M, Ihn H, Tada Y, Sugaya M, et al. Effects of the immunosuppressant rapamycin on the expression of human α2(I) collagen and matrix metalloproteinase 1 genes in scleroderma dermal fibroblasts. *J Dermatol Sci* (2014) 74:251–9. doi:10.1016/j.jdermsci.2014.02.002
54. Yoshizaki A, Yanaba K, Yoshizaki A, Iwata Y, Komura K, Ogawa F, et al. Treatment with rapamycin prevents fibrosis in tight-skin and bleomycin-induced mouse models of systemic sclerosis. *Arthritis Rheum* (2010) 62:2476–87. doi:10.1002/art.27498

55. Su TI, Khanna D, Furst DE, Danovitch G, Burger C, Maranian P, et al. Rapamycin versus methotrexate in early diffuse systemic sclerosis: results from a randomized, single-blind pilot study. *Arthritis Rheum* (2009) 60:3821–30. doi:10.1002/art.24986

Conflict of Interest Statement: The authors declare that the research was conducted in the absence of any commercial or financial relationships that could be construed as a potential conflict of interest.

frontiers in Immunology

CORRECTION
published: 12 April 2017
doi: 10.3389/fimmu.2017.00381

Corrigendum: Agonistic Anti-PDGF Receptor Autoantibodies from Patients with Systemic Sclerosis Impact Human Pulmonary Artery Smooth Muscle Cells Function *In Vitro*

*Silvia Svegliati[1†], Donatella Amico[1†], Tatiana Spadoni[1†], Colomba Fischetti[1], Doreen Finke[1], Gianluca Moroncini[1], Chiara Paolini[1], Cecilia Tonnini[1], Antonella Grieco[1], Marina Rovinelli[1], Ada Funaro[2] and Armando Gabrielli[1]**

[1] Clinica Medica, Dipartimento di Scienze Cliniche e Molecolari, Università Politecnica delle Marche, Ancona, Italy, [2] Dipartimento di Scienze Mediche, Università di Torino, Torino, Italy

OPEN ACCESS

Edited and Reviewed by:
Raffaele De Palma,
Università degli Studi della Campania "Luigi Vanvitelli" Caserta, Italy

***Correspondence:**
Armando Gabrielli
a.gabrielli@univpm.it

†These authors have contributed equally to this work.

Specialty section:
This article was submitted to Primary Immunodeficiencies, a section of the journal Frontiers in Immunology

Received: 07 March 2017
Accepted: 17 March 2017
Published: 12 April 2017

Citation:
Svegliati S, Amico D, Spadoni T, Fischetti C, Finke D, Moroncini G, Paolini C, Tonnini C, Grieco A, Rovinelli M, Funaro A and Gabrielli A (2017) Corrigendum: Agonistic Anti-PDGF Receptor Autoantibodies from Patients with Systemic Sclerosis Impact Human Pulmonary Artery Smooth Muscle Cells Function In Vitro. Front. Immunol. 8:381. doi: 10.3389/fimmu.2017.00381

Keywords: systemic sclerosis, autoantibodies, vascular smooth muscle cells, platelet-derived growth factor, synthetic phenotype

A corrigendum on

Agonistic Anti-PDGF Receptor Autoantibodies from Patients with Systemic Sclerosis Impact Human Pulmonary Artery Smooth Muscle Cells Function *In Vitro*
by Svegliati S, Amico D, Spadoni T, Fischetti C, Finke D, Moroncini G, et al. Front Immunol (2017) 8:75. doi:10.3389/fimmu.2017.00075

In the original article, we neglected to add Ada Funaro as an author. The correct author list and affiliation should be

Silvia Svegliati[1†], Donatella Amico[1†], Tatiana Spadoni[1†], Colomba Fischetti[1], Doreen Finke[1], Gianluca Moroncini[1], Chiara Paolini[1], Cecilia Tonnini[1], Antonella Grieco[1], Marina Rovinelli[1], Ada Funaro[2] and Armando Gabrielli[1*]

[1]Clinica Medica, Dipartimento di Scienze Cliniche e Molecolari, Università Politecnica delle Marche, Ancona, Italy

[2]Dipartimento di Scienze Mediche, Università di Torino, Torino, Italy

AUTHOR CONTRIBUTIONS

SS designed the experimental work analyzed results and wrote the first draft of the manuscript. DA, TS, and MR performed experimental work and analyzed results. CF and DF selected and provided samples and analyzed clinical data. GM, CP, CT, and AGR provided the monoclonal autoantibodies. AF contributed to write the final revised version of the manuscript. AGA designed, supervised, evaluated the experiments, and wrote the final version of the manuscript. All the authors read and approved the manuscript.

The authors apologize for this oversight.

This error does not change the scientific conclusions of the article in any way.

The original article has been updated.

Conflict of Interest Statement: The authors declare that the research was conducted in the absence of any commercial or financial relationships that could be construed as a potential conflict of interest.

frontiers in Immunology

ORIGINAL RESEARCH
published: 16 February 2017
doi: 10.3389/fimmu.2017.00124

Stretching Reduces Skin Thickness and Improves Subcutaneous Tissue Mobility in a Murine Model of Systemic Sclerosis

*Ying Xiong[1†], Lisbeth Berrueta[1], Katia Urso[2], Sara Olenich[1], Igla Muskaj[1], Gary J. Badger[3], Antonios Aliprantis[2†], Robert Lafyatis[4] and Helene M. Langevin[1,5]**

[1] Division of Preventive Medicine, Brigham and Women's Hospital, Harvard Medical School, Boston, MA, USA, [2] Division of Rheumatology, Immunology and Allergy, Brigham and Women's Hospital, Harvard Medical School, Boston, MA, USA, [3] Department of Medical Biostatistics, University of Vermont, Burlington, VT, USA, [4] University of Pittsburgh, School of Medicine, Pittsburgh, PA, USA, [5] Department of Neurological Sciences, University of Vermont, Burlington, VT, USA

Objective: Although physical therapy can help preserve mobility in patients with systemic sclerosis (SSc), stretching has not been used systematically as a treatment to prevent or reverse the disease process. We previously showed in rodent models that stretching promotes the resolution of connective tissue inflammation and reduces new collagen formation after injury. Here, we tested the hypothesis that stretching would impact scleroderma development using a mouse sclerodermatous graft-versus-host disease (sclGvHD) model.

Methods: The model consists in the adoptive transfer (allogeneic) of splenocytes from B10.D2 mice (graft) into Rag2$^{-/-}$ BALB/c hosts (sclGvHD), resulting in skin inflammation followed by fibrosis over 4 weeks. SclGvHD mice and controls were randomized to stretching *in vivo* for 10 min daily versus no stretching.

Results: Weekly ultrasound measurements of skin thickness and subcutaneous tissue mobility in the back (relative tissue displacement during passive trunk motion) successfully captured the different phases of the sclGvHD model. Stretching reduced skin thickness and increased subcutaneous tissue mobility compared to no stretching at week 3. Stretching also reduced the expression of CCL2 and ADAM8 in the skin at week 4, which are two genes known to be upregulated in both murine sclGvHD and the inflammatory subset of human SSc. However, there was no evidence that stretching attenuated inflammation at week 2.

Conclusion: Daily stretching for 10 min can improve skin thickness and mobility in the absence of any other treatment in the sclGvHD murine model. These pre-clinical results suggest that a systematic investigation of stretching as a therapeutic modality is warranted in patients with SSc.

Keywords: scleroderma, systemic sclerosis, GvHD, stretching, physical therapy, inflammation, fibrosis

OPEN ACCESS

Edited by:
Raffaele De Palma, Second University of Naples (SUN), Italy

Reviewed by:
Giuseppe Cirino, University of Naples Federico II, Italy
Emily Mace, Baylor College of Medicine, USA

****Correspondence:***
Helene M. Langevin
hlangevin@partners.org

†Present address:
Ying Xiong, Nanjing University of Chinese Medicine, Nanjing, China; Antonios Aliprantis, Merck Research Laboratories, Boston, MA, USA

Specialty section:
This article was submitted to Primary Immunodeficiencies, a section of the journal Frontiers in Immunology

Received: *21 September 2016*
Accepted: *25 January 2017*
Published: *16 February 2017*

Citation:
Xiong Y, Berrueta L, Urso K, Olenich S, Muskaj I, Badger GJ, Aliprantis A, Lafyatis R and Langevin HM (2017) Stretching Reduces Skin Thickness and Improves Subcutaneous Tissue Mobility in a Murine Model of Systemic Sclerosis. Front. Immunol. 8:124. doi: 10.3389/fimmu.2017.00124

INTRODUCTION

Systemic sclerosis (SSc, also known as scleroderma) is an autoimmune disorder characterized by chronic dysregulation of innate and adaptive immune systems, vasculopathy, and fibroblast dysfunction resulting in fibrosis (1). Although clinical manifestations of SSc are heterogeneous, their hallmark is skin fibrosis, including the dermis and subcutaneous tissue (1–3). When subcutaneous tissue becomes fibrotic, adhesions can form between the skin and underlying connective tissues, which leads to impaired movement between these tissue layers and decreased range of motion (4). Non-pharmacological treatments, including physical therapy and stretching, are thought to be important adjuncts to pharmacological treatment in patients with SSc (5). However, there is evidence that these types of interventions are underutilized, and stretching has not been used systematically to prevent or reverse the diseases process (6, 7). Conversely, the possibility that lack of movement may itself be an important contributor to the pathophysiology of the disease has not been investigated. Thus, the lack of a standardized approach to stretching, including the correct "dose," and dearth of insight into the mechanisms engaged at the tissue level by stretching has limited the application of this potentially powerful, yet non-invasive treatment (7–9).

We have previously developed an animal model in which mice or rats spontaneously stretch their whole body when they are partially lifted by the tail and allowed to grasp the edge of a surface with their front paws (10). When held in this position, the animals spontaneously extend both front and hind limbs, which increases the distance between shoulders and hips by ~25%. Using this model, we showed that stretching promotes the resolution of inflammation in subcutaneous connective tissues of the back and decreases newly formed collagen in a subcutaneous connective tissue injury model (10–12).

Because inflammation and fibrosis are known to contribute to the development of SSc pathology, the goal of this study was to test the effect of daily stretching in a murine model of SSc. The mouse sclerodermatous Graft-versus-host disease (sclGvHD) has been demonstrated to mimic a subset of SSc patients with an inflammatory gene signature (13, 14). In this model Rag2$^{-/-}$ BALB/c hosts (sclGvHD mice) receive adoptively transferred splenocytes from MHC-matched allogeneic B10.D2 mice (graft). The graft-versus-host reaction culminates in skin inflammation and fibrosis. Seven days after splenocyte transfer, the sclGvHD mice lose weight and inflammatory cells begin to infiltrate the skin. Over the course of the following 4 weeks, collagen accumulates in the skin and fibrosis is clinically manifested as alopecia (15) (15–17). We used novel high-frequency ultrasound methods to follow the course of the disease and measure the impact of stretching. Our ultrasound measures included the thickness of skin and subcutaneous tissue, as well as the relative motion between the skin and underlying subcutaneous connective tissue layers in dynamic ultrasound recordings during passive flexion of the trunk. We chose to focus our measurements on the skin and subcutaneous tissues of the back, which provide accessible flat tissue planes that can be measured reliably with both static and dynamic imaging as previously demonstrated in humans and large animals (18–20), and used high-frequency (50 MHz) ultrasound, which provides the high resolution needed to apply these techniques to rodents. We hypothesized that, in the absence of stretch, ultrasound measurement of skin thickness are increased and subcutaneous tissue mobility are decreased in sclGvHD compared with control mice. We further hypothesized that stretching attenuates these abnormalities in the sclGvHD mice. In addition, because sclGvHD demonstrates a gene expression pattern similar to the inflammatory subset of scleroderma (13, 14) and increased expression of extracellular matrix-associated pathways is evident in this inflammatory subset (13), we also examined the expressions of TGF-β, TIMP1, MMP-12, ADAM8, IL4RA, and CCL2 genes which have been previously shown to be upregulated in both murine sclGvHD and the inflammatory subset of SSc patients (13, 14, 21, 22).

MATERIALS AND METHODS

Mice and sclGvHD Model

The animal testing protocol used in this study was approved by the Harvard Medical School Institutional Animal Care and Use Committee. *Rag2*$^{-/-}$ mice on a BALB/c genetic background were generated as described previously in Ref. (13, 23). BALB/c and B10.D2, mice were obtained from the Jackson Laboratory (Bar Harbor, ME, USA). All mice were housed in a specific pathogen-free animal facility at the Harvard School of Public Health. Mice were housed and maintained in accordance with the Guide for Care and Use of Laboratory Animals. The drinking water of all *Rag2*$^{-/-}$ mice was supplemented with sulfamethoxazole and trimethoprim (Sulfatrim, Hi-Tech Pharmacal, 0.6 mg/ml drinking solution). The sclGvHD model was established as described previously (15).

Six- to nine-week-old males were used for all the experiments. Briefly, 20–40 million BALB/c (syngeneic) or B10.D2 (allogeneic) red-blood-cell-free splenocytes were transferred *via* tail-vein injection into host mice. Injection of allogeneic splenocytes produced the sclGvHD phenotype, while injection of syngeneic splenocytes served as controls. The mice were weighed and scored clinically once a week by a blinded observer as follows: 0 = no evidence of disease, 1 = fur ruffling or hunched posture, 2 = alopecia < 25% of body surface area, 3 = alopecia > 25% of body surface area, and 4 = death or a veterinary order to euthanize. Half a point was added for periorbital swelling.

Study Design

Mice were randomized into one of four groups ($N = 12$/group): syngeneic control/no stretch (Ctl-NS), syngeneic control/stretch (Ctl-S), sclGvHD/no stretch (Scl-NS), and sclGvHD/stretch (Scl-S). Allogeneic (sclGvHD) or Syngeneic (Control) splenocytes were injected on day 0. The control group was included to document the effect of scleroderma using ultrasound. The stretch (or no stretch) interventions were performed for 10 min once a day, 5 days per week, for 4 weeks, beginning 3 days after splenocyte injection. Ultrasound measurements were performed once a week during the 4-week intervention, except at week 0 due to barrier facility constraints. At all time points, ultrasound measurements were taken 1 h after the last stretching (or no

stretching) session. At the end of week 4, mice were euthanized by decapitation under deep isoflurane anesthesia immediately after the last ultrasound measurements, and skin samples from the back were excised for histology and gene expression analysis after shaving the back.

Intervention Methods

Stretching method: mice were stretched by gently lifting them by the base of the tail until reaching ~45° angle to the horizontal. While grasping onto a bar with their front paws, the mice spontaneously extend their hind limbs. The stretching, which exerted traction on the whole back, increases the distance between the shoulder and hip by ~25% (10). With minimal habituating, mice were able to hold this position comfortably for 10 min without struggling, vocalizing, or other signs of distress (**Figure 1A**). *No stretching (sham)*: mice were removed from their cage for 10 min but were neither lifted nor stretched (**Figure 1B**).

Ultrasound Data Acquisition

All ultrasound data acquisition and measurements were performed by investigators blinded to intervention condition. Ultrasound images of the back were acquired under isoflurane anesthesia. A high-frequency ultrasound scanner (Vevo 2100, Fujifilm VisualSonic, Toronto, ON, Canada) in B mode with a 50-MHz transducer (MS 700) was used for optimal spatial resolution, which provided a resolution of 30 μm × 75 μm (axial × lateral) and a focal length of 5.0 mm. A conductive gel was centrifuged for 5 min to remove air bubbles and spread over the skin. To ensure complete contact between the skin and the transducer, the fur in the back of the mice was parted after applying the gel and prior to imaging. This was done rather than shaving to avoid injury or irritation to the skin. The transducer was stabilized with a clamp and mounted into an articulated arm to control the distance and the angle between the transducer and the skin surface. For skin thickness measurements, the transducer was oriented transversely, perpendicular to the skin of the back and centered on the midline. Ultrasound images were acquired at two levels, one rostral and one caudal, on the left side of the back as shown in **Figure 1C**. For cumulative displacement measurement, the transducer was oriented longitudinally, 0.5 cm lateral and parallel to the midline and centered on the caudal level. Accurate positioning was achieved by regulating the micrometric screws and great care was taken to position the transducer in such a way as to avoid any compression of the skin (**Figure 1D**). In each mouse, an ultrasound cine-recording was acquired on the right and left sides of the back during cyclical passive trunk flexion using an articulated table with the hinge point of the table at the level of animal's axilla. The table moved up and down at 0.5 Hz at a 17° angle (**Figure 1E**) from the horizontal for a total of four cycles.

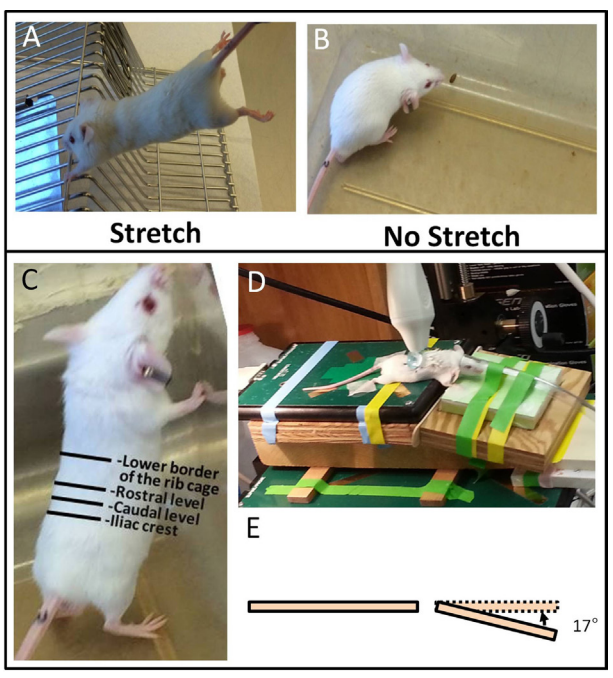

FIGURE 1 | Ultrasound imaging acquisition and stretching methods. **(A,B)**: Stretching **(A)** and no stretching **(B)** interventions. **(C)**: Location of rostral and caudal levels for acquisition of transverse ultrasound images. **(D)**: Position of mouse on articulated table during acquisition of dynamic ultrasound imaging during upward and downward table motion. **(E)**: Angle of table motion.

Ultrasound Image Measurement

For measurement of skin thickness, three zones were defined on the ultrasound images as illustrated in **Figures 2A–C**: Zone 1 (skin and subcutaneous tissue) extended from the superficial border of the dermis to the superficial border of the erector spinae muscle. Zone 2 (skin) extended from the superficial border of the dermis to the superficial border of the subcutaneous muscle, and Zone 3 from the superficial border of the subcutaneous muscle to the superficial border of the erector spinae muscle. Thickness measurements were performed at two fixed points, 1.5 mm (medial) and 2.5 mm (lateral) from the midline, respectively (**Figure 2B**). Thickness measurements at the four sites (upper and lower levels, medial, and lateral points) were averaged and taken as the outcome measure for Zones 1, 2, and 3 thickness.

For measurement of cumulative displacement, two segments were defined at the superficial border of the dermis (segment A) and the superficial border of the erector spinae perimuscular fascia (segment B), respectively (**Figure 2D**). Tissue displacement for each segment was measured using Vivovasc software as the tangential displacement during successive 40 ms increments over the two middle cycles of table motion (**Figure 2E**). Tangential displacement is defined as displacement along the direction of tissue planes (skin and perimuscular fascia). The absolute cumulative difference between the displacement of superficial and deep segments was calculated and taken as the outcome measure for relative tissue displacement. Ultrasound image measurement intra-rater reliability (ICCs) were $r = 0.98$ for tissue thickness and $r = 0.87$ for tissue displacement.

Histopathological Assessment

At 4 weeks after splenocyte transfer, tissue specimens including skin, subcutaneous tissue, and muscle were excised from the

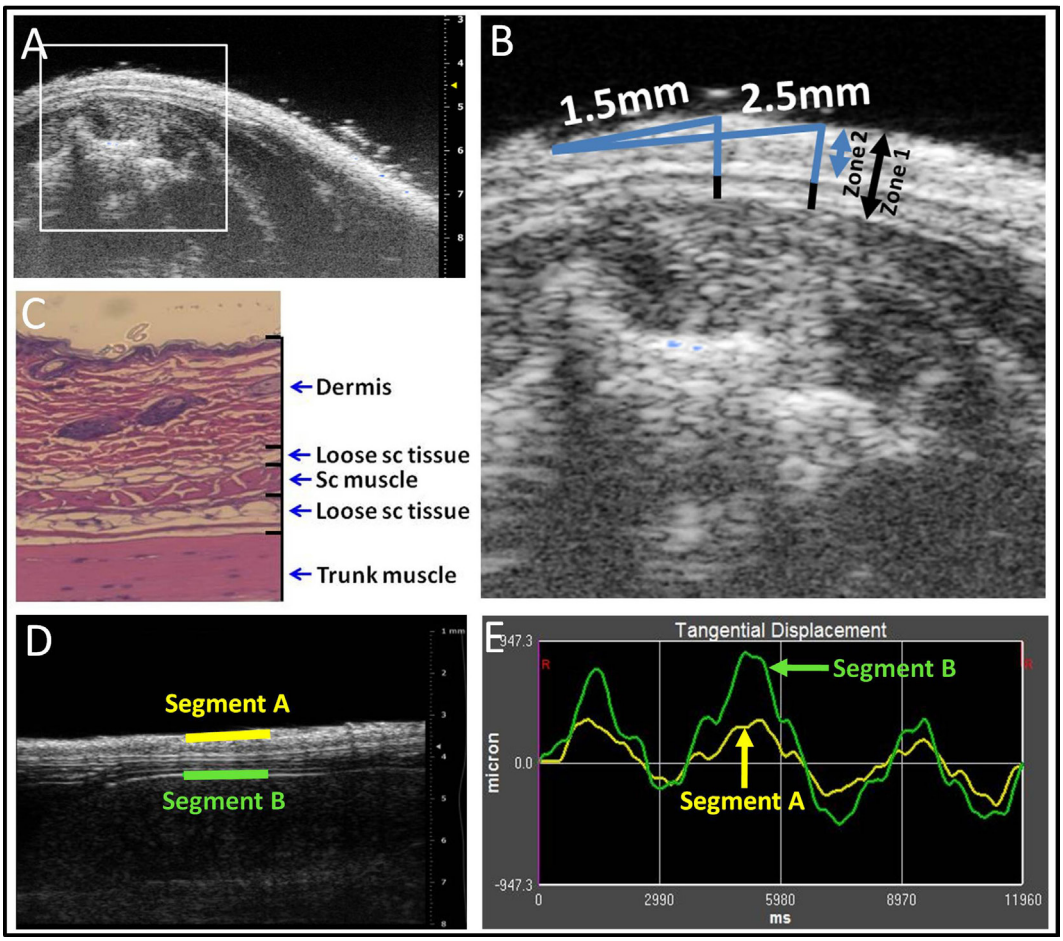

FIGURE 2 | **Ultrasound image analysis methods**. **(A–C)**: ultrasound thickness measurements. Medial and lateral locations are, respectively, 1.5 and 2.5 mm from the midline **(A,B)**. Zones 1–3 are shown in ultrasound **(B)** and corresponding histology **(C)** image shows relation to dermis, loose subcutaneous (sc) tissue, subcutaneous (sc) muscle, and trunk muscle (erector spinae). **(D,E)**: Ultrasound measurement of tissue differential displacement. Segments a and b are, respectively, located on the superficial border of the dermis and the superficial border of the erector spinae perimuscular fascia. **(E)**: representative tracing of tangential displacement of superficial and deep segments shown in **(D)** (segment A yellow and segment B green).

shaved skin of one side of the back between the rib cage and the highest point of iliac crest, fixed in 10% neutral-buffered formalin, embedded in paraffin, and stained with standard hematoxylin and eosin (H&E). A blinded observer experienced in SSc pathology (Robert Lafyatis) scored H&E-stained back skin tissue samples per mouse for four parameters (fibrosis, inflammation, fat loss, and epidermal hypertrophy), using a semi-quantitative scale from 0 to 4. Values were summed to derive a combined histopathological score (13).

Quantitative Real-time PCR

For mRNA expression studies, RNA was extracted from tissue samples corresponding to Zone 1 (skin and subcutaneous tissue) on the side contralateral to that used for histology. RNA was extracted using Trizol reagent (Qiagen, Santa Clarita, CA, USA) and reverse transcribed into cDNA with the Affinity Script CDNA Synthesis Kit (Agilent Technologies, Wilmington, DE, USA). Real-time quantitative PCR (qPCR) was performed using Sybr green reagent (Life Technologies, Grand Island, NY, USA). CT values for duplicate samples were averaged, and the amount of mRNA relative to a housekeeping gene transcript was calculated using the ΔCT method. Data were normalized to Hprt. The qPCR conditions were: 3 min 95°C, then 40 cycles of 10 s at 94°C, 10 s at 60°C, and 20 s at 72°C. Primers used for qPRC analysis are listed in **Table 1**.

Ex Vivo Tissue Explant Stretching Experiments and Fibroblast Morphological Measurements

Two separate *ex vivo* experiments were performed using subcutaneous connective tissue explants as previously described (24). In the first experiment, we compared four groups of mice without *in vivo* stretching ($N = 4$ mice per group): control mice euthanized at week 2, sclGvHD mice euthanized at week 2, control mice euthanized at week 4, and sclGvHD mice euthanized at week 4.

TABLE 1 | Q-PCR primer sequence.

Gene	Primer forward	Primer reverse
Adam8[a]	AGTTCCTGTTTATGCCCCAAAG	AAAGGTTGGCTTGACCTGCT
Ccl2[b]	GGCTCAGCCAGATGCAGTTAA	CCTACTCATTGGGATCATCTTGCT
Hprt[b]	GTTAAGCAGTACAGCCCCAAA	AGGGCATATCCAACAACAAACTT
Il4ra[b]	TCTGCATCCCGTTGTTTTGC	GCACCTGTGCATCCTGAATG
Mmp12[c]	GAACTTGCAGTCGGAGGGAA	TCTTGACAAGTACCATTCAGCA
Tgfb1[c]	CTTCAATACGTCAGACATTCGGG	GTAACGCCAGGAATTGTTGCTA
Timp1[a]	GCAACTCGGACCTGGTCATAA	CGGCCCGTGATGAGAAACT

[a]*Primers were selected from the Primer Bank website.*
[b]*Primers were described in Ref. (13).*
[c]*Primers were designed with Primer Blast website tool.*

The second experiment compared two groups: sclGVDH mice stretched *in vivo* for 4 weeks versus sclGVHD mice non-stretched (NS) *in vivo* for 4 weeks. In both experiments, immediately after euthanasia, a 8 cm × 3 cm tissue flap containing dermis, subcutaneous muscle, and subcutaneous tissue was excised from the back of the mouse. The tissue flap was cut into two pieces (right and left) that were randomized to *ex vivo* stretch versus control (no stretch). Each piece was placed transversely in grips and immersed in HEPES-physiological saline solution, pH 7.4 at 37°, containing (millimolars): NaCl 141.8, KCl 4.7, $MgSO_4$ 1.7, EDTA 0.39, $CaCl_2$ 2.8, HEPES 238.3, KH_2PO_4 1.2, and Glucose 5.0. The grips and tissues were placed vertically in a tissue bath with the proximal grip connected to a 500 g (4.9 N) capacity load cell. Samples randomized to *ex vivo* stretch were elongated a rate of 1 mm/s by advancing a micrometer connected to the distal tissue grip to 25% strain relative to the unloaded length (length of the tissue laying flat but not stretched) then maintained at that length for the duration of the incubation. Control samples (randomized to *ex vivo* no stretch) were incubated for the same duration without stretch. At the end of incubation, the tissue was immersion-fixed in 4% paraformaldehyde for 1 h. After fixation, areolar subcutaneous connective tissue samples (each 10 mm × 10 mm) were dissected and placed flat on a glass slide and stained with Texas Red conjugated phalloidin (4 U/ml; Molecular Probes, Eugene, OR, USA) for 40 min at 4°C then counterstained for 2 min with DAPI (Molecular Probes, Eugene, OR, USA). Samples were mounted on slides using 50% glycerol in PBS with 1% *N*-propylgallate as a mounting medium and overlaid with a glass coverslip. Three slides were prepared from each sample, with an average of 3–4 images taken from each slide, avoiding the edges, using a 63× immersion oil lens and a digital camera AxioCam MRC 5, Zeiss. Images were imported into the analysis software package Image J for morphometric analysis. An average of 30 fibroblasts were measured per excised tissue sample by a blinded investigator. A cell was excluded if part of its cell body perimeter is outside the image. For each cell, the cell body perimeter was traced as defined as the outline of the cell's cytoplasm projected in the plane of the image excluding cell processes (defined as an extension of a cell's cytoplasm longer than 2 μm and less than 2 μm in width at any portion of its length). Fibroblast cell body cross-sectional area was calculated as the area delimited by the cell body perimeter projected onto the image plane (see **Figure 8** for illustration of method).

Statistical Analysis

Repeated measures analyses of variance were performed to examine the effects of group, time, and their interaction. Dependent measures were zone-specific tissue thickness, relative tissue displacement, clinical score, and weights. Because group differences were found to be time-dependent (i.e., group × time interaction $p < 0.05$ for all outcome measures), partial *F*-tests were used to compare the four groups at each time point. If the partial *F*-test was significant, Fisher's Protected LSD was used to perform pairwise comparisons among groups at each time point to control type I error rate experiment-wise. For analyses of clinical score, control animals were excluded as all values were scored as 0. A one-way ANOVA was used to compare the four groups on histopathological score and mRNA expression. For mRNA, analyses of variance were performed on log fold change values, with results presented as geometric means and associated SEs. In a subset of animals ($N = 5$), estimates of intra-rater reliability were computed using on intraclass correlation coefficients for both tissue thickness and displacement. These estimates were based on variance components that were derived based on mixed model analyses of variance. Correlation between outcome variables were examined using Spearman's correlation. Repeated measures ANOVAs were used to examine *in vivo* and *ex vivo* stretch effects on fibroblast cross-sectional area. All statistical analyses were performed using SAS statistical software Version 9.4 (SAS Institute, Cary, NC, USA). Statistical significance was determined based on $\alpha = 0.05$.

RESULTS

Clinical Score, Animal Weight, and Histological Score

Clinical scores initially increased from baseline to week 1, subsequently decreased from week 1 to week 2 and rose again at weeks 3 and 4 (**Figure 3A**). This is consistent with previous studies that identified successive phases of skin involvement in the sclGvHD model, with an early predominantly inflammatory phase followed by fibrosis and atrophy (15–17). sclGvHD animal weights paralleled the clinical scores by first decreasing at week 1, rebounding at week 2 and decreasing again at weeks 3 and 4 compared with controls (**Figure 3B**). Mean combined histological scores at week 4 for the Scl-NS group was 5.3 ± 0.5 which is consistent with previous reports using this model (25) (**Figure 3C**). Animal weights

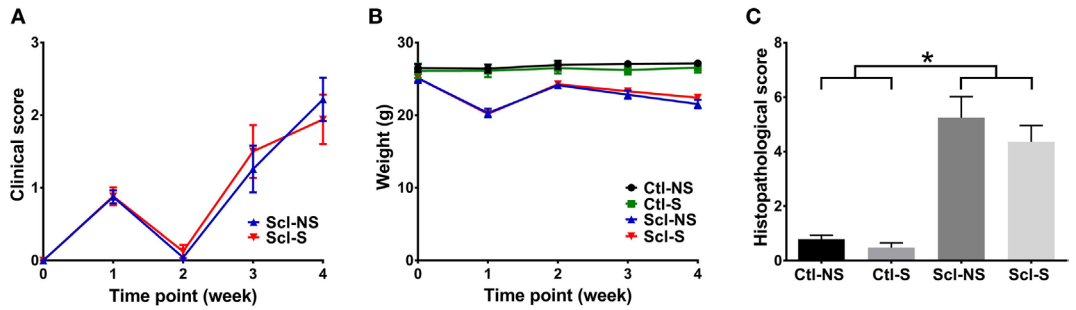

FIGURE 3 | Clinical and histological measures. (A,B): Clinical score **(A)** and animal weight **(B)** over the course of the 4-week experiment. **(C)**: Histological scores at week 4. Significant differences are shown between both sclGvHD/stretch (Scl-S) and sclGvHD/no stretch (Scl-NS) compared to both Con-S and Con-NS groups at week 2 (*$p < 0.05$). There were no significant differences between Scl-S and Scl-NS groups in any of the outcome measures ($N = 12$ mice per group).

TABLE 2 | Repeated measurements at weekly time points.

	Time point (week)	Control/no stretch $N = 12$	Control/stretch $N = 12$	sclGvHD/no stretch $N = 12$	sclGvHD/stretch $N = 12$	p-Value (ANOVA)
Thickness Zone 1 (μm)	1	489.14 ± 13.97^{a}	488.06 ± 17.77^{a}	472.77 ± 16.30^{ab}	462.60 ± 11.35^{b}	0.040
	2	486.50 ± 9.82^{a}	485.15 ± 14.84^{a}	606.08 ± 14.22^{b}	599.06 ± 15.76^{b}	<0.001
	3	491.67 ± 9.27^{a}	479.52 ± 16.30^{a}	554.85 ± 16.26^{b}	503.19 ± 13.50^{a}	<0.001
	4	473.29 ± 17.92	476.96 ± 18.47^{a}	463.04 ± 13.93^{ab}	448.40 ± 16.94^{b}	0.037
Thickness Zone 2 (μm)	1	327.29 ± 11.39^{a}	345.52 ± 16.10^{a}	327.54 ± 16.64^{a}	320.46 ± 9.75^{a}	0.060
	2	319.10 ± 9.27^{a}	320.38 ± 12.27^{a}	410.23 ± 11.06^{b}	410.75 ± 16.69^{b}	<0.001
	3	319.25 ± 12.75^{a}	324.75 ± 14.43^{a}	395.77 ± 15.91^{b}	355.75 ± 13.05^{a}	<0.001
	4	312.06 ± 17.48^{a}	326.40 ± 17.42^{a}	313.35 ± 12.91^{a}	309.46 ± 15.46^{a}	0.120
Thickness Zone 3 (μm)	1	161.17 ± 6.37^{a}	142.54 ± 5.50^{b}	145.23 ± 2.71^{b}	142.15 ± 4.79^{b}	0.040
	2	167.40 ± 4.46^{a}	164.77 ± 4.20^{a}	195.85 ± 8.38^{b}	188.31 ± 6.27^{b}	<0.001
	3	172.42 ± 7.61^{a}	154.77 ± 3.60^{b}	159.08 ± 4.98^{ab}	147.44 ± 4.44^{b}	0.011
	4	161.23 ± 3.70^{a}	150.56 ± 3.78^{ab}	149.69 ± 5.77^{ab}	138.94 ± 5.50^{b}	0.037
Cumulative displacement (μm)	1	429.98 ± 44.92^{a}	432.64 ± 28.59^{a}	381.75 ± 34.95^{a}	364.27 ± 42.33^{a}	0.238
	2	422.20 ± 52.54^{a}	464.33 ± 29.66^{a}	416.84 ± 37.61^{a}	455.58 ± 49.48^{a}	0.629
	3	456.93 ± 35.99^{a}	444.10 ± 33.98^{a}	344.88 ± 31.90^{b}	430.00 ± 30.34^{a}	0.037
	4	457.39 ± 33.13^{ab}	473.83 ± 23.88^{a}	331.28 ± 38.32^{c}	388.45 ± 22.28^{bc}	0.003
Clinical score	1	N/A	N/A	0.88 ± 0.09^{b}	0.88 ± 0.12^{b}	0.961
	2	N/A	N/A	0.04 ± 0.04^{b}	0.13 ± 0.09^{b}	0.864
	3	N/A	N/A	1.26 ± 0.32^{b}	1.50 ± 0.36^{b}	0.524
	4	N/A	N/A	2.22 ± 0.30^{b}	1.94 ± 0.34^{b}	0.378
Weight (g)	1	26.40 ± 0.55^{a}	26.10 ± 0.86^{a}	20.30 ± 0.58^{b}	20.17 ± 0.40^{b}	<0.001
	2	26.90 ± 0.58^{a}	26.46 ± 0.73^{a}	24.13 ± 0.44^{b}	24.26 ± 0.38^{b}	0.001
	3	27.06 ± 0.48^{a}	26.22 ± 0.63^{a}	22.83 ± 0.57^{b}	23.30 ± 0.45^{b}	<0.001
	4	27.13 ± 0.51^{a}	26.53 ± 0.70^{a}	21.53 ± 0.59^{b}	22.41 ± 0.48^{b}	<0.001

Results are expressed as mean ± SE. Means for experimental conditions within each time point. Not sharing a common letter are significantly different ($p < 0.05$, Fisher's protected LSD).

were lower in both Scl groups compared with both control groups at weeks 1–4. Differences in clinical scores, weight, and histological scores between Scl-NS and Scl-S groups were not statistically significant (**Figures 3A–C**; **Table 2**).

Ultrasound Measurement of Tissue Thickness

Figure 4 shows examples of ultrasound and corresponding histology images for control (**Figure 4A**) and sclGvHD (**Figures 4B,C**) mice illustrating the greater dermal thickness in the sclGvHD mice visible with both ultrasound and histology. Ultrasound measurements of Zone 1 (combined skin and subcutaneous tissue), Zone 2 (skin only), and Zone 3 (subcutaneous tissue only), all demonstrated time-dependent differences between the four experimental groups (ANOVA time by group interaction $p = 0.001$) (**Figure 5A**; **Table 2**). Skin and subcutaneous tissue thickness peaked at week 2 in the sclGvHD mice, which is consistent with the presence of early inflammatory edema.

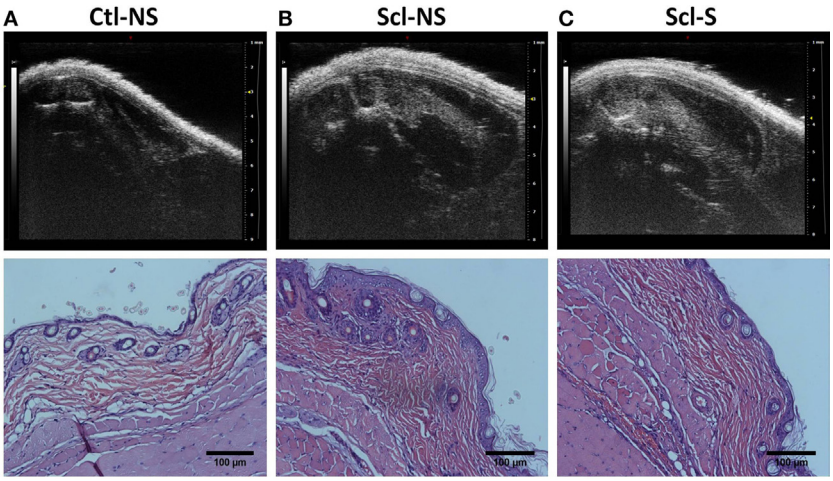

FIGURE 4 | Ultrasound and histology images at week 4. Ultrasound and corresponding histology images were taken from the same location on the back (at the location indicated in **Figure 2A**). **(A)** Control no stretch; **(B)** sclerodermatous graft-versus-host disease (SclGvHD) no stretch; **(C)** sclGvHD-stretch. Histological images show increased dermal collagen density in both non-stretched and stretched sclGvHD mice.

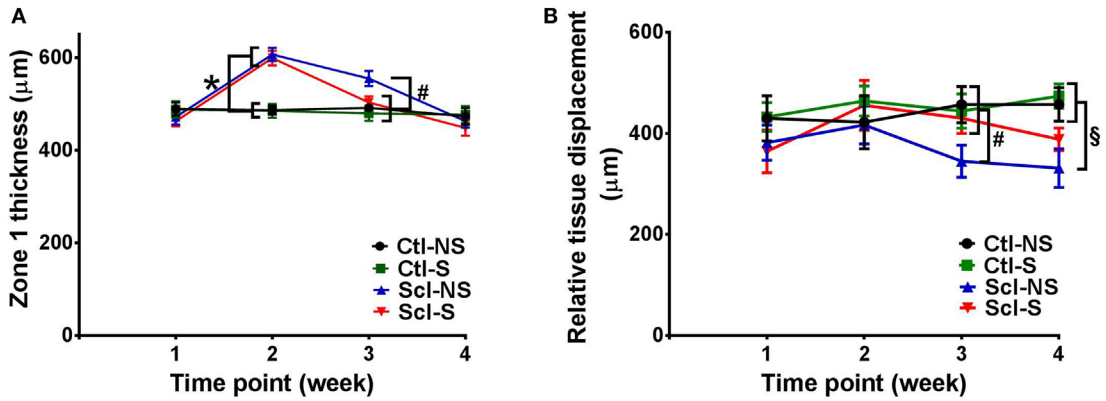

FIGURE 5 | Ultrasound measurement of tissue thickness (A) and relative tissue displacement (B) over the course of the 4-week experiment in the four experimental groups. **(A)** Significant differences ($p < 0.05$) are shown between both sclGvHD/stretch (Scl-S) and sclGvHD/no stretch (Scl-NS) compared to both Ctl-S and Ctl-NS groups at week 2 (*) and between Scl-NS and the other three groups at week 3 (#). **(B)** Significant differences are shown between Scl-NS and the other three groups at week 3 (#) and between the Scl-NS and both control groups at week 4 (¶). Scl-S and Scl-NS were not significantly different at week 4 ($N = 12$ mice per group).

Stretching had a significant effect on Zone 1 (combined skin and subcutaneous tissue) and Zone 2 (skin only) thickness, which were both reduced by 11% in the Scl-S group compared with the Scl-NS group at week 3 (**Figure 5A**; **Table 2**). Thus, while there was no difference between stretch and no stretch at the peak of inflammation (week 2), stretched sclGvHD mice became more similar to controls at week 3.

Ultrasound Measurement of Tissue Mobility

Ultrasound measurement of relative tissue displacement between skin and subcutaneous tissue during passive trunk flexion also showed significant differences between groups (ANOVA $p = 0.01$) (**Figure 5B**; **Table 2**). Although the interaction between group and time was not significant, differences between groups were significant at weeks 3 and 4. At week 3, relative tissue displacement was 26% greater in the Scl-S group compared with the Scl-NS group (**Figure 5B**; **Table 2**). At week 4, relative tissue displacement remained greater in the Scl-S compared with Scl-NS, but this difference was no longer statistically significant (**Figure 5B**; **Table 2**). There were no significant differences between experimental groups in the simple displacements of either skin or subcutaneous tissue during the passive trunk motion, indicating that stretching had a specific impact on the relative inter-layer mobility of tissues rather than the absolute amount of tissue displacement. Thus, as in the thickness measurements, stretching improved tissue mobility such that stretched sclGvHD mice were more similar to controls at week 3 only.

Gene Expression Analysis

At euthanasia (week 4), we measured markers of fibrosis (TGF-β, TIMP1, MMP12, ADAM8) and inflammation (IL4RA, CCL2) that have been previously shown to be upregulated in both sclG-vHD and SSc patients. RNA expression was significantly greater in the Scl-NS compared to the Ctl-NS group for TGF-β $p = 0.006$, TIMP1 $p = 0.012$, MMP12 $p < 0.001$, ADAM8 $p < 0.001$, and CCL2 $p < 0.001$ (**Figure 6**). Stretching significantly reduced the expression of ADAM8 and CCL2 compared with no stretching in sclGvHD mice ($p = 0.011$ and $p < 0.001$, respectively) (**Figures 6E,F**).

In order to further investigate possible anti-inflammatory effects of stretching suggested by the reduction in CCL2 at week 4, we conducted additional experiments in which mice randomined to *in vivo* stretch versus no stretch were euthanized at the peak of inflammation (week 2) for measurement of CCL2 along with additional markers of inflammation and matrix remodeling (COX2, PAK2, PLA2, YAP, CTGF, Adam8, MMP12, TGF-β, IL13, IL13ra1, IL4ra, and TIMP1). Although all markers were elevated in the SclGVHD mice compared with controls, we found no significant differences at week 2 between stretched and NS mice for any of the markers, including CCL2 (data not shown). This suggests that the reduced skin thickness and increased mobility observed at week 3 was not due to an early interruption of the inflammatory cascade.

Correlation Analysis

We did not observe any significant correlation between tissue thickness and either histological score, clinical score, or gene expression measures. However, relative tissue displacement was negatively correlated with both histopathological score ($r = -0.70$, $p = < 0.001$) and ADAM 8 expression in tissues of the back ($r = -0.69$, $p < 0.001$), and ADAM 8 was positively correlated with the histopathological score ($r = 0.77$, $p < 0.001$) (**Figure 7**).

Ex Vivo Stretching Experiments

In order to investigate the possible role of connective tissue fibroblasts in the response to stretching in the sclGvHD model, we conducted experiments in which connective tissue samples from control and sclGvHD mice are stretched *ex vivo*. We previously showed that connective tissue fibroblasts respond to tissue stretch *ex vivo* with cytoskeletal expansion accompanied by a drop in tissue tension (26) and that this fibroblast response is impaired in cross-linked collagen gels (27). We hypothesized that loss of fibroblast responsiveness to stretching may contribute to increased tissue stiffness in sclGvHd, and that stretching *in vivo* may help preserve fibroblast responsiveness as well as tissue mobility. We first tested whether fibroblast responsiveness to stretching *ex vivo* is impaired in sclGvHD compared with controls. We measured fibroblast cross sectional area in tissue explants stretched versus non-stretched *ex vivo* from four groups of mice: control week 2, sclGvHD week 2, control week 4, and sclGvHD week 4 (**Figure 8**). We found that, at week 2, fibroblasts in explants from control and Scl GvHD responded similarly to *ex vivo* stretching (main effect of *ex vivo* stretch $p < 0.001$). However, at week 4, fibroblast expansion was reduced in explants from sclGvHD mice compared with controls (group by stretch interaction $p < 0.01$) (**Figure 9A**). We then tested whether *in vivo* stretching for 10 min/day *in vivo* would prevent the

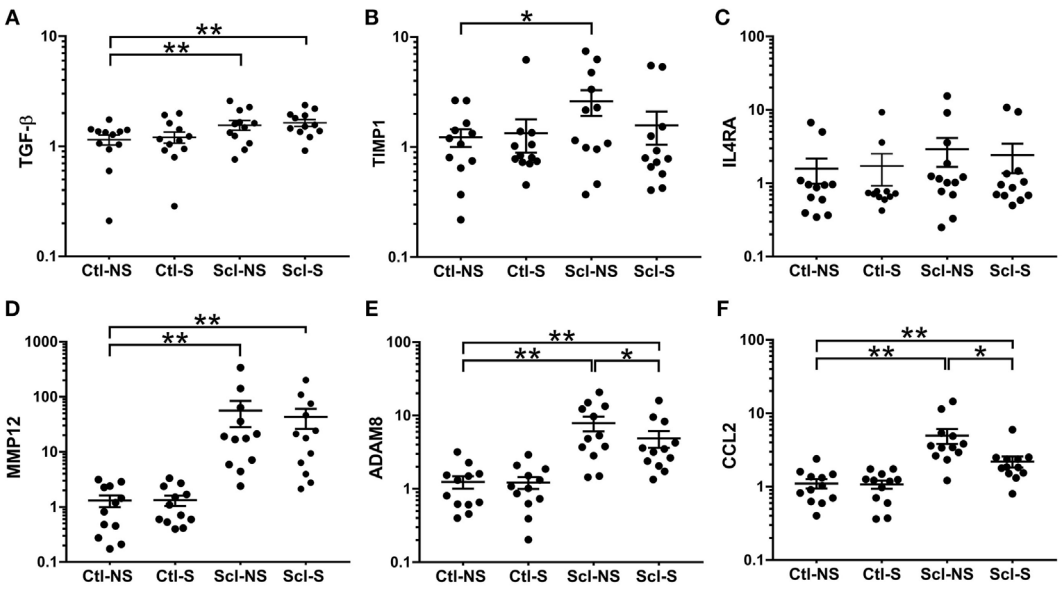

FIGURE 6 | mRNA expression (qPCR) analyses. (A–F): Significance levels for sclGvHD/no stretch and sclGvHD/stretch groups are shown relative to control/no stretch (Ctl-NS) group (*$p < 0.05$, **$p < 0.01$, $N = 12$ mice per group). There were no significant differences between Ctl-NS and Ctl/stretch groups for any of the outcome measures. Results are presented as geometric means and associated SEs, with the *y*-axis reflecting log scale.

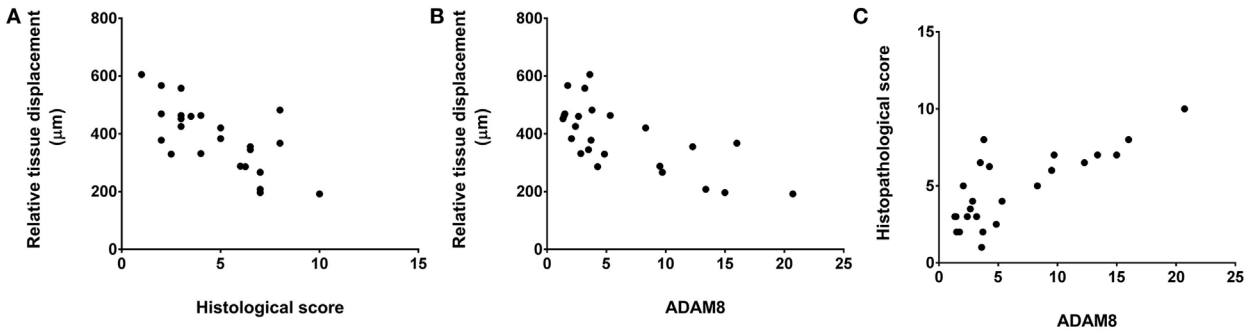

FIGURE 7 | Relationship of relative tissue displacement, histological score, and ADAM8 mRNA expression. Spearman's correlation coefficients were $r = -0.70$, $p \leq 0.001$ **(A)**, $r = -0.69$, $p < 0.001$ **(B)**, and $r = 0.77$, $p < 0.001$ **(C)**.

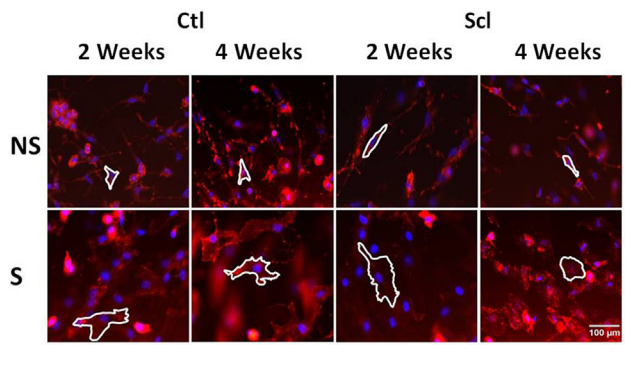

FIGURE 8 | Fibroblast cytoskeletal response to tissue stretch *ex vivo*. Tissue explants from Control and sclerodermatous graft-versus-host disease mice were excised immediately after euthanasia at week 2 or week 4, then stretched (S) versus non-stretched *ex vivo* for 2 h, followed by fixation and staining with phalloidin for measurement of cell body cross-sectional area (outlined as described in Section "Materials and Methods").

loss of fibroblast responsiveness *ex vivo* at week 4 and found no significant difference between mice that were stretched versus non-stretched *in vivo* (**Figure 9B**). Thus, while cytoskeletal expansion and remodeling of connective tissue fibroblasts is clearly impaired in sclGvHD, this response was not improved by *in vivo* stretching. This suggests that fibroblast-mediated tissue relaxation is not part of the mechanism underlying the beneficial effect of stretching.

DISCUSSION

In this study, we show that *in vivo* ultrasound is a valuable technique to monitor skin thickness and subcutaneous tissue mobility in the murine sclGvHD model. In addition, daily stretching produced a measurable beneficial effect since it reduced skin thickness and improved mobility during the fibrotic phase of the model (week 3). However, we found no differences in weight loss, clinical and histological scores between stretch and no stretch groups. A possible interpretation for these results is that our ultrasound findings were unrelated to any meaningful clinical improvement. On the other hand, it is also possible that ultrasound measurements are more sensitive than clinical and histological scores in following the course of the disease, since a marked increase in skin thickness in the sclGvHD mice was detectable with ultrasound at week 2 in the absence of clinical symptoms. This may be because the clinical score focuses on alopecia (and marginally periorbital swelling) which is more externally visible than skin swelling. Furthermore, clinicial scores do not reflect lack of tissue mobility which is one of the main sources of impairment in SSc. Even though clinical and histological scores were not different between stretch and no stretch groups, the correlation between skin mobility and histological scores suggests that skin mobility measured with ultrasound may be a useful and sensitive non-invasive marker in this model.

The mechanisms underlying any beneficial effect of stretching on skin thickness and mobility are at present unclear. Stretching reduced mRNA expression of CCL2 which is an important inflammatory mediator associated with the sclGvHD model (13, 14). The lack of accompanying reduction in clinical symptoms stands in contrast to a previous study using this model in which treatment with CCL2 antibodies completely prevented the development of clinical and tissue pathology (13). However, CCL2 antibodies were administered systemically beginning immediately after cell transfer while, in our study, we only saw stretch-induced reduction of CCL2 at week 4 and not at the peak of inflammation (week 2). It is, therefore, possible that reduction in CCL2 by stretching was not sufficient in magnitude or occurred too late to have a significant impact on the inflammatory process. Furthermore, we did not observe any reduction of inflammatory genes at week 2, suggesting that the reduced skin thickness and increased mobility observed at week 3 was not due to an early interruption of the inflammatory cascade.

Another possibility is that the effect of stretching is not primarily anti-inflammatory, but rather is mechanical in nature. Reduced shear plane mobility of subcutaneous connective tissue can result from a number of interrelated factors, including adhesions between tissue layers and increased connective tissue matrix stiffness due to increased collagen deposition and cross linking. We found no significant reduction in

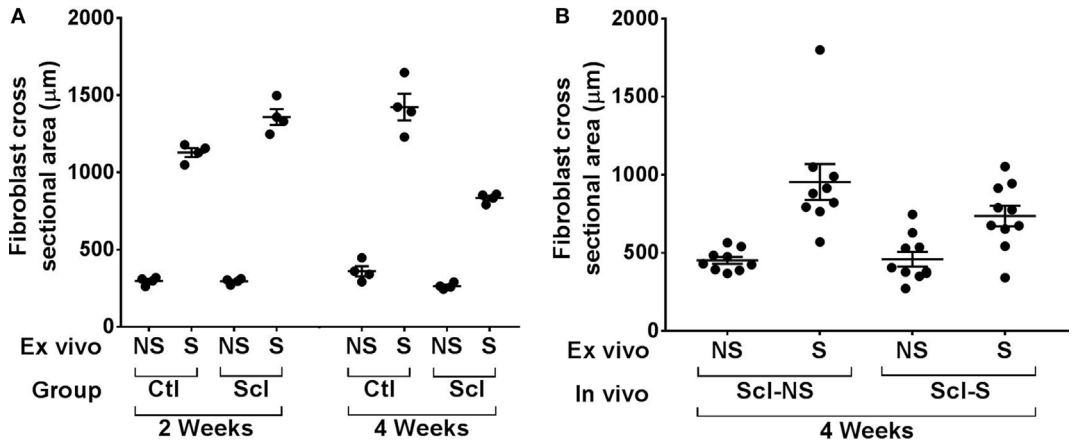

FIGURE 9 | ***Ex vivo* stretching experiments**. **(A)**: Connective tissue explants from control and sclerodermatous graft-versus-host disease (sclGvHD) mice were stretched (S) versus not stretched for 2 h *ex vivo*, then fixed and stained for measurement of fibroblast cross-sectional area as shown in **Figure 8**. Fibroblast response to *ex vivo* tissue stretch was reduced in sclGvHD mice that were euthanized at week 4 but not week 2, compared with controls. **(B)**: In sclGvHD mice, daily *in vivo* stretching did not result in an increased fibroblast responsiveness to *ex vivo* stretching at week 4.

TGF-β, TIMP-1, or MMP-12 with stretching, suggesting that stretching did not directly impact fibrotic matrix remodeling. We also found no improvement of fibroblast responsiveness to tissue stretch *ex vivo* in sclGvHD mice that had been stretched *in vivo*, suggesting that tissue stiffness remained higher than in controls in both stretched and NS sclGvHD mice at week 4. This is consistent with our ultrasound findings showing further reduction in tissue mobility from week 3 to week 4 in both sclGvHD groups compared with controls. On the other hand, although *in vivo* stretching did not fully reverse the pathology, the reduction of ADAM8 mRNA expression in stretched mice and positive correlation of ADAM8, tissue mobility, and histological scores suggests a role for cell–matrix interactions in the effect of stretching, since matricellular proteins of the ADAM family have been implicated in mechanical signaling as well as inflammation (28, 29). Further studies will be needed to specifically examine the contribution of extracellular matrix stiffness and cell–matrix interactions to the effects of *in vivo* stretching.

Although mechanisms are at this point unclear, it is important to note that the observed effects of stretching occurred in the absence of any other treatment. The implication of these preclinical findings is that a systematic investigation of stretching as a therapeutic modality is warranted in patients with SSc. This is particularly important in light of a recent report that only 10% of SSc patients received physical/occupational therapy and that a frequent complaint from patients is that physical therapists are often reluctant to treat patients with SSc (6). The magnitude of improvement in tissue mobility (25%) observed in our study was comparable to improvements in range of motion of joints and other tissues that are considered clinically significant in other conditions (30), as well as the magnitude of clinical improvement typically found with commonly prescribed pharmacological treatments in patients with diffuse sclerodermatous skin involvement (31, 32). Although the presence of deep tissue "friction rubs" has been reported as a clinical sign associated with poor prognosis and was suggested as a routine part of the rheumatologic physical examination (33), there are currently no established methods to quantify the involvement of deep tissues. Dynamic ultrasound imaging has been successfully used in humans to measure the mobility of connective tissues (19), but so far this technique has not been applied to scleroderma. Thus, a next step in the translation of our current results to humans would be the development and validation of a clinical protocol using dynamic ultrasound to first follow the course of the disease, and then quantify the effects of treatments, including stretching.

AUTHOR CONTRIBUTIONS

All the authors reviewed the final version and are accountable for the accuracy and integrity of results. YX contributed to data acquisition, analysis, and interpretation and drafted the manuscript. HL, AA, and LB designed the study, contributed to data analysis and interpretation, and revised the manuscript. KU, SO, IM, and RL contributed to data acquisition and revised the manuscript. GB contributed to the study design, data analysis and interpretation, and revised the manuscript.

ACKNOWLEDGMENTS

The authors thank Fred Roberts of Visualsonics for his assistance in developing the ultrasound imaging and measurement methods used in this study.

FUNDING

This work was supported by the Scleroderma Foundation, The Jiangsu Overseas Research and Training Program (YX), and The Burroughs Wellcome Foundation (AA and KU).

REFERENCES

1. Pattanaik D, Brown M, Postlethwaite BC, Postlethwaite AE. Pathogenesis of systemic sclerosis. *Front Immunol* (2015) 6:272. doi:10.3389/fimmu.2015.00272
2. Clements PJ, Lachenbruch PA, Ng SC, Simmons M, Sterz M, Furst DE. Skin score. A semiquantitative measure of cutaneous involvement that improves prediction of prognosis in systemic sclerosis. *Arthritis Rheum* (1990) 33:1256–63. doi:10.1002/art.1780330828
3. Ho YY, Lagares D, Tager AM, Kapoor M. Fibrosis – a lethal component of systemic sclerosis. *Nat Rev Rheumatol* (2014) 10:390–402. doi:10.1038/nrrheum.2014.53
4. Thaller SR, Cavina C, Kawamoto HK. Treatment of orthognathic problems related to scleroderma. *Ann Plast Surg* (1990) 24:528–33. doi:10.1097/00000637-199006000-00010
5. Willems LM, Vriezekolk JE, Schouffoer AA, Poole JL, Stamm TA, Bostrom C, et al. Effectiveness of nonpharmacologic interventions in systemic sclerosis: a systematic review. *Arthritis Care Res (Hoboken)* (2015) 67:1426–39. doi:10.1002/acr.22595
6. Bassel M, Hudson M, Baron M, Taillefer SS, Mouthon L, Poiraudeau S, et al. Physical and occupational therapy referral and use among systemic sclerosis patients with impaired hand function: results from a Canadian national survey. *Clin Exp Rheumatol* (2012) 30:574–7.
7. Thombs BD, Jewett LR, Assassi S, Baron M, Bartlett SJ, Maia AC, et al. New directions for patient-centred care in scleroderma: the Scleroderma Patient-Centred Intervention Network (SPIN). *Clin Exp Rheumatol* (2012) 30:S23–9.
8. Maddali Bongi S, Del Rosso A, Galluccio F, Tai G, Sigismondi F, Passalacqua M, et al. Efficacy of a tailored rehabilitation program for systemic sclerosis. *Clin Exp Rheumatol* (2009) 27:44–50.
9. Yuen HK, Marlow NM, Reed SG, Mahoney S, Summerlin LM, Leite R, et al. Effect of orofacial exercises on oral aperture in adults with systemic sclerosis. *Disabil Rehabil* (2012) 34:84–9. doi:10.3109/09638288.2011.587589
10. Corey SM, Vizzard MA, Bouffard NA, Badger GJ, Langevin HM. Stretching of the back improves gait, mechanical sensitivity and connective tissue inflammation in a rodent model. *PLoS One* (2012) 7:e29831. doi:10.1371/journal.pone.0029831
11. Bouffard NA, Cutroneo KR, Badger GJ, White SL, Buttolph TR, Ehrlich HP, et al. Tissue stretch decreases soluble TGF-beta1 and type-1 procollagen in mouse subcutaneous connective tissue: evidence from ex vivo and in vivo models. *J Cell Physiol* (2008) 214:389–95. doi:10.1002/jcp.21209
12. Berrueta L, Muskaj I, Olenich S, Butler T, Badger GJ, Colas RA, et al. Stretching impacts inflammation resolution in connective tissue. *J Cell Physiol* (2016) 231(7):1621-7. doi:10.1002/jcp.25263
13. Greenblatt MB, Sargent JL, Farina G, Tsang K, Lafyatis R, Glimcher LH, et al. Interspecies comparison of human and murine scleroderma reveals IL-13 and CCL2 as disease subset-specific targets. *Am J Pathol* (2012) 180:1080–94. doi:10.1016/j.ajpath.2011.11.024
14. Sargent JL, Li Z, Aliprantis AO, Greenblatt M, Lemaire R, Wu MH, et al. Interspecies comparative genomics identifies optimal mouse models of systemic sclerosis. *Arthritis Rheumatol* (2016) 68(8):2003–15. doi:10.1002/art.39658
15. Ruzek MC, Jha S, Ledbetter S, Richards SM, Garman RD. A modified model of graft-versus-host-induced systemic sclerosis (scleroderma) exhibits all major aspects of the human disease. *Arthritis Rheum* (2004) 50:1319–31. doi:10.1002/art.20160
16. Rodnan GP, Lipinski E, Luksick J. Skin thickness and collagen content in progressive systemic sclerosis and localized scleroderma. *Arthritis Rheum* (1979) 22:130–40. doi:10.1002/art.1780220205
17. Tedstone JL, Richards SM, Garman RD, Ruzek MC. Ultrasound imaging accurately detects skin thickening in a mouse scleroderma model. *Ultrasound Med Biol* (2008) 34:1239–47. doi:10.1016/j.ultrasmedbio.2008.01.013
18. Langevin HM, Stevens-Tuttle D, Fox JR, Badger GJ, Bouffard NA, Krag MH, et al. Ultrasound evidence of altered lumbar connective tissue structure in human subjects with chronic low back pain. *BMC Musculoskelet Disord* (2009) 10:151. doi:10.1186/1471-2474-10-151
19. Langevin HM, Fox JR, Koptiuch C, Badger GJ, Greenan-Naumann AC, Bouffard NA, et al. Reduced thoracolumbar fascia shear strain in human chronic low back pain. *BMC Musculoskelet Disord* (2011) 12:203. doi:10.1186/1471-2474-12-203
20. Bishop JH, Fox JR, Maple R, Loretan C, Badger GJ, Henry SM, et al. Ultrasound evaluation of the combined effects of thoracolumbar fascia injury and movement restriction in a porcine model. *PLoS One* (2016) 11:e0147393. doi:10.1371/journal.pone.0147393
21. Manetti M, Guiducci S, Romano E, Bellando-Randone S, Conforti ML, Ibba-Manneschi L, et al. Increased serum levels and tissue expression of matrix metalloproteinase-12 in patients with systemic sclerosis: correlation with severity of skin and pulmonary fibrosis and vascular damage. *Ann Rheum Dis* (2012) 71:1064–72. doi:10.1136/annrheumdis-2011-200837
22. Lafyatis R. Transforming growth factor beta – at the centre of systemic sclerosis. *Nat Rev Rheumatol* (2014) 10:706–19. doi:10.1038/nrrheum.2014.137
23. Urso K, Alvarez D, Cremasco V, Tsang K, Grauel A, Lafyatis R, et al. IL4RA on lymphatic endothelial cells promotes T cell egress during sclerodermatous graft versus host disease. *JCI Insight* (2016) 1:e88057. doi:10.1172/jci.insight.88057
24. Langevin HM, Bouffard NA, Badger GJ, Iatridis JC, Howe AK. Dynamic fibroblast cytoskeletal response to subcutaneous tissue stretch ex vivo and in vivo. *Am J Physiol Cell Physiol* (2005) 288:C747–56. doi:10.1152/ajpcell.00420.2004
25. Ni Z, Olsen JB, Guo X, Zhong G, Ruan ED, Marcon E, et al. Control of the RNA polymerase II phosphorylation state in promoter regions by CTD interaction domain-containing proteins RPRD1A and RPRD1B. *Transcription* (2011) 2:237–42. doi:10.4161/trns.2.5.17803
26. Langevin HM, Bouffard NA, Fox JR, Palmer BM, Wu J, Iatridis JC, et al. Fibroblast cytoskeletal remodeling contributes to connective tissue tension. *J Cell Physiol* (2011) 226:1166–75. doi:10.1002/jcp.22442
27. Abbott RD, Koptiuch C, Iatridis JC, Howe AK, Badger GJ, Langevin HM. Stress and matrix-responsive cytoskeletal remodeling in fibroblasts. *J Cell Physiol* (2013) 228:50–7. doi:10.1002/jcp.24102
28. Wolfsberg TG, Primakoff P, Myles DG, White JM. ADAM, a novel family of membrane proteins containing A disintegrin and metalloprotease domain: multipotential functions in cell-cell and cell-matrix interactions. *J Cell Biol* (1995) 131:275–8. doi:10.1083/jcb.131.2.275
29. Edwards DR, Handsley MM, Pennington CJ. The ADAM metalloproteinases. *Mol Aspects Med* (2008) 29:258–89. doi:10.1016/j.mam.2008.08.001
30. Witthaut J, Bushmakin AG, Gerber RA, Cappelleri JC, Le Graverand-Gastineau MP. Determining clinically important changes in range of motion in patients with Dupuytren's contracture: secondary analysis of the randomized, double-blind, placebo-controlled CORD I study. *Clin Drug Investig* (2011) 31:791–8. doi:10.2165/11592940-000000000-00000
31. Pope JE, Bellamy N, Seibold JR, Baron M, Ellman M, Carette S, et al. A randomized, controlled trial of methotrexate versus placebo in early diffuse scleroderma. *Arthritis Rheum* (2001) 44:1351–8. doi:10.1002/1529-0131(200106)44:6<1351::AID-ART227>3.0.CO;2-I
32. Volkmann ER, Furst DE. Management of systemic sclerosis-related skin disease: a review of existing and experimental therapeutic approaches. *Rheum Dis Clin North Am* (2015) 41:399–417. doi:10.1016/j.rdc.2015.04.004
33. Steen VD, Medsger TA Jr. The palpable tendon friction rub: an important physical examination finding in patients with systemic sclerosis. *Arthritis Rheum* (1997) 40:1146–51. doi:10.1002/art.1780400620

Conflict of Interest Statement: The authors declare that the research was conducted in the absence of any commercial or financial relationships that could be construed as a potential conflict of interest.

frontiers in Immunology

ORIGINAL RESEARCH
published: 06 March 2018
doi: 10.3389/fimmu.2018.00449

Gene Profiling in Patients with Systemic Sclerosis Reveals the Presence of Oncogenic Gene Signatures

Marzia Dolcino[1†], Andrea Pelosi[2†], Piera Filomena Fiore[2], Giuseppe Patuzzo[1], Elisa Tinazzi[1], Claudio Lunardi[1†] and Antonio Puccetti[2,3†]*

[1] Department of Medicine, University of Verona, Verona, Italy, [2] Immunology Area, Pediatric Hospital Bambino Gesù, Rome, Italy, [3] Department of Experimental Medicine – Section of Histology, University of Genova, Genova, Italy

Systemic sclerosis (SSc) is a rare connective tissue disease characterized by three pathogenetic hallmarks: vasculopathy, dysregulation of the immune system, and fibrosis. A particular feature of SSc is the increased frequency of some types of malignancies, namely breast, lung, and hematological malignancies. Moreover, SSc may also be a paraneoplastic disease, again indicating a strong link between cancer and scleroderma. The reason of this association is still unknown; therefore, we aimed at investigating whether particular genetic or epigenetic factors may play a role in promoting cancer development in patients with SSc and whether some features are shared by the two conditions. We therefore performed a gene expression profiling of peripheral blood mononuclear cells (PBMCs) derived from patients with limited and diffuse SSc, showing that the various classes of genes potentially linked to the pathogenesis of SSc (such as apoptosis, endothelial cell activation, extracellular matrix remodeling, immune response, and inflammation) include genes that directly participate in the development of malignancies or that are involved in pathways known to be associated with carcinogenesis. The transcriptional analysis was then complemented by a complex network analysis of modulated genes which further confirmed the presence of signaling pathways associated with carcinogenesis. Since epigenetic mechanisms, such as microRNAs (miRNAs), are believed to play a central role in the pathogenesis of SSc, we also evaluated whether specific cancer-related miRNAs could be deregulated in the serum of SSc patients. We focused our attention on miRNAs already found upregulated in SSc such as miR-21-5p, miR-92a-3p, and on miR-155-5p, miR 126-3p and miR-16-5p known to be deregulated in malignancies associated to SSc, i.e., breast, lung, and hematological malignancies. miR-21-5p, miR-92a-3p, miR-155-5p, and miR-16-5p expression was significantly higher in SSc sera compared to healthy controls. Our findings indicate the presence of modulated genes and miRNAs that can play a predisposing role in the development of malignancies in SSc and are important for a better risk stratification of patients and for the identification of a better individualized precision medicine strategy.

Keywords: systemic sclerosis, cancer, gene expression, miRNA, gene module, protein–protein interaction network

OPEN ACCESS

Edited by:
Raffaele De Palma, Università degli Studi della Campania Luigi Vanvitelli Caserta, Italy

Reviewed by:
Serena Vettori, Università degli Studi della Campania Luigi Vanvitelli Caserta, Italy
Hidenori Ohnishi, Gifu University Hospital, Japan

***Correspondence:**
Claudio Lunardi
claudio.lunardi@univr.it

[†]These authors have contributed equally to this work.

Specialty section:
This article was submitted to Primary Immunodeficiencies, a section of the journal Frontiers in Immunology

Received: *08 November 2017*
Accepted: *20 February 2018*
Published: *06 March 2018*

Citation:
Dolcino M, Pelosi A, Fiore PF, Patuzzo G, Tinazzi E, Lunardi C and Puccetti A (2018) Gene Profiling in Patients with Systemic Sclerosis Reveals the Presence of Oncogenic Gene Signatures. Front. Immunol. 9:449. doi: 10.3389/fimmu.2018.00449

INTRODUCTION

Systemic sclerosis (SSc) is a rare, chronic disease characterized by three pathogenetic hallmarks: vasculopathy, dysregulation of the immune system, and increased extracellular matrix deposition in the skin and internal organs, leading to extended fibrosis and to a remarkable heterogeneity in clinical features and course of the disease, resulting in high morbidity and mortality (1).

Several environmental factors alongside genetic susceptibility and epigenetic mechanisms contribute to the onset of the disease (2–5).

Increased frequency of a few types of cancer, namely breast, lung, and hematologic malignancies in SSc has been reported (6), and it seems to be associated with the presence of particular autoantibodies (7). Moreover, it is worthwhile mentioning that SSc may also be a paraneoplastic disease (8, 9), indicating a strong link between cancer and scleroderma.

Given the high incidence of tumors in patients with SSc, we wanted to assess whether this phenomenon may be supported by a particular gene modulation that can favor cancer development in patients with SSc. Thus, we analyzed transcriptional profiles of peripheral blood mononuclear cells (PBMCs) obtained from patients with SSc to evaluate the presence of modulated genes that are involved in signaling pathways associated with malignancy. Moreover, through a complex network analysis, we verified which pathways could play a pivotal role in cancer development in SSc patients.

Besides environmental and genetic factors, epigenetic mechanisms, such as microRNAs (miRNAs), are believed to play a central role in the pathogenesis of the disease.

microRNAs are a class of small non-coding RNAs that bind 3' untranslated region of messenger RNAs (mRNAs), negatively regulating target gene expression by either the repression of translation or degradation of target mRNAs (10). miRNAs are considered an important class of epigenetics regulators in many basic cellular processes as well as in the vast majority of diseases, including cancer and autoimmunity (11, 12). Little is known about the role of dysregulated expression of miRNAs in the pathogenesis of SSc (13). An altered expression of profibrotic and/or antifibrotic miRNAs has been suggested as an important factor in the development of fibrosis in SSc patients (14). Moreover, increased evidence suggests that serum miRNA levels may be promising biomarkers for the diagnosis, prognosis, and therapeutic approach in SSc (15). Serum levels of miR-21 and miR-92a have been found significantly higher in SSc samples compared to normal controls (16, 17). Their function is implicated in inflammation, in regulation of immune cells (18) and in favoring fibrosis (16, 17).

Since particular miRNAs have been associated with malignancies, we aimed at evaluating whether transcriptional profiles and dysregulation of particular miRNAs are shared by cancer and SSc.

MATERIALS AND METHODS

Patients

We enrolled 30 patients affected by SSc, attending the Unit of Autoimmune Disease at the University Hospital of Verona, and 30 sex and age matched healthy controls. All patients fulfilled the ACR/Eular classification criteria for SSc (19). The distinction between limited (lSSc) and diffuse cutaneous SSc (dSSc) was performed according to the criteria proposed by LeRoy et al. (20). Fifteen of the 30 patients were affected by lSSc and 15 by dSSc. The clinical and demographic features of the patients enrolled in the study are summarized in **Table 1**.

Samples obtained from 10 patients with lSSc, 10 patients with dSSc, and 10 healthy controls were used for the gene expression analysis, whereas samples obtained from all the patients and controls were used for the microRNA study. Blood samples were collected from patients with active disease and in the absence of immunosuppressive therapies.

A written informed consent was obtained by all the participants to the study and the study protocol was approved by the Ethical Committee of the Azienda Ospedaliera Universitaria Integrata di Verona. All the investigations have been performed according to the principles contained in the Helsinki declaration.

Gene Expression Analysis

Blood samples were collected in BD Vacutainer K2EDTA tubes using a 21-gage needle. PBMC were obtained upon stratification on Lympholyte® cell separation density gradient (Cedarlane, Burlington, Canada). Total RNA extraction from PBMC was performed with miRNeasy mini kit following manufacturer's protocol (Qiagen GmbH, Hilden, Germany). cRNA preparation, samples hybridization, and scanning were performed following the Affymetrix (Affymetrix, Santa Clara, CA, USA) provided protocols, by Cogentech Affymetrix microarray unit (Campus IFOM IEO, Milan, Italy). All samples were hybridized on Human Clariom D (Affymetrix) gene chip and were analyzed using the Transcriptome Analysis Console (TAC) 4.0 software (Applied Biosystem, Foster City, CA USA by Thermo Fisher Scientific,

TABLE 1 | Clinical and demographic features of the patients enrolled in the study.

Demographic and clinical features		Systemic sclerosis patients	
		lSSc	Diffuse cutaneous SSc
Patients		15	15
Male/female		2/13	1/15
Mean age (years)		56 ± 15	54 ± 12
Laboratory findings	ANA	14 (93%)	15 (100)
	Anti-centromere	9 (60%)	3 (20%)
	Scl-70	1 (6%)	11 (73%)
Lung involvement	Interstitial disease	4 (26%)	8 (53%)
	Pulmonary arterial hypertension	1 (6%)	2 (13%)
Skin involvement	mRSS	8 ± 3	14 ± 8
	Digital ulcers	5 (33%)	7 (46%)
Video Capillaroscopy	Early	1 (6%)	4 (26%)
	Active	8 (53%)	5 (33%)
	Late	6 (40%)	6 (40%)
Kidney involvement		0 (0%)	1 (6%)
Gastro-intestinal involvement		9 (60%)	14 (93%)

Waltham, MA, USA). The Signal Space Transformation (SST)-Robust Multi-Array Average algorithm (RMA) were applied to background-adjust, normalize, and log-transform signals intensity.

Relative gene expression levels of each transcript were validated applying a one-way analysis of variance (ANOVA) ($p \leq 0.01$) and multiple testing correction. Genes that displayed an expression level at least 1.5 fold different in the test sample versus control sample ($p \leq 0.01$) were submitted both to functional classification, using the Gene Ontology (GO) annotations, and to Pathway analysis, employing the Panther expression analysis tools[1] (21). The enrichment of all pathways and functional classes associated to the differentially expressed genes compared to the distribution of genes included on the Clariom D microarray was analyzed and p values ≤0.05, calculated by the binomial statistical test, were considered as significant enrichment.

Protein–Protein Interaction (PPI) Network Construction and Network Clustering

The Search Tool for the Retrieval of Interacting Genes (STRING version 10.5[2]) is a web-based database which comprises experimental as well as predicted interaction and covers >1,100 completely sequenced organisms (22). DEGs were mapped to the STRING database to detect protein–protein interactions (PPI) pairs that were validated by experimental studies (23) and the corresponding PPI network was constructed. A score of ≥0.7 for each PPI pair was selected to design the PPI network.

To detect high-flow areas (highly connected regions) of the network, we used the CFinder software tool, based on the Clique Percolation Method (CPM) (24). Finally, Cytoscape software (25) was used to define the topology of the built networks.

Cell-Free microRNA Expression in SSc Sera

To isolate cell-free circulating miRNA (cf-miRNA) in serum, we used miRNeasy serum/plasma kit (Qiagen, GmbH, Hilden, Germany). For all the samples, RNA was extracted from 200 µL of serum in accordance with manufacturer's instructions. In order to minimize the technical variation between samples in downstream PCR analysis we added, for all isolations, 0.90 fmol of spike-in non-human synthetic miRNA cel-39-3p into the sample after the addition of the lysis/denaturant buffer to the serum. After extraction, RNA was eluted in 14 µL of nuclease-free water.

Mature miRNA expression was assayed by TaqMan® Advanced miRNA assays chemistry (Applied Biosystems, Foster City, CA, USA). Briefly, 2 µL of serum RNA was reverse transcribed and pre-amplified with TaqMan® Advanced miRNA cDNA synthesis kit following manufacturer's instructions (Applied Biosystems, Foster City, CA, USA). Pre-amplified cDNA was diluted 1/10 in nuclease-free water and 5 µL of diluted cDNA for each replicate were loaded in PCR. 20 µL PCR reactions were composed by 2× Fast Advanced Master Mix and TaqMan® Advanced miRNA assays for hsa-miR-126-3p (477887_mir), hsa-miR-21-5p (477975_mir), hsa-miR-92a-3p (477827_mir), hsa-miR-155a-5p (477927_mir), and hsa-miR-16-5p (477860_mir). Since established consensus house-keeping miRNAs for data normalization are lacking for serum miRNAs, we used cel-39-3p expression (478293_mir) to normalize miRNA expression. Real time PCR were carried out in triplicate on a QuantStudio 6 Flex instrument (Applied Biosystems, Foster City, CA, USA). Expression values were obtained by ΔCt method using QuantStudio Real-time PCR system software v. 1.3.

RESULTS

Gene Array Analysis

In order to gain new insights into the pathogenesis of SSc, we compared the gene expression profiles of PBMC samples obtained from 10 lSSc and 10 dSSc patients with 10 PBMC samples obtained from age and sex matched healthy donors. Raw data have been deposited in the *ArrayExpress* database at EMBL-EBI[3] under accession number E-MTAB-6531.

When we analyzed lSSc samples, we found that 829 differently expressed genes (DEGs) satisfied the Bonferroni-corrected p value criterion ($p \leq 0.01$) and the fold change criterion (FC ≥ |1.5|), displaying robust and statistically significant variation between SSc and healthy controls samples. In particular, 736 and 93 transcripts resulted to be over- and underexpressed, respectively. The complete list of modulated genes can be found in Table S1 in Supplementary Material.

When the same Bonferroni-corrected p value and fold change criteria were used, 456 transcripts were differentially modulated in dSSc patients compared to healthy controls, 327 and 129 transcripts resulted to be up- and downregulated, respectively (Table S2 in Supplementary Material).

The Gene Ontology analysis of modulated genes in lSSc patients, showed that a large number of the modulated transcripts can be ascribed to biological processes that may play a role in SSc, including: apoptotic process, cell proliferation, growth factor and growth factor binding, inflammatory response, immune response, angiogenesis, endothelial cell activation, cell adhesion, and extracellular matrix organization process.

Moreover, a large number of modulated genes were ascribed to well-known signaling pathways encompassing Type I interferon, epidermal growth factor (EGF) receptor, transforming growth factor (TGF)-beta, interleukin, Wnt, glycolysis, platelet derived growth factor (PDGF), FAS, and Phosphoinositide 3 (PI3)-kinase signaling pathway.

Table 2 shows a selection of DEGs within the above-mentioned categories and also includes public gene accession numbers and fold changes.

Among genes involved in apoptosis, we found the upregulation of B-cell lymphoma 2 (BCL2); BCL2-like 1 (BCL2L1); BCL2-like 13 (BCL2L13); mitochondrial fission factor (MFF); translocase of inner mitochondrial membrane 50 homolog (TIMM50), and zinc finger and BTB domain containing 16 (ZBTB16). Interestingly,

[1] http://pantherdb.org/.
[2] http://string-db.org/.
[3] www.ebi.ac.uk/arrayexpress.

TABLE 2 | Selection of modulated genes in lSSc patients versus healthy controls.

ID	Gene symbol	Description	Fold change	*p*-Value	Public gene IDs
Inflammatory response					
TC0400011053.hg.1	CXCL10	Chemokine (C-X-C motif) ligand 10	5.20	0.0043	NM_001565
TC1100009225.hg.1	CXCR5	Chemokine (C-X-C motif) receptor 5	2.54	0.0036	NM_001716
TC1100008341.hg.1	FOLR2	Folate receptor 2	1.90	0.0065	NM_000803
TC0200008675.hg.1	IL18RAP	Interleukin 18 receptor accessory protein	-2.13	0.0027	NM_003853
TC1000009691.hg.1	IL2RA	Interleukin 2 receptor, alpha	2.35	0.0010	NM_000417
TC1900009297.hg.1	TBXA2R	Thromboxane A2 receptor	1.72	0.0043	NM_001060
TC0300011059.hg.1	GPX1	Glutathione peroxidase 1	1.81	0.0016	NM_000581
Apoptotic process					
TC1800008891.hg.1	BCL2	B-cell CLL/lymphoma 2	2.73	0.0012	NM_000633
TC2000008815.hg.1	BCL2L1	BCL2-like 1	1.71	0.0100	NM_001191
TC2200006521.hg.1	BCL2L13	BCL2-like 13 (apoptosis facilitator)	1.83	0.0076	NM_001270726
TC0200010972.hg.1	MFF	Mitochondrial fission factor	1.78	0.0012	NM_001277061
TC1900011729.hg.1	TIMM50	Translocase of inner mitochondrial membrane 50 homolog	2.12	<0.0001	NM_001001563
TC1100009101.hg.1	ZBTB16	Zinc finger and BTB domain containing 16	2.04	0.0033	NM_001018011
Immune response					
TC0800006746.hg.1	BLK	BLK proto-oncogene, Src family tyrosine kinase	2.60	0.0060	NM_001715
TC1900008166.hg.1	CD79A	CD79a molecule	3.45	0.0008	NM_001783
TC0600011491.hg.1	HLA-DRB5	Major histocompatibility complex, class II, DR β 5	44.50	0.0022	NM_002125
TC1400010492.hg.1	IGHV4-28	Immunoglobulin heavy variable 4-28	14.36	0.0076	AM233776.1
TC1400010806.hg.1	IGHV5-51	Immunoglobulin heavy variable 5-51	9.27	0.0001	FN550293.1
TS00000553.hg.1	IGKV1-27	Immunoglobulin kappa variable 1-27	12.72	0.0016	DQ101172.1
TC0200008384.hg.1	IGKV2D-29	Immunoglobulin kappa variable 2D-29	4.21	0.0030	DQ101153.1
TC2200006771.hg.1	IGLV1-50	Immunoglobulin lambda variable 1-50	4.80	0.0150	FM206563.1
TC1600007312.hg.1	IL4R	Interleukin 4 receptor	3.02	<0.0001	NM_000418
TC1600011368.hg.1	LAT	Linker for activation of T-cells	2.50	0.0001	NM_001014987
TC2200009231.hg.1	MIF	Macrophage migration inhibitory factor	2.27	0.0005	NM_002415
TC1100007771.hg.1	MS4A1	Membrane-spanning 4-domains, subfamily A, 1	2.33	0.0080	NM_021950
TC0300007067.hg.1	MYD88	Myeloid differentiation primary response 88	2.20	0.0008	NM_001172566
TC2200008183.hg.1	VPREB3	Pre-B lymphocyte 3	2.42	0.0090	NM_013378
TC0300013859.hg.1	CD200	CD200 molecule	4.02	<0.0001	NM_001004196
Angiogenesis					
TC1500010429.hg.1	CIB1	Calcium and integrin binding 1 (calmyrin)	2.56	<0.0001	NM_001277764
TC1700012274.hg.1	ITGB3	Integrin beta 3	4.29	0.0030	NM_000212
TC0700009977.hg.1	PDGFA	Platelet-derived growth factor alpha polypeptide	1.70	0.0041	NM_002607
TC1700008661.hg.1	PRKCA	Protein kinase C, alpha	1.73	0.0012	NM_002737
Endothelial cell activation					
TC0400011053.hg.1	CXCL10	Chemokine (C-X-C motif) ligand 10	5.24	0.0050	NM_001565
TC0300011485.hg.1	FOXP1	Forkhead box P1	1.61	0.0070	NM_001012505
TC1400008684.hg.1	PRMT5	Protein arginine methyltransferase 5	1.78	<0.0001	NM_001039619
TC0100016357.hg.1	SELP	Selectin P	2.66	0.0039	NM_003005
Cell adhesion					
TC1100006494.hg.1	CD151	CD151 molecule	1.52	0.0010	NM_001039490
TC1700011435.hg.1	ICAM2	Intercellular adhesion molecule 2	1.56	0.0046	NM_000873
TC1300009165.hg.1	PCDH9	Protocadherin 9	1.62	0.0028	NM_020403
TC1700012274.hg.1	ITGB3	Integrin beta 3	4.29	0.0024	NM_000212
TC1200010794.hg.1	ITGB7	Integrin beta 7	2.10	0.0050	NM_000889
Extracellular matrix organization					
TC0100010863.hg.1	LAMC1	Laminin, gamma 1 (formerly LAMB2)	2.06	0.0074	NM_002293
TC0600008462.hg.1	COL19A1	Collagen, type XIX, alpha 1	2.94	0.0012	NM_001858
TC2000008678.hg.1	CST3	Cystatin C	2.27	0.0030	NM_000099
TC0600006873.hg.1	BMP6	Bone morphogenetic protein 6	2.83	0.0023	NM_001718
TC0500012519.hg.1	SPARC	Secreted protein, acidic, cysteine-rich	3.56	0.0012	NM_001309443
Cell proliferation					
TC0800008845.hg.1	MYC	MYC proto-oncogene, bHLH transcription factor	2.05	0.0065	NM_002467
TC1900010696.hg.1	AKT2	v-Akt murine thymoma viral oncogene homolog 2	2.36	<0.0001	NM_001243027
TC0600007862.hg.1	PIM1	Pim-1 proto-oncogene, serine/threonine kinase	2.15	0.0122	NM_001243186
TC0200015887.hg.1	CUL3	Cullin 3	-1.54	0.0008	NM_001257197
TC0600011809.hg.1	CCND3	Cyclin D3	1.93	<0.0001	NM_001136017
TC1400010085.hg.1	TCL1A	T-cell leukemia/lymphoma 1 A	6.87	<0.0001	NM_001098725

(*Continued*)

TABLE 2 | Continued

ID	Gene symbol	Description	Fold change	*p*-Value	Public gene IDs
Growth factor and growth factor binding					
TC0700009977.hg.1	PDGFA	Platelet-derived growth factor alpha polypeptide	1.66	0.0013	NM_002607
TC0300007067.hg.1	MYD88	Myeloid differentiation primary response 88	2.04	0.0004	NM_001172566
TC0600006873.hg.1	BMP6	Bone morphogenetic protein 6	2.92	0.0041	NM_001718
Type I interferon signaling pathway					
TC0100015921.hg.1	ADAR	Adenosine deaminase, RNA-specific	1.84	0.0001	NM_001025107
TC0600007530.hg.1	HLA-E	Major histocompatibility complex, class I, E	1.72	0.0003	NM_005516
TC0600007487.hg.1	HLA-G	Major histocompatibility complex, class I, G	1.94	0.0015	NM_002127
TC0100013445.hg.1	IFI6	Interferon, alpha-inducible protein 6	1.83	0.0066	NM_002038
TC1400010584.hg.1	IRF9	Interferon regulatory factor 9	1.82	0.0031	NM_006084
TC1500008232.hg.1	ISG20	Interferon stimulated exonuclease gene 20 kDa	2.52	0.0001	NM_001303233
TC0300007067.hg.1	MYD88	Myeloid differentiation primary response 88	2.13	0.0006	NM_001172566
TC1200012708.hg.1	OAS1	2-5-Oligoadenylate synthetase 1	2.46	0.0108	NM_001032409
TC1200010908.hg.1	STAT2	Signal transducer and activator of transcription 2	1.58	0.0028	NM_005419
TC0400011053.hg.1	CXCL10	Chemokine (C-X-C motif) ligand 10	5.23	0.0040	NM_001565
TC1400010721.hg.1	PSME2	Proteasome activator subunit 2; microRNA 7703	1.70	0.0010	NM_002818
Epidermal growth factor receptor signaling pathway					
TC1900010696.hg.1	AKT2	v-Akt murine thymoma viral oncogene homolog 2	2.37	<0.0001	NM_001243027
TC1900006864.hg.1	MAP2K7	Mitogen-activated protein kinase kinase 7	2.24	0.0041	NM_001297555
TC0200008742.hg.1	NCK2	NCK adaptor protein 2	2.54	<0.0001	NM_001004720
TC1200009071.hg.1	PEBP1	Phosphatidylethanolamine binding protein 1	1.68	0.0007	NM_002567
Transforming growth factor-beta signaling pathway					
TC0600006873.hg.1	BMP6	Bone morphogenetic protein 6	2.91	0.0023	NM_001718
TC0600013126.hg.1	PTPRK	Protein tyrosine phosphatase, receptor type, K	3.07	0.0033	NM_001291983
TC1600009200.hg.1	TRAP1	TNF receptor-associated protein 1	1.96	0.0050	NM_001272049
TC1900011636.hg.1	UBE2M	Ubiquitin-conjugating enzyme E2M	1.73	0.0046	NM_003969
Interleukin signaling pathway					
TC1000009691.hg.1	IL2RA	Interleukin 2 receptor, alpha	2.46	0.0010	NM_000417
TC1600007312.hg.1	IL4R	Interleukin 4 receptor	2.94	<0.0001	NM_000418
TC0800008845.hg.1	MYC	MYC proto-oncogene, bHLH transcription factor	2.13	0.0065	NM_002467
TC0 × 00010196.hg.1	RPS6KA6	Ribosomal protein S6 kinase, 90 kDa, polypeptide 6	2.02	0.0012	NM_014496
TC1200010908.hg.1	STAT2	Signal transducer and activator of transcription 2	1.54	0.0022	NM_005419
Wnt signaling pathway					
TC1900009240.hg.1	GNG7	Guanine nucleotide binding protein, gamma 7	2.42	0.0010	NM_052847
TC0800008845.hg.1	MYC	MYC proto-oncogene, bHLH transcription factor	2.16	0.0066	NM_002467
TC1800007805.hg.1	NFATC1	Nuclear factor of activated T-cells, 1	2.02	0.0042	NM_001278669
TC0300012807.hg.1	SIAH2	Siah E3 ubiquitin protein ligase 2	1.94	0.0011	NM_005067
TC1900009176.hg.1	TCF3	Transcription factor 3	1.93	0.0032	NM_001136139
TC0900010543.hg.1	TLE1	Transducin-like enhancer of split 1 [E(sp1) homolog]	2.13	0.0012	NM_001303103
Glycolysis					
TC1000007891.hg.1	HK1	Hexokinase 1	1.91	0.0011	NM_000188
TC2100007355.hg.1	PFKL	Phosphofructokinase, liver	1.86	0.0030	NM_001002021
TC1500009952.hg.1	PKM	Pyruvate kinase, muscle	1.63	0.005	NM_001206796
TC1200006649.hg.1	TPI1	Triosephosphate isomerase 1	1.54	0.0029	NM_000365
Platelet derived growth factor (PDGF) signaling pathway					
TC1900010696.hg.1	AKT2	v-Akt murine thymoma viral oncogene homolog 2	2.34	<0.0001	NM_001243027
TC0 × 00009069.hg.1	ARHGAP6	Rho GTPase activating protein 6	2.54	0.0052	NM_001287242
TC0800008845.hg.1	MYC	MYC proto-oncogene, bHLH transcription factor	2.05	0.0080	NM_002467
TC0200008742.hg.1	NCK2	NCK adaptor protein 2	2.53	<0.0001	NM_001004720
TC0700009977.hg.1	PDGFA	Platelet-derived growth factor alpha polypeptide	1.52	0.0027	NM_002607
FAS signaling pathway					
TC1900010696.hg.1	AKT2	v-Akt murine thymoma viral oncogene homolog 2	2.32	<0.0001	NM_001243027
TC0800009239.hg.1	CYC1	Cytochrome c-1	1.81	0.0066	NM_001916
TC0900012167.hg.1	GSN	Gelsolin	1.66	0.0041	NM_000177
TC0100017528.hg.1	PARP1	Poly(ADP-ribose) polymerase 1	1.72	0.0012	NM_001618
TC0300007454.hg.1	PARP3	Poly(ADP-ribose) polymerase family member 3	2.05	0.0010	NM_001003931
Phosphoinositide 3 kinase signaling pathway					
TC1900010696.hg.1	AKT2	v-Akt murine thymoma viral oncogene homolog 2	2.40	<0.0001	NM_001243027
TC1300008688.hg.1	FOXO1	Forkhead box O1	2.03	0.0008	NM_002015
TC1500009452.hg.1	GNB5	Guanine nucleotide binding protein (G protein), β5	1.65	0.0023	NM_006578
TC1100008136.hg.1	RPS6KB2	Ribosomal protein S6 kinase, 70 kDa, polypeptide 2	1.72	0.0010	NM_003952

TIMM50 is an anti-apoptotic gene that has been involved in breast cancer cell proliferation (26).

The upregulation of apoptotic molecules was paralleled by the overexpression of genes involved in cell proliferation including MYC proto-oncogene, bHLH transcription factor (MYC); v-akt murine thymoma viral oncogene homolog 2 (AKT2); Pim-1 proto-oncogene, serine/threonine kinase (PIM); cyclin D3 (CCND3), and T-cell leukemia/lymphoma 1 A (TCL1A).

Interestingly, all these molecules have been previously associated to different type of cancer (27–30). Moreover, we found downregulation for cullin 3 (CUL3) a tumor suppressor molecule (31). All these observations may suggest that a dysregulation of proliferative genes in patients with SSc may predispose to the development of malignancies.

We also found upregulation of growth factors encoding molecules such as platelet-derived growth factor alpha polypeptide (PDGFA), bone morphogenetic factor 6 (BM6), and myeloid differentiation primary response 88 (MYD88) a fibrogenic molecule that controls pericyte migration and trans-differentiation of endothelial cells to myofibroblasts (32).

Chronic inflammation is a feature of SSc; therefore, the upregulation of genes involved in the inflammatory response, including chemokine (C-X-C motif) ligand 10 (CXCL10), chemokine (C-X-C motif) receptor 5 (CXCR5), folate receptor 2 (FOLR2), interleukin 2 receptor, alpha (IL2RA), thromboxane A2 receptor (TBXA2R), and glutathione peroxidase 1 (GPX1), is not surprising.

Scleroderma, like other autoimmune connective tissue diseases, is characterized by immune system alterations and the results of our analysis also highlighted this aspect, showing a modulation of a large number of genes involved in immune response. A selection of these molecules is reported in **Table 2** and includes: BLK proto-oncogene, Src family tyrosine kinase; CD79a molecule, immunoglobulin-associated alpha (CD79A); major histocompatibility complex, class II, DR beta 5 (HLA-DRB5); immunoglobulin heavy variable 4-28 (IGHV4-28); immunoglobulin heavy variable 5-51 (IGHV5-51); (IGKV1-27); immunoglobulin kappa variable 2D-29; immunoglobulin lambda variable 1-50 (IGLV1-50); interleukin 4 receptor (IL4R), linker for activation of T-cells (LAT); macrophage migration inhibitory factor (MIF); membrane-spanning 4-domains, subfamily A, member 1 (MS4A1); myeloid differentiation primary response 88 (MYD88); pre-B lymphocyte 3 (VPREB3), and CD200 molecule (CD200). Among the abovementioned molecules, MIF has been described as a lung metastasis inducer (33) and CD200 has been involved in the development of breast cancer metastasis (34) and of myeloid leukemia (35).

The initial stages of SSc are accompanied by an angiogenic response to tissue ischemia and vascular damage, that is later replaced by a deficient wound healing and by fibrosis (36). Indeed, several genes involved in angiogenesis were upregulated in lSSc samples including calcium and integrin binding 1 (CIB1); integrin beta 3 (ITGB3), platelet-derived growth factor alpha polypeptide (PDGFA), and protein kinase C, alpha (PRKCA). Interestingly, PDGF stimulates tumor cells, promotes angiogenesis, and the development of cancer associated fibroblasts (37) leading to tumor progression. In addition, aberrant expression of PKCA is associated with a range of malignancies and has recently become a target for anti-cancer therapies (38).

The upregulation of genes such as chemokine (C-X-C motif) ligand 10 (CXCL10), forkhead box P1(FOXP1), protein arginine methyltransferase 5(PRMT5), and selectin P (SELP) is consistent with the endothelial cells activation that is typical of SSc and is accompanied by the overexpression of cell adhesion molecules involved in endothelial cells and leukocytes interactions as well as in blood cells extravasation. We indeed found upregulation for intercellular adhesion molecule 2 (ICAM2), protocadherin 9 (PCDH9), integrin beta 3 (ITGB3), integrin beta 7 (ITGB7), and CD151 molecule that, importantly, is an emerging possible poor prognostic factor for solid tumors (39).

Systemic sclerosis is characterized by connective tissue fibrosis of skin and internal organs that is sustained by extracellular matrix (ECM) remodeling (40). Accordingly, we found an increased expression of transcripts that play a role in ECM organization including laminin gamma 1 (LAMC1), collagen, type XIX (COL19A1), bone morphogenetic protein 6 (BMP6), cystatin C (CST3), and secreted protein, acidic, cysteine-rich (SPARC), a secreted protein that is overexpressed in the fibroblasts of skin biopsy from patients with SSc (41). Noteworthy, remodeling of the stromal ECM by cancer-associated fibroblasts is crucial for tumor cell migration and invasion (42) and SPARC has been associated to these events (43). Interestingly, an elevated preoperative CST3 level was demonstrated to be related with worse survival in patients with renal cell carcinoma (44).

The pathway enrichment analysis that we performed to find signaling network that were overrepresented by modulated genes in lSSc samples, showed an enrichment in apoptosis, glycolysis, PDGF, 5HT4 type receptor, Fas cell surface death receptor (FAS), histamine H2 receptor, serine glycine biosynthesis, beta 3 adrenergic receptor, angiotensin (through G proteins and beta-arrestin), and interleukin signaling pathways (**Table 3**).

Interestingly, several of the abovementioned enriched pathways are involved in cancer development.

Other modulated transcripts belong to the epidermal growth factor (EGF), transforming growth factor (TGF) beta, Wnt, and PI3 kinase signalings, all involved not only in the development of the SSc associated fibrosis (45, 46) but also in cancer development (47–50). In particular, we observed overexpression of the AKT2 member of the EGF signaling pathway and of the FOXO1 component of the PI3K pathway. The deregulation of these genes

TABLE 3 | Pathways enriched in genes modulated in lSSc samples.

Panther pathways	*p*-Value
Apoptosis signaling pathway (P00006)	<0.01
Glycolysis (P00024)	<0.01
Platelet derived growth factor signaling pathway (P00047)	<0.01
5HT4 type receptor mediated signaling pathway (P04376)	0.01
FAS signaling pathway (P00020)	0.01
Histamine H2 receptor mediated signaling pathway (P04386)	0.01
Serine glycine biosynthesis (P02776)	0.02
Beta3 adrenergic receptor signaling pathway (P04379)	0.02
Angiotensin II-stimulated signaling through G proteins and beta-arrestin (P05911)	0.03
Interleukin signaling pathway (P00036)	0.05

has been associated with tumor progression and metastatic spread (29, 51).

The functional classification of DEGs in dSSc samples shows that they reflects the gene modulation observed in lSSC samples (see **Table 4**).

The apoptosis functional class accounted for several upregulated transcripts namely apoptosis enhancing nuclease (AEN), B-cell CLL/lymphoma 2 (BCL2), B-cell CLL/lymphoma 7 C (BCL7C), signal transducer and activator of transcription 1 (STAT1), TNF receptor-associated factor 2 (TRAF2), and translocase of inner

TABLE 4 | Selection of modulated genes in diffuse SSc patients versus healthy controls.

ID	Gene symbol	Description	Fold change	*p*-Value	Public gene IDs
Apoptosis					
TC1500008231.hg.1	AEN	Apoptosis enhancing nuclease	2.04	0.0024	NM_022767
TC1800008891.hg.1	BCL2	B-cell CLL/lymphoma 2	1.90	0.0090	NM_000633
TC1600009992.hg.1	BCL7C	B-cell CLL/lymphoma 7 C	1.56	0.0101	NM_001286526
TC0200015242.hg.1	STAT1	Signal transducer and activator of transcription 1	2.40	0.0042	NM_007315
TC1900011729.hg.1	TIMM50	Translocase of inner mitochondrial membrane 50	1.76	0.0024	NM_001001563
TC0900009242.hg.1	TRAF2	TNF receptor-associated factor 2	1.52	0.0089	NM_021138
Cell proliferation					
TC0300009916.hg.1	HES1	Hes family bHLH transcription factor 1	2.03	<0.0001	NM_005524
TC0900007863.hg.1	CKS2	CDC28 protein kinase regulatory subunit 2	1.50	0.0066	NM_001827
TC0200015887.hg.1	CUL3	Cullin 3	-1.94	0.0068	NM_001257197
TC0600011809.hg.1	CCND3	Cyclin D3	1.56	0.0007	NM_001136017
TC0800008845.hg.1	MYC	MYC proto-oncogene, bHLH transcription factor	2.09	0.0072	NM_002467
TC1900010696.hg.1	AKT2	v-Akt murine thymoma viral oncogene homolog 2	1.96	0.0012	NM_001243027
TC0600007862.hg.1	PIM1	Pim-1 proto-oncogene, serine/threonine kinase	2.12	0.0012	NM_001243186
Growth factor and growth factor binding					
TC1900011707.hg.1	GPI	Glucose-6-phosphate isomerase	1.82	0.0016	NM_000175
TC0300007067.hg.1	MYD88	Myeloid differentiation primary response 88	2.50	<0.0001	NM_001172566
TC1100011258.hg.1	FIBP	Fibroblast growth factor intracellular binding protein	1.70	0.0092	NM_004214
Inflammatory response					
TC0400011053.hg.1	CXCL10	Chemokine (C-X-C motif) ligand 10	6.69	0.0001	NM_001565
TC0400011054.hg.1	CXCL11	Chemokine (C-X-C motif) ligand 11	2.01	0.0023	NM_001302123
TC1100009225.hg.1	CXCR5	Chemokine (C-X-C motif) receptor 5	3.31	0.0066	NM_001716
TC0 × 00009667.hg.1	FCGR1B	Fc fragment of IgG, high affinity Ib, receptor (CD64)	2.52	0.0076	NM_001004340
TC1400009239.hg.1	FCGR3A	Fc fragment of IgG, low affinity IIIa, receptor (CD16a)	2.00	0.0012	NM_000569
TC1600011368.hg.1	LAT	Linker for activation of T-cells	1.80	0.0042	NM_001014987
TC1900009134.hg.1	PTGER4	Prostaglandin E receptor 4 (subtype EP4)	2.11	0.0020	NM_000958
Immune response					
TC1700009612.hg.1	CD79B	CD79b molecule immunoglobulin-associated beta	2.80	0.0020	NM_000626
TC1100011888.hg.1	CR2	Complement component receptor 2	1.90	0.0015	NM_001006658
TC1900011707.hg.1	FOXP3	Forkhead box P3	2.01	0.0066	NM_001114377
TC0600007530.hg.1	HLA-A	Major histocompatibility complex, class I, A	2.11	0.0002	NM_001242758
TC0600007487.hg.1	HLA-B	Major histocompatibility complex, class I, B	1.54	0.0022	D83043.1
TC1700012468.hg.1	HLA-E	Major histocompatibility complex, class I, E	1.66	0.0034	NM_005516
TC1700007931.hg.1	HLA-G	Major histocompatibility complex, class I, G	1.52	0.0045	NM_002127
TC1100008330.hg.1	IGHV3-66	Immunoglobulin heavy variable 3-66	3.50	0.0060	EU667609.1
TC1600007312.hg.1	IGHV4-61	Immunoglobulin heavy variable 4-61	3.51	0.0027	FN550331.1
TC1400010584.hg.1	IL4R	Interleukin 4 receptor	2.02	<0.0001	NM_000418
TC1500008668.hg.1	LAT	Linker for activation of T-cells	1.97	0.0011	NM_001014987
TC1100013178.hg.1	LST1	Leukocyte specific transcript 1	2.11	0.0052	NM_007161
TC1200008920.hg.1	MYD88	Myeloid differentiation primary response 88	2.09	0.0006	NM_001172566
TC1900011255.hg.1	RSAD2	Radical S-adenosyl methionine domain containing 2	8.34	0.0001	NM_080657
TC1000008236.hg.1	TAP1	Transporter 1, ATP-binding cassette, sub-family B	2.00	0.0017	NM_001292022
Angiogenesis					
TC1500010429.hg.1	CIB1	Calcium and integrin binding 1 (calmyrin)	2.08	0.0008	NM_001277764
TC1900011707.hg.1	GPI	Glucose-6-phosphate isomerase	1.50	0.0022	NM_000175
TC1700012468.hg.1	HN1	Hematological and neurological expressed 1	2.15	0.0001	NM_001002032
TC0700011770.hg.1	KRIT1	KRIT1, ankyrin repeat containing	−2.03	0.0054	NM_001013406
Endothelial cell activation					
TC1100009225.hg.1	CXCL10	Chemokine (C-X-C motif) ligand 10	5.94	0.0004	NM_001565
TC0600006967.hg.1	EDN1	Endothelin 1	2.23	0.0042	NM_001168319

(*Continued*)

TABLE 4 | Continued

ID	Gene symbol	Description	Fold change	*p*-Value	Public gene IDs
Extracellular matrix organization					
TC1900006470.hg.1	BSG	Basigin	2.05	0.0022	NM_001728
TC2000008678.hg.1	CST3	Cystatin C	2.13	0.0014	NM_000099
TC0800010204.hg.1	ADAM2	ADAM metallopeptidase domain 2	1.56	0.0084	NM_001278114
Type I interferon signaling pathway					
TC0100015921.hg.1	ADAR	Adenosine deaminase, RNA-specific	1.94	0.0006	NM_001025107
TC1700007931.hg.1	IFI35	Interferon-induced protein 35	1.70	0.0053	NM_005533
TC0100013445.hg.1	IFI6	Interferon, alpha-inducible protein 6	4.00	<0.0001	NM_002038
TC1000008400.hg.1	IFIT1	Interferon-induced protein with tetratricopeptide repeats 1	7.03	0.0030	NM_001270927
TC1000008396.hg.1	IFIT2	Interferon-induced protein with tetratricopeptide repeats 2	13.27	<0.0001	NM_001547
TC1000008397.hg.1	IFIT3	Interferon-induced protein with tetratricopeptide repeats 3	18.12	0.0010	NM_001031683
TC1100009657.hg.1	IFITM3	Interferon induced transmembrane protein 3	2.11	0.0008	NM_021034
TC0500012017.hg.1	IRF1	Interferon regulatory factor 1	1.73	0.0063	NM_002198
TC1400010584.hg.1	IRF9	Interferon regulatory factor 9	1.80	0.0007	NM_006084
TC0100006483.hg.1	ISG15	ISG15 ubiquitin-like modifier	2.36	0.0011	NM_005101
TC1500008232.hg.1	ISG20	Interferon stimulated exonuclease gene 20 kDa	2.00	0.0021	NM_001303233
TC0300007067.hg.1	MYD88	Myeloid differentiation primary response 88	2.27	0.0001	NM_001172566
TC1200012708.hg.1	OAS1	2-5-oligoadenylate synthetase 1	3.95	0.0004	NM_001032409
TC0200016402.hg.1	RSAD2	Radical S-adenosyl methionine domain containing 2	8.23	0.0003	NM_080657
Ras protein signal transduction					
TC0700007367.hg.1	DBNL	Drebrin-like	2.02	0.0027	NM_001014436
TC0300007432.hg.1	MAPKAPK3	Mitogen-activated protein kinase(PK)-activated PK 3	1.94	0.0031	NM_001243925
TC1600011368.hg.1	LAT	Linker for activation of T-cells	1.76	0.0020	NM_001014987
TC2200008641.hg.1	RAC2	Rho family, small GTP binding protein Rac2	1.88	0.0066	NM_002872
TC0100018463.hg.1	RHOC	Ras homolog family member C	2.59	0.0041	NM_001042678
p53 pathway					
TC2100008385.hg.1	SUMO3	Small ubiquitin-like modifier 3	2.44	0.0031	NM_001286416
TC1900007688.hg.1	CCNE1	Cyclin E1	1.70	0.0066	NM_001238
TC0900009242.hg.1	TRAF2	TNF receptor-associated factor 2	1.73	0.0043	NM_021138
TC1900010696.hg.1	AKT2	v-akt murine thymoma viral oncogene homolog 2	1.77	0.0002	NM_001243027
TC1900007688.hg.1	CCNE1	Cyclin E1	1.83	0.0027	NM_001238
JAK-STAT cascade					
TC0300007256.hg.1	CCR2	Chemokine (C-C motif) receptor 2	–3.18	0.0080	NM_001123041
TC0300009916.hg.1	HES1	Hes family bHLH transcription factor 1	2.08	0.0011	NM_005524
TC1200010908.hg.1	STAT2	Signal transducer and activator of transcription 2	2.04	0.0010	NM_005419
TC0200015242.hg.1	STAT1	Signal transducer and activator of transcription 1	2.56	0.0034	NM_007315
Wnt signaling pathway					
TC1400006718.hg.1	PSME1	Proteasome activator subunit 1	2.00	0.0013	NM_001281528
TC0600014110.hg.1	PSMB9	Proteasome subunit beta 9	2.40	0.0001	NM_002800
TC1400010721.hg.1	PSME2	Proteasome activator subunit 2; microRNA 7703	2.66	0.0001	NM_002818
TC1400007320.hg.1	DACT1	Disheveled-binding antagonist of beta-catenin 1	4.54	0.0007	NM_001079520
TC0800008845.hg.1	MYC	MYC proto-oncogene, bHLH transcription factor	2.61	0.0076	NM_002467
TC1000008942.hg.1	TCF7L2	Transcription factor 7-like 2 (T-cell specific, HMG-box)	1.76	0.0081	NM_001146274
Glycolysis					
TC1900011707.hg.1	GPI	Glucose-6-phosphate isomerase	1.60	0.0015	NM_000175
TC1200006649.hg.1	TPI1	Triosephosphate isomerase 1	2.00	0.0005	NM_000365
TC2100007355.hg.1	PFKL	Phosphofructokinase, liver	2.01	<0.0001	NM_001002021
Platelet derived growth factor signaling pathway					
TC1000007761.hg.1	ARID5B	AT rich interactive domain 5B (MRF1-like)	2.50	0.0033	NM_001244638
TC0800008845.hg.1	MYC	MYC proto-oncogene, bHLH transcription factor	2.43	0.0086	NM_002467
TC0300007432.hg.1	MAPKAPK3	Mitogen-activated protein kinase(PK)-activated PK 3	2.05	0.0032	NM_001243925
TC1900010696.hg.1	AKT2	v-Akt murine thymoma viral oncogene homolog 2	1.97	0.0001	NM_001243027
Interleukin signaling pathway					
TC1200010908.hg.1	STAT2	Signal transducer and activator of transcription 2	1.54	0.0002	NM_005419
TC0200015242.hg.1	STAT1	Signal transducer and activator of transcription 1	2.27	0.0012	NM_007315
TC0800008845.hg.1	MYC	MYC proto-oncogene, bHLH transcription factor	2.12	0.0078	NM_002467
TC1600007312.hg.1	IL4R	Interleukin 4 receptor	1.92	0.0001	NM_000418

(*Continued*)

TABLE 4 | Continued

ID	Gene symbol	Description	Fold change	*p*-Value	Public gene IDs
p38 signaling pathway					
TC2200008641.hg.1	RAC2	Rho family, small GTP binding protein Rac2	1.71	0.0054	NM_002872
TC1700008757.hg.1	MAP2K6	Mitogen-activated protein kinase kinase 6	−1.66	0.0042	NM_002758
TC0300007432.hg.1	MAPKAPK3	Mitogen-activated protein kinase(PK)-activated PK 3	1.92	0.0077	NM_001243925
Epidermal growth factor receptor signaling pathway					
TC0200007446.hg.1	PRKCE	Protein kinase C, epsilon	1.58	0.0020	NM_005400
TC2200008641.hg.1	RAC2	Rho family, small GTP binding protein Rac2	1.82	0.0031	NM_002872
TC1200010908.hg.1	STAT2	Signal transducer and activator of transcription 2	1.80	0.0003	NM_005419
TC0200015242.hg.1	STAT1	Signal transducer and activator of transcription 1	2.53	0.0042	NM_007315
TC1900010696.hg.1	AKT2	v-Akt murine thymoma viral oncogene homolog 2	2.06	0.0006	NM_001243027

mitochondrial membrane 50 homolog (TIMM50). In addition to genes that were also modulated in lSSc samples (i.e., MYC, AKT2, and PIM1), other genes involved in cell proliferation and also in tumor development were overexpressed. These genes include: hes family bHLH transcription factor 1(HES1), CDC28 protein kinase regulatory subunit 2 (CKS2), and cyclin D3 (CCND3) (52–54). Moreover, three upregulated transcripts were ascribed to the growth factor binding gene category: glucose-6-phosphate isomerase (GPI), fibroblast growth factor intracellular binding protein (FIBP), and MYD88 (also modulated in lSSc samples as mentioned above). Noteworthy, also in dSSc samples, we observed the down-modulation of the tumor suppressor CUL3.

Several modulated genes encode for inflammatory molecules including chemokine (C-X-C motif) ligand 11 (CXCL11), Fc fragment of IgG, high affinity Ib, receptor (FCGR1B), Fc fragment of IgG, low affinity IIIa, receptor (FCGR3A), linker for activation of T-cells (LAT), prostaglandin E receptor 4 (PTGER4), CXCL10, and CXCR5. These last two transcripts were also overexpressed in lSSc samples.

Genes involved in the immune response were modulated also in dSSc samples and, besides the genes overexpressed in lSSc samples (i.e., IL4R, LAT, and MYD88), we found upregulation of CD79b molecule, immunoglobulin-associated beta (CD79B), complement component receptor 2 (CR2), forkhead box P3 (FOXP3), major histocompatibility complex, class I, A (HLA-A), major histocompatibility complex, class I, B (HLA-B), major histocompatibility complex, class I, E (HLA-E), major histocompatibility complex, class I, G (HLA-G), immunoglobulin heavy variable 3-66 (IGHV3-66), immunoglobulin heavy variable 4-61 (IGHV4-61), radical S-adenosyl methionine domain containing 2 (RSAD2), and transporter 1, ATP-binding cassette, sub-family B (TAP1).

Among DEGs involved in angiogenesis there are: glucose-6-phosphate isomerase (GPI), hematological and neurological expressed 1 (HN1), KRIT1, ankyrin repeat containing (KRIT1) and CIB1 (also modulated in lSSc samples).

Endothelial activation was well represented in dSSc samples by the overexpression of gene encoding for endothelin 1 (EDN1) that is associated with diseases characterized by endothelial dysfunction and fibrosis (55).

Finally, we found upregulation of three transcripts that play a role in the ECM organization including ADAM metallopeptidase domain 2 (ADAM2), CST3 (increased also in lSSc samples), and basigin (BSG). BSG, also named ECM metalloproteinase inducer (EMMPRIN), is expressed on the surface of tumor cells and induces fibroblasts to synthesize matrix metalloproteinases (56).

Pathways enrichment analysis showed that pathways also overrepresented in lSSc samples were enriched in dSSc samples (i.e., glycolysis, apoptosis, and interleukin signaling pathway). Besides these signaling pathways, we found an enrichment in pathways involved in tumor development including: inflammation mediated by chemokine and cytokine, cell cycle, Ras (57), oxidative stress response (58), p53 (59), ubiquitin proteasome (60), JAK/STAT (61), p38 MAPK (62), angiogenesis, and EGF receptor signaling pathway (**Table 5**). Among modulated genes belonging to these pathways, we mention ras homolog family member C (RHOC), the overexpression of which indicates poor prognosis in breast cancer cells (63), and the abovementioned AKT2 and HES1.

As found in lSSc samples, among other DEGs involved in signal transduction, several transcripts were involved in Wnt, PDGF, and type I interferon signaling pathway and, their role in cancer development has been already stressed in our dissection of genes modulated in lSSc. Not surprisingly, type I interferon pathway accounted for a large amount of DEGs (14) and the evidence of the modulation of this molecular signaling both in lSSc and in dSSc further underlines its role in the pathogenesis of the disease.

TABLE 5 | Pathways enriched in genes modulated in diffuse SSc samples.

Panther pathways	*p*-Value
Glycolysis (P00024)	0.005
Apoptosis signaling pathway (P00006)	0.006
Inflammation mediated by chemokine and cytokine signaling pathway (P00031)	0.008
Cell cycle (P00013)	0.009
Ras pathway (P04393)	0.010
Oxidative stress response (P00046)	0.012
p53 pathway (P00059)	0.018
Ubiquitin proteasome pathway (P00060)	0.020
Interleukin signaling pathway (P00036)	0.026
JAK/STAT signaling pathway (P00038)	0.030
p38 MAPK pathway (P05918)	0.032
Angiogenesis (P00005)	0.035
Epidermal growth factor receptor signaling pathway (P00018)	0.044

Network Analysis of Modulated Genes in SSc

The gene expression profiling of SSc patients was complemented with a network analysis. With this purpose, by a bioinformatic analysis, we selected all the functional and experimentally validated interactions between the protein products of modulated genes and we constructed the two protein–protein interaction (PPI) networks that were representative of lSSc and dSSc dataset.

The lSSc-PPI network comprised 440 genes (nodes) and 1351 pairs of interactions (edges) (**Figure 1A**), whereas the dSSc included 225 genes and 870 pairs of interactions (**Figure 1B**).

The PPI networks were then submitted to a modular analysis to find set of highly interconnected nodes (modules) that participate in multiple activities in a coordinated manner and that are expected to play a prominent role in the development of biological phenomena.

In the lSSc-PPI network, we identified nine modules that are graphically represented in **Figure 2**. Moreover, a functional enrichment analysis was applied to find the associations between each module and relevant enriched "GO terms" and pathways. All the significantly enriched ($p < 0.05$) biological processes (BPs) and pathways in each module are showed in Table S3 in Supplementary Material and **Table 6** shows a selection of the most relevant terms. We observed that the most enriched BPs in module M0, were the signaling of G-protein coupled receptors (GPCRs) and mediated by chemokine. Interestingly, the GPCRs pathway is involved in cancer initiation and progression and GPCRs are emerging as anti-cancer drug targets (64). In the same module M0, we could highlight, among other, an enrichment in inflammation mediated by chemokine and cytokine, PI3 kinase and endothelin signaling pathway. Module M1 showed an enrichment in the positive regulation of type I interferon production BP whereas, among different enriched pathways, we found the glycolysis pathway and again, the endothelin signaling pathway. Module M2 and M4 were the most representative of the type I interferon response. In M2, the GO terms associated to the type I interferon signaling were the most enriched biological processes, followed by terms associated to the innate immune response (i.e., innate immune response, defense response to virus, interferon gamma mediate signaling) and to the adaptive immune response (i.e., antigen processing and presentation of exogenous peptides). Interestingly, the enriched pathways in M2 were related to the Jak/Stat and Interleukin signaling, both associated to tumor development as previously remarked.

In M4, the most enriched BPs were interferon-gamma-mediated signaling pathway and cellular response to interferon-gamma. Besides the BPs associated to type I interferon response, we found an enrichment in terms referred to the lymphocyte-associated immune response (i.e., regulation of lymphocyte activation, regulation of T cell activation, regulation of T cell proliferation and antigen processing, and presentation of peptide antigen *via* MHC class I and II). Most enriched pathways in M4 were referred to interferons (alpha, beta and gamma) pathways. Interestingly, in M4, we observed an enrichment in the PD-1 signaling, an immune-inhibitory-checkpoint that acts as crucial mediator for the escape phase of cancer immune editing (65). Module M3 and M5 were enriched in terms related to translation and other metabolic processes of proteins and, in module M6 the

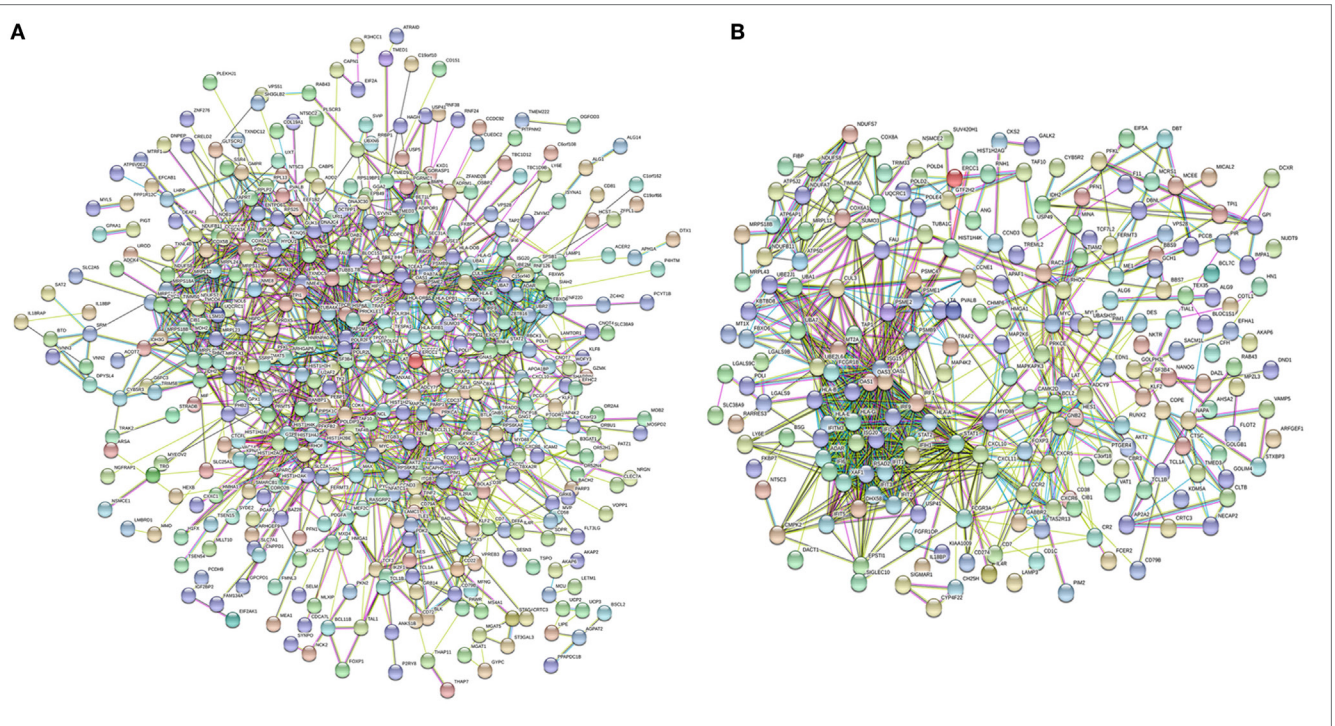

FIGURE 1 | Network analysis of modulated genes in systemic sclerosis (SSc) patients. Protein–protein interaction network of differently expressed genes in lSSc **(A)** and in diffuse cutaneous SSc **(B)** samples.

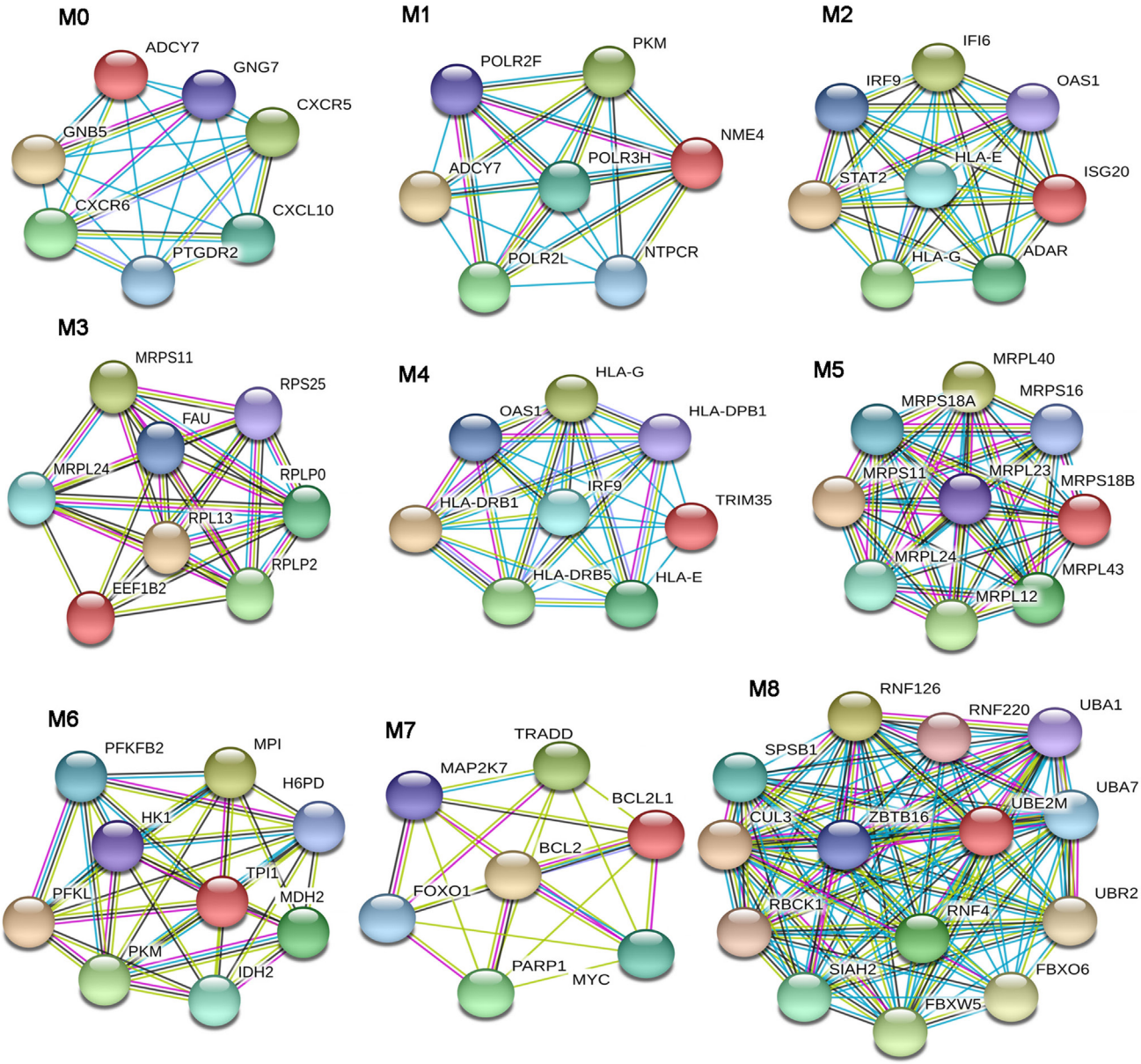

FIGURE 2 | Modular analysis of the lSSc-protein–protein interaction network. Modules originated from the interaction network of modulated genes in lSSc samples.

most enriched BPs and pathways were referred to the glycolytic pathway. In module M7, we observed an enrichment of many BPs associated to positive and negative regulation of apoptosis and concordantly, an enrichment in the apoptotic FAS and p53 pathways signaling. Moreover, in M7, several cancer-associated signaling pathways were included, including PI3 kinase, Ras, Interleukin, FGF, and EGF receptors signaling pathways. Finally, in module M8, the protein ubiquitination BP and the ubiquitin proteasome pathway were the most over-represented. Interestingly, tumor cells have a high dependency on the proteasome for survive and proteasome deregulation is frequently induced by many types of tumors (66).

From the dSSC-PPI network, we could extract seven modules (**Figure 3**) that were studied by a functional enrichment analysis. The results of this analysis are fully presented in Table S4 in Supplementary Material and the most relevant terms are showed in **Table 7**.

The BPs that we found enriched in the module M0 were mainly referred to the immune response. In particular, we observed an enrichment in the regulation of tumor necrosis factor superfamily cytokine production process. Moreover, the over-represented pathways in M0 reassumed nearly all signalings that were enriched in the entire dSSc dataset, including inflammation mediated by chemokine and cytokine, JAK/STAT, p53, oxidative stress response, Ras, interleukin, EGF receptor, and angiogenesis signaling pathway. Module M1 was largely enriched in ATP and purine ribo/nucleoside metabolic processes, whereas M2 was mostly represented by BPs referred

TABLE 6 | Most relevant biological processes and pathways enriched in lSSc modules.

Gene ontology biological processes	*p* Value	Panther pathways	*p* Value
M0			
G-protein coupled receptor signaling pathway	<0.001	inflammation mediated by chemokine and cytokine signaling pathway	<0.001
Chemokine-mediated signaling pathway	0.010	PI3 kinase pathway	0.013
		Endothelin signaling pathway	0.020
M1			
Positive regulation of type I interferon production	0.001	Glycolysis	0.010
		Endothelin signaling pathway	0.016
M2			
Type I interferon signaling pathway	<0.001	JAK/STAT signaling pathway	0.001
Cellular response to type I interferon	<0.001	Interleukin signaling pathway	0.026
Response to type I interferon	<0.001		
Cytokine-mediated signaling pathway	<0.001		
Innate immune response	<0.001		
Immune response	<0.001		
Defense response to virus	<0.001		
Interferon-gamma-mediated signaling pathway	<0.001		
Antigen processing and presentation of exogenous peptide *via* MHC class I	0.030		
M3			
Translation	<0.001	None	
Protein metabolic process	<0.001		
rRNA metabolic process	0.033		
M4			
Interferon-gamma-mediated signaling pathway	<0.001	Interferon gamma signaling	<0.001
Cellular response to interferon-gamma	<0.001	Interferon Signaling	<0.001
Response to interferon-gamma	<0.001	Interferon alpha/beta signaling	<0.001
Type I interferon signaling pathway	<0.001	PD-1 signaling	<0.001
Cellular response to type I interferon	<0.001		
Positive regulation of T cell activation	<0.001		
Response to type I interferon	<0.001		
Regulation of T cell activation	<0.001		
Regulation of T cell proliferation	0.001		
Regulation of lymphocyte activation	0.027		
Antigen processing and presentation of exogenous peptide *via* MHC class I	0.032		
Antigen processing and presentation of exogenous peptide *via* MHC class II	0.050		
M5			
Translation	0.008	None	
M6			
Glycolysis	<0.001	Glycolysis	<0.001
Generation of precursor metabolites and energy	<0.001	Pyruvate metabolism	<0.001
Monosaccharide metabolic process	0.007		
Carbohydrate metabolic process	0.009		
M7			
Apoptotic process	<0.001	Apoptosis signaling pathway	<0.001
Programmed cell death	<0.001	FAS signaling pathway	0.010
Regulation of apoptotic process	<0.001	p53 pathway feedback loops 2	0.013
Positive regulation of apoptotic process	0.008	Phosphoinositide 3 kinase pathway	0.016
Negative regulation of apoptotic process	0.027	Ras Pathway	0.030
Extrinsic apoptotic signaling pathway	0.033	Interleukin signaling pathway	0.035
		FGF signaling pathway	0.042
		Epidermal growth factor receptor signaling pathway	0.042
M8			
Protein ubiquitination	<0.001	Ubiquitin proteasome pathway	0.001

to the type I interferon signaling followed by BPs involved in both innate and adaptive immune response. In addition, DEGs in M2 mainly play a role in ubiquitin proteasome, Jak/Stat, interleukin, EGF receptor, and PDGF signaling pathways. In M3, the most enriched BP was cellular response to TNF and, not surprising, the most over-represented pathway was the apoptosis signaling. Other pathways, statistically representative of module M3 were toll-like receptor (TLR), ubiquitin proteasome, and p53 pathway. In particular, the enrichment of TLR signaling is interesting since it is well known that inducing pro-inflammatory cytokines and co-stimulatory molecules, it contributes to the development of an excessive inflammatory response, leading to both autoimmune disorders and tumor growth (67). Module M4 was mostly enriched in G-protein coupled receptor signaling, and we also observed enriched BPs related to leukocyte/lymphocyte chemotaxis, whereas the most over-represented pathway was inflammation mediated by chemokine and cytokine signaling pathways. The Wnt signaling pathway was preeminent in module M5. In addition, DEGs in this module were also primarily involved in the p53 pathway. Response to virus was the most representative BP of module M6: is worthwhile mentioning that numerous viruses have been proposed as possible triggering factors in SSc (68), and indeed, it has been estimated that up to a quarter of human tumors are connected to infection or infection-associated chronic inflammation (69).

A large number of BPs involved in immune cells activation, proliferation, and differentiation and in type I interferon signaling, were prevalent in M6. The over-represented pathways in this module were again signalings also involved in cancer and already

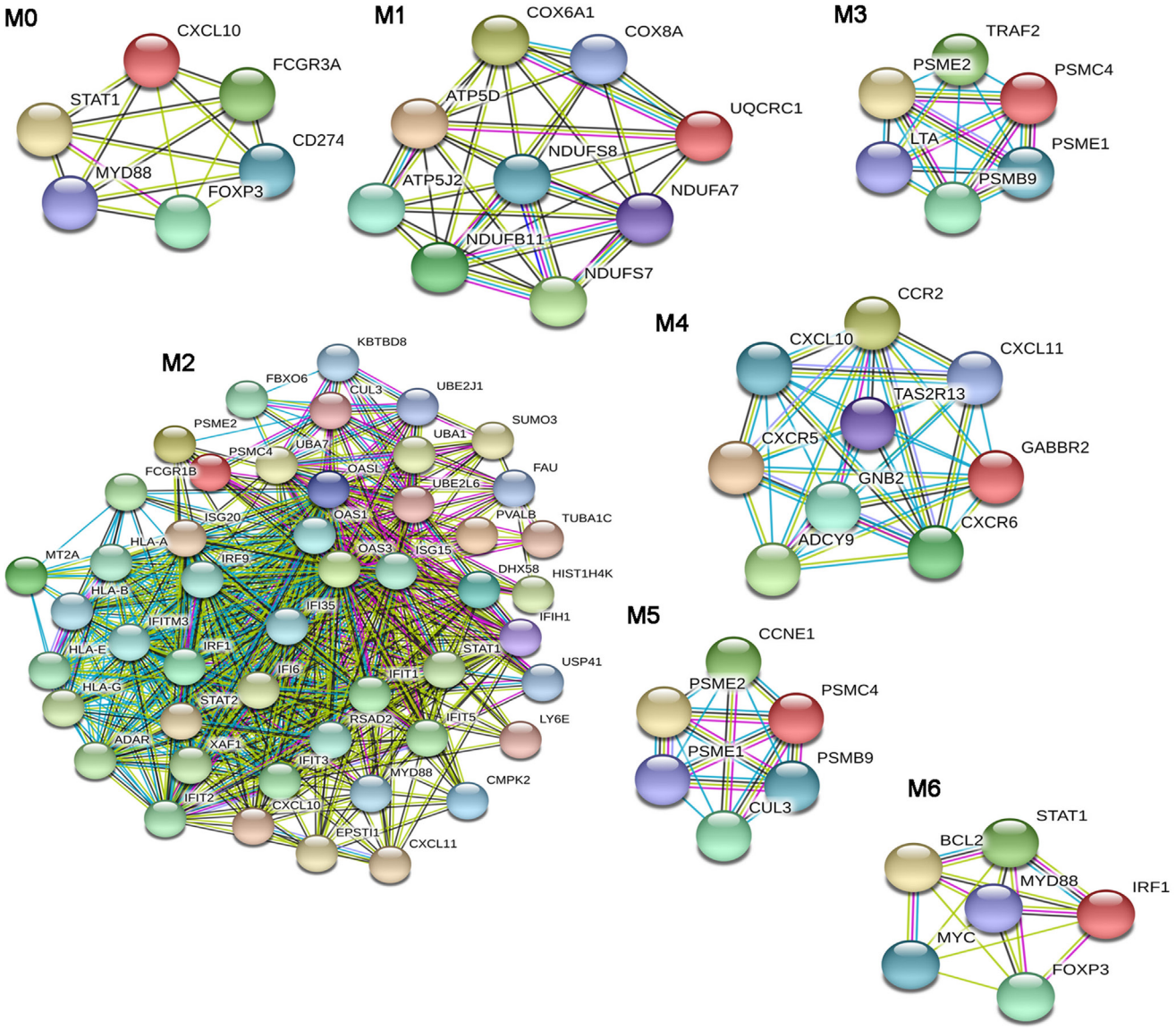

FIGURE 3 | Modular analysis of the diffuse SSc (dSSc)-protein–protein interaction network. Modules originated from the interaction network of modulated genes in dSSc samples.

mentioned in this analysis (i.e., p53, interleukin, PDGF, Jak/Stat, TLR, Ras, and apoptosis signaling pathway).

MicroRNAs in SSc Sera

Systemic sclerosis is associated with an increased risk of malignancies, and in the present study, we found a modulation of genes encoding for molecules that have been previously associated to different types of cancers. An important role of miRNAs in human cancers is well established (12). The higher incidence of cancer in SSc patients prompted us to investigate whether specific cancer-related miRNAs could be deregulated in the serum of SSc patients as compared to healthy controls.

Since SSc patients are mainly affected by breast, lung, or hematological malignancies (70), we selected miRNAs with a solid evidence in literature for deregulation in these kind of cancers. We focused on miR-155-5p, miR-126-3p, and miR-16-5p. Furthermore, we decided to analyze miR-21-5p and miR-92a, since they play key roles in many cancers, and to confirm their upregulation in our cohort of SSc patients (**Table 8**). Cell-free miRNAs (cf-miRNA) in limited and diffuse SSc and in healthy sera was evaluated by real time PCR, as represented in **Figure 4**. A significant higher expression of 4/5 of the miRNAs tested in SSc sera was found as compared to healthy controls. miR-126-3p expression also showed a trend of upregulation in SSc samples although it did not reach statistically significant differences in the samples tested compared to controls. Moreover, no significant differences between limited and diffuse SSc were found in our analysis. miR-21-5p and miR-92a-3p were upregulated,

TABLE 7 | Most relevant biological processes and pathways enriched in diffuse SSc modules.

Gene ontology biological processes	*p* Value	Panther pathways	*p* Value
M0			
Positive regulation of immune system process	<0.001	Inflammation mediated by chemokine and cytokine signaling pathway	0.001
Regulation of immune system process	0.001	JAK/STAT signaling pathway	0.003
Immune response	0.004	Interferon-gamma signaling pathway	0.010
Regulation of tumor necrosis factor superfamily cytokine production	0.030	p53 pathway feedback loops 2	0.013
Negative regulation of activated T cell proliferation	0.040	Oxidative stress response	0.022
Positive regulation of lymphocyte proliferation	0.050	Toll-like receptor signaling pathway	0.024
Positive regulation of mononuclear cell proliferation	0.050	Ras Pathway	0.026
		Interleukin signaling pathway	0.030
		Epidermal growth factor (EGF) receptor signaling pathway	0.033
		Platelet derived growth factor (PDGF) signaling pathway	0.040
		Angiogenesis	0.050
M1			
ATP metabolic process	<0.001	None	
Purine ribonucleoside triphosphate metabolic process	<0.001		
Purine nucleoside triphosphate metabolic process	<0.001		
Purine ribonucleoside monophosphate metabolic process	<0.001		
Purine nucleoside monophosphate metabolic process	<0.001		
Ribonucleoside monophosphate metabolic process	<0.001		
ATP synthesis coupled electron transport	<0.001		
M2			
Type I interferon signaling pathway	<0.001	Ubiquitin proteasome pathway	< 0.001
Cellular response to type I interferon	<0.001	JAK/STAT signaling pathway	0.011
Response to type I interferon	<0.001	Interleukin signaling pathway	0.016
Immune system process	<0.001	EGF receptor signaling pathway	0.043
Interferon-gamma-mediated signaling pathway	<0.001	PDGF signaling pathway	0.048
Antigen processing and presentation of exogenous peptide *via* MHC class I	<0.001		
Regulation of immune response	<0.001		
M3			
Cellular response to tumor necrosis factor	<0.001	Apoptosis signaling pathway	0.009
Response to tumor necrosis factor	<0.001	Toll-like receptor signaling pathway	0.016
Tumor necrosis factor-mediated signaling pathway	<0.001	Ubiquitin proteasome pathway	0.020
		p53 pathway	0.025
M4			
G-protein coupled receptor signaling pathway	<0.001	Inflammation mediated by chemokine and cytokine signaling pathway	<0.001
T cell chemotaxis	<0.001	Heterotrimeric G-protein signaling pathway-Gi alpha and Gs alpha	0.001
Leukocyte chemotaxis	0.012		
Lymphocyte chemotaxis	0.020		
M5			
Cell–cell signaling by wnt	<0.001	Cell cycle	<0.001
Wnt signaling pathway	<0.001	p53pathway feedback loops 2	0.010
		Ubiquitin proteasome pathway	0.020
		p53 pathway	0.022
M6			
Response to virus	<0.001	Oxidative stress response	<0.001
Regulation of lymphocyte proliferation	0.001	p53 pathway feedback loops 2	<0.001
Alpha-beta T cell differentiation	0.004	Interleukin signaling pathway	<0.001
Alpha-beta T cell activation	0.004	PDGF signaling pathway	0.001
Type I interferon signaling pathway	0.005	JAK/STAT signaling pathway	0.005
Cellular response to type I interferon	0.006	Interferon-gamma signaling pathway	0.009
Response to type I interferon	0.012	Toll-like receptor signaling pathway	0.013
Regulation of type I interferon production	0.027	Ras Pathway	0.020
		Apoptosis signaling pathway	0.028
		EGF receptor signaling pathway	0.028
		Angiogenesis	0.032

TABLE 8 | Cancer-related miRNAs selected for expression analysis in SSc serum.

miRNA	Modulation in cancer	Cancer	Reference
miR-21-5p	Upregulated	Breast; lung; leukemias	(71–73)
miR-92a-3p	Upregulated	Lung	(74, 75)
miR-155-5p	Upregulated	Breast; lung; leukemias	(71, 72, 76)
miR-126-3p	Downregulated	Breast	(72, 77)
miR-16-5p	Downregulated	Leukemias	(78)

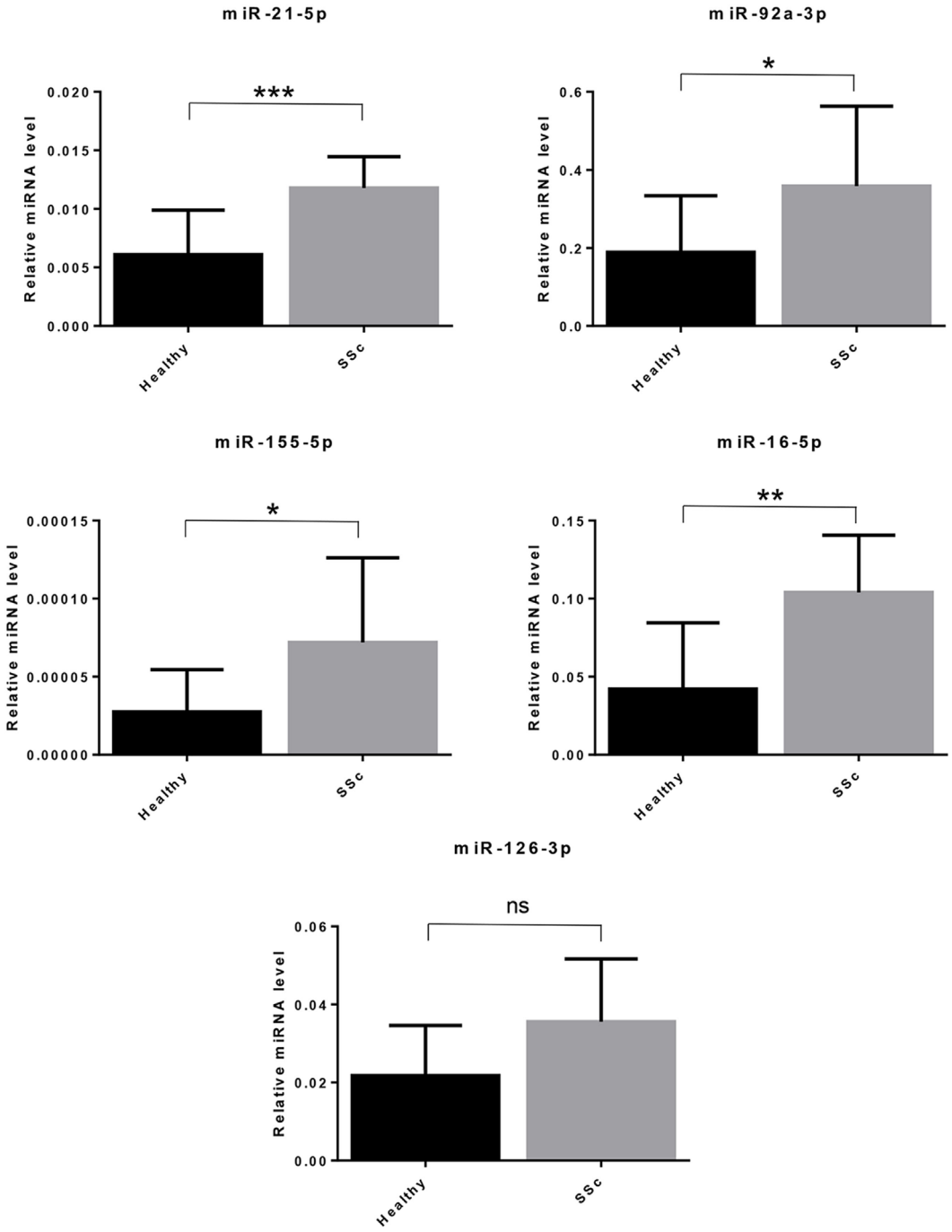

FIGURE 4 | Cell-free circulating miRNA expression in systemic sclerosis (SSc) sera. The expression of the indicated miRNAs was evaluated by real-time PCR in serum of systemic sclerosis patients (*SSc*; $n = 30$) and of healthy controls (*Healthy*; $n = 30$). Expression values of mature miRNAs were calculated using the comparative ΔCt method and normalized to spike-in cel-39-3p. Histograms represent mean ± SD. *p*-values (ns = not significant; $^{*}p \leq 0.05$; $^{**}p \leq 0.01$; $^{***}p \leq 0.001$) were determined using the Mann–Whitney rank sum test.

as reported in literature, further supporting the hypothesis of their involvement in SSc pathogenesis. To our knowledge, upregulation of miR-155-5p and miR-16-5p in SSc sera has not been reported yet, and it suggests a role of these miRNAs in the disease.

DISCUSSION

Systemic sclerosis represents a major medical challenge and many unmet needs in the treatment of the disease still remain. However, advances have been made thanks to the increased understanding

of the pathogenesis of SSc and the overall patients' survival is improved.

The increased risk of malignancies in SSc is a major source of concern and the identification of risk factors for both disorders may have implications for the prognosis and for the treatment.

We therefore wanted to carry out a gene expression profile and an epigenetic analysis in scleroderma patients to verify the presence of common bases for the development of malignancies and SSc.

We have noticed that the functional classes, to which the genes modulated in limited and diffuse forms of SSc belong, were virtually overlapping and, in both cases, we observed the modulation of genes and pathways previously associated with malignancy. Although it has been reported a higher incidence of some tumors in patients with dSSc than in those with lSSc, our data seem to suggest that in both forms of the disease there is a genetic modulation that may be linked to the onset of a neoplastic transformation. Indeed, from our analysis has emerged that the various classes comprising genes potentially linked to the pathogenesis of SSc (such as apoptosis, endothelial cell activation, extracellular matrix remodeling, immune response, and inflammation), include genes that directly participate in the development of malignancies or that are involved in pathways known to be associated with carcinogenesis.

In this regard, several pathways enriched in lSSc and/or dSSc (apoptosis, glycolysis, PDGF, Fas cell surface death receptor, FAS, angiogenesis, interleukin, Ras, Jak/Stat, and EGFR signaling pathways) are involved in cancer development.

Indeed, altered apoptosis has a crucial role in the induction of a malignant phenotype, and it is well known that some oncogenic mutations block apoptosis, leading to cancer progression (79). Moreover, some cancer cells express FAS ligand (FasL) and the activation of FAS pathway may favor immune privilege to tumors by inducing apoptosis of anti-tumor lymphocytes (80).

The modulation of genes involved in the glycolytic pathway is not surprising, given that upregulation of glycolysis is a well-documented property of cancers, and this mechanism confers to tumor cells a significant growth advantage (81).

Platelet derived growth factors and PDGF receptors have substantial role in regulating cell growth during embryonal development. An enhancement of PDGF receptor signaling, may also sustain tumor cell growth. Moreover, fibroblasts, and myofibroblasts of solid tumors stroma express PDGF receptors, and PDGF stimulates these cells promoting tumorigenesis (82). Noteworthy, PDGF enhances c-myc expression and stimulates the c-myc promoter (83). This gene, found overexpressed in our lSSc dataset, coordinates cell growth and cell proliferation and its deregulation is a near-universal property of primary and metastatic cancers (84).

Ras proteins are key elements in malignant transformation; moreover, the Jak/stat signaling pathway sustains epithelial mesenchymal transition and generates a pro-tumorigenic microenvironment. The EGF receptor signaling pathway modulates migration and survival of cancer cells.

It has been established that inflammation caused by either chronic disease or infection is an important risk factor in cancer development and that a variety of interleukins are involved in both inflammation and carcinogenesis (85). In particular, among genes involved in the interleukin signaling pathways that was enriched in lSSc modulated genes, we found overexpression of the interleukin 2 receptor alpha (IL2RA) gene. The soluble form of this molecule is released from neoplastic cells and is expressed on the surface of both lymphoid and non-lymphoid cancer cells (86).

Pathway analysis also highlighted the modulation of a large number of genes (11) involved in the Type 1 interferon signaling pathway. This pathway is a hallmark of many systemic autoimmune diseases (87) including SSc (88) and has also been considered as a "double-edged sword" in cancer. Indeed, in cancer, it promotes both T cell responses and a negative feedback leading to immunosuppression. Tumor cells can take advantage from this counter-regulatory effects induced by IFN type I to avoid immune cell killing (89).

This suggests that there are multiple points of contact between the signaling pathways leading to scleroderma and those that predispose to the development of a malignancy. However, these pathways may lead to different outcomes in different tissues in which they are expressed, and indeed in patients with scleroderma, some malignancies are more frequent such as those affecting breast, lung, and lymphoid tissue.

Endothelial cell apoptosis is among the first manifestations of vasculopathy associated with the development of SSc, and fibroblasts activation and proliferation lead to the fibrotic characteristics of the disease. Gene expression profiles obtained from the PBMC of patients with SSc indicate an altered modulation of genes involved in apoptosis and in cell proliferation that could, at tissue level, exert a mitogenic effect on some cellular populations or lead to down-modulation of oncosuppressor genes, as suggested by the downregulation of CUL3 (31) in both lSSc and dSSc.

Our data also suggest the presence of a genetic modulation that can favor angiogenesis, a common feature associated to the development and progression of any type of cancer.

Modulation of many genes involved in the immune response, including genes inducible by type I interferon, reflects the strong immune system dysregulation associated with excessive antigenic stimulation typical of autoimmune diseases. Such dysregulation can either induce proliferation of cells of the immune system, leading to malignancy in susceptible individuals or modify the immune system's regulatory mechanisms that inhibit the development of naturally occurring cancers.

Several modulated genes participate in the remodeling process of the extracellular tissue matrix. Excessive deposition of ECM promotes the development of fibrosis, hallmark of SSc, and the fibrotic and inflammatory processes of the lung have been considered the basis for the eventual onset of lung cancer in SSc. On the other hand, within these functional classes, we have also observed over-expression of metalloproteases (i.e., ADAM2) or ECM metalloproteases inducers (i.e., BSG) typically induced by several tumor cells (56, 90). Moreover, genes associated with the migration of tumor cells such as SPARC (43), a glycoprotein associated with ECM, are involved in the development of non-small cell lung cancer. Therefore, while ECM deposition and related profibrotic events may favor carcinogenesis through different

mechanisms such as blocking lymphatic channels and creating niches in which carcinogens may eventually accumulate, on the other hand, there is a genetic modulation that favors cancer cells spreading.

A crucial issue in basic and clinical research is to understand gene modulation in terms of biological networks since proteins usually function in protein–protein interacting networks. We therefore wanted to dissect meaningful relationships among modulated genes in SSc, analyzing the PPI network in which their protein products can be involved. Moreover, since it is known that the deregulation of protein expression may provoke more drastic biological effects when genes/proteins with more interacting partners are involved, we focused our attention on the most connected genes/proteins that "as a matter of fact" (by definition) are included in the network areas called modules. This is particularly important when studying gene regulation in certain diseases in order to identify the molecular pathways that are most relevant in disease pathogenesis. The pathway enrichment analysis of modulated genes included in the modules confirmed the enrichment of signaling pathways (i.e., the aforementioned Jak/stat, glycolysis, Ras, PDGF, EGF receptor, Wnt, and type I interferon signaling pathways) associated with carcinogenesis in both datasets.

The genes participating to these pathways are indeed comprised in network areas (modules), whereas gene interactions are concentrated and generally underline significant biological processes.

These molecular pathways also emerged from our first global analysis of the two datasets, but the network analysis further underlined their involvement in SSc. Indeed, members of these signaling networks are concentrated in modules were the molecules that are supposed to play a prominent role in shaping the typical features of the disease, are positioned.

Another aspect we have investigated is the expression of microRNAs in SSc. Altered expression of miRNAs in SSc, as well as their involvement in inflammation and fibrosis, has been described (14, 91). Similarly, the implication of miRNAs in human cancers is well established (12). A fascinating hypothesis is that a dysregulated epigenetic control mediated by miRNAs in SSc could promote tumorigenesis. Deregulated expression of miRNAs has been found in blood of SSc patients and it could exert oncogenic effects at distant sites from SSc lesions. Indeed, the upregulation of miR-21 and miR-92a in SSc (16, 92) may support this hypothesis, since these miRNAs play a role in many tumors, repressing important oncosuppressor genes (74, 93). Thus, the higher incidence of breast, lung and hematological malignancies in SSc patients (70) prompted us to investigate whether specific cancer-related miRNAs could be deregulated in the serum of SSc patients. We found that miR-21-5p, miR-92a-3p, miR-155-5p, and miR-16-5p expression was significantly higher in SSc sera compared to healthy controls. miR-21 can play a role in SSc since it is also upregulated in SSc fybroblasts and it is implicated in TGF-β-regulated fibrosis (17). Interestingly, miR-21 upregulation promotes proliferation, migration, and invasion in lung cancer (71). Elevated miR-92a levels in serum and in dermal fibroblasts of SSc patients have also been reported (16), and this miRNA is implicated in angiogenesis and proliferation in lung cancer and it can promote leukemogenesis (74, 75). MiR-155-5p expression was also increased in SSc sera. Notably, miR-155 was found upregulated in SSc fybroblasts, and it was associated to the progression of lung fibrosis in dSSc patients (94, 95). miR-155 upregulation also sustains survival and proliferation in hematological disorders and breast cancer (72, 76). We found increased miR-16-5p levels in SSc sera despite this miRNA is frequently associated to oncosuppressor functions and it is frequently absent in human leukemias (78). Since this miRNA inhibits cell proliferation and promotes apoptosis (96), it could participate to the apoptotic process of endothelial cells, considered the first pathogenic event in SSc. A release of miR-16 in the bloodstream from apoptotic endothelial cells could explain the increased levels of the miRNA in SSc sera. We also decided to evaluate miR-126 in SSc sera since it was found downregulated in breast and lung cancer (76, 77). Moreover, miR-126 plays an important role in angiogenic signaling and in vascular integrity (97), and we found several genes involved in angiogenesis upregulated in SSc by microarray analysis. We did not find statistically significant differences in the miR-126 expression levels between SSc patients and healthy controls, although we observed a trend toward upregulation in SSc samples. In conclusion, we describe here interesting findings on deregulated cancer-related miRNAs in SSc patients. However, further studies are needed to elucidate the potential role of these miRNA in SSc. In particular, since the levels of circulating microRNAs can be affected by different cell types, interesting points will be to elucidate which cells mainly contribute to these circulating oncogenic miRNAs and whether they can play an active role in the increased tumorigenesis associated to the disease.

Taken together, our data suggest the presence of modulated genes and miRNAs that can play a predisposing role in the development of malignancies in SSc. The findings of genetic and epigenetic features that are shared by SSc and cancer shed new light on the pathogenesis of the disease and strengthen the idea that autoimmunity plays a central role in the initiation and progression of SSc, since the presence or development of malignancies is associated with particular autoantibodies. These aspects are central to a better risk stratification of patients and to develop an individualized precision medicine strategy.

ETHICS STATEMENT

This study was carried out in accordance with the recommendations of "local ethical committee Azienda integrata Università di Verona e Ospedale Borgo Roma Verona, Italy" with written informed consent from all subjects. All subjects gave written informed consent in accordance with the Declaration of Helsinki. The protocol was approved by the "name of committee."

AUTHOR CONTRIBUTIONS

APu, CL, MD, APe, and APu conceived and designed the experiments. MD, APe, and PF performed the experiments. MD, APe and APu analyzed the data. GP and ET contributed reagents. ET, GP, and CL contributed materials. MD and APe wrote the paper.

FUNDING

The work was funded by the University of Verona and by donation of the Italian Association of Sclerodermic Patients (AILS).

SUPPLEMENTARY MATERIAL

The Supplementary Material for this article can be found online at http://www.frontiersin.org/articles/10.3389/fimmu.2018.00449/full#supplementary-material.

REFERENCES

1. Denton CP, Khanna D. Systemic sclerosis. *Lancet* (2017) 390:1685–99. doi:10.1016/S0140-6736(17)30933-9
2. Dolcino M, Puccetti A, Barbieri A, Bason C, Tinazzi E, Ottria A, et al. Infections and autoimmunity: role of human cytomegalovirus in autoimmune endothelial cell damage. *Lupus* (2015) 24:419–32. doi:10.1177/0961203314558677
3. Lunardi C, Bason C, Navone R, Millo E, Damonte G, Corrocher R, et al. Systemic sclerosis immunoglobulin G autoantibodies bind the human cytomegalovirus late protein UL94 and induce apoptosis in human endothelial cells. *Nat Med* (2000) 6:1183–6. doi:10.1038/80533
4. Luo Y, Wang Y, Wang Q, Xiao R, Lu Q. Systemic sclerosis: genetics and epigenetics. *J Autoimmun* (2013) 41:161–7. doi:10.1016/j.jaut.2013.01.012
5. Murdaca G, Contatore M, Gulli R, Mandich P, Puppo F. Genetic factors and systemic sclerosis. *Autoimmun Rev* (2016) 15:427–32. doi:10.1016/j.autrev.2016.01.016
6. Bernal-Bello D, de Tena JG, Guillen-Del Castillo A, Selva-O'Callaghan A, Callejas-Moraga EL, Marin-Sanchez AM, et al. Novel risk factors related to cancer in scleroderma. *Autoimmun Rev* (2017) 16:461–8. doi:10.1016/j.autrev.2017.03.012
7. Shah AA, Xu G, Rosen A, Hummers LK, Wigley FM, Elledge SJ, et al. Brief report: anti-RNPC-3 antibodies as a marker of cancer-associated scleroderma. *Arthritis Rheumatol* (2017) 69:1306–12. doi:10.1002/art.40065
8. Monfort JB, Lazareth I, Priollet P. Paraneoplastic systemic sclerosis: about 3 cases and review of literature. *J Mal Vasc* (2016) 41:365–70. doi:10.1016/j.jmv.2016.07.001
9. Shah AA, Casciola-Rosen L. Cancer and scleroderma: a paraneoplastic disease with implications for malignancy screening. *Curr Opin Rheumatol* (2015) 27:563–70. doi:10.1097/BOR.0000000000000222
10. Bartel DP. MicroRNAs: target recognition and regulatory functions. *Cell* (2009) 136:215–33. doi:10.1016/j.cell.2009.01.002
11. Ceribelli A, Satoh M, Chan EK. MicroRNAs and autoimmunity. *Curr Opin Immunol* (2012) 24:686–91. doi:10.1016/j.coi.2012.07.011
12. Garzon R, Calin GA, Croce CM. MicroRNAs in cancer. *Annu Rev Med* (2009) 60:167–79. doi:10.1146/annurev.med.59.053006.104707
13. Miao CG, Xiong YY, Yu H, Zhang XL, Qin MS, Song TW, et al. Critical roles of microRNAs in the pathogenesis of systemic sclerosis: new advances, challenges and potential directions. *Int Immunopharmacol* (2015) 28:626–33. doi:10.1016/j.intimp.2015.07.042
14. Zhu H, Luo H, Zuo X. MicroRNAs: their involvement in fibrosis pathogenesis and use as diagnostic biomarkers in scleroderma. *Exp Mol Med* (2013) 45:e41. doi:10.1038/emm.2013.71
15. Babalola O, Mamalis A, Lev-Tov H, Jagdeo J. The role of microRNAs in skin fibrosis. *Arch Dermatol Res* (2013) 305:763–76. doi:10.1007/s00403-013-1410-1
16. Sing T, Jinnin M, Yamane K, Honda N, Makino K, Kajihara I, et al. microRNA-92a expression in the sera and dermal fibroblasts increases in patients with scleroderma. *Rheumatology* (2012) 51:1550–6. doi:10.1093/rheumatology/kes120
17. Zhu H, Luo H, Li Y, Zhou Y, Jiang Y, Chai J, et al. MicroRNA-21 in scleroderma fibrosis and its function in TGF-beta-regulated fibrosis-related genes expression. *J Clin Immunol* (2013) 33:1100–9. doi:10.1007/s10875-013-9896-z
18. Kumarswamy R, Volkmann I, Thum T. Regulation and function of miRNA-21 in health and disease. *RNA Biol* (2011) 8:706–13. doi:10.4161/rna.8.5.16154
19. van den Hoogen F, Khanna D, Fransen J, Johnson SR, Baron M, Tyndall A, et al. 2013 classification criteria for systemic sclerosis: an American College of Rheumatology/European League against Rheumatism collaborative initiative. *Arthritis Rheum* (2013) 65:2737–47. doi:10.1002/art.38098
20. LeRoy EC, Black C, Fleischmajer R, Jablonska S, Krieg T, Medsger TA Jr, et al. Scleroderma (systemic sclerosis): classification, subsets and pathogenesis. *J Rheumatol* (1988) 15:202–5.
21. Mi H, Thomas P. PANTHER pathway: an ontology-based pathway database coupled with data analysis tools. *Methods Mol Biol* (2009) 563:123–40. doi:10.1007/978-1-60761-175-2_7
22. Franceschini A, Szklarczyk D, Frankild S, Kuhn M, Simonovic M, Roth A, et al. STRING v9.1: protein-protein interaction networks, with increased coverage and integration. *Nucleic Acids Res* (2013) 41:D808–15. doi:10.1093/nar/gks1094
23. Jensen LJ, Kuhn M, Stark M, Chaffron S, Creevey C, Muller J, et al. STRING 8 – a global view on proteins and their functional interactions in 630 organisms. *Nucleic Acids Res* (2009) 37:D412–6. doi:10.1093/nar/gkn760
24. Palla G, Derenyi I, Farkas I, Vicsek T. Uncovering the overlapping community structure of complex networks in nature and society. *Nature* (2005) 435:814–8. doi:10.1038/nature03607
25. Cline MS, Smoot M, Cerami E, Kuchinsky A, Landys N, Workman C, et al. Integration of biological networks and gene expression data using Cytoscape. *Nat Protoc* (2007) 2:2366–82. doi:10.1038/nprot.2007.324
26. Gao SP, Sun HF, Jiang HL, Li LD, Hu X, Xu XE, et al. Loss of TIM50 suppresses proliferation and induces apoptosis in breast cancer. *Tumour Biol* (2016) 37:1279–87. doi:10.1007/s13277-015-3878-0
27. Fallah Y, Brundage J, Allegakoen P, Shajahan-Haq AN. MYC-driven pathways in breast cancer subtypes. *Biomolecules* (2017) 7:E53. doi:10.3390/biom7030053
28. Horiuchi D, Camarda R, Zhou AY, Yau C, Momcilovic O, Balakrishnan S, et al. PIM1 kinase inhibition as a targeted therapy against triple-negative breast tumors with elevated MYC expression. *Nat Med* (2016) 22:1321–9. doi:10.1038/nm.4213
29. Pereira L, Horta S, Mateus R, Videira MA. Implications of Akt2/Twist crosstalk on breast cancer metastatic outcome. *Drug Discov Today* (2015) 20:1152–8. doi:10.1016/j.drudis.2015.06.010
30. Pignataro L, Sambataro G, Pagani D, Pruneri G. Clinico-prognostic value of D-type cyclins and p27 in laryngeal cancer patients: a review. *Acta Otorhinolaryngol Ital* (2005) 25:75–85.
31. Dorr C, Janik C, Weg M, Been RA, Bader J, Kang R, et al. Transposon mutagenesis screen identifies potential lung cancer drivers and CUL3 as a tumor suppressor. *Mol Cancer Res* (2015) 13:1238–47. doi:10.1158/1541-7786.MCR-14-0674-T
32. Leaf IA, Nakagawa S, Johnson BG, Cha JJ, Mittelsteadt K, Guckian KM, et al. Pericyte MyD88 and IRAK4 control inflammatory and fibrotic responses to tissue injury. *J Clin Invest* (2017) 127:321–34. doi:10.1172/JCI87532
33. Wang C, Zhou X, Li W, Li M, Tu T, Ba X, et al. Macrophage migration inhibitory factor promotes osteosarcoma growth and lung metastasis through activating the RAS/MAPK pathway. *Cancer Lett* (2017) 403:271–9. doi:10.1016/j.canlet.2017.06.011
34. Podnos A, Clark DA, Erin N, Yu K, Gorczynski RM. Further evidence for a role of tumor CD200 expression in breast cancer metastasis: decreased metastasis in CD200R1KO mice or using CD200-silenced EMT6. *Breast Cancer Res Treat* (2012) 136:117–27. doi:10.1007/s10549-012-2258-3
35. Damiani D, Tiribelli M, Raspadori D, Sirianni S, Meneghel A, Cavalllin M, et al. Clinical impact of CD200 expression in patients with acute myeloid leukemia and correlation with other molecular prognostic factors. *Oncotarget* (2015) 6:30212–21. doi:10.18632/oncotarget.4901
36. Mulligan-Kehoe MJ, Simons M. Current concepts in normal and defective angiogenesis: implications for systemic sclerosis. *Curr Rheumatol Rep* (2007) 9:173–9. doi:10.1007/s11926-007-0013-2
37. Heldin CH, Lennartsson J, Westermark B. Involvement of platelet-derived growth factor ligands and receptors in tumorigenesis. *J Intern Med* (2017) 283(1):16–44. doi:10.1111/joim.12690

38. Michie AM, Nakagawa R. The link between PKCalpha regulation and cellular transformation. *Immunol Lett* (2005) 96:155–62. doi:10.1016/j.imlet.2004.08.013
39. Zeng P, Wang YH, Si M, Gu JH, Li P, Lu PH, et al. Tetraspanin CD151 as an emerging potential poor prognostic factor across solid tumors: a systematic review and meta-analysis. *Oncotarget* (2017) 8:5592–602. doi:10.18632/oncotarget.13532
40. Leask A. Matrix remodeling in systemic sclerosis. *Semin Immunopathol* (2015) 37:559–63. doi:10.1007/s00281-015-0508-2
41. Zhou X, Tan FK, Guo X, Arnett FC. Attenuation of collagen production with small interfering RNA of SPARC in cultured fibroblasts from the skin of patients with scleroderma. *Arthritis Rheum* (2006) 54:2626–31. doi:10.1002/art.21973
42. Erdogan B, Webb DJ. Cancer-associated fibroblasts modulate growth factor signaling and extracellular matrix remodeling to regulate tumor metastasis. *Biochem Soc Trans* (2017) 45:229–36. doi:10.1042/BST20160387
43. Hung JY, Yen MC, Jian SF, Wu CY, Chang WA, Liu KT, et al. Secreted protein acidic and rich in cysteine (SPARC) induces cell migration and epithelial mesenchymal transition through WNK1/snail in non-small cell lung cancer. *Oncotarget* (2017) 8:63691–702. doi:10.18632/oncotarget.19475
44. Guo S, Xue Y, He Q, He X, Guo K, Dong P, et al. Preoperative serum cystatin-C as a potential biomarker for prognosis of renal cell carcinoma. *PLoS One* (2017) 12:e0178823. doi:10.1371/journal.pone.0178823
45. Asano Y, Ihn H, Yamane K, Jinnin M, Mimura Y, Tamaki K. Phosphatidylinositol 3-kinase is involved in alpha2(I) collagen gene expression in normal and scleroderma fibroblasts. *J Immunol* (2004) 172:7123–35. doi:10.4049/jimmunol.172.11.7123
46. Bergmann C, Distler JH. Canonical Wnt signaling in systemic sclerosis. *Lab Invest* (2016) 96:151–5. doi:10.1038/labinvest.2015.154
47. Janku F. Phosphoinositide 3-kinase (PI3K) pathway inhibitors in solid tumors: from laboratory to patients. *Cancer Treat Rev* (2017) 59:93–101. doi:10.1016/j.ctrv.2017.07.005
48. Li J, Ji L, Chen J, Zhang W, Ye Z. Wnt/beta-Catenin signaling pathway in skin carcinogenesis and therapy. *Biomed Res Int* (2015) 2015:964842. doi:10.1155/2015/964842
49. Sasaki T, Hiroki K, Yamashita Y. The role of epidermal growth factor receptor in cancer metastasis and microenvironment. *Biomed Res Int* (2013) 2013:546318. doi:10.1155/2013/546318
50. Shen W, Tao GQ, Zhang Y, Cai B, Sun J, Tian ZQ. TGF-beta in pancreatic cancer initiation and progression: two sides of the same coin. *Cell Biosci* (2017) 7:39. doi:10.1186/s13578-017-0168-0
51. Kim CG, Lee H, Gupta N, Ramachandran S, Kaushik I, Srivastava S, et al. Role of Forkhead Box Class O proteins in cancer progression and metastasis. *Semin Cancer Biol* (2017) S1044-579X:30092–5. doi:10.1016/j.semcancer.2017.07.007
52. Liu ZH, Dai XM, Du B. Hes1: a key role in stemness, metastasis and multidrug resistance. *Cancer Biol Ther* (2015) 16:353–9. doi:10.1080/15384047.2015.1016662
53. Wang J, Xu L, Liu Y, Chen J, Jiang H, Yang S, et al. Expression of cyclin kinase subunit 2 in human breast cancer and its prognostic significance. *Int J Clin Exp Pathol* (2014) 7:8593–601.
54. Weng AP, Aster JC. No T without D3: a critical role for cyclin D3 in normal and malignant precursor T cells. *Cancer Cell* (2003) 4:417–8. doi:10.1016/S1535-6108(03)00305-2
55. Ohura N, Yamamoto K, Ichioka S, Sokabe T, Nakatsuka H, Baba A, et al. Global analysis of shear stress-responsive genes in vascular endothelial cells. *J Atheroscler Thromb* (2003) 10:304–13. doi:10.5551/jat.10.304
56. Guo H, Majmudar G, Jensen TC, Biswas C, Toole BP, Gordon MK. Characterization of the gene for human EMMPRIN, a tumor cell surface inducer of matrix metalloproteinases. *Gene* (1998) 220:99–108. doi:10.1016/S0378-1119(98)00400-4
57. Fernandez-Medarde A, Santos E. Ras in cancer and developmental diseases. *Genes Cancer* (2011) 2:344–58. doi:10.1177/1947601911411084
58. Reuter S, Gupta SC, Chaturvedi MM, Aggarwal BB. Oxidative stress, inflammation, and cancer: how are they linked? *Free Radic Biol Med* (2010) 49:1603–16. doi:10.1016/j.freeradbiomed.2010.09.006
59. Ozaki T, Nakagawara A. Role of p53 in cell death and human cancers. *Cancers (Basel)* (2011) 3:994–1013. doi:10.3390/cancers3010994
60. Devoy A, Soane T, Welchman R, Mayer RJ. The ubiquitin-proteasome system and cancer. *Essays Biochem* (2005) 41:187–203. doi:10.1042/EB0410187
61. Pencik J, Pham HT, Schmoellerl J, Javaheri T, Schlederer M, Culig Z, et al. JAK-STAT signaling in cancer: from cytokines to non-coding genome. *Cytokine* (2016) 87:26–36. doi:10.1016/j.cyto.2016.06.017
62. Bradham C, McClay DR. p38 MAPK in development and cancer. *Cell Cycle* (2006) 5:824–8. doi:10.4161/cc.5.8.2685
63. Xu XD, Shen HB, Zhu L, Lu JQ, Zhang L, Luo ZY, et al. Anti-RhoC siRNAs inhibit the proliferation and invasiveness of breast cancer cells via modulating the KAI1, MMP9, and CXCR4 expression. *Onco Targets Ther* (2017) 10:1827–34. doi:10.2147/OTT.S93164
64. Nieto Gutierrez A, McDonald PH. GPCRs: emerging anti-cancer drug targets. *Cell Signal* (2017) 41:65–74. doi:10.1016/j.cellsig.2017.09.005
65. Alsaab HO, Sau S, Alzhrani R, Tatiparti K, Bhise K, Kashaw SK, et al. PD-1 and PD-L1 checkpoint signaling inhibition for cancer immunotherapy: mechanism, combinations, and clinical outcome. *Front Pharmacol* (2017) 8:561. doi:10.3389/fphar.2017.00561
66. Chen Y, Zhang Y, Guo X. Proteasome dysregulation in human cancer: implications for clinical therapies. *Cancer Metastasis Rev* (2017) 36:703–16. doi:10.1007/s10555-017-9704-y
67. Vidya MK, Kumar VG, Sejian V, Bagath M, Krishnan G, Bhatta R. Toll-like receptors: significance, ligands, signaling pathways, and functions in mammals. *Int Rev Immunol* (2018) 37:20–36. doi:10.1080/08830185.2017.1380200
68. Randone SB, Guiducci S, Cerinic MM. Systemic sclerosis and infections. *Autoimmun Rev* (2008) 8:36–40. doi:10.1016/j.autrev.2008.07.022
69. Goldszmid RS, Dzutsev A, Trinchieri G. Host immune response to infection and cancer: unexpected commonalities. *Cell Host Microbe* (2014) 15:295–305. doi:10.1016/j.chom.2014.02.003
70. Zeineddine N, Khoury LE, Mosak J. Systemic sclerosis and malignancy: a review of current data. *J Clin Med Res* (2016) 8:625–32. doi:10.14740/jocmr2606w
71. Xue X, Liu Y, Wang Y, Meng M, Wang K, Zang X, et al. MiR-21 and MiR-155 promote non-small cell lung cancer progression by downregulating SOCS1, SOCS6, and PTEN. *Oncotarget* (2016) 7:84508–19. doi:10.18632/oncotarget.13022
72. Tahiri A, Leivonen SK, Luders T, Steinfeld I, Ragle Aure M, Geisler J, et al. Deregulation of cancer-related miRNAs is a common event in both benign and malignant human breast tumors. *Carcinogenesis* (2014) 35:76–85. doi:10.1093/carcin/bgt333
73. Riccioni R, Lulli V, Castelli G, Biffoni M, Tiberio R, Pelosi E, et al. miR-21 is overexpressed in NPM1-mutant acute myeloid leukemias. *Leuk Res* (2015) 39:221–8. doi:10.1016/j.leukres.2014.11.001
74. Li Y, Vecchiarelli-Federico LM, Li YJ, Egan SE, Spaner D, Hough MR, et al. The miR-17-92 cluster expands multipotent hematopoietic progenitors whereas imbalanced expression of its individual oncogenic miRNAs promotes leukemia in mice. *Blood* (2012) 119:4486–98. doi:10.1182/blood-2011-09-378687
75. Ren P, Gong F, Zhang Y, Jiang J, Zhang H. MicroRNA-92a promotes growth, metastasis, and chemoresistance in non-small cell lung cancer cells by targeting PTEN. *Tumour Biol* (2016) 37:3215–25. doi:10.1007/s13277-015-4150-3
76. Joyce CE, Novina CD. miR-155 in acute myeloid leukemia: not merely a prognostic marker? *J Clin Oncol* (2013) 31:2219–21. doi:10.1200/JCO.2012.48.3180
77. Sun Y, Bai Y, Zhang F, Wang Y, Guo Y, Guo L. miR-126 inhibits non-small cell lung cancer cells proliferation by targeting EGFL7. *Biochem Biophys Res Commun* (2010) 391:1483–9. doi:10.1016/j.bbrc.2009.12.098
78. Pekarsky Y, Balatti V, Croce CM. BCL2 and miR-15/16: from gene discovery to treatment. *Cell Death Differ* (2017) 25(1):21–6. doi:10.1038/cdd.2017.159
79. Lowe SW, Lin AW. Apoptosis in cancer. *Carcinogenesis* (2000) 21:485–95. doi:10.1093/carcin/21.3.485
80. Houston A, O'Connell J. The Fas signalling pathway and its role in the pathogenesis of cancer. *Curr Opin Pharmacol* (2004) 4:321–6. doi:10.1016/j.coph.2004.03.008
81. Gatenby RA, Gillies RJ. Why do cancers have high aerobic glycolysis? *Nat Rev Cancer* (2004) 4:891–9. doi:10.1038/nrc1478
82. Heldin CH. Targeting the PDGF signaling pathway in tumor treatment. *Cell Commun Signal* (2013) 11:97. doi:10.1186/1478-811X-11-97

83. Chiariello M, Marinissen MJ, Gutkind JS. Regulation of c-myc expression by PDGF through Rho GTPases. *Nat Cell Biol* (2001) 3:580–6. doi:10.1038/35078555
84. Kalkat M, De Melo J, Hickman KA, Lourenco C, Redel C, Resetca D, et al. MYC deregulation in primary human cancers. *Genes* (2017) 8:E151. doi:10.3390/genes8060151
85. Balkwill F, Mantovani A. Inflammation and cancer: back to Virchow? *Lancet* (2001) 357:539–45. doi:10.1016/S0140-6736(00)04046-0
86. Bien E, Balcerska A. Serum soluble interleukin 2 receptor alpha in human cancer of adults and children: a review. *Biomarkers* (2008) 13:1–26. doi:10.1080/13547500701674063
87. Picard C, Belot A. Does type-I interferon drive systemic autoimmunity? *Autoimmun Rev* (2017) 16:897–902. doi:10.1016/j.autrev.2017.07.001
88. Wu M, Assassi S. The role of type 1 interferon in systemic sclerosis. *Front Immunol* (2013) 4:266. doi:10.3389/fimmu.2013.00266
89. Snell LM, McGaha TL, Brooks DG. Type I interferon in chronic virus infection and cancer. *Trends Immunol* (2017) 38:542–57. doi:10.1016/j.it.2017.05.005
90. Atanackovic D, Arfsten J, Cao Y, Gnjatic S, Schnieders F, Bartels K, et al. Cancer-testis antigens are commonly expressed in multiple myeloma and induce systemic immunity following allogeneic stem cell transplantation. *Blood* (2007) 109:1103–12. doi:10.1182/blood-2006-04-014480
91. Ciechomska M, van Laar JM, O'Reilly S. Emerging role of epigenetics in systemic sclerosis pathogenesis. *Genes Immun* (2014) 15:433–9. doi:10.1038/gene.2014.44
92. Zhou B, Zuo XX, Li YS, Gao SM, Dai XD, Zhu HL, et al. Integration of microRNA and mRNA expression profiles in the skin of systemic sclerosis patients. *Sci Rep* (2017) 7:42899. doi:10.1038/srep42899
93. Pfeffer SR, Yang CH, Pfeffer LM. The role of miR-21 in Cancer. *Drug Dev Res* (2015) 76:270–7. doi:10.1002/ddr.21257
94. Artlett CM, Sassi-Gaha S, Hope JL, Feghali-Bostwick CA, Katsikis PD. Mir-155 is overexpressed in systemic sclerosis fibroblasts and is required for NLRP3 inflammasome-mediated collagen synthesis during fibrosis. *Arthritis Res Ther* (2017) 19:144. doi:10.1186/s13075-017-1331-z
95. Christmann RB, Wooten A, Sampaio-Barros P, Borges CL, Carvalho CR, Kairalla RA, et al. miR-155 in the progression of lung fibrosis in systemic sclerosis. *Arthritis Res Ther* (2016) 18:155. doi:10.1186/s13075-016-1054-6
96. Aqeilan RI, Calin GA, Croce CM. miR-15a and miR-16-1 in cancer: discovery, function and future perspectives. *Cell Death Differ* (2010) 17:215–20. doi:10.1038/cdd.2009.69
97. Fish JE, Santoro MM, Morton SU, Yu S, Yeh RF, Wythe JD, et al. miR-126 regulates angiogenic signaling and vascular integrity. *Dev Cell* (2008) 15:272–84. doi:10.1016/j.devcel.2008.07.008

Conflict of Interest Statement: The research was conducted in the absence of any commercial or financial relationships that could be construed as a potential conflict of interest.

The reviewer SV and handling editor declared their shared affiliation.

frontiers in Immunology

ORIGINAL RESEARCH
published: 04 April 2018
doi: 10.3389/fimmu.2018.00574

N-Formyl Peptide Receptors Induce Radical Oxygen Production in Fibroblasts Derived From Systemic Sclerosis by Interacting With a Cleaved Form of Urokinase Receptor

Filomena Napolitano[1†], Francesca Wanda Rossi[1,2†], Ada Pesapane[1], Silvia Varricchio[3], Gennaro Ilardi[3], Massimo Mascolo[3], Stefania Staibano[3], Antonio Lavecchia[4], Pia Ragno[5], Carmine Selleri[6], Gianni Marone[1,2,7], Marco Matucci-Cerinic[8,9], Amato de Paulis[1,2] and Nunzia Montuori[1,2]*

[1] Department of Translational Medical Sciences, University of Naples Federico II, Naples, Italy, [2] Center for Basic and Clinical Immunology Research (CISI), WAO Center of Excellence, University of Naples Federico II, Naples, Italy, [3] Department of Advanced Functional Sciences, Pathology Section, University of Naples Federico II, Naples, Italy, [4] Department of Pharmacy, Drug Discovery Laboratory, University of Naples Federico II, Naples, Italy, [5] Department of Chemistry and Biology, University of Salerno, Salerno, Italy, [6] Department of Medicine and Surgery, University of Salerno, Salerno, Italy, [7] Institute of Experimental Endocrinology and Oncology (IEOS), Consiglio Nazionale delle Ricerche (CNR), Naples, Italy, [8] Department of Experimental and Clinical Medicine, University of Florence, Florence, Italy, [9] Department of Geriatric Medicine, Division of Rheumatology AOUC, University of Florence, Florence, Italy

OPEN ACCESS

Edited by:
Isabelle Meyts,
KU Leuven, Belgium

Reviewed by:
Ruben Martinez-Barricarte,
Rockefeller University,
United States
Yun Ling,
Shanghai Public Health
Clinical Center, China

***Correspondence:**
Amato de Paulis
depaulis@unina.it

[†]These authors have equally contributed to this work.

Specialty section:
This article was submitted to Primary Immunodeficiencies, a section of the journal Frontiers in Immunology

Received: 25 October 2017
Accepted: 07 March 2018
Published: 04 April 2018

Citation:
Napolitano F, Rossi FW, Pesapane A, Varricchio S, Ilardi G, Mascolo M, Staibano S, Lavecchia A, Ragno P, Selleri C, Marone G, Matucci-Cerinic M, de Paulis A and Montuori N (2018) N-Formyl Peptide Receptors Induce Radical Oxygen Production in Fibroblasts Derived From Systemic Sclerosis by Interacting With a Cleaved Form of Urokinase Receptor. Front. Immunol. 9:574. doi: 10.3389/fimmu.2018.00574

Systemic sclerosis (SSc) is a chronic autoimmune disease characterized by fibrosis, alteration in the microvasculature and immunologic abnormalities. It has been hypothesized that an abnormal redox state could regulate the persistent fibrotic phenotype in SSc patients. *N*-Formyl peptide receptors (FPRs) are chemotactic receptors overexpressed in fibroblasts derived from SSc patients. In this study, we demonstrated that stimulation of FPRs promotes the generation of reactive oxygen species (ROS) in skin fibroblasts. In fibroblast cells, ROS production was due to FPRs interaction with the urokinase receptor (uPAR) and to β_1 integrin engagement. FPRs cross-talk with uPAR and integrins led to Rac1 and ERKs activation. FPRs stimulation increased gp91phox and p67phox expression as well as the direct interaction between GTP-Rac1 and p67phox, thus promoting assembly and activation of the NADPH oxidase complex. FPRs functions occur through interaction with a specific domain of uPAR (residues $_{88}$SRSRY$_{92}$) that can be exposed on the cell membrane by protease-mediated receptor cleavage. Immunohistochemistry analysis with a specific anti-SRSRY antibody showed increased expression of uPAR in a cleaved form, which exposes the SRSRY sequence at its N-terminus (DIIDIII-uPAR88–92) in skin biopsies from SSc patients. As expected by the increased expression of both FPRs and DII-DIII-uPAR$_{88\text{-}92}$, fibroblasts derived from SSc patients showed a significantly increase in ROS generation both at a basal level than after FPRs stimulation, as compared to fibroblasts from normal subjects. C37, a small molecule blocking the interaction between FPRs and uPAR, and selumetinib, a clinically approved MAPKK/ERK inhibitor, significantly inhibited FPRs-mediated ROS production in fibroblasts derived from SSc patients. Thus, FPRs, through the interaction with the uPA/uPAR system, can induce ROS generation in fibroblasts by activating the NADPH oxidase, playing a role in the alteration of the redox state observed in SSc.

Keywords: inflammation, fibrosis, systemic sclerosis, FPRs, uPAR, integrin, ROS, fibroblasts

INTRODUCTION

Systemic sclerosis (SSc) is an autoimmune disorder characterized by thickening of the skin and a severe and often progressive fibrosis of multiple internal organs. Fibrosis is a process characterized by a deregulated repair with an excessive deposition of collagen and other extracellular matrix components, which follows the features of the embryonic development and of the physiological wound healing (1, 2).

The release of reactive oxygen species (ROS) (3) as well as the secretion of chemokines and growth factors, i.e., platelet-derived growth factor (PDGF), transforming growth factor beta (TGF-β), connective tissue growth factor (CTGF), interleukin-6 (IL-6), and interleukin-13 (IL-13), all significantly higher in SSc patients than in controls (1–3), can promote fibroblast activation, fibroblast to myofibroblast transition, and collagen deposition in fibrosis (4).

High levels of ROS and oxidative stress have been directly or indirectly implicated in SSc (1). Indeed, free radicals through a direct profibrogenic effect on fibroblasts contribute to the production of key factors implicated in fibrosis, such as TGF-β (1–4).

In SSc, high levels of ROS are observed in fibroblasts, due to the stimulation of the membrane NADPH oxidase system (5–7). Early in the disease, inflammation generates a mild oxidative stress. Low levels of ROS stabilize and increase the Ras protein level that, in turn, determines increased sensitivity of fibroblast cells to growth factors. ROS also inhibits tyrosine phosphatases and maintains MEK, and ERK1/2 in the active state. Subunits p67 and p47 of the NADPH oxidase undergo phosphorylation by ERK1/2 and further stimulate the production of ROS (1, 8). In addition, a ROS-mediated loop increases the expression of NADPH oxidase 2 and 4 in skin fibroblasts from SSc patients (9).

The circuit linking Ras with ERK1/2 and ROS amplifies and maintains the cytokines and growth factors and their cognate receptors in an autocrine amplification loop (1).

N-formyl peptide receptors (FPRs) are a family of pattern recognition receptors, regulating innate responses (10). FPRs, by interacting with several structurally diverse pro- and anti-inflammatory ligands, possess important regulatory effects in multiple pathophysiological conditions, including inflammation and cancer (10, 11).

We have previously demonstrated that skin fibroblasts from SSc patients overexpress all the three FPRs (FPR1, FPR2, and FPR3) (12). Leoni et al. recently identified a novel intestinal epithelial FPR signaling pathway that is activated by an endogenous FPR1 ligand, annexin A1, and its cleavage product Ac2-26, which determines generation of ROS through NOX1, an epithelial NADPH oxidase (13). The redox signaling pathway resulting from the epithelial FPR1/NOX-1-activation promotes mucosal wound repair.

Since inappropriate NADPH oxidase activation seems to play a fundamental role in determining fibrosis in SSc (1, 4, 8, 9), and FPRs are able to activate NADPH oxidase, both in leukocytes (14) and epithelial cells (13), we sought to investigate whether FPRs could be involved in ROS generation in fibroblasts derived from normal and SSc subjects, through the interaction with the urokinase (uPA)/urokinase receptor (uPAR) system.

Indeed, several functions of FPRs occur through the interaction with uPAR. uPAR is characterized by three homologous domains (DI, DII, DIII) anchored to the cell membrane by a glycosyl-phosphatidylinositol (GPI) tail. uPAR is able to interact with FPRs, tyrosine kinase receptors and integrins, regulating main signal transduction pathways engaged in wound repair, angiogenesis, and tumor progression (15). In the flexible linker connecting uPAR domains DI and DII, a specific region of uPAR, corresponding to amino acids 88–92 (SRSRY), interacts with FPRs, mediating uPA or fMLF-dependent cell migration. uPA or its aminoterminal fragment (ATF), upon binding to the receptor, can promote uPAR interaction with FPRs, through the exposure of the $uPAR_{88–92}$ region. Moreover, the removal of DI, uPA-mediated, results in the expression on the cell surface of a truncated uPAR form that can contain the chemotactic peptide that is able to interact with FPRs and to regulate their signal (DII-DIII-$uPAR_{88–92}$) (16).

Besides FPRs, uPAR can also interact with other cell surface receptors, such as integrins and receptor tyrosine kinases (16–22). uPAR-integrin interactions activate the MAPK cascade, in particular ERK 1/2, with the involvement of non-receptor tyrosine kinase src, tyrosine-kinase family src (Hck, Fgr, Fyn), and focal adhesion-associated protein kinase (FAK) (18). Furthermore, uPAR-mediated cell migration, allowed by uPAR interactions with FPRs and β1 integrins, involves as signaling mediators, specifically, small Rac1 and Rho GTPases (15).

In this study, we investigated FPRs-uPAR-integrin cross-talk as a potential player in ROS generation skin fibroblasts derived from normal subjects and SSc patients.

MATERIALS AND METHODS

Peptides and Chemicals

The hexapeptide Trp-Lys-Tyr-Met-Val-D-Met-NH2 (WKYMVm) was synthesized and HPLC purified (95%) by Innovagen (Lund, Sweden); the peptide $uPAR_{84–95}$ was synthesized by PRIMM (Milan, Italy) and *N*-Formyl-L-methionyl-L-leucyl-L-phenylalanine (fMLF) was obtained from Calbiochem (La Jolla, CA, USA). Protein concentration was determined with a modified Bradford assay (Bio-Rad Laboratories). ECL Plus was obtained from GE Healthcare (Buckinghamshire, UK), and 29, 79-dichlorodihydrofluorescein diacetate (DCHF-DA) was obtained from Molecular Probes (Invitrogen, Paisley, UK). The protease and phosphatase inhibitors cocktail was obtained from Calbiochem. Monoclonal mouse anti-FPR1 phycoerythrin (PE)-conjugated, anti-FPRL1/FPR2 fluorescein (FITC)-conjugated, anti-FPRL2/FPR3 allophycocyanin (APC)-conjugated antibodies were from R&D System (Minneapolis, MN, USA). Mouse anti-$gp91^{phox}$, rabbit anti-$p67^{phox}$, mouse anti-phospho-ERK, and rabbit anti-ERK 2 were from Santa Cruz Biotechnology (Santa Cruz, CA, USA); rabbit anti-actin was obtained from Sigma-Aldrich (St. Louis, MO, USA); mouse anti-uPAR monoclonal antibody R4 was kindly provided by Dr G. Hoyer-Hansen (Finsen Laboratory, Copenhagen, Denmark); secondary anti-mouse and anti-rabbit Abs coupled to HRP were from Bio-Rad (Munchen, Germany). The rabbit antibody anti-$uPAR_{84–95}$ peptide IB (15) was obtained from PRIMM (Milan,

Italy), mouse monoclonal anti-uPAR ADG3937 was obtained from American Diagnostica (Greenwich, CT, USA), mouse anti-uPAR monoclonal antibody R3 was kindly provided by Dr G. Hoyer-Hansen (Finsen Laboratory, Copenhagen, Denmark). Diphenyleneiodonium (DPI), PD98059, and NSC23766 were from Calbiochem; P25 peptide and a peptide with the exact composition of amino acids of P25 but in scrambled control peptide (Scp) were from PRIMM; selumetinib (AZD6244) from AstraZeneca; and C37 from the NCI/DTP Open Chemical Repository (Available from: http://dtp.cancer.gov). They were dissolved in dimethyl sulfoxide (DMSO), stored at −20°C, and added to the culture at final concentrations indicated in the text.

Tissues and Patients' Samples

Eleven females and three males affected by SSc, admitted to the Department of Translational Medical Sciences of the University of Naples Federico II, were diagnosed by following the ACR/EULAR criteria (23) in limited cutaneous ($n=8$) or diffuse cutaneous (dcSSc; $n=6$) subsets (24). The mean age of patients was 49.5 years (range, 30–69 years). Patients according to the disease duration (<5 years for early-stage limited cutaneous SSc and <2 years for early-stage diffuse cutaneous SSc) and skin histopathology were stratified as having an early-stage ($n = 6$) or late-stage ($n = 8$) SSc (25). All patients showing serum positivity for antinuclear Abs (ANA), anti-SCL-70 topoisomerase, and anticentromere (CENP-B) I positivity were included in the study. After obtaining written informed consent, all patients were washed out from steroid treatment at least 30 days before skin biopsy was done. Proton pump inhibitors and vasodilators were allowed. Patients were excluded if severe organ complications prevented steroid treatment washout. All patients with overlapping symptoms of other autoimmune, rheumatic, and/or connective tissue diseases were excluded from the study. Control donors (eight females and two males; mean ± SD age, 45 ± 15 years) were matched with each scleroderma patient (age, sex, and biopsy site) and processed in parallel.

Cell Cultures

Surgical specimens were mechanically dissociated and trypsinizated, as described previously (26). Cells were plated and cultured in monolayer in DMEM (Life Technologies Carlsbad, CA, USA) supplemented with 10% heat inactivated FBS (Life Technologies), 100 U/ml penicillin G sodium, and 100 mg/ml streptomycin sulfate, at 37°C, in a humidified atmosphere of 5% CO_2. Fibroblasts from normal subjects and from patients with SSc were used between the 3rd and 10th passage in culture.

The BJ (human foreskin fibroblasts; ATCC accession number CRL-2522), the HGF-1 (human gingival fibroblasts; ATCC accession number CRL-2014), and the MRC-5 (human lung fibroblasts; ATCC accession number CCL-171) were from ATCC (LGC Standards, Milan, Italy) and were grown in DMEM (Life Technologies) with 10% FBS. BJ cells were obtained from ATCC at the sixth passage, subcultured and frozen in stock vials; they were used between the 1st and 10th passage in culture.

The H460 (cell lung cancer; ATCC accession number HTB-177), as a positive control for uPAR expression, was obtained from ATCC and grown in RPMI 1640 medium (Life Technologies) supplemented with 10% FBS.

Flow Cytometric Analysis of Surface Molecules

Flow cytometric analysis of cell surface molecules was performed as previously described (27). Briefly, after saturation of non-specific binding sites with total rabbit IgG, cells (1×10^6) were incubated for 20 min at +4°C with specific or isotype control antibodies. Finally, cells were washed and analyzed with a FACSCalibur Cytofluorometer using Cell Quest software (Becton & Dickinson, San Fernando, CA, USA). A total of 10^4 events for each sample were acquired in all cytofluorimetric analyses.

Western Blot Analysis

Cells were harvested in lysis buffer (50 mM HEPES, 150 mM NaCl, 10% glycerol, 1% Triton X-100, 1 mM EGTA, 1.5 mM $MgCl_2$, 10 mM NaF, 10 mM sodium pyrophosphate, and 1 mM Na_3VO_4) supplemented with a cocktail of proteases and phosphatases inhibitors. Fifty micrograms of protein was electrophoresed on a 10% SDS-PAGE and transferred onto a polyvinylidene fluoride membrane. The membrane was blocked with 5% nonfat dry milk and probed with specific Abs: mouse anti-uPAR ADG3937 (1 μg/ml), mouse anti-Rac1 (1 μg/ml), mouse anti phospho-ERK (5 μg/ml), rabbit anti-ERK 2 (1 μg/ml), mouse anti-gp91^{phox} (1 μg/ml), rabbit anti-p67^{phox} (1 μg/ml), and rabbit anti-actin (0.5 μg/ml). Finally, washed filters were incubated with HRP-conjugated anti-rabbit or antimouse Abs. The immunoreactive bands were detected by a chemiluminescence kit and quantified by densitometry (ChemiDoc XRS, BioRad) (12).

ROS Detection

The BJ cells were plated overnight at 2×10^4 cells/well in 96-well plates using DMEM with 10% FBS. Cells were incubated with 5 μM 2′,7′-dichlorodihydrofluorescein diacetate (DCHF-DA) for 30 min in the dark at 37°C. The esterified form of DCHF-DA can permeate cell membranes before being deacetylated by intracellular esterases. The resulting compound, dichlorodihydrofluorescein, reacts with ROS, producing an oxidized fluorescent compound, dichlorofluorescein (DCF), which can be detected by a multiplate reader. After incubation with DCHF-DA, cells were washed twice and treated with medium alone, fMLF (10^{-4} M; 10^{-8} M), uPAR$_{84–95}$ (10^{-8} M), WKYMVm peptide (10^{-8} M), and TGF-β (20 ng/ml) as positive control, in the presence or in the absence of P25 peptide (50 μM), anti-uPAR$_{84–95}$ antibody (5 μg/ml), DPI (10 μM), PD98059 (50 μM), NSC23766 (25 μM), C37 (10 μM), and selumetinib (2.5 μM) for 5, 15, 30, and 60 min at 37°C in a humidified 5% CO_2 incubator. DCF was detected at a wavelength of 535 nm by a microplate reader (Tecan Trading AG, Switzerland).

Determination of Rac1 Activity and Association With p67^{phox}

BJ cell lysates were *in vitro* treated with GDP and GTPγS (Upstate) to generate Rac1-GDP and Rac1-GTP, respectively. Rac1-GDP and Rac1-GTP containing lysates were precipitated using the p21-binding domain (PBD) of PAK1, bound to agarose beads. Eluted proteins were subjected to SDS-page and Western blot analysis was performed with antip67^{phox}, anti-gp91^{phox} antibodies and anti-Rac1 antibody as a control.

BJ cells (1×10^6) were incubated at 37°C with or without specific FPRs agonists for the indicated times. Same amount of total protein from clarified lysates were precipitated using the p21-binding domain (PBD) of PAK1, and eluted proteins were subjected to SDS-page and Western blot analysis was performed using anti-$p67^{phox}$, anti-$gp91^{phox}$ antibodies and anti-Rac1 antibody, as a loading control.

Histology and Immunohistochemistry

A 3-mm skin punch biopsy was taken from a representative area of 14 SSc patients and from 10 controls. Specimens were fixed in 10% buffered formalin, embedded in paraffin, and serial sectioned (4-mm-thick sections). One section for each case was stained with H&E and the others were stained by immunohistochemistry (streptavidin-biotin standard technique) with the specific primary antibodies (12). Cells showing a definite black staining confined to the nucleus or cytoplasm were judged positive. All slides were examined in a double-blinded fashion by two investigators, and the final staining for each case was expressed as the percentage of positive cells among the total number of counted cells (at least five high-power representative fields).

Statistical Analyses

All statistical analyses were performed using GraphPad Prism 5.0 software (GraphPad). All the experiments have been executed at least in triplicate. The results are expressed as mean ± SEM. Values from groups were compared using a paired Student's *t*-test (28). Differences were considered significant when $p < 0.05$.

RESULTS

Expression of FPRs and Effects of Their Ligands on ROS Production by Normal Human Fibroblasts

In order to study ROS generation *via* FPRs-uPAR cross-talk in human fibroblasts, we sought a fibroblast cell line to be used as a model. To this aim we investigated, by cytofluorimetric analysis, FPRs expression in three human fibroblast cell lines from different sources: BJ cells (normal foreskin fibroblasts), HGF-1 cells (normal gingival fibroblasts), and MRC5 cells (normal lung fibroblasts). Fibroblasts from the three cell lines, even with a different pattern of expression, synthesized all the three members of the FPRs family (**Figure 1**). Given their derivation from human normal foreskin, all the experiments were conducted on BJ non-immortalized fibroblasts capable to proliferate to a maximum of 72 population doublings before the onset of senescence.

We have demonstrated that in normal fibroblasts the FPRs/uPAR cross-talk is able to mediate several functions such as migration, proliferation, and induction of a myofibroblast phenotype through ROS generation, matrix deposition, and α-SMA overexpression (12).

We investigated the effects of FPRs activation and cross-talk with uPAR on ROS release from normal fibroblasts, using BJ cells as a model. To this aim, we evaluated ROS levels after stimulation with a wide range of concentrations of specific FPRs agonists, fMLF (10^{-4}M–10^{-10}M), the synthetic peptide WKYMVm (10^{-6}M–10^{-9}M), and the synthetic soluble $uPAR_{84\text{-}95}$ peptide (10^{-7}M–10^{-9}M), containing the uPAR-derived ^{88}SRSRY^{92} sequence and able to interact with FPRs on the cell surface and to activate their signals. The intracellular ROS levels were determined after 5, 15, 30, and 60 min of stimulation and compared with unstimulated cells (**Figures 2A–D**).

Figure 2 shows that ROS production from BJ cells was increased in a significant manner after FPRs stimulation with all the three agonists ($p < 0.05$). In particular, we observed that fMLF induced an optimal response both at high concentrations (10^{-4}M), which activate the high affinity receptor FPR1, and lower concentrations, active on FPR2. Indeed, the WKMVYm and $uPAR_{84-95}$ peptides exert their effects with a bell-shaped dose response curve, similar to the typical response observed with

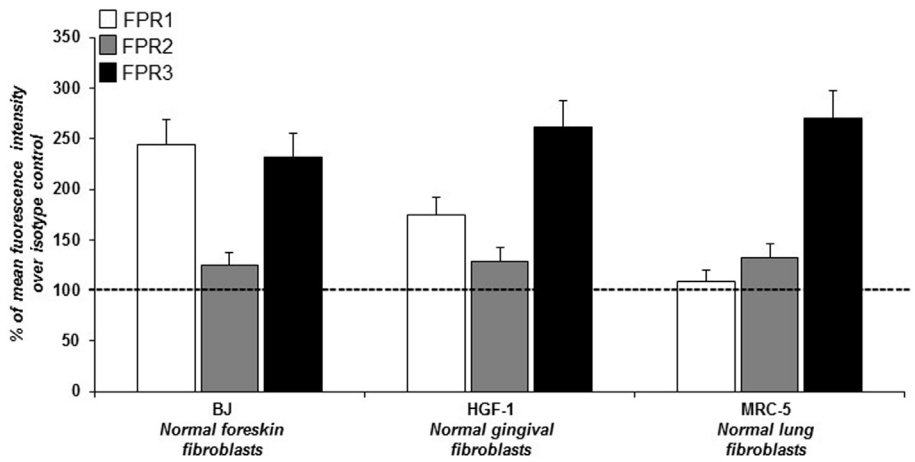

FIGURE 1 | Cytofluorimetric analysis of *N*-formyl peptide receptors (FPRs) expression in human normal fibroblasts. Mean fluorescence intensity of FPR1 (white column), FPR2 (gray column), and FPR3 (black column) expression in BJ (human normal foreskin fibroblasts), HGF-1 (human normal gingival fibroblasts) and MRC-5 (human normal lung fibroblasts) cell lines expressed as a percentage of increase of mean fluorescence intensity of antibody-treated cells over mean fluorescence intensity of isotype control treated cells (considered as 100%).

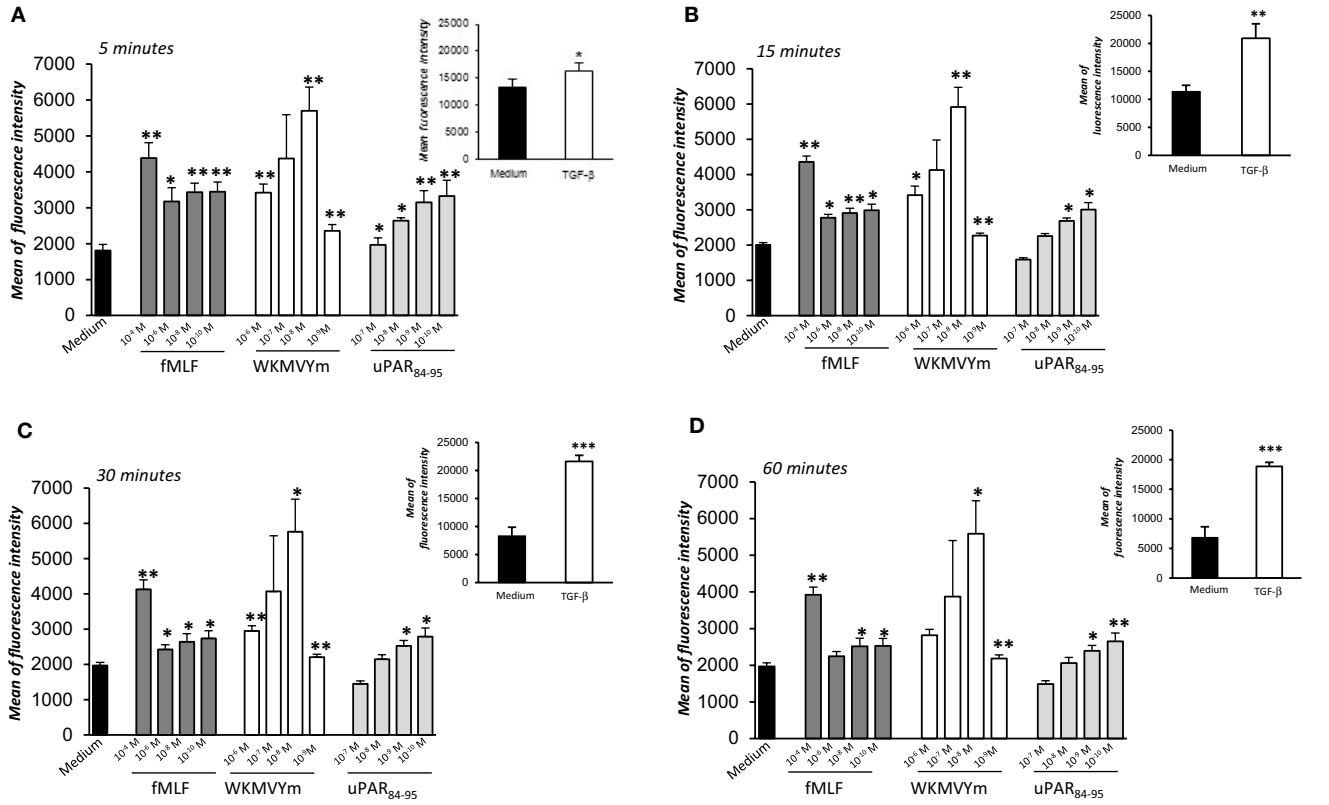

FIGURE 2 | Effects of *N*-Formyl-L-methionyl-L-leucyl-L-phenylalanine (fMLF), WKYMVm peptide, and $uPAR_{84-95}$ on reactive oxygen species (ROS) production in BJ cells. Cells were plated in a 96-well plate and treated with DCHF-DA. At the end of incubation, cells were treated with medium alone (black columns), fMLF (dark gray columns), WKYMVm peptide (white columns), and $uPAR_{84-95}$ peptide (light gray columns). ROS release was measured as dichlorofluorescein (DCF) fluorescence intensity at 5, 15, 30, and 60 min **(A–D)**. Results are expressed as mean fluorescence intensity of DCHF-DA-loaded cells. DCHF-DA-loaded unstimulated cells and TGF-β stimulated cells were examined in parallel, as controls, and are shown in insets. Values are the mean ± SEM of three experiments performed in triplicate. $^{*}p < 0.05$; $^{**}p < 0.001$.

fMLF in inflammatory cells (27). As a control, the effect of TGF-β (20 ng/ml), able to stimulate ROS release by a FPRs independent pathway (4), was examined in parallel in BJ cells (**Figure 2**, panel A–D; insets).

Role of FPRs-uPAR-Integrin Cross-Talk in ROS Generation by Normal Human Fibroblasts

The observation that ^{88}SRSRY^{92} stimulates ROS production (**Figure 2**) suggests that FPRs cross-talk with cell surface uPAR may mediate the same effect. Indeed, uPAR is an important signaling partner of FPRs at the cell-surface (21). Moreover, several studies show that uPAR also requires integrins as co-receptors (15). In fact, uPAR over-expression in tumor cells, controls cell migration and invasion by the recruitment of integrins and FPR1 on cell surface and regulating their signaling pathways (15). Thus, we first investigated the expression of uPAR, both in the native and in the cleaved form (DII-DIII-uPAR), by Western blot, in BJ cells at different time of culture (first and fifth passage). **Figure 3A** shows that BJ cells markedly over-expressed uPAR in the native form; DII-DIII-uPAR was also expressed although to a lesser extent (lane 2 and 3).

Then to test the hypothesis that FPRs could regulate ROS production in fibroblasts through the recruitment, at cell surface of the uPAR/integrins complex, we performed the ROS production assay in the presence of IB, a polyclonal antibody directed against the region involved in uPAR interaction with FPRs, corresponding precisely to the ^{88}SRSRY^{92} region (17) and in the presence of the P25 peptide, which disrupts uPAR interactions with β1 or β2 integrins (29).

Treatment of BJ cells with the IB antibody (5 μg/ml) and the P25 peptide (50 μM) completely inhibited FPRs-mediated ROS production, in response to their specific agonists, fMLF 10^{-4}M and WKYWM peptide 10^{-8}M, whereas non-immune immunoglobulins and a Scp did not exert any effect. As a control, the IB antibody and the P25 peptide did not affect TGF-β induced ROS release by BJ cells (**Figure 3B**).

These results suggest that FPRs could control ROS production by interacting with uPAR, thus participating to a supramolecular complex including integrins, as already demonstrated for cell migration and invasion (15).

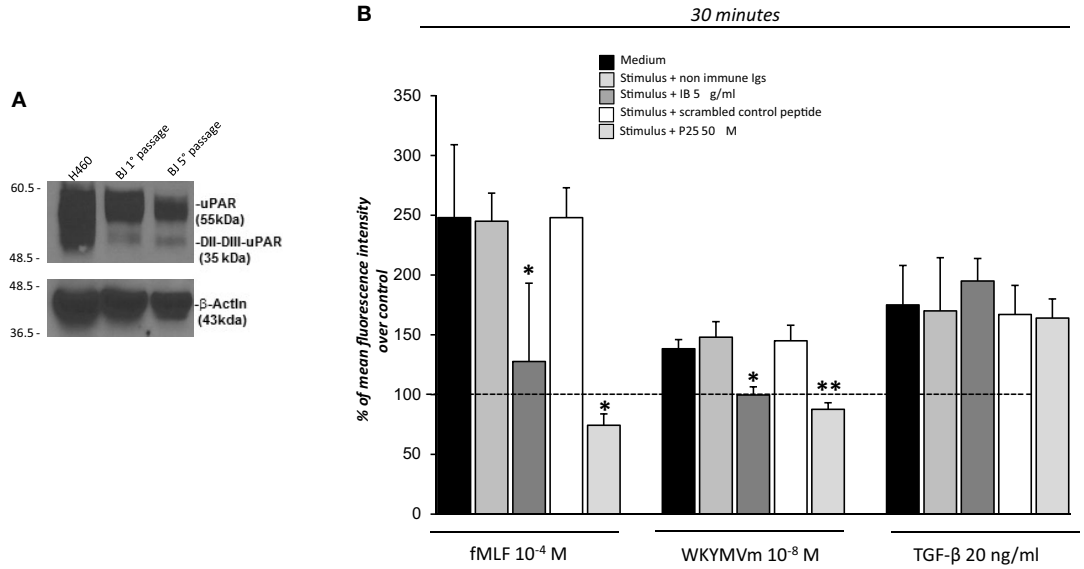

FIGURE 3 | Effects of the inhibition of the cross-talk between FPRs-uPAR-Integrins on reactive oxygen species (ROS) induction in BJ cells. **(A)** Western blot analysis of uPAR expression in H460 cell line as a positive control (lane 1), BJ cells at first passage (lane 2) and fifth passage (lane 3) in culture with the R4 anti-uPAR mAb and with an anti-β-actin Ab, as a loading control. **(B)** BJ cells were plated in a 96-well plate and treated with DCHF-DA. At the end of incubation, cells were treated with medium alone, *N*-formyl-L-methionyl-L-leucyl-L-phenylalanine (fMLF), WKYMVm or TGF-β in the absence (black columns) or in the presence of nonimmune immunoglobulins (medium gray columns), IB antibody (dark gray columns), scrambled control peptide (Scp) (white columns), and P25 peptide (light gray columns). ROS release was measured as dichlorofluorescein (DCF) fluorescence at 30 min. Results are expressed as a percentage of increase of mean fluorescence intensity of stimulated DCHF-DA-loaded cells in respect to unstimulated DCHF-DA-loaded cells (considered as 100%). Values are the mean ± SEM of three experiments performed in triplicate. $^{*}p < 0.05$; $^{**}p < 0.001$.

Rac1 and ERK1/2 Role in FPRs-Mediated ROS Production in Normal Human Fibroblasts

In order to study the signaling pathways involved in FPRs-mediated ROS generation in fibroblasts, we focused on the small GTPase Rac1 and on the ERK1/2 pathway.

uPAR-mediated cell migration, allowed by uPAR interactions with FPRs and β1 integrins, involves as signaling mediators specifically small Rac1 and Rho GTPases (15).

One important effector of Rac1 activity is $p67^{phox}$, which combines with other components of the NADPH oxidase system to generate a functional complex for producing ROS (30). NADPH oxidase system-derived ROS can also activate other downstream signals, such as ERK 1/2 signaling pathways (9). Interestingly, also uPAR-dependent signaling pathways lead to the activation of ERK MAPKs through the activation of PI3K (18).

We analyzed the effects of FPRs stimulation with optimal concentrations of fMLF (10^{-4}M), WKYMVm peptide (10^{-8}M), and $uPAR_{84–95}$ (10^{-8}M) on Rac1 and ERK1/2 activation. All the stimuli increased the levels of Rac1-GTP and p-ERK 1/2 (**Figures 4A,B**). Furthermore, we evaluated ROS levels after stimulation with the same agonists, in the absence or in the presence of an inhibitor of Rac-specific GEF (guanine nucleotide exchange factor) Trio and Tiam1 (NSC23766) (25 μM) and of a specific MEK 1/2 inhibitor (PD98059) (50 μM). BJ cells, which responded to all the three stimuli, were unable to produce ROS in presence of NSC23766 and PD98059 (**Figure 4C**). These results are compatible with the hypothesis that FPRs stimulation in normal fibroblasts determines ROS production by activating Rac1- and ERK 1/2-dependent signals.

FPRs-Mediated ROS Production and NADPH Oxidase-2 Activation in Normal Human Fibroblasts

Having established that FPRs activation induced ROS production through Rac1 and ERK 1/2 signaling in BJ cells, we assessed whether ROS were generated by the NADPH oxidase complex through cell pretreatment with the NOX-inhibitor DPI (10 μM, 1 h) before the addition of fMLF (10^{-4}M), WKYMVm peptide (10^{-8}M), and $uPAR_{84–95}$ (10^{-8}M). **Figure 5A** shows that treatment with DPI in BJ cells determined a significant reduction in ROS levels compared to untreated cells ($p < 0.001$).

Diphenyleneiodonium treatment did not significantly affect ROS release by BJ cells (**Figure 5A**). Indeed, in fibroblast cells, TGF-β mostly induces mitochondrial ROS through the complex III of the electron transport chain (31).

Recently, it has been demonstrated that in SSc fibroblasts, NOX2 and NOX4 are constitutively overexpressed and are responsible for ROS production in these cells (9).

To investigate whether FPRs stimulation could induce ROS production through upregulation and/or activation of the NOX2 complex, we evaluated, by Western blot, the expression levels of $gp91^{phox}$ and $p67^{phox}$ after stimulation with specific agonists of FPRs. **Figure 5** shows that BJ cells responded to fMLF (10^{-4}M), WKYMVm peptide (10^{-8}M), and $uPAR_{84–95}$ (10^{-8}M) by

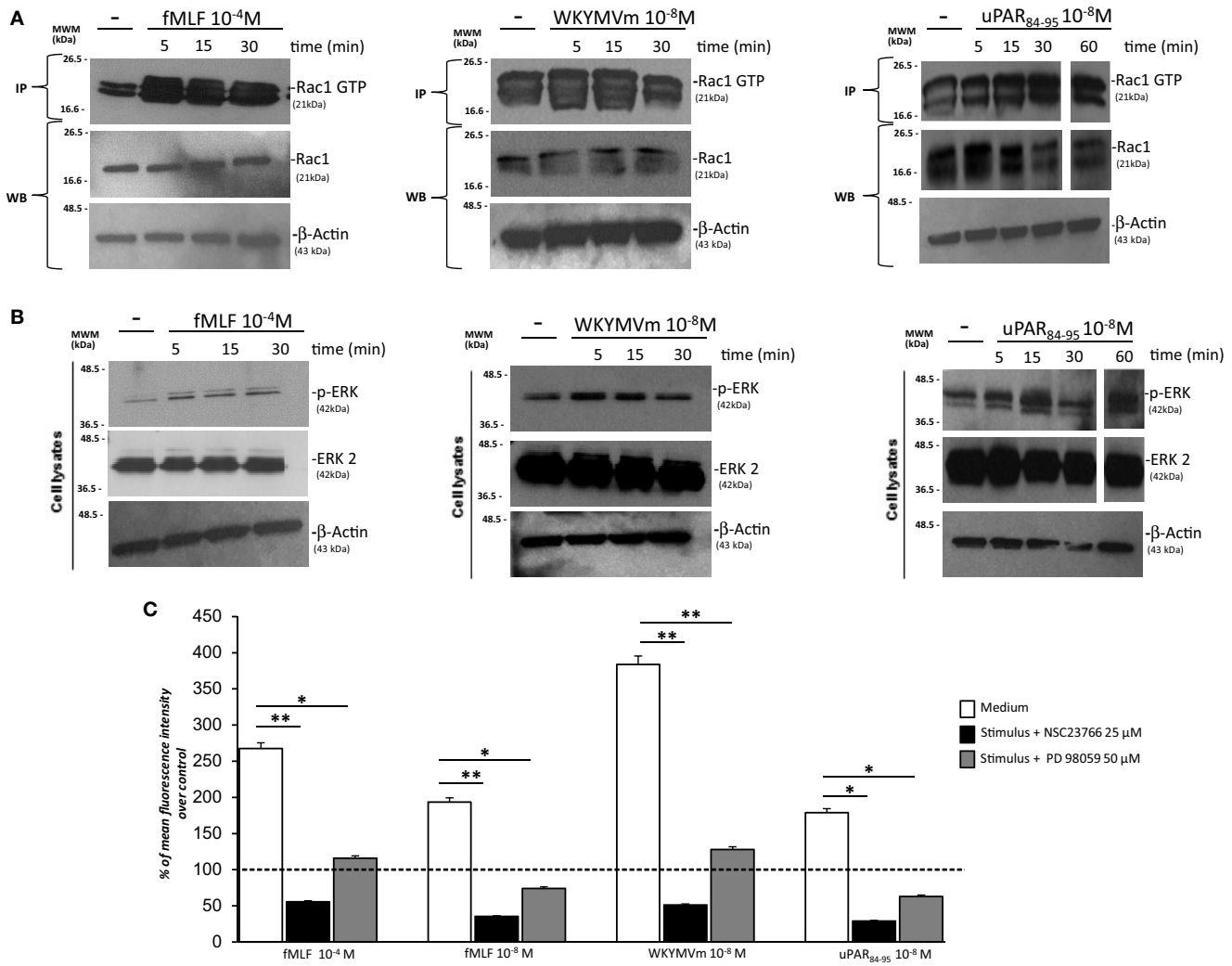

FIGURE 4 | FPRs-mediated Rac1 and ERK activation in BJ cells. **(A)** BJ cells, treated with medium alone (-),*N*-formyl-L-methionyl-L-leucyl-L-phenylalanine (fMLF), WKYMVm peptide, or uPAR$_{84–95}$ peptide, were lysed and subjected to Rac1 activity assay using PAK-PBD-glutathione sepharose beads. Immunoprecipitates and the corresponding total lysates, as an input control, were subjected to Western blot analysis with an anti-Rac1-specific Ab and with an anti-β-actin Ab, as a loading control. **(B)** BJ cells, treated with medium alone, fMLF, WKYMV peptide, or uPAR$_{84–95}$ peptide were lysed and subjected to Western blot analysis with an anti phospho-ERK 1/2 (p-ERK)-specific Ab and then with anti ERK-2 and anti-β-actin Abs, as a loading control. **(C)** BJ cells were plated in a 96-well plate and treated with DCHF-DA. At the end of incubation, cells were treated with fMLF, WKYMVm peptide, and uPAR$_{84–95}$ peptide in the absence (white columns) or in the presence of NSC23766 (black columns) or PD98059 (gray columns). ROS release was measured as dichlorofluorescein (DCF) fluorescence intensity at 5 min. Results are expressed as a percentage of increase of mean fluorescence intensity of stimulated DCHF-DA-loaded cells in respect to unstimulated DCHF-DA-loaded cells (considered as 100%). Values are the mean ± SEM of three experiments performed in triplicate. *$p < 0.05$; **$p < 0.001$.

slightly upregulating the expression of both gp91^{phox} and p67^{phox} (**Figure 5B**).

Upon stimulation, activated GTP bound-Rac1 and/or Rac2 translocate to the plasma membrane and recruit p67^{phox} by binding to its N-terminal (30, 32). In order to demonstrate that the binding of p67^{phox} to Rac1/2-GTP is the limiting step in the assembly of the active NADPH oxidase complex, BJ cell lysates were treated with GDP and GTPγS to generate Rac1-GDP and Rac1-GTP, respectively. Cell lysates containing Rac1-GDP and Rac1-GTP were incubated with the p21-binding domain (PBD) of PAK1, bound to agarose beads. Western blot analysis of precipitated with a polyclonal anti-p67^{phox} antibody revealed that Rac1-GTP binds to p67^{phox} (**Figure 6A**). As a control, Western blot analysis with anti-gp91^{phox} antibody did not show any association with Rac1-GTP (not showed).

To investigate whether FPRs stimulation could induce the interaction between Rac1-GTP and p67^{phox}, the same pull-down experiments were carried out in BJ cells, after stimulation with the specific FPRs agonists, fMLF (10^{-4}M), WKYMVm peptide (10^{-8}M), and uPAR$_{84–95}$ (10^{-8}M). Western blot analysis of precipitated polyclonal anti-p67^{phox} antibody revealed that FPRs stimulation increased interaction between Rac1-GTP and p67^{phox}, thus allowing the assembly of the active NOX2 complex (**Figure 6B**) (33).

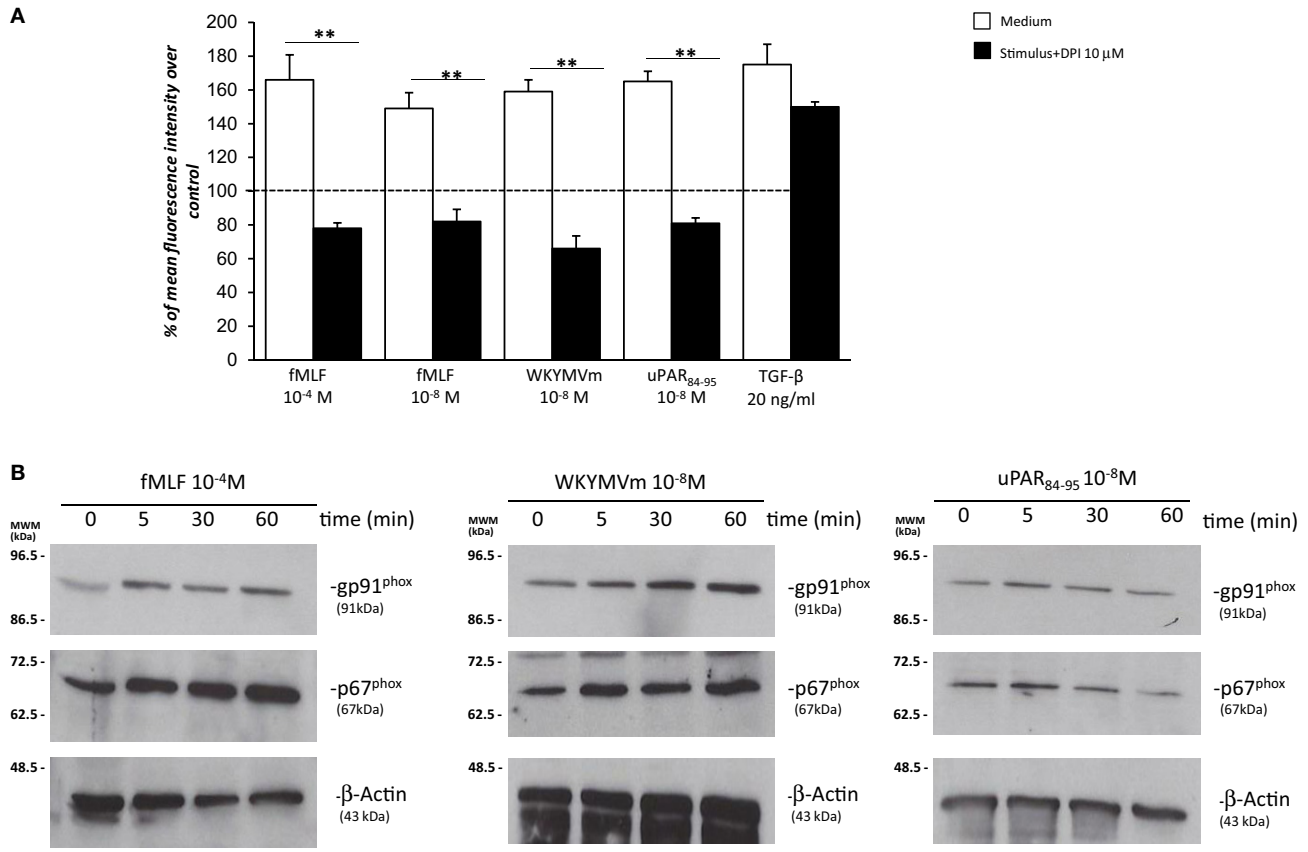

FIGURE 5 | Effects of the NOX-inhibitor diphenyleneiodonium (DPI) on *N*-formyl peptide receptor (FPR)-mediated reactive oxygen species (ROS) production and FPRs-induced modulation of gp91^{phox} and p67^{phox} expression in BJ cells. **(A)** BJ cells were plated in a 96-well plate and pretreated for 1 h at 37°C with 10 μM of the NOX-inhibitor DPI. At the end of incubation, cells were treated with *N*-formyl-L-methionyl-L-leucyl-L-phenylalanine (fMLF), WKYMVm peptide, uPAR$_{84-95}$ peptide, or TGF-β. Results are expressed as percentage of increase of mean fluorescence intensity of stimulated DCHF-DA-loaded cells in respect to unstimulated DCHF-DA-loaded cells (considered as 100%). Values are the mean ± SEM of three experiments performed in triplicate. $^{**}p < 0.001$. **(B)** Western blot analysis with anti-gp91^{phox}, -p67^{phox}, and β-actin antibodies of lysates from BJ cells stimulated with fMLF, WKYMVm peptide, and uPAR$_{84-95}$ peptide for 0, 5, 30, and 60 min.

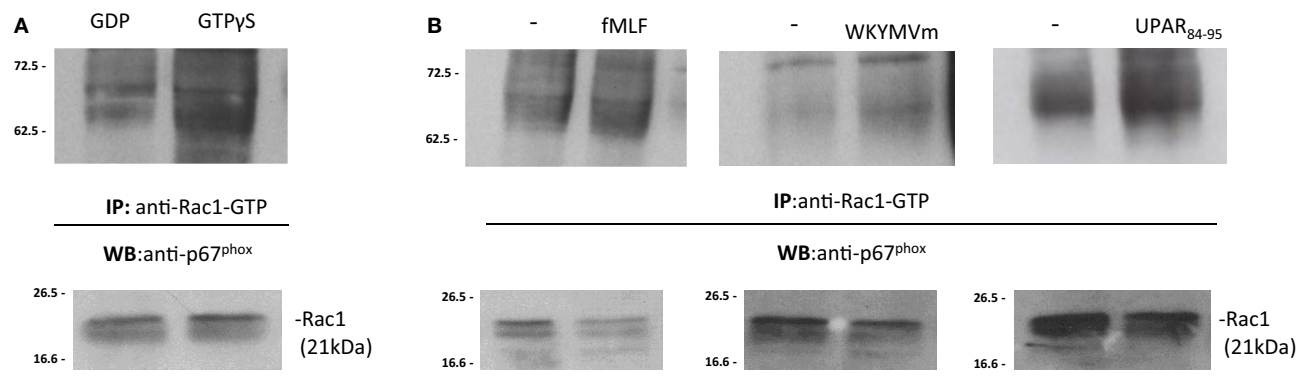

FIGURE 6 | FPRs-mediated Rac1 GTP-p67^{phox} interaction in BJ cells. **(A)** BJ cells lysates were treated with GDP and GTPγS (Upstate) to generate Rac1-GDP and Rac1-GTP, respectively. Rac1-GDP and Rac1-GTP containing lysates were precipitated using the p21-binding domain (PBD) of PAK1, bound to agarose beads. Eluted samples and the corresponding total lysates were subjected to Western blot analysis with a polyclonal anti-p67^{phox} antibody and with anti-Rac1 antibody as a loading control, respectively. **(B)** BJ cells, after incubation with medium alone (-),*N*-formyl-L-methionyl-L-leucyl-L-phenylalanine (fMLF), WKYMVm peptide, for 5 min, or uPAR$_{84-95}$ (10^{-8}M) for 30 min at 37°C in a humidified (5% CO_2) incubator, were lysed and subjected to Rac1 activity assay. Active Rac1 (Rac1-GTP) was precipitated from cell lysates using the PBD of PAK1, bound to agarose beads. Eluted samples and the corresponding total lysates were subjected to Western blot analysis with a polyclonal anti-p67^{phox} antibody and with anti-Rac1 antibody as a loading control, respectively.

After stimulation with specific FPRs agonists, association between Rac1-GTP and gp91^{phox} did not increase (not showed). Thus, our data demonstrate that FPRs/uPAR-mediated ROS generation in fibroblast cells is mediated by a direct binding of Rac1 to p67^{phox} that, in turn, could interact with gp91^{phox} and probably p22^{phox} membrane subunits to generate the active NOX2 complex as described (33).

Ex Vivo Expression of Different uPAR Forms in Human Fibroblasts

Urokinase receptor cleavage contributes to the impaired angiogenesis observed in SSc patients (34, 35). uPAR gene inactivation causes dermal and pulmonary fibrosis and peripheral microvasculopathy in mice. Moreover, native full-length uPAR expression is significantly decreased in the skin of SSc patients, as assessed by a monoclonal anti-uPAR/domain DI antibody (36).

Although full-length uPAR expression is downregulated in SSc dermis, we hypothesized that the DII-DIII-uPAR$_{88–92}$ form, able to interact with FPRs, could instead be increased. To confirm our hypothesis, we investigated the expression of the different uPAR forms in SSc and normal skin biopsies by IHC. In particular, we used the R3 mAb that recognizes domain DI (37), thus the full-length uPAR; the IB polyclonal antibody specifically directed against the ^{88}Ser-Arg-Ser-Arg-Tyr^{92} sequence of uPAR, which is mostly exposed only in the truncated uPAR form (38); the ADG3937 mAb, recognizing an epitope located in the domains DII + DIII which, also, identifies the full-length receptor. SSc skin biopsies revealed dermal fibrosis showing prominent involvement of the deep dermis and the subcutaneous fat, admixed with chronic inflammatory infiltrate, mostly confined deeply around vessels of the subcutis. All biopsies showed an absent/low staining for R3 in fibroblasts, endothelial cells, and lymphocytes. Conversely, IB was found positive in fibroblasts, endothelial cells, and lymphocytes of all specimens; finally, ADG3937 was expressed only in 4 out 14 selected cases. By contrast, skin fibroblasts from control donors showed positivity for the three antibodies (**Figure 7A**).

Effect of Selumetinib and C37 on FPRs/uPAR-Mediated ROS Production in Fibroblasts Derived From SSc Patients

We next aimed to investigate whether inhibition of the structural and functional interaction between FPRs and uPAR by new compounds or tested drugs could affect ROS generation in fibroblasts from SSc patients.

First, fibroblasts derived from primary cultures of three healthy controls and three SSc patients were tested for their ability to produce ROS in basal conditions (**Figure 7B**). To this aim, fluorescence was measured in both cell types after loading with DCHF-DA without any stimulation. Fibroblasts from SSc patients showed an increased level of basal ROS generation at all time points examined, as compared to normal primary fibroblasts.

Then, fibroblasts derived from primary cultures of three healthy controls (**Figure 7C**) and three SSc patients (**Figure 7D**) were tested for their ability to produce ROS after stimulation with fMLF (10^{-4}M), WKYMVm (10^{-8}M) peptide and uPAR$_{84–95}$ (10^{-8}M) peptide, in the absence or in the presence of C37 (10 μM) and selumetinib (2.5 μM). C37 is a small molecule identified by our group by structure-based virtual screening able to target the ^{88}SRSRY^{92} sequence of uPAR in the hot-spot residue Arg^{91} (39); for this reason, its effect on FPRs/uPAR-mediated ROS production was evaluated after stimulations with fMLF and WKYMVm. The effect of selumetinib, a highly selective MEK1 inhibitor currently approved for various anticancer therapies (40), on ROS release mediated by FPRs/uPAR activation was evaluated in parallel, after all the three stimuli. Indeed, we have demonstrated ERK 1/2 involvement in ROS generation induced by FPRs/uPAR activation.

Figure 7C shows that in primary fibroblasts from healthy controls, which significantly responded to all the three stimuli, neither C37 nor selumetinib were able to inhibit FPRs/uPAR-mediated ROS production.

Figure 7D shows that in primary fibroblasts from SSc patients, which responded more efficiently than normal fibroblasts to all the three stimuli, both C37 and selumetinib were significantly active.

The results from these studies show that C37 and selumetinib, through inhibition of FPRs-mediated ROS generation, may lead to the development of novel antifibrotic therapeutic strategies.

DISCUSSION

N-formyl peptide receptors involvement in different inflammatory conditions and in innate immune responses is well established (11). We have already demonstrated that FPRs and their cross-talk with uPAR are involved in the pathogenesis of SSc. Here, we investigated whether FPRs stimulation and their cross-talk with uPAR could induce ROS generation in fibroblasts, thus playing a role in some ROS-mediated processes such as tissue remodeling and fibrosis.

In order to study the molecular mechanisms of FPRs-mediated ROS generation in fibroblast cells, we pursued our studies on the BJ cell line. We demonstrated that FPRs stimulation induces ROS generation in fibroblasts by interacting with uPAR and integrins, as shown in epithelial cell migration and invasion (15). Our study also reported that FPRs/uPAR/β1integrin cross-talk determines ROS production through Rac1 and ERKs activation in human skin fibroblasts.

One important effector of Rac1 activity is p67^{phox}, which combines with the NADPH oxidase system to generate a functional complex for producing ROS. Upon activation by GTP-Rac1, p67^{phox} translocates to the membrane where it associates with gp91^{phox}. FPRs stimulation promoted gp91^{phox} and p67^{phox} expression as well as a direct interaction between GTP-Rac1 and p67^{phox}.

We already provided *in vitro* and *in vivo* evidence that human normal skin fibroblasts expressed FPRs and that SSc fibroblasts overexpress these receptors (12). Here, we evaluated the role of FPRs interaction with uPAR and integrins in the pathogenesis of SSc.

It has been reported that skin sections from uPAR-deficient mice showed increased dermal thickness, collagen content and

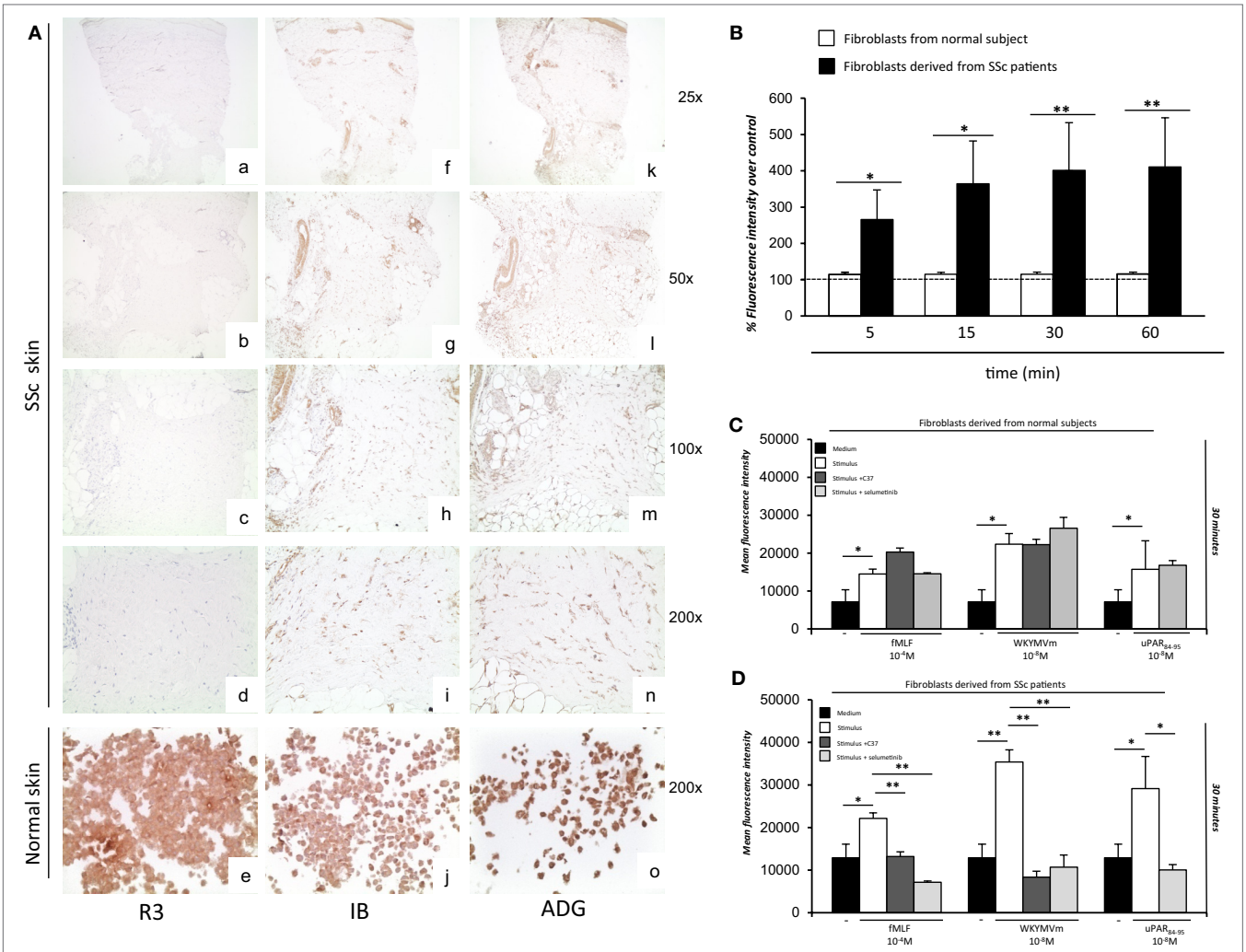

FIGURE 7 | *Ex vivo* expression of uPAR forms and analysis of the effects of C37 and selumetinib on FPRs-mediated reactive oxygen species (ROS) production in fibroblasts derived from normal subjects and systemic sclerosis (SSc) patients. **(A)** (a–d) staining for R3 in localized scleroderma: fibroblasts, lymphocytes, and endothelial cells were negative for R3 (a: original magnification, ×25; b: original magnification, ×50, c: original magnification, ×100; d: original magnification, ×200); (e) staining for R3 in normal human fibroblast cell line: fibroblasts were positive for this antibody [original magnification, ×200] (f–i) staining for IB in localized scleroderma: most fibroblasts, lymphocytes and endothelial cells were positive for IB (f: original magnification, ×25; g: original magnification, ×50, h: original magnification, ×100; i: original magnification, ×200); (j) staining for IB in normal human fibroblast cell line: fibroblasts were positive for this antibody (original magnification, ×200) (k–n) staining for ADG3937 in localized scleroderma: positivity for ADG3937 was observed in fibroblasts, lymphocytes and endothelial cells (k: original magnification, ×25; l: original magnification, ×50, m: original magnification, ×100; *n* original magnification, ×200); (o) staining for ADG3937 in normal human fibroblast cell line: fibroblasts were positive for this antibody (original magnification, ×200) **(B)** Fibroblasts derived from normal subjects (white columns) and SSc patients (gray columns) were plated in a 96-well plate and treated with DCHF-DA. At the end of incubation, cells were washed, and ROS release was measured as dichlorofluorescein (DCF) fluorescence intensity. Results are expressed as a percentage of increase of mean fluorescence intensity of DCHF-DA–loaded cells, as compared with DCHF-DA–unloaded cells (considered as 100%). Values are the mean ± SEM of three experiments performed in triplicate. *$p < 0.05$; **$p < 0.001$. **(C)** Fibroblasts derived from primary cultures of three normal subjects were plated in a 96-well plate and treated with DCHF-DA. At the end of incubation, cells were treated with fMLF, WKYMVm peptide, or $uPAR_{84–95}$ peptide in the absence (white columns) and in the presence of C37 (medium gray columns) or selumetinib (light gray columns). ROS release was measured as dichlorofluorescein (DCF) fluorescence intensity at 30 min. Values are the mean ± SEM of three experiments performed in triplicate. *$p < 0.05$. **(D)** Fibroblasts derived from primary cultures of three SSc patients were plated in a 96-well plate and treated with DCHF-DA. At the end of incubation, cells were treated with *N*-formyl-L-methionyl-L-leucyl-L-phenylalanine (fMLF), WKYMVm peptide, or $uPAR_{84–95}$ peptide in the absence (white columns) and in the presence of C37 (medium gray columns), selumetinib (light gray columns). ROS release was measured as DCF fluorescence intensity. Values are the mean ± SEM of three experiments performed in triplicate. *$p < 0.05$; **$p < 0.001$.

a significantly greater myofibroblast count than uPAR wild-type mice, mimicking the histopathological features of SSc. Moreover, the expression of full length uPAR was decreased in skin biopsies of SSc patients (36). Since the cleavage of uPAR is crucial in fibroblast-to-myofibroblast transition (12, 41) and has been implicated in SSc microvasculopathy (34), we hypothesized that the DII-DIII-$uPAR_{88–92}$ form, able to interact with FPRs, could instead be increased. To confirm our hypothesis,

we analyzed the expression of the different uPAR forms on SSc skin biopsies. We demonstrated that SSc fibroblasts showed increased membrane levels of DII-DIII-uPAR$_{88–92}$, expressing at the N-terminus the chemotactic sequence able to interact with overexpressed FPRs.

According to their increased expression levels, *in vitro* treatment of SSc fibroblasts with C37, a new small molecule able to inhibit the cross-talk between FPRs and uPAR, inhibited ROS production, after stimulation of FPRs with specific ligands. Inhibition of the MAPK/ERK pathway with selumetinib also blocked ROS production upon FPRs stimulation in the same cells.

In conclusion, the results of the present study show that FPRs, through the interaction with the uPA/uPAR system and integrins, induce increased levels of ROS. Both FPRs and a cleaved form of uPAR were able to interact with FPRs, which appear to be overexpressed in skin biopsies of SSc patients when compared to normal controls. This observation reinforces our previous hypothesis of the possible involvement of FPRs/uPAR in the pathogenesis of SSc. Since FPRs functional interaction with uPAR and their signal can be efficiently inhibited by new small molecules, our observations can also help in the development of novel therapeutic strategies in the treatment of SSc.

ETHICS STATEMENT

The study was conducted on samples already obtained for diagnostic purposes, and all patients signed a written informed consent.

AUTHOR CONTRIBUTIONS

FN: responsible for cell cultures, responsible for cellular treatments, WB, Co-IP, and was a contributor in writing the manuscript; FWR: performed cytometric analysis and ROS assay, analyzed the data, and was a contributor in writing the manuscript AP: performed cytometric analysis and ROS assay; SV, GI, MM, SS: performed immunohistochemistry analysis; AL, PR, CS, GM, MMC, AdP: performed data analysis; NM: analyzed the data and was the main contributor in writing the manuscript.

FUNDING

This work was supported by grant from Ministero dell'Istruzione, dell'Università e della Ricerca (MIUR), Campania Bioscience, award number PON03PE_00060_8. The funders had no role in study design, data collection and analysis, decision to publish, or preparation.

REFERENCES

1. Gabrielli A, Avvedimento EV, Krieg T. Scleroderma. *N Engl J Med* (2009) 360:1989–2003. doi:10.1056/NEJMra0806188
2. Jimenez SA, Derk CT. Following the molecular pathways toward an understanding of the pathogenesis of systemic sclerosis. *Ann Intern Med* (2004) 140:37–50. doi:10.7326/0003-4819-140-1-200401060-00010
3. Richter K, Kietzmann T. Reactive oxygen species and fibrosis: further evidence of a significant liaison. *Cell Tissue Res* (2016) 365:591–605. doi:10.1007/s00441-016-2445-3
4. Morry J, Ngamcherdtrakul W, Yantasee W. Oxidative stress in cancer and fibrosis: opportunity for therapeutic intervention with antioxidant compounds, enzymes, and nanoparticles. *Redox Biol* (2017) 11:240–53. doi:10.1016/j.redox.2016.12.011
5. Bedard K, Krause KH. The NOX family of ROS-generating NADPH oxidases: physiology and pathophysiology. *Physiol Rev* (2007) 87:245–313. doi:10.1152/physrev.00044.2005
6. Babio BM. NADPH oxidase. *Curr Opin Immunol* (2004) 16:42–7. doi:10.1016/j.coi.2003.12.001
7. Droge W. Free radicals in the physiological control of cell function. *Physiol Rev* (2002) 82:47–95. doi:10.1152/physrev.00018.2001
8. Sambo P, Baroni SS, Luchetti M, Paroncini P, Dusi S, Orlandini G, et al. Oxidative stress in scleroderma: maintenance of scleroderma fibroblast phenotype by the constitutive up-regulation of reactive oxygen species generation through the NADPH oxidase complex pathway. *Arthritis Rheum* (2001) 44:2653–64. doi:10.1002/1529-0131(200111)44:11<2653::AID-ART445>3.0.CO;2-1
9. Spadoni T, Svegliati Baroni S, D'Amico G, Albani L, Moroncini G, Avvedimento EV, et al. A reactive oxygen species-mediated loop maintains increased expression of NADPH oxidases 2 and 4 in skin fibroblasts from patients with systemic sclerosis. *Arthritis Rheumatol* (2015) 67:1611–22. doi:10.1002/art.39084
10. Le Y, Murphy PM, Wang JM. Formyl-peptide receptors revisited. *Trends Immunol* (2002) 23:541–8. doi:10.1016/S1471-4906(02)02316-5
11. Prevete N, Liotti F, Marone G, Melillo RM, de Paulis A. Formyl peptide receptors at the interface of inflammation, angiogenesis and tumor growth. *Pharmacol Res* (2015) 102:184–91. doi:10.1016/j.phrs.2015.09.017
12. Rossi FW, Napolitano F, Pesapane A, Mascolo M, Staibano S, Matucci-Cerinic M, et al. Upregulation of the N-formyl peptide receptors in scleroderma fibroblasts fosters the switch to myofibroblasts. *J Immunol* (2015) 194:5161–73. doi:10.4049/jimmunol.1402819
13. Leoni G, Alam A, Neumann PA, Lambeth JD, Cheng G, McCoy J, et al. Annexin A1, formyl peptide receptor, and NOX1 orchestrate epithelial repair. *J Clin Invest* (2013) 123:443–54. doi:10.1172/JCI65831
14. Pick E. Role of the Rho GTPase Rac in the activation of the phagocyte NADPH oxidase: outsourcing a key task. *Small GTPases* (2014) 5:e27952. doi:10.4161/sgtp.27952
15. Gorrasi A, Li Santi A, Amodio G, Alfano D, Remondelli P, Montuori N, et al. The urokinase receptor takes control of cell migration by recruiting integrins and FPR1 on the cell surface. *PLoS One* (2014) 9:e86352. doi:10.1371/journal.pone.0086352
16. Montuori N, Ragno P. Multiple activities of a multifaceted receptor: roles of cleaved and soluble uPAR. *Front Biosci* (2009) 14:2494–503. doi:10.2741/3392
17. Resnati M, Pallavicini I, Wang JM, Oppenheim J, Serhan CN, Romano M, et al. The fibrinolytic receptor for urokinase activates the G protein-coupled chemotactic receptor FPRL1/LXA4R. *Proc Natl Acad Sci U S A* (2002) 99:1359–64. doi:10.1073/pnas.022652999
18. Smith HW, Marshall CJ. Regulation of cell signalling by uPAR. *Nat Rev Mol Cell Biol* (2010) 11:23–36. doi:10.1038/nrm2821
19. Degryse B, Resnati M, Czekay RP, Loskutoff DJ, Blasi F. Domain 2 of the urokinase receptor contains an integrin-interacting epitope with intrinsic signaling activity: generation of a new integrin inhibitor. *J Biol Chem* (2005) 280:24792–803. doi:10.1074/jbc.M413954200
20. Chaurasia P, Aguirre-Ghiso JA, Liang OD, Gardsvoll H, Ploug M, Ossowski L. A region in urokinase plasminogen receptor domain III controlling a functional association with alpha5beta1 integrin and tumor growth. *J Biol Chem* (2006) 281:14852–63. doi:10.1074/jbc.M512311200
21. Montuori N, Carriero MV, Salzano S, Rossi G, Ragno P. The cleavage of the urokinase receptor regulates its multiple functions. *J Biol Chem* (2002) 277:46932–9. doi:10.1074/jbc.M207494200
22. Jo M, Takimoto S, Montel V, Gonias SL. The urokinase receptor promotes cancer metastasis independently of urokinase-type plasminogen activator in mice. *Am J Pathol* (2009) 175:190–200. doi:10.2353/ajpath.2009.081053
23. van den Hoogen F, Khanna D, Fransen J, Johnson SR, Baron M, Tyndall A, et al. 2013 classification criteria for systemic sclerosis: an American College of Rheumatology/European League against Rheumatism collaborative initiative. *Arthritis Rheum* (2013) 65:2737–47. doi:10.1002/art.38098

24. LeRoy EC, Black C, Fleischmajer R, Jablonska S, Krieg T, Medsger TA Jr, et al. Scleroderma (systemic sclerosis): classification, subsets and pathogenesis. *J Rheumatol* (1988) 15:202–5.
25. Manetti M, Guiducci S, Romano E, Rosa I, Ceccarelli C, Mello T, et al. Differential expression of junctional adhesion molecules in different stages of systemic sclerosis. *Arthritis Rheum* (2013) 65:247–57. doi:10.1002/art.37712
26. Postiglione L, Montuori N, Riccio A, Di Spigna G, Salzano S, Rossi G, et al. The plasminogen activator system in fibroblasts from systemic sclerosis. *Int J Immunopathol Pharmacol* (2010) 23:891–900. doi:10.1177/039463201002300325
27. de Paulis A, Montuori N, Prevete N, Fiorentino I, Rossi FW, Visconte V, et al. Urokinase induces basophil chemotaxis through a urokinase receptor epitope that is an endogenous ligand for formyl peptide receptor-like 1 and -like 2. *J Immunol* (2004) 173:5739–48. doi:10.4049/jimmunol.173.9.5739
28. Snedecor GW, Cochran WG. *Statistical Methods*. 7th ed. Ames, IA: Iowa State University Press (1980).
29. Wei Y, Lukashev M, Simon DI, Bodary SC, Rosenberg S, Doyle MV, et al. Regulation of integrin function by the urokinase receptor. *Science* (1996) 273:1551–5. doi:10.1126/science.273.5281.1551
30. Lapouge K, Smith SJ, Walker PA, Gamblin SJ, Smerdon SJ, Rittinger K. Structure of the TPR domain of p67phox in complex with Rac GTP. *Mol Cell* (2000) 6:899–907. doi:10.1016/S1097-2765(05)00091-2
31. Jain M, Rivera S, Monclus EA, Synenki L, Zirk A, Eisenbart J, et al. Mitochondrial reactive oxygen species regulate transforming growth factor-β signaling. *J Biol Chem* (2013) 288:770–7. doi:10.1074/jbc.M112.431973
32. Koga H, Terasawa H, Nunoi H, Takeshige K, Inagaki F, Sumimoto H. Tetratricopeptide repeat (TPR) motifs of p67phox participate in interaction with the small GTPase Rac and activation of the phagocyte NADPH oxidase. *J Biol Chem* (1999) 274:25051–60. doi:10.1074/jbc.274.35.25051
33. Grizot S, Fieschi F, Dagher MC, Takeshige K, Inagaki F, Sumimoto H. The active N-terminal region of p67phox: structure at 1.8 A resolution and biochemical characterizations of the A128V mutant implicated in chronic granulomatous disease. *J Biol Chem* (2001) 276:21627–31. doi:10.1074/jbc.M100893200
34. D'Alessio S, Fibbi G, Cinelli M, Guiducci S, Del Rosso A, Margheri F, et al. Matrix metalloproteinase 12 dependent cleavage of urokinase receptor in systemic sclerosis microvascular endothelial cells results in impaired angiogenesis. *Arthritis Rheum* (2004) 50:3275–85. doi:10.1002/art.20562
35. Matucci-Cerinic M, Manetti M, Bruni C, Chora I, Bellando-Randone S, Lepri G, et al. The "myth" of loss of angiogenesis in systemic sclerosis: a pivotal early pathogenetic process or just a late unavoidable event? *Arthritis Res Ther* (2017) 19:162. doi:10.1186/s13075-017-1370-5
36. Manetti M, Rosa I, Milia AF, Guiducci S, Carmeliet P, Ibba-Manneschi L, et al. Inactivation of urokinase-type plasminogen activator receptor (uPAR) gene induces dermal and pulmonary fibrosis and peripheral microvasculopathy in mice: a new model of experimental scleroderma? *Ann Rheum Dis* (2014) 73:1700–9. doi:10.1136/annrheumdis-2013-203706
37. Ronne E, Behrendt N, Ellis V, Ploug M, Danø K, Høyer-Hansen G. Cell-induced potentiation of the plasminogen activation system is abolished by a monoclonal antibody that recognizes the NH2-terminal domain of the urokinase receptor. *FEBS Lett* (1991) 288:233–6. doi:10.1016/0014-5793(91)81042-7
38. Montuori N, Bifulco K, Carriero MV, La Penna C, Visconte V, Alfano D, et al. The cross-talk between the urokinase receptor and fMLP receptors regulates the activity of the CXCR4 chemokine receptor. *Cell Mol Life Sci* (2011) 68:2453–67. doi:10.1007/s00018-010-0564-7
39. Rea VE, Lavecchia A, Di Giovanni C, Rossi FW, Gorrasi A, Pesapane A, et al. Discovery of new small molecules targeting the vitronectin-binding site of the urokinase receptor that block cancer cell invasion. *Mol Cancer Ther* (2013) 12:1402–16. doi:10.1158/1535-7163.MCT-12-1249
40. Holt SV, Logié A, Odedra R, Heier A, Heaton SP, Alferez D, et al. The MEK1/2 inhibitor, selumetinib (AZD6244; ARRY-142886), enhances anti-tumour efficacy when combined with conventional chemotherapeutic agents in human tumour xenograft models. *Br J Cancer* (2012) 106:858–66. doi:10.1038/bjc.2012.8
41. Bernstein AM, Twining SS, Warejcka DJ, Tall E, Masur SK. Urokinase receptor cleavage: a crucial step in fibroblast-to-myofibroblast differentiation. *Mol Biol Cell* (2007) 18:2716–27. doi:10.1091/mbc.E06-10-0912

Conflict of Interest Statement: The authors declare that the research was conducted in the absence of any commercial or financial relationships that could be construed as a potential conflict of interest.

frontiers in Immunology

ORIGINAL RESEARCH
published: 01 October 2018
doi: 10.3389/fimmu.2018.02191

Single Cell RNA Sequencing Identifies HSPG2 and APLNR as Markers of Endothelial Cell Injury in Systemic Sclerosis Skin

Sokratis A. Apostolidis[1†], Giuseppina Stifano[2†], Tracy Tabib[1], Lisa M. Rice[2], Christina M. Morse[1], Bashar Kahaleh[3] and Robert Lafyatis[1]*

[1] Division of Rheumatology, Department of Medicine, University of Pittsburgh Medical Center, Pittsburgh, PA, United States, [2] Boston University School of Medicine, Boston, MA, United States, [3] Division of Rheumatology and Immunology, Department of Medicine, University of Toledo, Toledo, OH, United States

OPEN ACCESS

Edited by:
Megan Anne Cooper, Washington University in St. Louis, United States

Reviewed by:
Mirko Manetti, Università degli Studi di Firenze, Italy
Elisha D. O. Roberson, Washington University in St. Louis, United States

***Correspondence:**
Robert Lafyatis
rlafyatis@gmail.com

[†] *These authors have contributed equally to this work*

Specialty section:
This article was submitted to Primary Immunodeficiencies, a section of the journal Frontiers in Immunology

Received: *01 February 2018*
Accepted: *04 September 2018*
Published: *01 October 2018*

Citation:
Apostolidis SA, Stifano G, Tabib T, Rice LM, Morse CM, Kahaleh B and Lafyatis R (2018) Single Cell RNA Sequencing Identifies HSPG2 and APLNR as Markers of Endothelial Cell Injury in Systemic Sclerosis Skin. Front. Immunol. 9:2191. doi: 10.3389/fimmu.2018.02191

Objective: The mechanisms that lead to endothelial cell (EC) injury and propagate the vasculopathy in Systemic Sclerosis (SSc) are not well understood. Using single cell RNA sequencing (scRNA-seq), our goal was to identify EC markers and signature pathways associated with vascular injury in SSc skin.

Methods: We implemented single cell sorting and subsequent RNA sequencing of cells isolated from SSc and healthy control skin. We used t-distributed stochastic neighbor embedding (t-SNE) to identify the various cell types. We performed pathway analysis using Gene Set Enrichment Analysis (GSEA) and Ingenuity Pathway Analysis (IPA). Finally, we independently verified distinct markers using immunohistochemistry on skin biopsies and qPCR in primary ECs from SSc and healthy skin.

Results: By combining the t-SNE analysis with the expression of known EC markers, we positively identified ECs among the sorted cells. Subsequently, we examined the differential expression profile between the ECs from healthy and SSc skin. Using GSEA and IPA analysis, we demonstrated that the SSc endothelial cell expression profile is enriched in processes associated with extracellular matrix generation, negative regulation of angiogenesis and epithelial-to-mesenchymal transition. Two of the top differentially expressed genes, *HSPG2* and *APLNR*, were independently verified using immunohistochemistry staining and real-time qPCR analysis.

Conclusion: ScRNA-seq, differential gene expression and pathway analysis revealed that ECs from SSc patients show a discrete pattern of gene expression associated with vascular injury and activation, extracellular matrix generation and negative regulation of angiogenesis. HSPG2 and APLNR were identified as two of the top markers of EC injury in SSc.

Keywords: ScRNA-seq, HSPG2, APLNR, systemic sclerosis, endothelial dysfunction

INTRODUCTION

Vascular injury is a hallmark event in the pathogenesis of Systemic Sclerosis (SSc) (1). Endothelial dysfunction happens early in the course of the disease and drives some of the most prominent clinical manifestations of SSc, including Raynaud's phenomenon (RP), telangiectasias, gastric antral vascular ectasias (GAVE), pulmonary arterial hypertension (PAH), and SSc renal crisis (SRC) (1, 2). Loss of nailfold capillaries, nailfold microhemorrhages, and "giant" capillaries are a very useful tool for physicians to diagnose SSc and underlines the importance of microvascular damage in the disease progression (3). Histopathologic examination of the affected vessels reveals extensive intimal hyperplasia, adventitial fibrosis and vascular smooth muscle hypertrophy that lead to luminal narrowing and ultimately occlusion and thrombosis (4, 5). The result is progressive tissue hypoxia, recurrent cycles of ischemia—reperfusion injury and inflammatory changes. In the majority of SSc patients, vascular changes precede the onset of fibrosis suggesting that endothelial injury is central in the pathogenesis of the disease (6–8) and can involve organs in which fibrosis is not traditionally seen such as the kidneys.

The exact mechanisms that lead to endothelial cell injury and propagate the vasculopathy in SSc are not well understood. The presence of tissue hypoxia should promote compensatory angiogenesis. However, this process is defective in SSc patients who exhibit impaired neovascularization and loss of capillaries and arterioles leading to painful digital ulcerations, PAH and SRC (1, 9, 10). A complex network of interactions between endothelial cells, pericytes, myofibroblasts, and the extracellular matrix (ECM) has been implicated in the pathogenesis of SSc (8). It is currently unclear what drives the activation of fibroblasts and the increased ECM deposition responsible for the fibrotic changes seen in SSc. The endothelial cell injury has been proposed to play a prominent role through the production of activating cytokines by SSc endothelial cells (2, 11), disruption of vascular permeability and extravasation of growth factors (1), induction of hypoxia (2), and possibly by contributing to the pool of myofibroblasts through endothelial-to-mesenchymal transition (12).

Altered gene expression, alternative splicing and epigenetic mechanisms have been shown to contribute to the aberrant endothelial function (13–15). Prior gene expression profiling studies (16–19) and proteome-side analyses (13) have shed light onto the molecular pathways affected in SSc patients. However, these studies do not address the discrete contributions of the implicated cell subsets or individual cells and they do not account for cellular heterogeneity and differential cell composition of the target tissues. Thus, interpretation of their results is limited.

In this report, we implemented single cell sorting and subsequent RNA sequencing of cells isolated from SSc and healthy control (HC) skin. We present evidence that scRNA-seq provides a robust platform for cellular identification that allows for gene expression analysis at the single cell level and accounts for cellular heterogeneity. We focus on skin endothelial cells and define the differential *in situ* gene expression profile in SSc patients. Using pathway analysis software, we highlight the implicated molecular pathways. Finally, we verify independently on skin biopsies using immunohistochemistry and on primary endothelial cells using qPCR that APLNR and HSPG2 represent markers highly expressed in endothelial cells from SSc skin and can potentially be used as surrogates of endothelial dysfunction in SSc patients.

MATERIALS AND METHODS

Study Participants

The Boston University Medical Center Institutional Review Board (Boston, MA, USA) reviewed and approved the conduct of this study. Informed consent was obtained from patients with diffuse cutaneous SSc [according to diagnostic (20) and subtype (21) criteria] and healthy subjects. Skin biopsies were obtained from the dorsal mid forearm and immediately collected in PBS for single cell isolation. The modified Rodnan skin score (MRSS) was determined for each patient on the day of the biopsy (22).

For the qPCR studies with primary endothelial cells, human microvascular endothelial cells (MVECs) were isolated as described previously (23) from skin biopsies of four diffuse cutaneous SSc patients and four age and sex-matched healthy controls. Informed consent was obtained in compliance with the Institutional Review Board of Human Studies of University of Toledo. All patients fulfilled the American College of Rheumatology criteria for the diagnosis of SSc; they were not on immunosuppressive or steroid therapy and none had digital ulcers or PAH.

Skin Digestion and Single Cell Suspension Preparation

Skin digestion was performed using the whole skin dissociation kit for human (130-101-540, Macs Miltenyi Biotec). Enzymatic digestion was completed in 2 h, followed by mechanical dissociation using gentleMacs Dissociator running the gentleMACS program h_skin_01.

MoFlo Analysis

Live cells were stained using NucBlue Live Cell Stain ReadyProbes reagent (Hoechst33342), and sorted using fluorescence-activated cell sorting (FACS) with a Beckman Coulter MoFlo Legacy, excited with multi line UV and detected with 450/20 band pass filter. Cells were deposited with cyclone in TCL buffer (Qiagen) on a 96-well plate, and stored at −80°C until RNA-seq processing.

RNA-seq Protocol and Data Analysis

RNA-seq was performed using the SmartSeq2 protocol. The SmartSeq2 libraries were prepared according to the SmartSeq2 protocol (24) with some modifications (25). The Smart-Seq2 data was processed at the Broad Institute using a standard computational pipeline. Libraries were barcoded by cell. They were sequenced using Illumina NextSeq platform. Data was deconvoluted by barcode and aligned using Tophat version 2.0.10 (26). Transcripts were quantified using the Cufflinks suite version 2.2.1 (27). Cuffnorm files were analyzed using the R environment for statistical computing (version 3.2.1).

Using R, we performed t-distributed stochastic neighbor embedding (t-SNE) analysis, k-means clustering and hierarchical clustering. The following packages were used in R: tsne, rtsne, heatmap.2, rorc, gplots, ggplot2, hmisc, reshape, stringr, mixtools, reshape2, vioplot, seurat. The following parameters were used for t-SNE plots: perplexity 30, max iterations at default of 1000, initial dimensions at 10 and theta 0.0. Pathway analysis was performed using the Gene Set Enrichment Analysis software (GSEA) developed by the Broad Institute (28). Our dataset was compared against the following reference genesets: extracellular matrix, KEGG ECM receptor interactions, hallmark epithelial mesenchymal transition, positive regulation of angiogenesis, negative regulation of angiogenesis. Data was also analyzed with the Ingenuity Pathway Analysis (IPA, QIAGEN Inc., https://www.qiagenbioinformatics.com/products/ingenuity-pathway-analysis).

MVEC Cultures

Microvascular endothelial cells (MVECs) were isolated from the biopsy samples and purified using CD31 magnetic beads as previously described (23) and cultured in Clonetics Endothelial Cell Basal Medium-2 (EBM-2) supplemented with EGM-2-MV growth factors (EGM-2) at 37°C in 5% CO2. Normal control dermal MVECs were similarly derived from healthy adult donors who were matched with the SSc patients for age, sex and race.

Immunohistochemistry, Immunofluorescence, and qPCR

Immunohistochemistry for HSPG2 was performed using an anti-HSPG2 antibody (anti-Perlecan, mouse IgG1 Antibody, clone 5D7-2E4, Millipore Sigma), using a staining protocol as previously described (29). Four healthy control skin biopsies and six scleroderma skin biopsies were stained with anti-HSPG2 antibody. Quantitative real-time PCR was performed using primary endothelial cells (MVECs) for *APLNR* and *ACTB* control, using the ddCT method as previously described (30), with the following TaqMan probes on a 7300 Real-Time PCR system (Applied Biosystems):

APLNR: Hs00270873_s1, FAM-MGB, Cat. #4453320 (ThermoFisher Scientific, Applied Biosystems).
ACTB: Hs01060665_g1, FAM-MGB, Cat. #4448892 (ThermoFisher Scientific, Applied Biosystems).

Immunofluorescent single and dual antibody staining using tyramide signal amplification (Tyramide SuperBoost Kits with Alexa Fluor Tyramides; ThermoFisher Scientific, Waltham, MA) were performed on formalin fixed paraffin embedded SSc skin tissues. Tissue sections (5 μm thick) were depariffinized and rehydrated followed by heat induced antigen retrieval in citrate buffer pH6.0 (Vector Labs, Burlingame, CA) for 10 min then allowed to cool for 10 min. Blocking was achieved by using 3% H2O2 followed by 10% goat serum (ThermoFisher Scientific, Waltham, MA) for 1 h each. Dual antibody staining was performed using combinations of mouse monoclonal anti-HSPG Perlecan antibody (1:100; Millipore, Temecula, CA); anti-human Von Willebrand Factor mouse monoclonal antibody (1:100; Dako, Santa Clara, CA); anti-human Von Willebrand Factor rabbit polyclonal antibody (1:50); Sigma Aldrich, St. Louis,MO) and Apelin receptor rabbit monoclonal antibody(clone: 5H5L9, 1:500, ThermoFisher Scientific, Waltham, MA). All primary antibodies were incubated overnight at 4°C. Enzymatic development was performed using appropriate goat anti-rabbit or goat anti-mouse Poly-HRP conjugated secondary antibodies (ThermoFisher Scientific, Waltham, MA) for 1 h followed by Alexa Fluor 488 or 594 labeled tyramide solution and completed with reaction stop solution (ThermoFisher Scientific, Waltham, MA) Dual antibody stained samples underwent the same staining process; after the first antibody development was complete tissue again underwent an additional heat induced antigen retrieval, blocking, incubation with compatible primary antibody, poly-HRP secondary antibody and development with spectrally compatible tryamide Alexa Fluor. Slides underwent nuclear staining with Hoeschst stain (1:2000; ThermoFisher Scientific, Waltham, MA). All wash steps consisted of PBS washes 3 times 10 min each. Finally, slides were cover slipped, using ProLong Diamnond Antifade Mountant (ThermoFisher Scientific, Waltham, MA). Images were taken using an Olympus FLUOVIEW FV1000 (Olympus, Waltham, MA) confocal laser-scanning microscope.

RESULTS

Dimensionality Reduction and Clustering of the Dataset

In order to discover the altered regulation of gene expression in diffuse cutaneous systemic sclerosis (dcSSc), we analyzed skin biopsies from one dcSSc patient and one age and sex-matched healthy control. **Supplementary Figure 1** shows H&E staining of the skin of the dSSc patient with notable fibrosis and inflammatory infiltration. The skin biopsies were digested and single cell suspensions were used to FACS sort single cells in individual wells, which were subsequently used for cDNA library creation and down-stream RNA sequencing. We successfully sequenced 88 cells from the healthy skin biopsy and 96 cells from the SSc skin biopsy.

For our initial goal to visualize and ultimately define the various cell subsets in the dataset, we used t-distributed stochastic neighbor embedding (t-SNE), a method of unsupervised learning for dimensionality reduction. 2D projection of the t-SNE effectively reduced the dimensionality of the data, revealing clustering patterns that represent distinct cellular populations (**Supplementary Figure 2**). Next, we performed K-means clustering analysis of the t-SNE output. First, we calculated the recommended number of k-means centers to be 10 using the "elbow criterion" (**Supplementary Figure 3**). Subsequently, we overlaid the k-means clustering on the t-SNE projection to visualize individual clusters (**Figure 1A**).

Identification of Individual Cell Subpopulations

In order to define the cluster that represents the endothelial cell population in our dataset we employed known endothelial

cell markers. Von Willebrand factor (gene name *VWF*), platelet endothelial cell adhesion molecule (gene name *PECAM1*) and vascular endothelial cadherin (gene name *CDH5*) were expressed in a distinct group of cells in our dataset (**Figure 1B**). Furthermore, plotting *VWF* against *PECAM1* and *CDH5* demonstrated that the cells expressing high levels of *VWF* were also the cells that expressed increased levels of *PECAM1* and *CDH5* (**Figure 1C**). Next, we overlaid the expression of these genes on the t-SNE projection plot (**Figure 1D**) and were able to identify cluster 4 as the endothelial cell cluster (see **Figure 1** for cluster numbering). This cluster contained 9 cells from healthy control skin and 8 cells from SSc skin. We used the gene expression profiles of these cells for the rest of the analysis.

Differential Gene Expression Profile of Endothelial Cells in SSc vs. Healthy Skin

After defining the endothelial cells in our dataset, we identified differentially expressed genes between HC and SSc ECs of the skin. We focused on the two-fold up-regulated or two-fold down-regulated genes in SSc compared to HC endothelial cells (**Supplementary Figure 4** and **Supplementary Table 1**). Differential expression was performed using excel. Pair-wise comparison was done with t-test and FDR applied to account for multiple tests. Only genes that that had >2.0 or < -2.0 FC in a statistically significant manner were included. **Figure 2A** shows the genes upregulated by at least two-fold in a statistically significant manner (top bin) that contain already established markers of endothelial injury and activation, such as the Apelin receptor *APLNR* (31–36), as well as previously identified markers of vascular dysfunction in SSc, such as *THBS1* (16, 37–39) and *VWF* (13, 40–44). The top bin also includes components of the extracellular matrix, including the heparan sulfate proteoglycan 2 (gene name *HSPG2*) that was previously shown to be implicated in fibrotic processes (45–47) including SSc-associated fibrosis (48), wound healing (49, 50) and TGF-β signaling (51, 52). Violin plots for the expression of *VWF, THBS1, APLNR,* and *HSPG2* demonstrate that these genes are upregulated in endothelial cells from SSc skin compared to HC skin (**Figure 2B**).

Pathway Enrichment Analysis

In order to understand the pathways enriched in our dataset and to find gene signatures that are positively or negatively regulated in SSc endothelial cells compared to their healthy counterparts, we used Gene Set Enrichment Analysis (GSEA) (28) and Ingenuity Pathway Analysis (IPA, Qiagen). GSEA provides a software platform to analyze gene expression data through pairwise comparison of the dataset of interest with known biological processes and pathways. ECM alterations are a prominent feature in SSc pathogenesis. Intimal thickening and adventitial fibrosis are commonly seen in biopsies of SSc skin and are the pathologic representations of defective angiogenesis, skin fibrosis and vascular wall remodeling. Previous functional studies have shown that endothelial cells play a central role by promoting the fibrotic intimal lesions through interaction with vascular smooth muscle cells and pericytes (1, 53) and possibly by TGF-β mediated endothelial-to-mesenchymal transition (1, 54, 55). Using genesets that represent the ECM production and

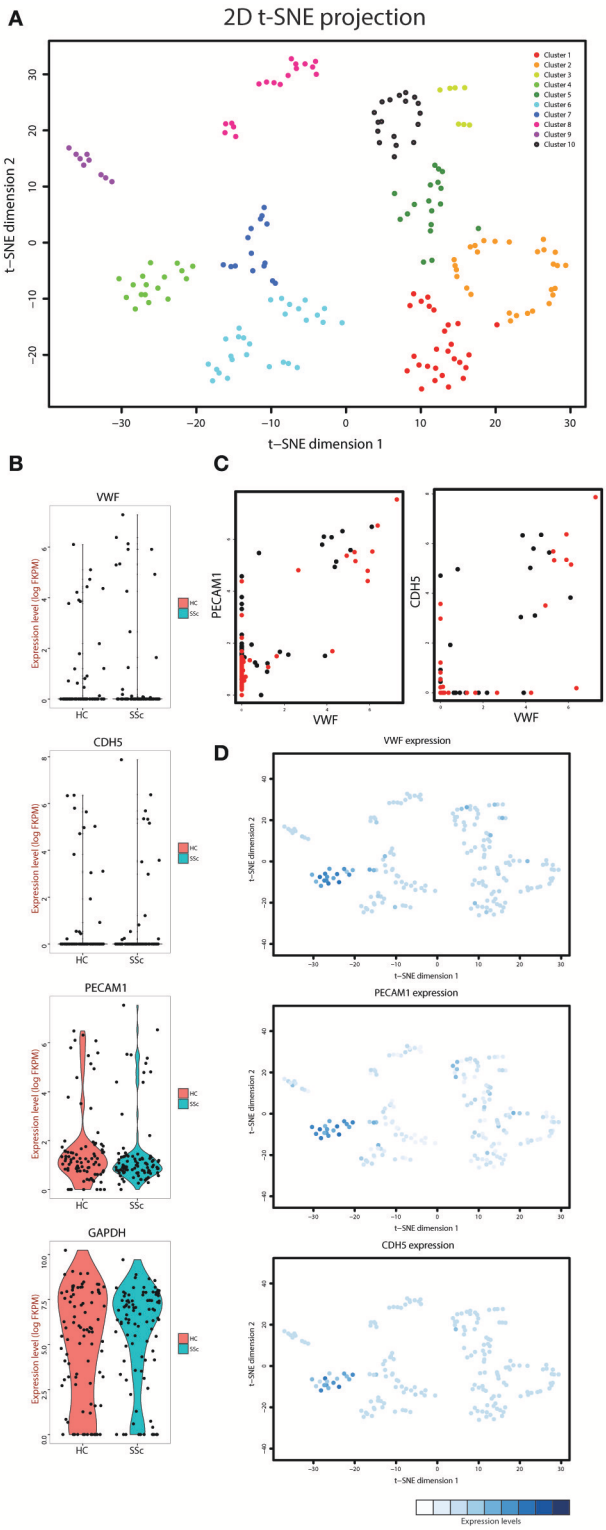

FIGURE 1 | (A) t-SNE analysis of the cells isolated from the systemic sclerosis (SSc) and healthy control (HC) skin. Overlaid is k-means clustering with a defined number of 10 clusters with every cluster represented by a different color. **(B)** Violin plots showing the expression levels and density of expression

(Continued)

FIGURE 1 | for the *VWF*, *CDH5*, *PECAM1,* and *GAPDH* genes in the cells derived from HC and SSc skin. **(C)** Co-expression plots of *VWF* with *PECAM1* (left) and *CDH5* (right) in both HC (black dots) and SSc (red dots) skin cells. **(D)** Overlay of the t-SNE analysis with the expression level of *VWF*, *PECAM1,* and *CDH5* for each cell. The expression levels for each gene were normalized within the respective graph.

ECM receptor interactions, we found that the SSc endothelial cell gene expression profile correlated weakly with ECM ($p = 0.38$, **Figure 3A**, ECM) but more strongly in the complex interactions associated with ECM formation and receptor interactions ($p = 0.0001$, **Figure 3A**, ECM receptor interaction). Using a signature geneset for epithelial-to-mesenchymal transition (EMT), we show that SSc endothelial cells showed a trend toward enrichment in EMT-associated genes ($p = 0.284$, **Figure 3B**). Finally, in order to better understand the effect of SSc in angiogenesis, we employed two different GSEA sets: one corresponding to negative and one to positive regulation of angiogenesis. SSc endothelial cells demonstrated enrichment of genes associated with negative regulation of angiogenesis ($p = 0.018$, **Figure 3C**); conversely, genes associated with the positive regulation of angiogenesis showed a trend toward downregulation in SSc. ($p = 0.2703$, **Figure 3D**). Thus, GSEA demonstrates that the SSc endothelial cell expression profile is enriched in processes associated with ECM generation, weakly associated with EMT, and detects angiogenesis to be negatively regulated in SSc endothelial cells.

In order to find the top biologic processes, signatures, and pathways associated with our dataset, we used Ingenuity Pathway Analysis (Qiagen). Examining the canonical pathways enriched in our database, we found the SSc endothelial cells show enrichment in pathways associated with inhibition of angiogenesis, acute phase response, complement activation and matrix metalloproteinases (**Figure 4**).

Independent Verification of Sentinel Markers

Complementing our scRNA-seq experiments, we independently verified our findings using distinct experimental protocols. First, we stained skin biopsies of SSc skin and HC skin with the extracellular matrix protein HSPG2, one of the differentially expressed genes in the scRNA-seq experiments (**Figure 2**). HSPG2 staining was more robust in SSc skin, especially in the perivascular areas (**Figure 5A**). HSPG2 has been shown to be regulated in a TGF-β dependent manner (51, 52). Both APLNR and HSPG2 co-stained by immunoflorescence with VWF, confirming that they are

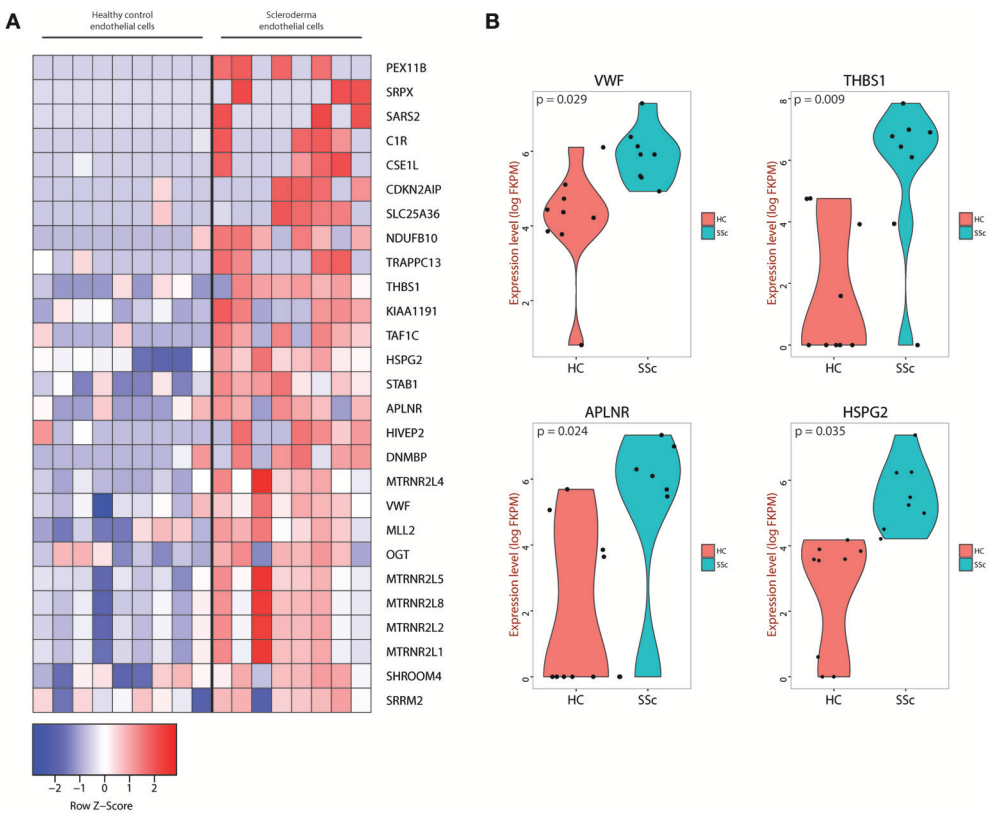

FIGURE 2 | (A) Heatmap of genes that were at least two-fold upregulated in SSc endothelial cells compared to endothelial cells isolated from healthy skin. **(B)** Violin plots for the *VWF*, *THBS1*, *APLNR, and HSPG2* genes showing the expression level and density of expression for the endothelial cells from HC and SSc skin. The corresponding *p*-values are also depicted for each gene.

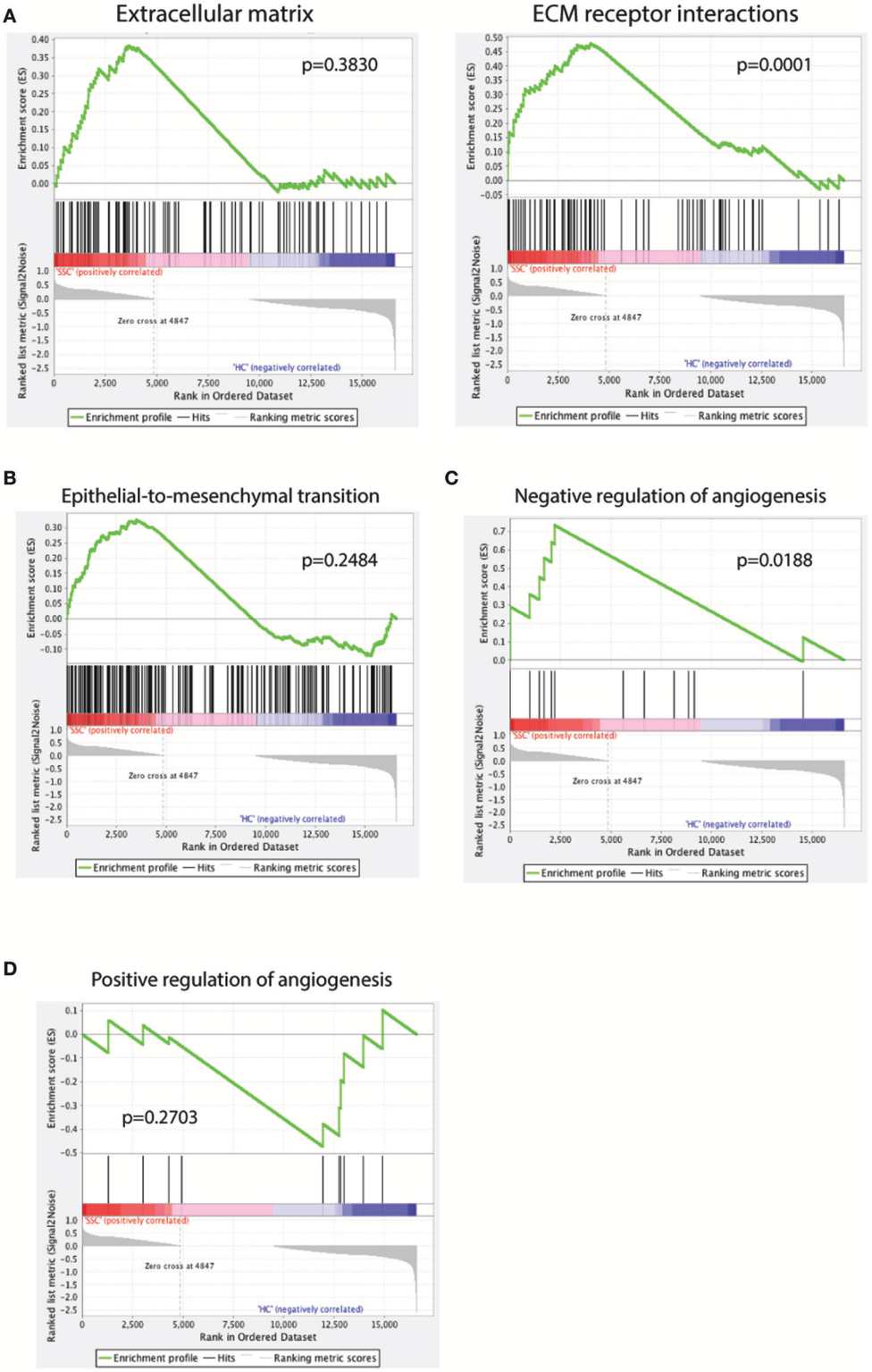

FIGURE 3 | GSEA analysis of the scRNAseq dataset against the GSEA geneset for extracellular matrix (**A**, left) and extracellular matrix (ECM) receptor interactions (**A**, right), epithelial-to-mesenchymal transition **(B)**, negative regulation of angiogenesis **(C)** and positive regulation of angiogenesis **(D)**. A positive enrichment score on the y-axis indicates positive correlation with the SSc endothelial cell group and a negative enrichment score indicates a negative correlation.

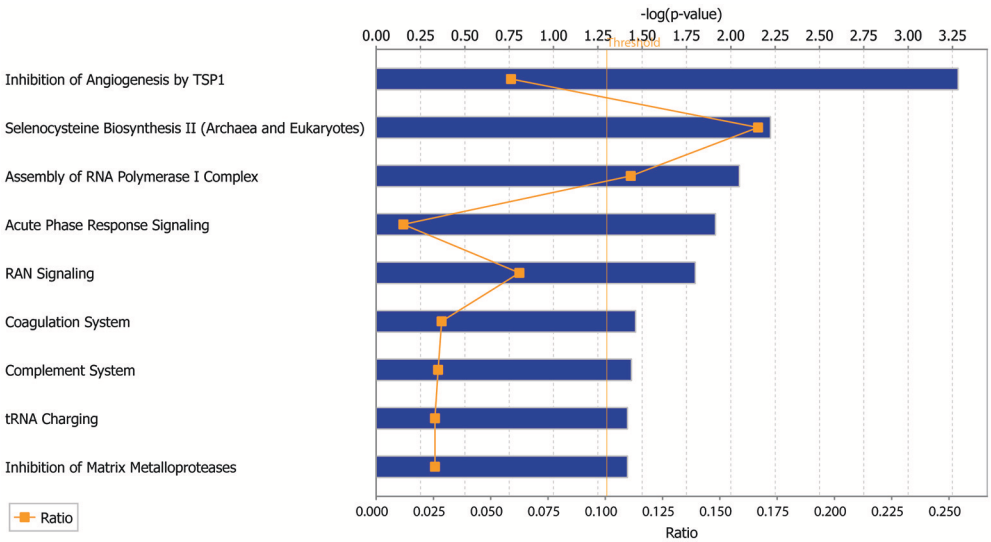

FIGURE 4 | Ingenuity Pathway Analysis (IPA) of the scRNAseq database showing the top canonical pathways enriched in the endothelial cells derived from SSc skin compared to those from healthy control skin.

expressed by endothelial cells in SSc skin (**Figure 5D**). In order to explore the effect of TGF-β signaling blockade on HSPG2 in SSc patients, we used our previously generated microarray data from our clinical trial of a TGF-β blocking antibody, fresolimumab (for patient characteristics, study details, outcomes and microarray data, refer to (16), Clinicaltrials.gov NCT01284322, GEO database accession number GSE55036). In this trial, SSc patients were treated for 7 and 24 weeks with fresolimumab (**Figure 5B**) and HSPG2 expression was reduced by the end of 24 weeks in a statistically significant manner (ANOVA, *p* value 0.027), indicating that HSPG2 expression is inhibited by TGF-β blockade, coincident with the decrease in disease activity and skin inflammation seen with fresolimumab.

APLNR was another gene found to be increased in the SSc endothelial cells using scRNA-seq (**Figure 2**). To independently verify this result, we studied *APLNR* gene expression in microvascular endothelial cells (MVECs) isolated from the skin of four distinct SSc patients and four healthy controls using qPCR. *APLNR* was more highly expressed by SSc primary endothelial cells compared to HC endothelial cells (**Figure 5C**).

DISCUSSION

Vascular injury is a central event in the pathophysiology of SSc. However, our knowledge regarding the pathogenesis and pathways involved in the generation of endothelial cell injury is limited. Here, we provide a comprehensive analysis of scRNA-seq data generated from cells derived from SSc and healthy skin. We show that scRNA-seq provides a robust platform for identifying specific cell subtypes and more importantly differential gene expression profiles and signatures in the cell subpopulations of interest at the single cell level.

Using scRNA-seq, we identified distinct markers that can provide insight in the development of endothelial cell injury, including markers that have been previously linked with the pathogenesis of SSc, such as Thrombospondin 1 and Von Willebrand Factor (13, 16, 37–44). Additional genes identified by our analysis, notably *APLNR* and *HSPG2*, have not been previously linked to SSc pathogenesis. These genes are of particular interest as they have been associated with vascular activation and dysfunction as well as fibrosis in different settings (31–36, 45–50, 56).

Apelin and Elabela are both ligands of the Apelin receptor (*APLNR/APJ*), a G-protein coupled receptor found on endothelial cells (57). These ligands play central roles in cardiovascular development and angiogenesis (31, 35, 56, 58). The Apelin/Elabela-APLNR signaling is critical in regulating vascular maturation and APLNR –/– mice are embryonically lethal secondary to cardiovascular defects (33). APLNR expression is induced in conditions of hypoxia (32, 36). APLNR signaling has not been investigated in SSc other than data suggesting that elevated Apelin levels are associated with more severe vascular disease (59). The Apelin/Elabela-APLNR signaling has been implicated in pulmonary arterial hypertension, one of the major complications of SSc (60, 61). In this setting, increased Apelin activity appears beneficial and receptor agonists are being considered as therapies. In this context, increased APLNR expression might represent a positive adaptive response to hypoxia, fibrosis and/or other vascular injury in the SSc skin microenvironment. On the other hand, APLNR has been associated with pathological retinal angiogenesis and telangectasias (34, 62) and, thus, it might contribute to the dysregulated angiogenesis seen in SSc.

The *HSPG2* gene codes for the extracellular matrix protein perlecan, which represents a main component of the blood vessel basement membrane (63). HSPG2 has been implicated in several

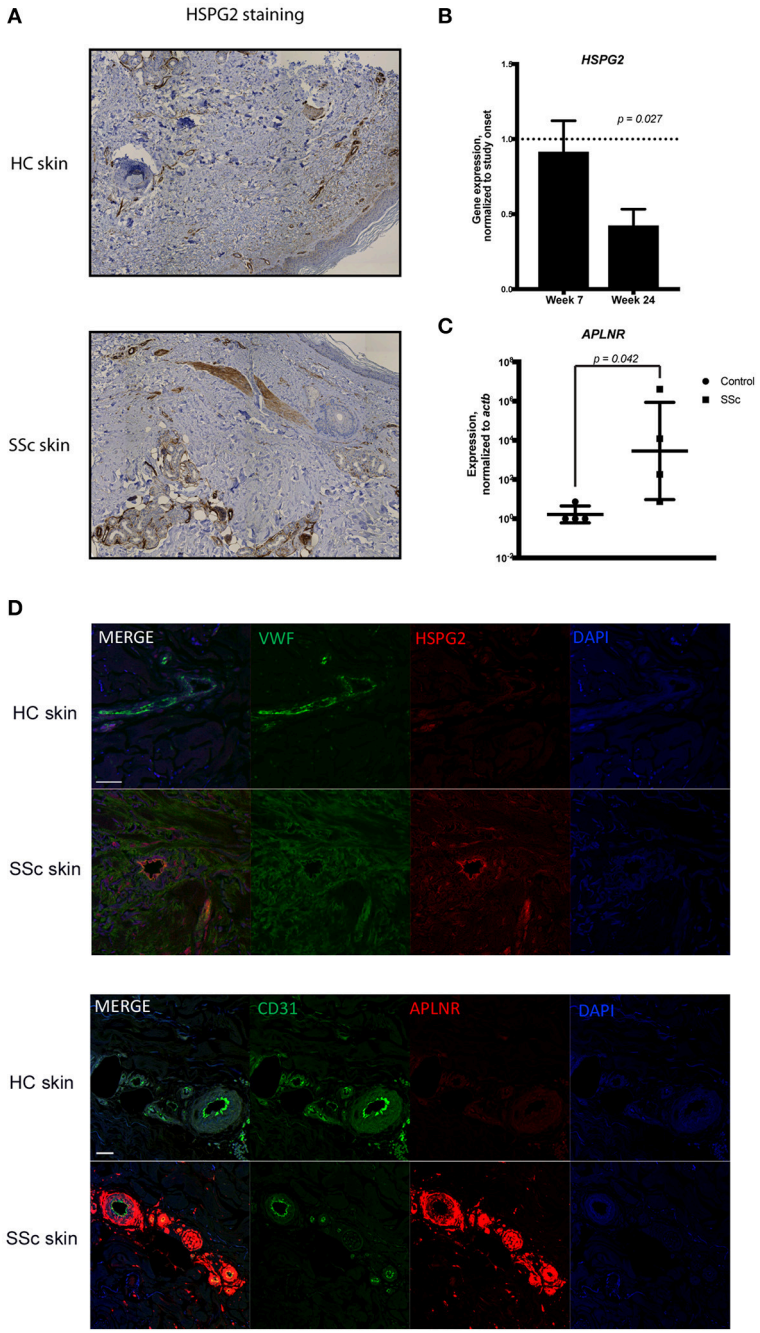

FIGURE 5 | (A) Immunohistochemistry of skin biopsies from healthy and SSc skin showing the expression of HSPG2. **(B)** The microarray data from the Fresolimumab clinical trial were analyzed to show the expression of *HSPG2* gene within the study subjects during treatment with fresolimumab at week 7 and week 24. Expression levels are normalized to the onset of study at the time of enrollment. Data were analyzed using ANOVA and shown is the *p*-value. **(C)** qPCR analysis of the expression of *APLNR* in MVECs isolated from healthy and scleroderma skin. Data are normalized to *ACTB*. *t*-test analysis was performed and the *p*-value is shown. **(D)** Dual antibody immunofluorescent (IF) staining of formalin fixed paraffin embedded scleroderma and control skin biopsies sectioned in 5 μm sections. Upper panels show dual IF staining of HSPG2 (green) and Von Willebrand factor (red) co-localizing on blood vessels. Lower panels show dual IF staining of Von Willebrand factor (green) and APLNR (red) co-localizing on blood vessels in scleroderma skin with DAPI nuclear stain. Scale bar = 50mm.

fibrotic processes, including liver fibrosis and desmoplastic tumors (45–47). Interestingly, a C-terminal fragment of HSPG2 was found to be a main fibrogenic mediator produced by apoptotic SSc endothelial cells (48). Specifically, the C-terminal HSPG2 fragment produced by apoptotic SSc endothelial cells induced PI3K-dependent resistance to apoptosis in fibroblasts and activated myofibroblast differentiation (48). HSPG2-deficient mice exhibit delayed wound healing (49),

impaired angiogenesis (49, 52) and decreased TGF-β production in the mouse skin (50). Reciprocally, TGF-β signaling induces HSPG2 promoter activity (51). Analysis of the fresolimumab clinical trial microarray data suggests that *HSPG2* gene expression in SSc skin is regulated by TGF-β. Thus, TGFβ up-regulation of HSPG2 may mediate a profibrotic response to vascular injury in SSc skin.

Our pathway analysis on the single-cell platform demonstrates that the pathways of extracellular matrix generation, inhibition of angiogenesis, epithelial to mesenchymal transition and matrix metalloproteinase production are highly activated and centrally involved in the pathophysiology of endothelial cell injury in SSc patients. A recent study has highlighted the potential importance of endothelial-mesenchymal transition in SSc (64). Our pathway analysis, showing a trend toward upregulated epithelial-mesenchymal transition, supports this notion.

A limitation of the current study is that only one patient and one control biopsy were analyzed by scRNA-seq. However, ancillary studies examining RNA expression in cells and skin immunohistochemistry support the generalizability of the scRNA-seq findings. We anticipate with emerging technologies that more cells and more robust signatures might be found.

Vascular injury occurs early in the disease course of SSc. Raynaud's phenomenon and other vascular malformations can precede the development of overt disease for years to decades. Understanding the endothelial cell injury pathways has the potential of allowing early identification of patients and more accurate prognostication. In addition, our data point to several upregulated endothelial cell genes in SSc skin and implicate these genes in distinct pathways in SSc pathogenesis. Our results provide the framework for the development of biomarkers representing vascular injury and therapeutic targets to be further explored.

ETHICS STATEMENT

This study was carried out in accordance with the recommendations of IRB committee of Boston University Medical Center. All subjects gave written informed consent in accordance with the Declaration of Helsinki.

AUTHOR CONTRIBUTIONS

SA, GS, TT, LR, and CM designed and performed experiments, analyzed the data, and prepared the manuscript. BK analyzed the data and prepared the manuscript. RL designed experiments, analyzed the data and prepared the manuscript.

FUNDING

Research reported in this publication was supported by the National Institute of Arthritis and Musculoskeletal and Skin Diseases under award number 2P50 AR060780 of the National Institutes of Health. The content is solely the responsibility of the authors and does not necessarily represent the official views of the National Institutes of Health.

SUPPLEMENTARY MATERIAL

The Supplementary Material for this article can be found online at: https://www.frontiersin.org/articles/10.3389/fimmu.2018.02191/full#supplementary-material

Supplementary Figure 1 | H&E staining of the skin from the dcSSc patients used for the scRNA-seq showing the extensive fibrosis (arrows) and inflammatory infiltration (arrowheads).

Supplementary Figure 2 | Two-dimensional projection of the t-SNE analysis of the cells isolated from the systemic sclerosis (SSc) and healthy control (HC) skin. Cells were pooled together to facilitate cell subset identification.

Supplementary Figure 3 | The "elbow" criterion used to determine the optimal number of clusters to be used for the k-means clustering used in conjunction with the t-SNE analysis.

Supplementary Figure 4 | Heatmap with hierarchical clustering of genes that were at least two-fold up-regulated or down-regulated in SSc endothelial cells compared to endothelial cells isolated from healthy skin.

Supplementary Table 1 | Genes regulated <2-fold in SSc compared to healthy skin endothelial cells.

REFERENCES

1. Matucci-Cerinic M, Kahaleh B, Wigley FM. Review: evidence that systemic sclerosis is a vascular disease. *Arthritis Rheum.* (2013) 65:1953–62. doi: 10.1002/art.37988
2. Altorok N, Wang Y, Kahaleh B. Endothelial dysfunction in systemic sclerosis. *Curr Opin Rheumatol.* (2014) 26:615–20. doi: 10.1097/BOR.0000000000000112
3. Cutolo M, Sulli A, Pizzorni C, Accardo S. Nailfold videocapillaroscopy assessment of microvascular damage in systemic sclerosis. *J Rheumatol.* (2000) 27:155–60.
4. D'Angelo WA, Fries JF, Masi AT, Shulman LE. Pathologic observations in systemic sclerosis (scleroderma). A study of fifty-eight autopsy cases and fifty-eight matched controls. *Am J Med.* (1969) 46:428–40. doi: 10.1016/0002-9343(69)90044-8
5. Norton WL, Nardo JM. Vascular disease in progressive systemic sclerosis (scleroderma). *Ann Intern Med.* (1970) 73:317–24.
6. Cipriani P, Marrelli A, Liakouli V, Di Benedetto P, Giacomelli R. Cellular players in angiogenesis during the course of systemic sclerosis. *Autoimmun Rev.* (2011) 10:641–6. doi: 10.1016/j.autrev.2011.04.016
7. Kahaleh B. Vascular disease in scleroderma: mechanisms of vascular injury. *Rheum Dis Clin North Am.* (2008) 34:57–71. doi: 10.1016/j.rdc.2007.12.004
8. Wigley FM. Vascular disease in scleroderma. *Clin Rev Allergy Immunol.* (2009) 36:150–75. doi: 10.1007/s12016-008-8106-x
9. Kuwana M, Okazaki Y. Brief report: impaired *in vivo* neovascularization capacity of endothelial progenitor cells in patients with systemic sclerosis. *Arthritis Rheumatol.* (2014) 66:1300–5. doi: 10.1002/art.38326
10. Manetti M, Guiducci S, Ibba-Manneschi L, Matucci-Cerinic M. Impaired angiogenesis in systemic sclerosis: the emerging role of the antiangiogenic VEGF(165)b splice variant. *Trends Cardiovasc Med.* (2011) 21:204–10. doi: 10.1016/j.tcm.2012.05.011
11. Serrati S, Chilla A, Laurenzana A, Margheri F, Giannoni E, Magnelli L, et al. Systemic sclerosis endothelial cells recruit and activate dermal fibroblasts by induction of a connective tissue growth factor (CCN2)/transforming growth factor beta-dependent mesenchymal-to-mesenchymal transition. *Arthritis Rheum.* (2013) 65:258–69. doi: 10.1002/art.37705
12. Hashimoto N, Phan SH, Imaizumi K, Matsuo M, Nakashima H, Kawabe T, et al. Endothelial-mesenchymal transition in bleomycin-induced pulmonary fibrosis. *Am J Respir Cell Mol Biol.* (2010) 43:161–72. doi: 10.1165/rcmb.2009-0031OC

13. van Bon L, Affandi AJ, Broen J, Christmann RB, Marijnissen RJ, Stawski L, et al. Proteome-wide analysis and CXCL4 as a biomarker in systemic sclerosis. *N Engl J Med*. (2014) 370:433–43. doi: 10.1056/NEJMoa1114576
14. Manetti M, Guiducci S, Romano E, Ceccarelli C, Bellando-Randone S, Conforti ML, et al. Overexpression of VEGF165b, an inhibitory splice variant of vascular endothelial growth factor, leads to insufficient angiogenesis in patients with systemic sclerosis. *Circ Res*. (2011) 109:e14–26. doi: 10.1161/CIRCRESAHA.111.242057
15. Noda S, Asano Y, Takahashi T, Akamata K, Aozasa N, Taniguchi T, et al. Decreased cathepsin V expression due to Fli1 deficiency contributes to the development of dermal fibrosis and proliferative vasculopathy in systemic sclerosis. *Rheumatology* (2013) 52:790–9. doi: 10.1093/rheumatology/kes379
16. Rice LM, Padilla CM, McLaughlin SR, Mathes A, Ziemek J, Goummih S, et al. Fresolimumab treatment decreases biomarkers and improves clinical symptoms in systemic sclerosis patients. *J Clin Invest*. (2015) 125:2795–807. doi: 10.1172/JCI77958
17. Whitfield ML, Finlay DR, Murray JI, Troyanskaya OG, Chi JT, Pergamenschikov A, et al. Systemic and cell type-specific gene expression patterns in scleroderma skin. *Proc Natl Acad Sci USA*. (2003) 100:12319–24. doi: 10.1073/pnas.1635114100
18. Gardner H, Shearstone JR, Bandaru R, Crowell T, Lynes M, Trojanowska M, et al. Gene profiling of scleroderma skin reveals robust signatures of disease that are imperfectly reflected in the transcript profiles of explanted fibroblasts. *Arthritis Rheum*. (2006) 54:1961–73. doi: 10.1002/art.21894
19. Milano A, Pendergrass SA, Sargent JL, George LK, McCalmont TH, Connolly MK, et al. Molecular subsets in the gene expression signatures of scleroderma skin. *PLoS ONE* (2008) 3:e2696. doi: 10.1371/annotation/05bed72c-c6f6-4685-a732-02c78e5f66c2
20. Masi AT, Rodnan G, Medsger T Jr, Altman R, D'Angelo W, Fries J. Subcommittee for scleroderma criteria of the American Rheumatism Association Diagnostic and Therapeutic Criteria Committee. Preliminary criteria for the classification of systemic sclerosis (scleroderma). *Arthritis Rheum*. (1980) 23:581–90.
21. LeRoy EC, Black C, Fleischmajer R, Jablonska S, Krieg T, Medsger TA Jr, et al. Scleroderma (systemic sclerosis): classification, subsets and pathogenesis. *J Rheumatol*. (1988) 15:202–5.
22. Furst DE, Clements PJ, Steen VD, Medsger T Jr, Masi AT, D'Angelo WA, et al. The modified Rodnan skin score is an accurate reflection of skin biopsy thickness in systemic sclerosis. *J Rheumatol*. (1998) 25:84–8.
23. Normand J, Karasek MA. A method for the isolation and serial propagation of keratinocytes, endothelial cells, and fibroblasts from a single punch biopsy of human skin. *In Vitro Cell Dev Biol Anim*. (1995) 31:447–55. doi: 10.1007/BF02634257
24. Picelli S, Faridani OR, Björklund ÅK, Winberg G, Sagasser S, Sandberg R. Full-length RNA-seq from single cells using Smart-seq2. *Nat Protoc*. (2014) 9:171–81. doi: 10.1038/nprot.2014.006
25. Trombetta JJ, Gennert D, Lu D, Satija R, Shalek AK, Regev A. Preparation of single-cell RNA-seq libraries for next generation sequencing. *Curr Protoc Mol Biol.* (2014) suppl 107:4.22.1–4.22.17. doi: 10.1002/0471142727.mb0422s107
26. Kim D, Pertea G, Trapnell C, Pimentel H, Kelley R, Salzberg SL. TopHat2: accurate alignment of transcriptomes in the presence of insertions, deletions and gene fusions. *Genome Biol*. (2013) 14:R36. doi: 10.1186/gb-2013-14-4-r36
27. Trapnell C, Roberts A, Goff L, Pertea G, Kim D, Kelley DR, et al. Differential gene and transcript expression analysis of RNA-seq experiments with TopHat and Cufflinks. *Nat Protoc*. (2012) 7:562–78. doi: 10.1038/nprot.2012.016
28. Subramanian A, Tamayo P, Mootha VK, Mukherjee S, Ebert BL, Gillette MA, et al. Gene set enrichment analysis: a knowledge-based approach for interpreting genome-wide expression profiles. *Proc Natl Acad Sci USA*. (2005) 102:15545–50. doi: 10.1073/pnas.0506580102
29. Nazari B, Rice LM, Stifano G, Barron AM, Wang YM, Korndorf T, et al. Altered dermal fibroblasts in systemic sclerosis display podoplanin and CD90. *Am J Pathol*. (2016) 186:2650–64. doi: 10.1016/j.ajpath.2016.06.020
30. Farina G, Lafyatis D, Lemaire R, Lafyatis R. A four-gene biomarker predicts skin disease in patients with diffuse cutaneous systemic sclerosis. *Arthritis Rheum*. (2010) 62:580–8. doi: 10.1002/art.27220
31. Cox CM, D'Agostino SL, Miller MK, Heimark RL, Krieg PA. Apelin, the ligand for the endothelial G-protein-coupled receptor, APJ, is a potent angiogenic factor required for normal vascular development of the frog embryo. *Dev Biol*. (2006) 296:177–89. doi: 10.1016/j.ydbio.2006.04.452
32. Eyries M, Siegfried G, Ciumas M, Montagne K, Agrapart M, Lebrin F, et al. Hypoxia-induced apelin expression regulates endothelial cell proliferation and regenerative angiogenesis. *Circ Res*. (2008) 103:432–40. doi: 10.1161/CIRCRESAHA.108.179333
33. Kang Y, Kim J, Anderson JP, Wu J, Gleim SR, Kundu RK, et al. Apelin-APJ signaling is a critical regulator of endothelial MEF2 activation in cardiovascular development. *Circ Res*. (2013) 113:22–31. doi: 10.1161/CIRCRESAHA.113.301324
34. Kasai A, Ishimaru Y, Higashino K, Kobayashi K, Yamamuro A, Yoshioka Y, et al. Inhibition of apelin expression switches endothelial cells from proliferative to mature state in pathological retinal angiogenesis. *Angiogenesis* (2013) 16:723–34. doi: 10.1007/s10456-013-9349-6
35. Kasai A, Shintani N, Oda M, Kakuda M, Hashimoto H, Matsuda T, et al. Apelin is a novel angiogenic factor in retinal endothelial cells. *Biochem Biophys Res Commun*. (2004) 325:395–400. doi: 10.1016/j.bbrc.2004.10.042
36. Zhang J, Liu Q, Hu X, Fang Z, Huang F, Tang L, et al. Apelin/APJ signaling promotes hypoxia-induced proliferation of endothelial progenitor cells via phosphoinositide-3 kinase/Akt signaling. *Mol Med Rep*. (2015) 12:3829–34. doi: 10.3892/mmr.2015.3866
37. Chen Y, Leask A, Abraham DJ, Kennedy L, Shi-Wen X, Denton CP, et al. Thrombospondin 1 is a key mediator of transforming growth factor beta-mediated cell contractility in systemic sclerosis via a mitogen-activated protein kinase kinase (MEK)/extracellular signal-regulated kinase (ERK)-dependent mechanism. *Fibrogenesis Tissue Repair* (2011) 4:9. doi: 10.1186/1755-1536-4-9
38. Macko RF, Gelber AC, Young BA, Lowitt MH, White B, Wigley FM, et al. Increased circulating concentrations of the counteradhesive proteins SPARC and thrombospondin-1 in systemic sclerosis (scleroderma). Relationship to platelet and endothelial cell activation. *J Rheumatol*. (2002) 29:2565–70.
39. Mimura Y, Ihn H, Jinnin M, Asano Y, Yamane K, Tamaki K. Constitutive thrombospondin-1 overexpression contributes to autocrine transforming growth factor-beta signaling in cultured scleroderma fibroblasts. *Am J Pathol*. (2005) 166:1451–63. doi: 10.1016/S0002-9440(10)62362-0
40. Scheja A, Akesson A, Geborek P, Wildt M, Wollheim CB, Wollheim FA, et al. Von Willebrand factor propeptide as a marker of disease activity in systemic sclerosis (scleroderma). *Arthritis Res*. (2001) 3:178–82. doi: 10.1186/ar295
41. Blann AD, Sheeran TP, Emery P. von Willebrand factor: increased levels are related to poor prognosis in systemic sclerosis and not to tissue autoantibodies. *Br J Biomed Sci*. (1997) 54:5–9.
42. Herrick AL, Illingworth K, Blann A, Hay CR, Hollis S, Jayson MI. Von Willebrand factor, thrombomodulin, thromboxane, beta-thromboglobulin and markers of fibrinolysis in primary Raynaud's phenomenon and systemic sclerosis. *Ann Rheum Dis*. (1996) 55:122–7. doi: 10.1136/ard.55.2.122
43. Kahaleh MB, Osborn I, LeRoy EC. Increased factor VIII/von Willebrand factor antigen and von Willebrand factor activity in scleroderma and in Raynaud's phenomenon. *Ann Intern Med*. (1981) 94(4 pt 1):482–4. doi: 10.7326/0003-4819-94-4-482
44. Pendergrass SA, Hayes E, Farina G, Lemaire R, Farber HW, Whitfield ML, et al. Limited systemic sclerosis patients with pulmonary arterial hypertension show biomarkers of inflammation and vascular injury. *PLoS ONE* (2010) 5:e12106. doi: 10.1371/journal.pone.0012106
45. Gallai M, Kovalszky I, Knittel T, Neubauer K, Armbrust T, Ramadori G. Expression of extracellular matrix proteoglycans perlecan and decorin in carbon-tetrachloride-injured rat liver and in isolated liver cells. *Am J Pathol*. (1996) 148:1463–71.
46. Warren CR, Grindel BJ, Francis L, Carson DD, Farach-Carson MC. Transcriptional activation by NFkappaB increases perlecan/HSPG2 expression in the desmoplastic prostate tumor microenvironment. *J Cell Biochem*. (2014) 115:1322–33. doi: 10.1002/jcb.24788
47. Baiocchini A, Montaldo C, Conigliaro A, Grimaldi A, Correani V, Mura F, et al. Extracellular matrix molecular remodeling in human liver fibrosis evolution. *PLoS ONE* (2016);11:e0151736. doi: 10.1371/journal.pone.0151736
48. Laplante P, Raymond MA, Gagnon G, Vigneault N, Sasseville AM, Langelier Y, et al. Novel fibrogenic pathways are activated in response to endothelial apoptosis: implications in the pathophysiology of systemic sclerosis. *J Immunol*. (2005) 174:5740–9. doi: 10.4049/jimmunol.174.9.5740

49. Zhou Z, Wang J, Cao R, Morita H, Soininen R, Chan KM, et al. Impaired angiogenesis, delayed wound healing and retarded tumor growth in perlecan heparan sulfate-deficient mice. *Cancer Res.* (2004) 64:4699–702. doi: 10.1158/0008-5472.CAN-04-0810
50. Shu C, Smith SM, Melrose J. The heparan sulphate deficient Hspg2 exon 3 null mouse displays reduced deposition of TGF-beta1 in skin compared to C57BL/6 wild type mice. *J Mol Histol*. (2016) 47:365–74. doi: 10.1007/s10735-016-9677-0
51. Iozzo RV, Pillarisetti J, Sharma B, Murdoch AD, Danielson KG, Uitto J, et al. Structural and functional characterization of the human perlecan gene promoter. Transcriptional activation by transforming growth factor-beta via a nuclear factor 1-binding element. *J Biol Chem*. (1997) 272:5219–28. doi: 10.1074/jbc.272.8.5219
52. Sharma B, Handler M, Eichstetter I, Whitelock JM, Nugent MA, Iozzo RV. Antisense targeting of perlecan blocks tumor growth and angiogenesis *in vivo*. *J Clin Invest*. (1998) 102:1599–608. doi: 10.1172/JCI3793
53. Rajkumar VS, Sundberg C, Abraham DJ, Rubin K, Black CM. Activation of microvascular pericytes in autoimmune Raynaud's phenomenon and systemic sclerosis. *Arthritis Rheum*. (1999) 42:930–41. doi: 10.1002/1529-0131(199905)42:5<930::AID-ANR11>3.0.CO;2-1
54. Zvaifler NJ. Relevance of the stroma and epithelial-mesenchymal transition (EMT) for the rheumatic diseases. *Arthritis Res Ther*. (2006) 8:210. doi: 10.1186/ar1963
55. Li Z, Jimenez SA. Protein kinase Cdelta and c-Abl kinase are required for transforming growth factor beta induction of endothelial-mesenchymal transition *in vitro*. *Arthritis Rheum*. (2011) 63:2473–83. doi: 10.1002/art.30317
56. Kidoya H, Takakura N. Biology of the apelin-APJ axis in vascular formation. *J Biochem*. (2012) 152:125–31. doi: 10.1093/jb/mvs071
57. Ho L, van Dijk M, Chye STJ, Messerschmidt DM, Chng SC, Ong S, et al. ELABELA deficiency promotes preeclampsia and cardiovascular malformations in mice. *Science* (2017) 357:707–13. doi: 10.1126/science.aam6607
58. Chng SC, Ho L, Tian J, Reversade B. ELABELA: a hormone essential for heart development signals via the apelin receptor. *Dev Cell* (2013) 27:672–80. doi: 10.1016/j.devcel.2013.11.002
59. Aozasa N, Asano Y, Akamata K, Noda S, Masui Y, Yamada D, et al. Serum apelin levels: clinical association with vascular involvements in patients with systemic sclerosis. *J Eur Acad Dermatol Venereol*. (2013) 27:37–42. doi: 10.1111/j.1468-3083.2011.04354.x
60. Yang P, Read C, Kuc RE, Buonincontri G, Southwood M, Torella R, et al. Elabela/toddler is an endogenous agonist of the apelin APJ receptor in the adult cardiovascular system, and exogenous administration of the peptide compensates for the downregulation of its expression in pulmonary arterial hypertension. *Circulation* (2017) 135:1160–73. doi: 10.1161/CIRCULATIONAHA.116.023218
61. Andersen CU, Hilberg O, Mellemkjaer S, Nielsen-Kudsk JE, Simonsen U. Apelin and pulmonary hypertension. *Pulm Circ*. (2011) 1:334–46. doi: 10.4103/2045-8932.87299
62. McKenzie JA, Fruttiger M, Abraham S, Lange CA, Stone J, Gandhi P, et al. Apelin is required for non-neovascular remodeling in the retina. *Am J Pathol*. (2012) 180:399–409. doi: 10.1016/j.ajpath.2011.09.035
63. Noonan DM, Fulle A, Valente P, Cai S, Horigan E, Sasaki M, et al. The complete sequence of perlecan, a basement membrane heparan sulfate proteoglycan, reveals extensive similarity with laminin A chain, low density lipoprotein-receptor, and the neural cell adhesion molecule. *J Biol Chem*. (1991) 266:22939–47.
64. Manetti M, Romano E, Rosa I, Guiducci S, Bellando-Randone S, De Paulis A, et al. Endothelial-to-mesenchymal transition contributes to endothelial dysfunction and dermal fibrosis in systemic sclerosis. *Ann Rheum Dis*. (2017) 76:924–34. doi: 10.1136/annrheumdis-2016-210229

Conflict of Interest Statement: The authors declare that the research was conducted in the absence of any commercial or financial relationships that could be construed as a potential conflict of interest.

frontiers in Immunology

REVIEW
published: 17 October 2018
doi: 10.3389/fimmu.2018.02383

Ubiquitination in Scleroderma Fibrosis and Its Treatment

*Ying Long, Weilin Chen, Qian Du, Xiaoxia Zuo and Honglin Zhu**

Department of Rheumatology, Xiangya Hospital, Central South University, Changsha, China

Scleroderma (systemic sclerosis, SSc) is a highly heterogeneous rheumatic disease, and uncontrolled fibrosis in visceral organs is the major cause of death in patients. The transforming growth factor-β (TGF-β) and WNT/β-catenin signaling pathways, along with signal transducer and activator of transcription 3 (STAT3), play crucial roles in this fibrotic process. Currently, no therapy is available that effectively arrests or reverses the progression of fibrosis in patients with SSc. Ubiquitination is an important post-translational modification that controls many critical cellular functions. Dysregulated ubiquitination events have been observed in patients with systemic lupus erythematosus, rheumatoid arthritis and fibrotic diseases. Inhibitors targeting the ubiquitination pathway have considerable potential for the treatment of rheumatic diseases. However, very few studies have examined the role and mechanism of ubiquitination in patients with SSc. In this review, we will summarize the molecular mechanisms of ubiquitination in patients with SSc and explore the potential targets for treatment.

Keywords: SSc, ubiquitination, TGF-β, WNT/β-catenin, STAT3

OPEN ACCESS

Edited by:
Raffaele De Palma,
Università degli Studi della Campania "Luigi Vanvitelli" Caserta, Italy

Reviewed by:
Gianluca Moroncini,
Università Politecnica delle Marche, Italy
Luigi Racioppi,
Università degli Studi di Napoli Federico II, Italy

****Correspondence:***
Honglin Zhu
honglinzhu@csu.edu.cn

Specialty section:
This article was submitted to Primary Immunodeficiencies, a section of the journal Frontiers in Immunology

Received: *19 June 2018*
Accepted: *25 September 2018*
Published: *17 October 2018*

Citation:
Long Y, Chen W, Du Q, Zuo X and Zhu H (2018) Ubiquitination in Scleroderma Fibrosis and Its Treatment. Front. Immunol. 9:2383. doi: 10.3389/fimmu.2018.02383

INTRODUCTION

Scleroderma (systemic sclerosis, SSc) is a complicated heterogeneous rheumatic disease that is characterized by progressive fibrosis in the skin and multiple other organs. Both environmental and genetic factors contribute to the etiology of SSc and trigger a chronic self-amplifying inflammatory process, leading to vascular alterations, autoimmunity and fibrosis (1). Many molecules and signaling pathways participate in the progression of fibrosis, such as the transforming growth factor-β (TGF-β) and WNT/β-catenin signaling pathways, signal transducer and activator of transcription 3 (STAT3), platelet-derived growth factor (PDGF), endothelin 1, interleukin 6, interleukin 13, autoantibodies, and numerous biologically active substances. Among these pathways, the TGF-β and WNT/β-catenin signaling pathways and STAT3 play key roles. Based on accumulating evidence, post-translational modifications have important regulatory roles in these pathways, such as acetylation, phosphorylation and ubiquitination, suggesting that these modifications are potential targets for the treatment of fibrosis (2–4).

Ubiquitin is a highly evolutionarily conserved protein that modifies other proteins for degradation. Ubiquitination is a process by which target protein is covalently bound to ubiquitin through an enzymatic cascade that is orchestrated sequentially by activating (E1), conjugating (E2) and ligating (E3) enzymes (5). E1 enzymes activate ubiquitin and transfer it onto the E2 conjugating enzyme, and then E3 ligases interact with the ubiquitin-loaded E2 enzyme and substrate protein to mediate the formation of polyubiquitin chains. Subsequently, the polyubiquitin chain is recognized by the 26S proteasome complex and degraded into individual amino acids.

The human genome contains two E1 enzymes, approximately forty E2 enzymes and >600 E3 ligases. The diverse E3 ligases have important roles in the selective recognition of each targeted protein. Additionally, >100 deubiquitinating enzymes (DUBs) have been identified that remove ubiquitin from the substrate proteins (6).

Ubiquitination plays important roles in the proteasomal degradation of proteins, inflammatory signaling, immune responses, autophagy, and T cell activation and differentiation (7). Dysregulation of ubiquitination has been observed in many autoimmune diseases, such as systemic lupus erythematous (8), rheumatoid arthritis (RA) (9) and fibrotic diseases (10). Anti-ubiquitin antibodies are present in 42% of patients with SSc and are associated with anti-histone antibodies. The latter might be positively correlated with the severity of pulmonary fibrosis in patients with SSc (11). According to results from whole-exome sequencing, an E3 ubiquitin ligase-related gene was associated with a higher risk of SSc. Therefore, ubiquitination might play an important role in SSc (12). However, little is known about ubiquitination in the pathology of SSc. Herein, we will summarize the role of ubiquitination in SSc and then discuss the future perspectives for SSc therapy.

MUTATIONS IN UBIQUITINATION-RELATED ENZYMES IN PATIENTS WITH SSC

Many susceptibility regions have been identified in patients with SSc by genome-wide association studies (GWAS), and the most common and confirmed susceptibility locus is the HLA locus. Recently, non-HLA susceptibility genes have also been identified, and most are correlated with inflammation, T cell differentiation and autoantibodies (13).

The susceptibility genes TNF-α-induced protein 3 (TNFAIP3), TNF receptor-interacting protein (TNIP1), ankyrin repeat and SOCS box-containing 10 (ASB10), and autophagy-related 5 (ATG5) are involved in the ubiquitination-proteasome system (UPS). TNFAIP3 expression (encodes A20) is rapidly induced by TNF-α. TNFAIP3 possesses both E3 ubiquitin ligase and deubiquitinase activities and negatively regulates the inflammatory response by deubiquitinating proteins in the NF-κB pathway, such as IKKg/NEMO, RIP1 and RIP2. TNFAIP3 is associated with diffuse cutaneous SSc, anti-topoisomerase I antibody, lung fibrosis and pulmonary arterial hypertension (14). TNIP1 interacts with A20 and represses the activity of the TLR-induced NF-κB signaling pathway, decreasing the production of proinflammatory cytokines in patients with SSc. Recombinant TNIP1 downregulates inflammatory cytokine-induced collagen synthesis (15). ASB10 belongs to the E3 ubiquitin ligase complex and may be involved in the pathogenesis of SSc and pulmonary vascular complications (12, 16). The protein encoded by the ATG5 gene interacts with ATG12 and forms a complex that functions as an E1-like activating enzyme. ATG5 is also associated with RA, juvenile idiopathic arthritis and primary biliary cirrhosis. However, the function of ATG5 in patients with SSc requires further investigation (17).

UBIQUITIN MODIFICATION OF PROTEINS IN KEY SIGNALING PATHWAYS INVOLVED IN SSC

TGF-β Signaling Is Regulated by Ubiquitination

Definition

The TGF-β superfamily consists of TGF-βs, bone morphogenetic proteins (BMPs) and activin. These proteins activate TGF-β signaling by binding to their membrane-anchored serine/threonine kinase receptors TGF-βRI or TGF-βRII. The canonical TGF-β signaling pathway is regulated by Smad proteins. Smad proteins are divided into three types. R-Smads are receptor-regulated Smads, including TGF-β/activin-specific Samd2 and Smad3, BMP-specific Smad1, Smad5 and Smad8. I-Smads are inhibitory Smads and include Smad6 and Smad7. Co-Smad is the common Smad and is represented by Smad4. The Smad proteins regulate the transcription of various genes. Many transcription factors and co-factors are also involved in this process; transcription factors include Mixer, FoxH1, E2F, and Runx-related proteins, co-activators include p300 and CBP, and co-repressors include c-Ski and SnoN (18) (**Figure 1A**).

The Role of TGF-β Signaling in SSc

TGF-β is commonly viewed as playing a critical role in the fibrosis process. Dysregulation of the TGF-β signaling pathway is involved in the pathogenesis of SSc (19). High levels of TGF-β and its regulated genes have been detected in skin biopsies and were positively correlated with the severity of SSc (20). The TGF-β neutralizing antibody fresolimumab exerts anti-fibrotic effects on patients with SSc, but its use is also accompanied by a high incidence of keratoacanthomas, which limits its use in long-term treatment. Therefore, the development of new drugs that target downstream mediators of TGF-β signaling is important (21, 22).

Ubiquitin Enzymes in TGF-β/SMAD Signaling

Many E3 ligases are involved in TGF-β/SMAD signaling, including Smurfs (E6-accessory protein C-terminus, HECT), WWP family (HECT type), NEDD4L (HECT type), Arkadia (RING-H2 finger domain), CHIP (C-terminus of HSC70-interacting protein), β-TrCP (Skp1-Cullin-F-box (SCF)-type ubiquitin ligase), and Fbxw7 (SCF type). TGF-β/SMAD signaling regulates the transcription of various genes, including negative regulators, such as I-Smads and Smurfs. When TGF-β signaling is activated, I-Smads and Smurfs interact in the nucleus and translocate to the cytoplasm (23, 24). Smad7 recruits WWP1 and NEDD4L to the active TGF-β receptor complexes and induces the degradation of the complexes (25, 26). Smurf1 ubiquitinates Smad1 and Smad5 (27, 28), and Smurf2 ubiquitinates Smad1 and Smad2 under steady-state conditions (29, 30). Arkadia and NEDD4L ubiquitinate phospho-Smad2/3 (31, 32), whereas CHIP regulates the abundance of Smad1 and Smad3 (33, 34). Smurfs, WWP1, NEDD4-2, CHIP, and β-TrCP conjugate polyubiquitin chains onto Smad4 and mediate its degradation (35). As mentioned above, E3 ligases mainly function as inhibitors of TGF-β signaling. However, they have also been shown to enhance TGF-β signaling. Arkadia degrades the negative

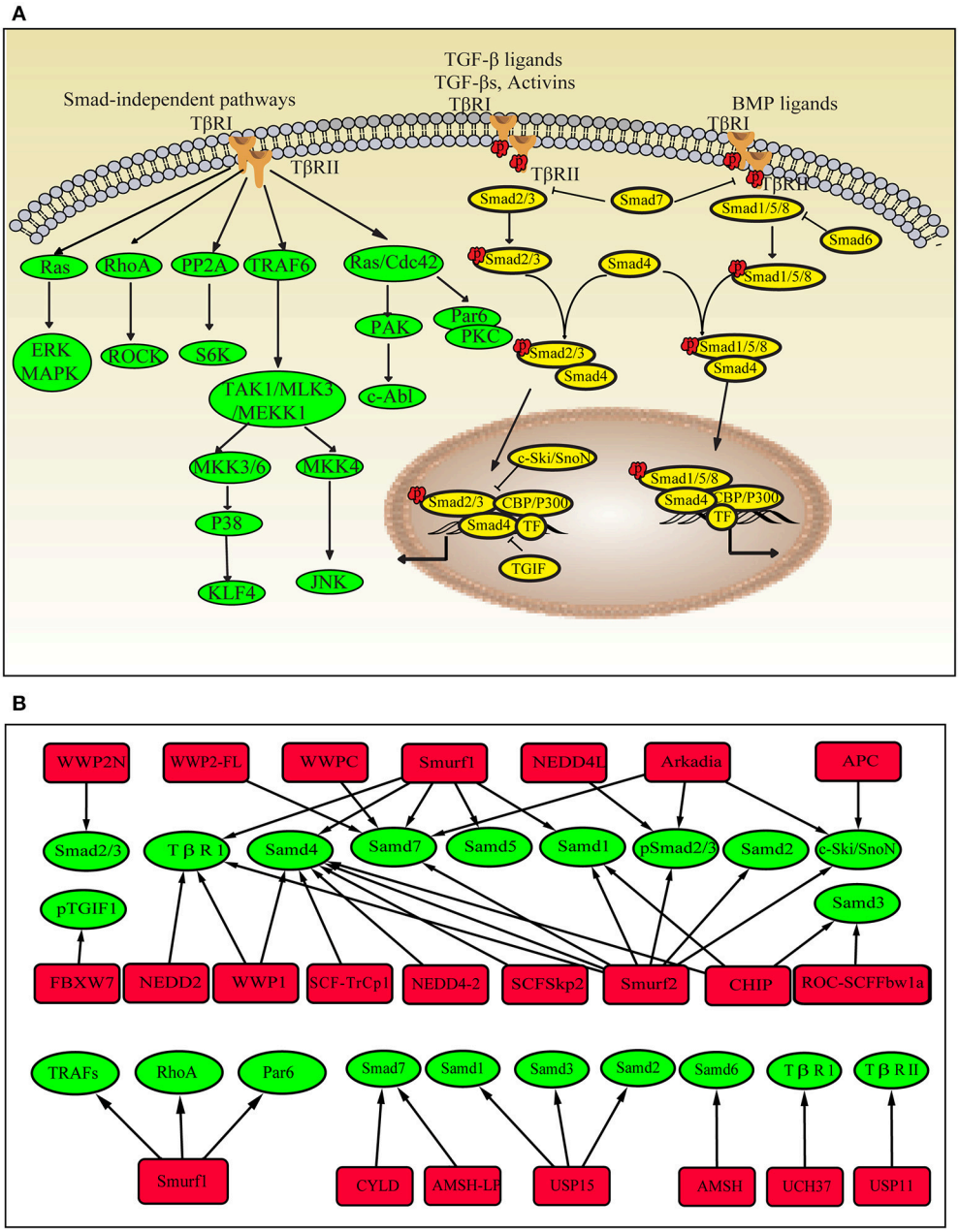

FIGURE 1 | Ubiquitin modifications in the TGF-β pathway. **(A)** Schematic showing the Smad-dependent and Smad-independent TGF-β signaling pathways. **(B)** Ubiquitinating enzymes, DUBs and target proteins in the TGF-β pathway. Red square nodes represent enzymes, green circles represent target proteins.

regulators of TGF-β signaling, such as Smad7, c-Ski, and SnoN (36). Smad7 is also ubiquitinated by WWP-C and WWP2-FL (37). Phosphorylated TGIF1 (TGF-β-induced factor 1) is a transcriptional repressor of TGF-β signaling that is degraded by the ubiquitin ligase complex containing Fbxw7 (38).

Ubiquitin Enzymes in Smad-Independent TGF-β Signaling

Ubiquitination also plays important roles in Smad-independent TGF-β pathways. TGF-β induces the ubiquitination and degradation of KLF4 (Krüppel-like factor 4), which is important for TGF-β-mediated regulation of transcription (39). The TGF-β/RhoA pathway is required for the progression of the epithelial-mesenchymal transition (EMT). Smurf1 targets RhoA for degradation (40). In TGF-β-induced anti-inflammatory signaling, Smurf1 ubiquitinates TRAFs (TNF receptor-associated factors), and Smurf2 interacts with TRAF2 and ubiquitinates TNF receptor 2, thereby inhibiting downstream signaling (41). In fibroblasts from patients with SSc, Smurf2 is upregulated after stimulation with TGF-β (42), and the Smad7-Smurf-mediated

inhibitory effect is impaired (43). Ubiquitination also promotes Smad2/3 signaling and increases collagen I accumulation by stabilizing Ha-Ras, which is independent of TGF-β activation. All of these mechanisms eventually contribute to collagen overproduction. The dysregulation of E3 ubiquitin ligases involved in TGF-β signaling has also been observed in patients with other fibrotic diseases and in animal models. The levels of MDM2 (RING-type) and FIEL1 (HECT-Type E3) are increased in lung tissues from patients with idiopathic pulmonary fibrosis (IPF) (44, 45). Smurf2 is upregulated in the fibroblasts present in hypertrophic scars (46). Smurf1, Smurf2, Arkadia and Hrd1 (Synoviolin, RING-type) levels are increased in animals with unilateral ureteral obstruction-induced renal fibrosis (47–49). Smurf2 and Synoviolin are upregulated in a liver fibrosis model (50–52). NEDD4 and Pellino1 (RING-type) expression are increased in keloid fibroblasts (53) and cardiac fibroblasts, respectively (54). These E3 ubiquitin ligases not only directly mediate the degradation of components of the TGF-β signaling pathway but also participate in inducing the transition of epithelial cells to mesenchymal cells, enhancing fibroblast proliferation and invasiveness, and increasing TGF-β production.

DUBs

DUBs have also been implicated in TGF-β signaling. UCH37 and USP11 were shown to deubiquitinate TβRI or TβRII, which is important for early steps in the TGF-β signaling pathway (55–57). High levels of USP11 have been detected in lung tissues from patients with IPF and bleomycin-induced mice, whereas inhibition of USP11 expression attenuates TGF-β signaling (57). CYLD deubiquitinates Smad7 and inhibits TGF-β signaling (58). In mice with liver fibrosis, CYLD ameliorates hepatocellular damage and liver fibrogenesis (59). USP15 deubiquitinates mono-ubiquitinated R-Smads and is required for proper TGF-β signaling. Other DUBs, such as AMSH (the associated molecule with the Src homology 3 domain of the signal-transducing adaptor molecule) and AMSH-like protein cleave K63-linked ubiquitin chains, which are associated with I-Smads and inhibit their functions (60–62) (**Figure 1B**).

The WNT/β-Catenin Pathway Is Regulated by Ubiquitination

Definition

The canonical WNT pathway is closely related to the regulation of β-catenin and its potential to modulate transcription. When WNT signaling is inactivated, β-catenin is phosphorylated (pβ-catenin) in the cytoplasm by a multiprotein complex (Axin/APC complex) composed of Axin, APC, CK1 and GSKβ. The pβ-catenin protein is immediately degraded by the UPS and is rarely detected in normal cells. Upon stimulation, WNT binds to the receptor Frizzled (Fz) and the coreceptors LRP5/6, recruits the cytoplasmic effector protein Disheveled (Dvl) and inhibits the Axin/APC complex. Consequently, the high levels of cytosolic β-catenin are translocated to the nucleus and regulate the transcription of target genes via β-catenin/TCF complexes. Based on accumulating evidence from recent studies, ubiquitin modification also plays important roles in regulating the WNT pathway (63).

The Role of WNT/β-Catenin Pathway in SSc

WNT signaling plays pivotal roles in developmental processes and tissue homeostasis. The canonical WNT/β-catenin pathway elicits fibrotic responses both directly and through TGF-β (2). High levels of activated β-catenin and its regulated gene AXIN2 have been in skin and lung tissues from patients with SSc, as well as in animal models of fibrosis (64, 65). SSc autoantibodies and oxidative DNA damage mediate Wnt inhibitor factor 1 (WIF-1) silencing and promote WNT activation and subsequent fibrosis. Strategies that restore the expression of WIF-1 prevent collagen accumulation *in vivo*. Microarray studies have also revealed the activation of WNT/β-catenin pathways in the skin tissues from patients with SSc. According to the results from clinical trials, treatments targeting the WNT/β-catenin pathway (tankyrase and porcupine inhibitors) are effective, well-tolerated and safe for long-term application (66). C-82, which targets the β-catenin/CBP interaction, is now in phase I/II clinical trials for SSc therapy. Therefore, the molecular mechanisms regulating the WNT/β-catenin pathway must be completely identified (67, 68).

Ubiquitin Enzymes and DUBs in WNT Signaling

The cell-surface receptor Fz is ubiquitinated by the transmembrane E3 ligases ZNRF3 and RNF43 and is deubiquitinated by UBPY/Ub-specific protease 8 (USP8) for recycling to the plasma membrane (69, 70). LRP6 is retained in the endoplasmic reticulum due to palmitoylation and monoubiquitylation, suggesting that an E3 ligase and DUBs participate in this process; however, the types of ubiquitin chains remain unknown (71). Dvl proteins (Dvl1, Dvl2 and Dvl3) play key roles in both canonical and noncanonical WNT signaling. Multiple E3 ligases that ubiquitinate Dvl negatively regulate WNT signaling (72). The DUBs CYLD and USP14 remove the K63-linked polyubiquitin chain from Dvl (73, 74). Axin is degraded by the E3 ligase RNF146 and Smurf1 and Smurf2, which interact with LRP5/6 (75–77). HectD1 ubiquitinates APC, promotes its interaction with Axin and negatively regulates WNT signaling (78), whereas USP15 protects the APC from ubiquitin-mediated degradation (79). β-TrCP assembles K48-linked polyubiquitin chains onto β-catenin and mainly regulates the nuclear pool of β-catenin (80). The ubiquitin ligase Jade-1 also mediates β-catenin ubiquitination and is responsible for degrading cytoplasmic β-catenin (81). Unlike β-TrCP and Jade-1, Rad6B (an E2 ubiquitin-conjugating enzyme) and EDD (an E3 ubiquitin ligase) ubiquitinate β-catenin and increase its activity (82, 83) (**Figure 2**).

STAT3 Regulation by Ubiquitination

STAT3 belongs to the transcription factor family that transduces cellular signals from a number of soluble growth factors and cytokines, including PDGF, epidermal growth factor (EGF) and IL-6 family cytokines. STAT3 plays critical roles in several biological processes, including cell proliferation, differentiation and migration. Upon stimulation, cytoplasmic STAT3 is phosphorylated, dimerizes, and then translocates to the nucleus to regulate the transcription of target genes. Recently, STAT3 was shown to integrate multiple profibrotic signals and was identified as a key checkpoint in fibroblast activation. STAT3 is

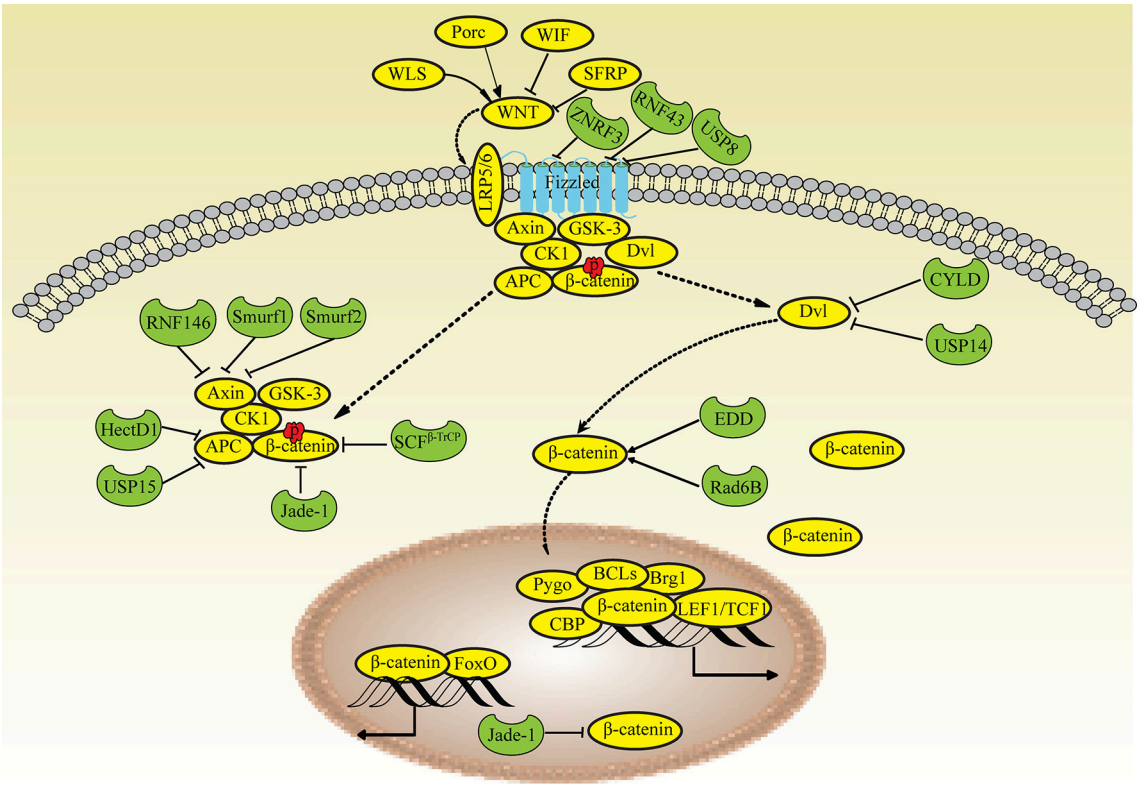

FIGURE 2 | Ubiquitin modifications in the WNT/β-catenin pathway. When WNT signaling is inactivated, β-catenin is phosphorylated (pβ-catenin) in the cytoplasm by the Axin/APC complex and degraded by Jade-1 and β-TrCP. Upon stimulation, WNT binds to the receptor Frizzled and the coreceptors LRP5/6, recruits Dvl and inhibits the Axin/APC complex, leading to the translocation of high levels of cytosolic β-catenin into the nucleus. Fz is ubiquitinated by ZNRF3 and RNF43 and deubiquitinated by USP8. Dvl is deubiquitinated by CYLD and USP14. Axin is degraded by RNF146, Smurf2, and Smurf1. APC is ubiquitinated by HectD1 and deubiquitinated by USP15. Rad6B and EDD ubiquitinate β-catenin; Jade-1 also ubiquitinates β-catenin in the nucleus.

considered a potential target for SSc treatment (4, 84). The STAT3 dimerization inhibitor S3I-201 exerts strong anti-fibrotic effects on animal models of SSc. STAT3 is ubiquitinated with lysine-63-linked ubiquitin chains by TRAF6 (tumor necrosis factor receptor-associated factor 6) (85), which exhibits E3 ubiquitin ligase activity. STAT3 is also ubiquitinated and degraded by the E3 ligase COP1 (86).

Treatment of SSc by Strategies Targeting the UPS

Bortezomib is a reversible 20S proteasome inhibitor and the first drug approved to treat multiple myeloma. In the UPS, the proteasome is the final step in protein degradation and a valuable target for developing potential drugs. Bortezomib derivatives, such as carfilzomib and marizomib, are in various phases of clinical trials as potential treatments for several malignancies (87). In fibroblasts from patients with SSc, proteasome inhibitors replenish human dermal fibroblasts, degrade the extracellular matrix and exert anti-fibrotic effects (88). The proteasome inhibitor MG-132, synthetic lactacystin, and bortezomib decrease the expression of type I collagen and tissue inhibitor of metalloproteinase-1 and increase the production of metalloproteinase-1 in a dose-dependent manner (89). However, proteasome inhibitors have been reported to induce resistance and side effects, and a combination of several UPS inhibitors targeting different components may overcome this challenge (6).

Studies of E1 enzyme inhibitors are rare due to their lack of specificity as therapies. Several inhibitors of E2 enzymes are in preclinical research stages, but their role in SSc has been poorly investigated. The specificity of the UPS depends mainly on E3 ubiquitin ligases. The FIEL1 inhibitor BC-1485 ameliorates lung fibrosis in a mouse model (44). The Synoviolin inhibitor LS-102 reduces endoplasmic reticulum stress-induced collagen secretion from lung epithelial cells, suggesting that it might be a potential treatment for IPF (90). In patients with SSc, the TGF-β and WNT/β-catenin signaling pathways and STAT3 are mainly regulated by E3 ligases at multiple levels, which presents the potential for specific substrates for drug target design. Erioflorin, which is isolated from *Eriophyllum lanatum*, has been shown to block β-TrCP and affect WNT/β-catenin signaling (91). Specific inhibitors or antagonists of other E3 ligases, such as Smurf1, Smurf2 and NEDD4, have not yet been discovered.

DUBs deubiquitinate and rescue substrates from proteasomal degradation, and thus are regarded other potential targets

for drug development. WP1130 has been shown to suppress the activity of several DUBs, including UCH37 and USP14, which regulate both TGF-β and WNT/β-catenin signaling. The combination of WP1130 and bortezomib exerts pro-apoptosis and anti-proliferation effects on tumor cells (92). b-AP15 is a small-molecule inhibitor of USP14 and UCHL5. b-AP15 blocks USP14 in a reversible manner and regulates WNT/β-catenin signaling (93). UCHL5 levels are elevated in lung tissues from patients with IPF (80). b-AP15 also reduces the levels of the fibronectin, type I collagen, and SMAD2/3 proteins in lung tissues from mice with fibrosis (94). The USP11 inhibitor mitoxantrone attenuates TGF-β signaling in lung fibroblasts and has been indicated as a potential antifibrotic drug for subjects with fibrosis.

In animal models and clinical trials, the UPS has been validated as a valuable molecular target for the treatment of cancer, asthma and arthritis, as >1,000 proteins have been identified in the UPS. These proteins represent substantial opportunities and challenges for researchers to investigate the molecular mechanisms underlying the addition of ubiquitin chains and the main components. The identification and validation of these components will expand the pool of targets for drug discovery for fibrosis (95).

CONCLUSIONS AND FUTURE PERSPECTIVES

In this review, we highlight the mechanisms regulating ubiquitination in patients with SSc and explore potential anti-fibrosis drugs. Effective therapies for many fibrotic manifestations in patients with SSc are currently unavailable. Considering the central role of TGF-β signaling, WNT/β-catenin signaling and STAT3 in SSc, the use of UPS inhibitors to selectively disrupt the formation of receptor or co-receptor complexes or block intracellular signaling may yield advances in the development of urgently needed treatments. These drugs are very powerful and might also induce severe side effects because of their unselective action that would limit their widespread use. In the near future, the elucidation of new, potent and highly specific drugs targeting specific UPS components is required. Therefore, investigations of the enzymology of ubiquitination will be of paramount importance in the next few years. Moreover, more studies are needed of enzymes involved in ubiquitination that represent promising drug targets to ameliorate fibrosis in patients with SSc.

AUTHOR CONTRIBUTIONS

YL wrote the first draft. WC, QD, and XZ revised the manuscript. HZ revised the final version and inserted additional information.

FUNDING

This study was funded by grants from the Hunan Provincial Natural Science Foundation (2018JJ3823) and the National Natural Science Foundation of China (81771765, 81373206, and 81671622).

REFERENCES

1. Denton CP, Khanna D. Systemic sclerosis. *Lancet* (2017) 390:1685–99. doi: 10.1016/S0140-6736(17)30933-9
2. Allanore Y, Simms R, Distler O, Trojanowska M, Pope J, Denton CP, et al. Systemic sclerosis. *Nat Rev Dis Primers* (2015) 1:15002. doi: 10.1038/nrdp.2015.2
3. Ho YY, Lagares D, Tager AM, Kapoor M. Fibrosis–a lethal component of systemic sclerosis. *Nat Rev Rheumatol.* (2014) 10:390–402. doi: 10.1038/nrrheum.2014.53
4. McHugh J. Systemic sclerosis: STAT3–a key integrator of profibrotic signalling. *Nat Rev Rheumatol.* (2017) 13:693. doi: 10.1038/nrrheum.2017.190
5. Yau R, Rape M. The increasing complexity of the ubiquitin code. *Nat Cell Biol.* (2016) 18:579–86. doi: 10.1038/ncb3358
6. Popovic D, Vucic D, Dikic I. Ubiquitination in disease pathogenesis and treatment. *Nat Med.* (2014) 20:1242–53. doi: 10.1038/nm.3739
7. Ebner P, Versteeg GA, Ikeda F. Ubiquitin enzymes in the regulation of immune responses. *Crit Rev Biochem Mol Biol.* (2017) 52:425–60. doi: 10.1080/10409238.2017.1325829
8. Guo Y, Zhao M, Lu Q. Transcription factor RFX1 is ubiquitinated by E3 ligase STUB1 in systemic lupus erythematosus. *Clin Immunol.* (2016) 169:1–7. doi: 10.1016/j.clim.2016.06.003
9. Fakhfakh Karray E, Bendhifallah I, Zakraoui L, Hamzaoui K. Association of small ubiquitin-like modifier 4 gene polymorphisms with rheumatoid arthritis in a Tunisian population. *Clin Exp Rheumatol.* (2011) 29:751.
10. Fukasawa H, Fujigaki Y, Yamamoto T, Hishida A, Kitagawa M. Protein degradation by the ubiquitin-proteasome pathway and organ fibrosis. *Curr Med Chem.* (2012) 19:893–900. doi: 10.2174/092986712799034941
11. Fujimoto M, Sato S, Ihn H, Kikuchi K, Tamaki T, Tamaki K, et al. Antiubiquitin antibody in localised and systemic scleroderma. *Ann Rheum Dis.* (1996) 55:399–402. doi: 10.1136/ard.55.6.399
12. Gao L, Emond MJ, Louie T, Cheadle C, Berger AE, Rafaels N, et al. Identification of rare variants in ATP8B4 as a risk factor for systemic sclerosis by whole-exome sequencing. *Arthritis Rheumatol.* (2016) 68:191–200. doi: 10.1002/art.39449
13. Zuo X, Zhang L, Luo H, Li Y, Zhu H. Systematic approach to understanding the pathogenesis of systemic sclerosis. *Clin Genet.* (2017) 92:365–71. doi: 10.1111/cge.12946
14. Dieude P, Guedj M, Wipff J, Ruiz B, Riemekasten G, Matucci-Cerinic M, et al. Association of the TNFAIP3 rs5029939 variant with systemic sclerosis in the European Caucasian population. *Ann Rheum Dis.* (2010) 69:1958–64. doi: 10.1136/ard.2009.127928
15. Allanore Y, Saad M, Dieude P, Avouac J, Distler JH, Amouyel P, et al. Genome-wide scan identifies TNIP1, PSORS1C1, and RHOB as novel risk loci for systemic sclerosis. *PLoS Genet.* (2011) 7:e1002091. doi: 10.1371/journal.pgen.1002091
16. Keller KE, Yang YF, Sun YY, Sykes R, Acott TS, Wirtz MK. Ankyrin repeat and suppressor of cytokine signaling box containing protein-10 is associated with ubiquitin-mediated degradation pathways in trabecular meshwork cells. *Mol Vis.* (2013) 19:1639–1655.
17. Mayes MD, Bossini-Castillo L, Gorlova O, Martin JE, Zhou X, Chen WV, et al. Immunochip analysis identifies multiple susceptibility loci for systemic sclerosis. *Am J Hum Genet.* (2014) 94:47–61. doi: 10.1016/j.ajhg.2013.12.002
18. Biernacka A, Dobaczewski M, Frangogiannis NG. TGF-beta signaling in fibrosis. *Growth Factors* (2011) 29:196–202. doi: 10.3109/08977194.2011.595714

19. Varga J, Pasche B. Transforming growth factor beta as a therapeutic target in systemic sclerosis. *Nat Rev Rheumatol*. (2009) 5:200–6. doi: 10.1038/nrrheum.2009.26
20. Farina G, Lafyatis D, Lemaire R, Lafyatis R. A four-gene biomarker predicts skin disease in patients with diffuse cutaneous systemic sclerosis. *Arthritis Rheum*. (2010) 62:580–8. doi: 10.1002/art.27220
21. Rice LM, Padilla CM, McLaughlin SR, Mathes A, Ziemek J, Goummih S, et al. Fresolimumab treatment decreases biomarkers and improves clinical symptoms in systemic sclerosis patients. *J Clin Invest*. (2015) 125:2795–807. doi: 10.1172/JCI77958
22. Lacouture ME, Morris JC, Lawrence DP, Tan AR, Olencki TE, Shapiro GI, et al. Cutaneous keratoacanthomas/squamous cell carcinomas associated with neutralization of transforming growth factor beta by the monoclonal antibody fresolimumab (GC1008). *Cancer Immunol Immunother*. (2015) 64:437–46. doi: 10.1007/s00262-015-1653-0
23. Ebisawa T, Fukuchi M, Murakami G, Chiba T, Tanaka K, Imamura T, et al. Smurf1 interacts with transforming growth factor-beta type I receptor through Smad7 and induces receptor degradation. *J Biol Chem*. (2001) 276:12477–80. doi: 10.1074/jbc.C100008200
24. Kavsak P, Rasmussen RK, Causing CG, Bonni S, Zhu H, Thomsen GH, et al. Smad7 binds to Smurf2 to form an E3 ubiquitin ligase that targets the TGF beta receptor for degradation. *Mol Cell* (2000) 6:1365–75. doi: 10.1016/S1097-2765(00)00134-9
25. Komuro A, Imamura T, Saitoh M, Yoshida Y, Yamori T, Miyazono K, et al. Negative regulation of transforming growth factor-beta (TGF-beta) signaling by WW domain-containing protein 1 (WWP1). *Oncogene* (2004) 23:6914–23. doi: 10.1038/sj.onc.1207885
26. Kuratomi G, Komuro A, Goto K, Shinozaki M, Miyazawa K, Miyazono K, et al. NEDD4-2 (neural precursor cell expressed, developmentally down-regulated 4-2) negatively regulates TGF-beta (transforming growth factor-beta) signalling by inducing ubiquitin-mediated degradation of Smad2 and TGF-beta type I receptor. *Biochem J*. (2005) 386(Pt 3):461–70. doi: 10.1042/BJ20040738
27. Zhu H, Kavsak P, Abdollah S, Wrana JL, Thomsen GH. A SMAD ubiquitin ligase targets the BMP pathway and affects embryonic pattern formation. *Nature* (1999) 400:687–93. doi: 10.1038/23293
28. Murakami G, Watabe T, Takaoka K, Miyazono K, Imamura T. Cooperative inhibition of bone morphogenetic protein signaling by Smurf1 and inhibitory Smads. *Mol Biol Cell* (2003) 14:2809–17. doi: 10.1091/mbc.e02-07-0441
29. Lin X, Liang M, Feng XH. Smurf2 is a ubiquitin E3 ligase mediating proteasome-dependent degradation of Smad2 in transforming growth factor-beta signaling. *J Biol Chem*. (2000) 275:36818–22. doi: 10.1074/jbc.C000580200
30. Zhang Y, Chang C, Gehling DJ, Hemmati-Brivanlou A, Derynck R. Regulation of Smad degradation and activity by Smurf2, an E3 ubiquitin ligase. *Proc Natl Acad Sci USA*. (2001) 98:974–9. doi: 10.1073/pnas.98.3.974
31. Gao S, Alarcon C, Sapkota G, Rahman S, Chen PY, Goerner N, et al. Ubiquitin ligase Nedd4L targets activated Smad2/3 to limit TGF-beta signaling. *Mol Cell* (2009) 36:457–68. doi: 10.1016/j.molcel.2009.09.043
32. Mavrakis KJ, Andrew RL, Lee KL, Petropoulou C, Dixon JE, Navaratnam N, et al. Arkadia enhances Nodal/TGF-beta signaling by coupling phospho-Smad2/3 activity and turnover. *PLoS Biol*. (2007) 5:e67. doi: 10.1371/journal.pbio.0050067
33. Xin H, Xu X, Li L, Ning H, Rong Y, Shang Y, et al. CHIP controls the sensitivity of transforming growth factor-beta signaling by modulating the basal level of Smad3 through ubiquitin-mediated degradation. *J Biol Chem*. (2005) 280:20842–50. doi: 10.1074/jbc.M412275200
34. Wang L, Liu YT, Hao R, Chen L, Chang Z, Wang HR, et al. Molecular mechanism of the negative regulation of Smad1/5 protein by carboxyl terminus of Hsc70-interacting protein (CHIP). *J Biol Chem*. (2011) 286:15883–94. doi: 10.1074/jbc.M110.201814
35. Moren A, Imamura T, Miyazono K, Heldin CH, Moustakas A. Degradation of the tumor suppressor Smad4 by WW and HECT domain ubiquitin ligases. *J Biol Chem*. (2005) 280:22115–23. doi: 10.1074/jbc.M414027200
36. Nagano Y, Mavrakis KJ, Lee KL, Fujii T, Koinuma D, Sase H, et al. Arkadia induces degradation of SnoN and c-Ski to enhance transforming growth factor-beta signaling. *J Biol Chem*. (2007) 282:20492–501. doi: 10.1074/jbc.M701294200
37. Soond SM, Chantry A. Selective targeting of activating and inhibitory smads by distinct WWP2 ubiquitin ligase isoforms differentially modulates TGFbeta signalling and EMT. *Oncogene* (2011) 30:2451–62. doi: 10.1038/onc.2010.617
38. Bengoechea-Alonso MT, Ericsson J. Tumor suppressor Fbxw7 regulates TGFbeta signaling by targeting TGIF1 for degradation. *Oncogene* (2010) 29:5322–8. doi: 10.1038/onc.2010.278
39. Hu D, Wan Y. Regulation of Kruppel-like factor 4 by the anaphase promoting complex pathway is involved in TGF-beta signaling. *J Biol Chem*. (2011) 286:6890–901. doi: 10.1074/jbc.M110.179952
40. Andrews PS, Schneider S, Yang E, Michaels M, Chen H, Tang J, et al. Identification of substrates of SMURF1 ubiquitin ligase activity utilizing protein microarrays. *Assay Drug Dev Technol*. (2010) 8:471–87. doi: 10.1089/adt.2009.0264
41. Carpentier I, Coornaert B, Beyaert R. Smurf2 is a TRAF2 binding protein that triggers TNF-R2 ubiquitination and TNF-R2-induced JNK activation. *Biochem Biophys Res Commun*. (2008) 374:752–7. doi: 10.1016/j.bbrc.2008.07.103
42. Zuscik MJ, Rosier RN, Schwarz EM. Altered negative regulation of transforming growth factor beta signaling in scleroderma: potential involvement of SMURF2 in disease. *Arthritis Rheum*. (2003) 48:1779–80. doi: 10.1002/art.11158
43. Asano Y, Ihn H, Yamane K, Kubo M, Tamaki K. Impaired Smad7-Smurf-mediated negative regulation of TGF-beta signaling in scleroderma fibroblasts. *J Clin Invest*. (2004) 113:253–64. doi: 10.1172/JCI16269
44. Lear T, McKelvey AC, Rajbhandari S, Dunn SR, Coon TA, Connelly W, et al. Ubiquitin E3 ligase FIEL1 regulates fibrotic lung injury through SUMO-E3 ligase PIAS4. *J Exp Med*. (2016) 213:1029–46. doi: 10.1084/jem.20151229
45. Kusko RL, Brothers JF II, Tedrow J, Pandit K, Huleihel L, Perdomo C, et al. Integrated genomics reveals convergent transcriptomic networks underlying chronic obstructive pulmonary disease and idiopathic pulmonary fibrosis. *Am J Respir Crit Care Med*. (2016) 194:948–60. doi: 10.1164/rccm.201510-2026OC
46. Zhang Z, Finnerty CC, He J, Herndon DN. Smad ubiquitination regulatory factor 2 expression is enhanced in hypertrophic scar fibroblasts from burned children. *Burns* (2012) 38:236–46. doi: 10.1016/j.burns.2011.08.012
47. Li L, Shen Y, Ding Y, Liu Y, Su D, Liang X. Hrd1 participates in the regulation of collagen I synthesis in renal fibrosis. *Mol Cell Biochem*. (2014) 386:35–44. doi: 10.1007/s11010-013-1843-z
48. Fukasawa H, Yamamoto T, Togawa A, Ohashi N, Fujigaki Y, Oda T, et al. Down-regulation of Smad7 expression by ubiquitin-dependent degradation contributes to renal fibrosis in obstructive nephropathy in mice. *Proc Natl Acad Sci USA*. (2004) 101:8687–92. doi: 10.1073/pnas.0400035101
49. Liu FY, Li XZ, Peng YM, Liu H, Liu YH. Arkadia-Smad7-mediated positive regulation of TGF-beta signaling in a rat model of tubulointerstitial fibrosis. *Am J Nephrol*. (2007) 27:176–83. doi: 10.1159/000100518
50. Hasegawa D, Fujii R, Yagishita N, Matsumoto N, Aratani S, Izumi T, et al. E3 ubiquitin ligase synoviolin is involved in liver fibrogenesis. *PLoS ONE* (2010) 5:e13590. doi: 10.1371/journal.pone.0013590
51. Cai Y, Shen XZ, Zhou CH, Wang JY. Abnormal expression of Smurf2 during the process of rat liver fibrosis. *Chin J Dig Dis*. (2006) 7:237–45. doi: 10.1111/j.1443-9573.2006.00275.x
52. Cai Y, Zhou CH, Fu D, Shen XZ. Overexpression of Smad ubiquitin regulatory factor 2 suppresses transforming growth factor-beta mediated liver fibrosis. *J Dig Dis*. (2012) 13:327–34. doi: 10.1111/j.1751-2980.2012.00592.x
53. Chung S, Nakashima M, Zembutsu H, Nakamura Y. Possible involvement of NEDD4 in keloid formation; its critical role in fibroblast proliferation and collagen production. *Proc Jpn Acad Ser B Phys Biol Sci*. (2011) 87:563–73. doi: 10.2183/pjab.87.563
54. Song J, Zhu Y, Li J, Liu J, Gao Y, Ha T, et al. Pellino1-mediated TGF-beta1 synthesis contributes to mechanical stress induced cardiac fibroblast activation. *J Mol Cell Cardiol*. (2015) 79:145–56. doi: 10.1016/j.yjmcc.2014.11.006
55. Wicks SJ, Haros K, Maillard M, Song L, Cohen RE, Dijke PT, et al. The deubiquitinating enzyme UCH37 interacts with Smads and regulates

TGF-beta signalling. *Oncogene* (2005) 24:8080–4. doi: 10.1038/sj.onc.1208944
56. Cutts AJ, Soond SM, Powell S, Chantry A. Early phase TGFbeta receptor signalling dynamics stabilised by the deubiquitinase UCH37 promotes cell migratory responses. *Int J Biochem Cell Biol.* (2011) 43:604–12. doi: 10.1016/j.biocel.2010.12.018
57. Jacko AM, Nan L, Li S, Tan J, Zhao J, Kass DJ, et al. De-ubiquitinating enzyme, USP11, promotes transforming growth factor β-1 signaling through stabilization of transforming growth factor β receptor II. *Cell Death Dis.* (2016) 7:e2474. doi: 10.1038/cddis.2016.371
58. Zhao Y, Thornton AM, Kinney MC, Ma CA, Spinner JJ, Fuss IJ, et al. The deubiquitinase CYLD targets Smad7 protein to regulate transforming growth factor beta (TGF-beta) signaling and the development of regulatory T cells. *J Biol Chem*. (2011) 286:40520–30. doi: 10.1074/jbc.M111.292961
59. Pannem RR, Dorn C, Hellerbrand C, Massoumi R. Cylindromatosis gene CYLD regulates hepatocyte growth factor expression in hepatic stellate cells through interaction with histone deacetylase 7. *Hepatology* (2014) 60:1066–81. doi: 10.1002/hep.27209
60. Inui M, Manfrin A, Mamidi A, Martello G, Morsut L, Soligo S, et al. USP15 is a deubiquitylating enzyme for receptor-activated SMADs. *Nat Cell Biol.* (2011) 13:1368–75. doi: 10.1038/ncb2346
61. Itoh F, Asao H, Sugamura K, Heldin CH, ten Dijke P, Itoh S. Promoting bone morphogenetic protein signaling through negative regulation of inhibitory Smads. *EMBO J.* (2001) 20:4132–42. doi: 10.1093/emboj/20.15.4132
62. Ibarrola N, Kratchmarova I, Nakajima D, Schiemann WP, Moustakas A, Pandey A, et al. Cloning of a novel signaling molecule, AMSH-2, that potentiates transforming growth factor beta signaling. *BMC Cell Biol.* (2004) 5:2. doi: 10.1186/1471-2121-5-2
63. Nusse R, Clevers H. Wnt/beta-catenin signaling, disease, and emerging therapeutic modalities. *Cell* (2017) 169:985–99. doi: 10.1016/j.cell.2017.05.016
64. Lam AP, Herazo-Maya JD, Sennello JA, Flozak AS, Russell S, Mutlu GM, et al. Wnt coreceptor Lrp5 is a driver of idiopathic pulmonary fibrosis. *Am J Respir Crit Care Med*. (2014) 190:185–95. doi: 10.1164/rccm.201401-0079OC
65. Wei J, Fang F, Lam AP, Sargent JL, Hamburg E, Hinchcliff ME, et al. Wnt/beta-catenin signaling is hyperactivated in systemic sclerosis and induces Smad-dependent fibrotic responses in mesenchymal cells. *Arthritis Rheum*. (2012) 64:2734–45. doi: 10.1002/art.34424
66. Beyer C, Reichert H, Akan H, Mallano T, Schramm A, Dees C, et al. Blockade of canonical Wnt signalling ameliorates experimental dermal fibrosis. *Ann Rheum Dis*. (2013) 72:1255–8. doi: 10.1136/annrheumdis-2012-202544
67. Distler JH, Feghali-Bostwick C, Soare A, Asano Y, Distler O, Abraham DJ. Review: frontiers of antifibrotic therapy in systemic sclerosis. *Arthritis Rheumatol*. (2017) 69:257–67. doi: 10.1002/art.39865
68. Kahn M. Can we safely target the WNT pathway? *Nat Rev Drug Discov*. (2014) 13:513–32. doi: 10.1038/nrd4233
69. Koo BK, Spit M, Jordens I, Low TY, Stange DE, van de Wetering M, et al. Tumour suppressor RNF43 is a stem-cell E3 ligase that induces endocytosis of Wnt receptors. *Nature* (2012) 488:665–9. doi: 10.1038/nature11308
70. Hao HX, Xie Y, Zhang Y, Charlat O, Oster E, Avello M, et al. ZNRF3 promotes Wnt receptor turnover in an R-spondin-sensitive manner. *Nature* (2012) 485:195–200. doi: 10.1038/nature11019
71. Abrami L, Kunz B, Iacovache I, van der Goot FG. Palmitoylation and ubiquitination regulate exit of the Wnt signaling protein LRP6 from the endoplasmic reticulum. *Proc Natl Acad Sci USA*. (2008) 105:5384–9. doi: 10.1073/pnas.0710389105
72. Gao C, Xiao G, Hu J. Regulation of Wnt/beta-catenin signaling by posttranslational modifications. *Cell Biosci.* (2014) 4:13. doi: 10.1186/2045-3701-4-13
73. Tauriello DV, Haegebarth A, Kuper I, Edelmann MJ, Henraat M, Canninga-van Dijk MR, et al. Loss of the tumor suppressor CYLD enhances Wnt/beta-catenin signaling through K63-linked ubiquitination of Dvl. *Mol Cell.* (2010) 37:607–19. doi: 10.1016/j.molcel.2010.01.035
74. Jung H, Kim BG, Han WH, Lee JH, Cho JY, Park WS, et al. Deubiquitination of dishevelled by Usp14 is required for Wnt signaling. *Oncogenesis* (2013) 2:e64. doi: 10.1038/oncsis.2013.28
75. Zhang Y, Liu S, Mickanin C, Feng Y, Charlat O, Michaud GA, et al. RNF146 is a poly(ADP-ribose)-directed E3 ligase that regulates axin degradation and Wnt signalling. *Nat Cell Biol.* (2011) 13:623–9. doi: 10.1038/ncb2222
76. Kim S, Jho EH. The protein stability of Axin, a negative regulator of Wnt signaling, is regulated by Smad ubiquitination regulatory factor 2 (Smurf2). *J Biol Chem*. (2010) 285:36420–26. doi: 10.1074/jbc.M110.137471
77. Fei C, Li Z, Li C, Chen Y, Chen Z, He X, et al. Smurf1-mediated Lys29-linked nonproteolytic polyubiquitination of axin negatively regulates Wnt/beta-catenin signaling. *Mol Cell Biol*. (2013) 33:4095–105. doi: 10.1128/MCB.00418-13
78. Tran H, Bustos D, Yeh R, Rubinfeld B, Lam C, Shriver S, et al. HectD1 E3 ligase modifies adenomatous polyposis coli (APC) with polyubiquitin to promote the APC-axin interaction. *J Biol Chem*. (2013) 288:3753–67. doi: 10.1074/jbc.M112.415240
79. Huang X, Langelotz C, Hetfeld-Pechoc BK, Schwenk W, Dubiel W. The COP9 signalosome mediates beta-catenin degradation by deneddylation and blocks adenomatous polyposis coli destruction via USP15. *J Mol Biol.* (2009) 391:691–702. doi: 10.1016/j.jmb.2009.06.066
80. Wu G, Xu G, Schulman BA, Jeffrey PD, Harper JW, Pavletich NP. Structure of a beta-TrCP1-Skp1-beta-catenin complex: destruction motif binding and lysine specificity of the SCF(beta-TrCP1) ubiquitin ligase. *Mol Cell.* (2003) 11:1445–56. doi: 10.1016/S1097-2765(03)00234-X
81. Chitalia VC, Foy RL, Bachschmid MM, Zeng L, Panchenko MV, Zhou MI, et al. Jade-1 inhibits Wnt signalling by ubiquitylating beta-catenin and mediates Wnt pathway inhibition by pVHL. *Nat Cell Biol*. (2008) 10:1208–16. doi: 10.1038/ncb1781
82. Shekhar MP, Gerard B, Pauley RJ, Williams BO, Tait L. Rad6B is a positive regulator of beta-catenin stabilization. *Cancer Res*. (2008) 68:1741–50. doi: 10.1158/0008-5472.CAN-07-2111
83. Hay-Koren A, Caspi M, Zilberberg A, Rosin-Arbesfeld R. The EDD E3 ubiquitin ligase ubiquitinates and up-regulates beta-catenin. *Mol Biol Cell* (2011) 22:399–411. doi: 10.1091/mbc.e10-05-0440
84. Chakraborty D, Sumova B, Mallano T, Chen CW, Distler A, Bergmann C, et al. Activation of STAT3 integrates common profibrotic pathways to promote fibroblast activation and tissue fibrosis. *Nat Commun*. (2017) 8:1130. doi: 10.1038/s41467-017-01236-6
85. Wei J, Yuan Y, Jin C, Chen H, Leng L, He F, et al. The ubiquitin ligase TRAF6 negatively regulates the JAK-STAT signaling pathway by binding to STAT3 and mediating its ubiquitination. *PLoS ONE* (2012) 7:e49567. doi: 10.1371/journal.pone.0049567
86. Dallavalle C, Albino D, Civenni G, Merulla J, Ostano P, Mello-Grand M, et al. MicroRNA-424 impairs ubiquitination to activate STAT3 and promote prostate tumor progression. *J Clin Invest*. (2016) 126:4585–602. doi: 10.1172/JCI86505
87. Ao N, Chen Q, Liu G. The small molecules targeting ubiquitin-proteasome system for cancer therapy. *Comb Chem High Throughput Screen.* (2017) 20:403–13. doi: 10.2174/1386207320666170710124746
88. Koca SS, Ozgen M, Dagli F, Tuzcu M, Ozercan IH, Sahin K, et al. Proteasome inhibition prevents development of experimental dermal fibrosis. *Inflammation* (2012) 35:810–7. doi: 10.1007/s10753-011-9380-y
89. Fineschi S, Reith W, Guerne PA, Dayer JM, Chizzolini C. Proteasome blockade exerts an antifibrotic activity by coordinately down-regulating type I collagen and tissue inhibitor of metalloproteinase-1 and up-regulating metalloproteinase-1 production in human dermal fibroblasts. *FASEB J.* (2006) 20:562–4. doi: 10.1096/fj.05-4870fje
90. Nakajima F, Aratani S, Fujita H, Yagishita N, Ichinose S, Makita K, et al. Synoviolin inhibitor LS-102 reduces endoplasmic reticulum stress-induced collagen secretion in an *in vitro* model of stress-related interstitial pneumonia. *Int J Mol Med*. (2015) 35:110–6. doi: 10.3892/ijmm.2014.1984
91. Blees JS, Bokesch HR, Rubsamen D, Schulz K, Milke L, Bajer MM, et al. Erioflorin stabilizes the tumor suppressor Pdcd4 by inhibiting its interaction with the E3-ligase beta-TrCP1. *PLoS ONE* (2012) 7:e46567. doi: 10.1371/journal.pone.0046567
92. Kapuria V, Peterson LF, Fang D, Bornmann WG, Talpaz M, Donato NJ. Deubiquitinase inhibition by small-molecule WP1130 triggers aggresome formation and tumor cell apoptosis. *Cancer Res*. (2010) 70:9265–76. doi: 10.1158/0008-5472.CAN-10-1530

93. Tian Z, D'Arcy P, Wang X, Ray A, Tai YT, Hu Y, et al. A novel small molecule inhibitor of deubiquitylating enzyme USP14 and UCHL5 induces apoptosis in multiple myeloma and overcomes bortezomib resistance. *Blood* (2014) 123:706–16. doi: 10.1182/blood-2013-05-500033
94. Nan L, Jacko AM, Tan J, Wang D, Zhao J, Kass DJ, et al. Ubiquitin carboxyl-terminal hydrolase-L5 promotes TGFbeta-1 signaling by de-ubiquitinating and stabilizing Smad2/Smad3 in pulmonary fibrosis. *Sci Rep*. (2016) 6:33116. doi: 10.1038/srep33116
95. Huang X, Dixit VM. Drugging the undruggables: exploring the ubiquitin system for drug development. *Cell Res.* (2016) 26:484–98. doi: 10.1038/cr.2016.31

Conflict of Interest Statement: The authors declare that the research was conducted in the absence of any commercial or financial relationships that could be construed as a potential conflict of interest.

frontiers in Immunology

ORIGINAL RESEARCH
published: 27 February 2020
doi: 10.3389/fimmu.2020.00220

T-Cell Proapoptotic and Antifibrotic Activity Against Autologous Skin Fibroblasts *in vitro* Is Associated With IL-17A Axis Upregulation in Systemic Sclerosis

Serena Vettori[1], Giusi Barra[2], Barbara Russo[1], Alessia Borgia[1], Giuseppe Pasquale[2], Luciana Pellecchia[1], Lucia Vicedomini[1] and Raffaele De Palma[2,3]*†*

[1] *Rheumatology Unit, Department of Precision Medicine, University of Campania "Luigi Vanvitelli", Naples, Italy,* [2] *Clinical Immunology Unit, Department of Precision Medicine, University of Campania "Luigi Vanvitelli", Naples, Italy,* [3] *Institute of Protein Biochemistry (IBP-CNR), Naples, Italy*

OPEN ACCESS

Edited by:
Isabelle Meyts,
KU Leuven, Belgium

Reviewed by:
Yun Ling,
Fudan University, China
Tadashi Ariga,
Hokkaido University, Japan

***Correspondence:**
Serena Vettori
serenavettori@libero.it
Raffaele De Palma
raffaele.depalma@unicampania.it

†Present address:
Raffaele De Palma,
Department of Internal Medicine (DIMI), University of Genova, Genova, Italy

Specialty section:
This article was submitted to Primary Immunodeficiencies, a section of the journal Frontiers in Immunology

Received: *06 August 2019*
Accepted: *27 January 2020*
Published: *27 February 2020*

Citation:
Vettori S, Barra G, Russo B, Borgia A, Pasquale G, Pellecchia L, Vicedomini L and De Palma R (2020) T-Cell Proapoptotic and Antifibrotic Activity Against Autologous Skin Fibroblasts in vitro Is Associated With IL-17A Axis Upregulation in Systemic Sclerosis. Front. Immunol. 11:220. doi: 10.3389/fimmu.2020.00220

Background: Systemic sclerosis (SSc) T cells can induce apoptosis of autologous skin fibroblasts *in vitro*. Th17 cells have been reported to increase in SSc patients, and interleukin-17A (IL-17A) has a profibrotic function. We used a system based on T-cell-autologous fibroblast co-cultures to further investigate a possible role of IL-17A in SSc.

Methods: T cells from diffuse SSc patients were co-cultured with autologous skin fibroblasts. *IL17A* mRNA was assessed by real-time PCR in co-cultured and control T cells, while *IL17RA*, *CXCL1*, *CCL2*, *CCL3*, *COL1A1*, *COL3A1*, *CTGF*, *TGFBR2*, and *SMAD3* mRNAs were assessed in co-cultured and control fibroblasts. In subset experiments, co-cultures and control cells were treated with either IL-17A or IL-17A *plus* anti-IL17 receptor monoclonal antibody (α-IL-17RA mAb). Chemokine and procollagen type I (PCI) production was further investigated at the protein level in cell culture supernatants by multiple suspension immunoassay and sandwich ELISA, respectively. Co-cultured and control fibroblasts were also stained with Annexin V and analyzed by flow cytometry.

Results: T cell–fibroblast co-cultures overexpressed *IL17A* and *IL17RA*. Furthermore, co-cultured fibroblasts upregulated IL-17A targets *CXCL1*, *CCL2*, and *CCL3*, while *COL1A1*, *COL3A1*, *CTGF*, and two key effectors of the TGF-β signaling, *TGFBR2* and *SMAD3*, were found downregulated. Consistently, chemokine concentrations were increased in co-culture supernatants, while PCI levels were reduced, especially after stimulation with ectopic IL-17A. Finally, simultaneous α-IL-17RA mAb treatment restored PCI levels and reduced fibroblast apoptosis in IL-17A-stimulated co-cultures.

Conclusion: These data suggest that IL-17A upregulation might play a role in modulating T cell-mediated antifibrotic and proapoptotic effects in co-cultured autologous skin fibroblasts.

Keywords: systemic sclerosis, T cells, fibroblasts, co-cultures, apoptosis, IL-17A, IL-17RA, chemokines

INTRODUCTION

Systemic sclerosis (SSc) is a chronic multiorgan disease characterized by microvascular injury, autoimmune phenomena, and fibroblast activation, leading to uncontrolled extracellular matrix (ECM) deposition in the skin and visceral organs and increased mortality due to vital organ dysfunction (1, 2). The etiopathogenesis of the disease remains unknown. However, endothelial, immune cell, and fibroblast activation, and most notably T cell–fibroblast cross-talk, play a role (3). In the past years, we and others showed that the skin of patients with diffuse SSc (dcSSc) of recent onset (<3 years) is predominantly infiltrated by oligoclonally expanded CD4+ T cells (4, 5). Furthermore, we demonstrated that SSc T cells co-cultured with autologous skin fibroblasts up to 10 days display the same clonotypes found in the skin of these patients and can induce fibroblast apoptosis *in vitro* (6). These data suggest that an antigen-driven T-cell response could be initially devoted to control the aberrant fibroblast activation found in SSc. In line with our observations, other authors reported that chemically pre-activated peripheral γδT cells from SSc patients can also induce autologous fibroblast apoptosis after a short-term exposure *in vitro* (7). In those experiments, both T cell–fibroblast interaction and activation of γδT cells was paralleled by a cytokine burst in which profibrotic cues were more prominent (5, 6, 8, 9). These events may account for the escape of fibroblasts from a control attempted by T cells and for the resistance to apoptosis *in vivo*.

More recent evidences suggest that, among other immune-inflammatory mediators, interleukin-17A (IL-17A) and Th17 could play a key function in the pathogenesis of SSc (10), even though their role remains unclear (11). IL-17A seems to promote the production of proinflammatory mediators and metalloproteinases in human fibroblasts. Moreover, this cytokine suppresses collagen type I and connective tissue growth factor (CTGF) synthesis and counteracts alpha-smooth muscle actinin (α-SMA)-mediated myofibroblast transdifferentiation *in vitro* (12–15). However, in animal models of lung and skin fibrosis, IL-17A deficiency seems to protect against collagen deposition (16–18), and IL-17A stimulation of mouse fibroblast lines induces CTGF and transforming growth factor-β (TGF-β) overexpression (18). A possible explanation for this dual role of IL-17A in SSc has been provided by Dufour et al., who showed that IL-17A plays different effects on cultured SSc fibroblasts, depending on the prevalent activation of either IL-17A or TGF-β signaling pathway (19). In this context, the assessment of IL-17A levels in our co-cultures and a better knowledge of the effects of its modulation in T cell–fibroblast co-cultures could be helpful to add details on T cell–fibroblast dynamics in SSc *in vitro*.

METHOD

Patients

Nine dcSSc patients (20) with a disease duration from Raynaud's phenomenon (RP) onset ≤ 3 years, all meeting ACR/EULAR 2013 classification criteria (21), underwent whole blood drawing for peripheral blood mononuclear cell (PBMC) isolation and punch skin biopsy as described elsewhere according to international standards (6, 22), after giving informed written consent. **Supplementary Table 1** summarizes demographic, clinical, and serological features of the patients enrolled. All biospecimens were obtained at first observation before initiating any immunomodulatory treatment.

The study protocol was approved by the Ethics Committee of the Department of Internal and Experimental Medicine "F.Magrassi-A. Lanzara" of the Second University of Naples (protocol n. 303/March 16th 2017).

Cultures and Reagents

Fibroblasts were obtained by outgrowth culture from two to three 1-mm^2 skin pieces into Petri dishes with DMEM added with 10% heat-inactivated fetal calf serum (FCS), 1 mM penicillin–streptomycin, and 2 mM l-glutamine. After 2–3 weeks, cells reached confluence, were harvested by trypsin treatment, and re-seeded in RPMI1640. Cells at passages 3–7 were used to set co-cultures. For each experiment, at least five cell batches were assayed in duplicate. All reagents were purchased from Invitrogen, ThermoFisher Scientific Inc., Waltham, MA, USA.

PBMCs were isolated from 20 ml of peripheral blood by centrifugation in a density gradient (Ficoll-Hypaque, Pharmacia LKB Biotechnology, New Brunswick, NJ, USA), washed, counted, and co-cultured up to 10 days with autologous fibroblasts in a 10:1 ratio in the presence of human recombinant IL-2 (hrIL-2) at a concentration of 20 U/ml, as described previously (5, 6), to sustain fibroblast-induced T-cell expansion (23). Fibroblasts alone and PBMCs alone *plus* hrIL-2 were cultured separately as controls. In subset experiments, co-cultures were added with human recombinant IL-17A (hrIL-17A) at a concentration of 6.25 ng/ml and/or IL-17RA neutralizing monoclonal antibody (α-IL-17RA mAb) at a concentration of 16 μg/ml. Human BSA 0.1% and goat isotype IgG were used as irrelevant controls for IL-17A and α-IL-17RA mAb treatment, respectively (IL-17A from Gibco, ThermoFisher Inc., Waltham, MA, USA; α-IL-17RA from R&D Systems Inc., Minneapolis, MN, USA). Minimal effective concentrations of both hrIL-17A and α-IL-17RA mAb were assessed by titration experiments measuring target gene expression induction, according to manufacturer instructions (**Supplementary Figure 1**).

RNA Isolation and Gene Expression Analysis

RNA isolation was performed on cultured cells after trypsinization, washing in PBS and addition of Trizol Reagent (Invitrogen, ThermoFisher Scientific Inc., Waltham, MA, USA) according to manufacturer instructions. Then, 100 ng of total RNA was reverse transcribed using random hexamers, Multiscribe reverse transcriptase 50 U/μl, RT buffer, dNTPs, and RNase inhibitor 20 U/μl. 18S rRNA was used as endogenous control and analyzed by TaqMan-based real-time PCR using a pre-developed FAM-labeled primer-probe system (Hs99999901_s1; Applied Biosystems, ThermoFisher Scientific Inc., Waltham, MA, USA), while *IL17A*, *IL17RA*, *IL17RC*, *CXCL1*, *CCL2*, *CCL3*, *TGFBR2*, *SMAD3*, *CTGF*, *COL1A1*, and *COL3A1* mRNAs were analyzed by real-time PCR in a Sybr

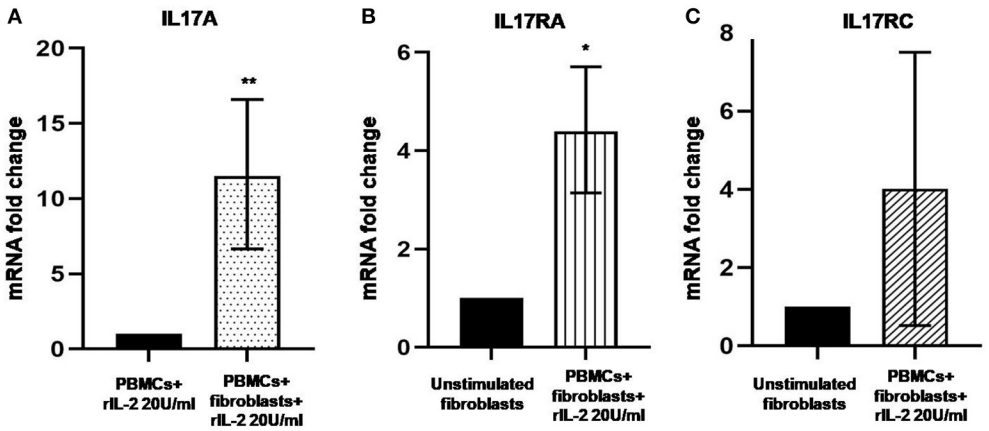

FIGURE 1 | Levels of *IL17A*, *IL17RA*, and *IL17RC* in co-cultured PBMCs and fibroblasts from early dcSSc patients. Results are fold changes in mRNA levels of target genes in real-time PCR. **(A)** Shows the expression of *IL17A* in PBMCs co-cultured with autologous skin fibroblasts and hrIL-2 20 U/ml as compared to PBMCs cultured in the presence of hrIL-2 20 U/ml only. **(B)** Shows the expression of *IL-17RA* in fibroblasts co-cultured with autologous PBMCs and hrIL-2 20 U/ml as compared to fibroblasts alone. **(C)** Shows the expression of *IL-17RC* in fibroblasts co-cultured with autologous PBMCs and hrIL-2 20 U/ml as compared to fibroblasts alone. Data are median and IQR ranges, Wilcoxon signed rank test in panels **(A,B)**. Data are mean and SD, one sample *t*-test in panel **(C)** because of normal data distribution. $^{*}p < 0.05$; $^{**}p < 0.01$; number of samples per group = 6.

Green Master Mix, using 1 μl of cDNA and 11.25 μM self-designed primer pairs (all Applied Biosystems, ThermoFisher Scientific Inc., Waltham, MA, USA). Samples without the enzyme in the RT reaction were used as negative controls to exclude genomic contamination, and the quality of the primer amplification was tested by dissociation curve analysis (24). For relative quantification, the comparative threshold cycle (Ct) method was used (25). Primer sequences are reported in **Supplementary Table 2**.

Protein Analysis

CXCL1, CCL2, and CCL3 levels were measured in culture supernatants by immunosuspension assay. Tests were performed with spectrally encoded beads coupled with capture antibodies each specific to the analyte of interest as the solid support, and a biotinylated detection antibody–streptavidin–phycoerythrin complex, as the reporter system (Merk Millipore, Billerica, MA, USA) to be read by a double laser-based fluorimetric instrument (Luminex 200, Luminex Corporation, Austin, TX, USA). Concentrations obtained by interpolation of sample fluorescence intensities with a standard curve were expressed as pg/ml.

Serum procollagen type I (PCI) levels were measured by sandwich ELISA and concentrations were also expressed in pg/ml by interpolation of sample optical densities with standard curves (Elabscience Biotechnology Co, Whu Han, PRC).

Apoptosis Analysis

The Annexin V-FITC-labeled Apoptosis Detection Kit (Roche Diagnostics GmbH, Penzberg, Germany) was used to detect and quantify apoptosis by flow cytometry according to the manufacturer instructions. Cells were collected by centrifugation for 10 min at 500 *g* and then re-suspended at a density of 1×10^5 cells/ml in 1 binding buffer (HEPES buffer, 10 mM, pH 7.4, 150 mM NaCl, 5 mM KCl, 1 mM $MgCl^2$, and 1.8 mM $CaCl_2$) and stained simultaneously with FITC-labeled Annexin V and propidium iodide (PI). PI was used as a cell viability marker. Cells were analyzed using a FACScalibur flow cytometer.

Statistical Analysis

GraphPad Prism software version 6.0 (GraphPad software Inc., San Diego, CA, USA) was used for statistical analysis. Continuous variables were expressed as mean ± SD and medians with interquartile range (IQR). The D'Agostino-Pearson test was applied to test normality data distribution and the Student's paired or unpaired *t*-test or the Mann–Whitney and the Wilcoxon tests were used as appropriate. The one-way ANOVA test was used for multiple group comparison. Results were considered statistically significant for $p < 0.05$.

RESULTS

IL-17A Is Upregulated in Co-cultured PBMCs and IL-17RA Is Upregulated and Activated in Autologous Co-cultured Skin Fibroblasts From Early dcSSc Patients

In **Figure 1A**, we show IL-17A expression in SSc PBMCs co-cultured with autologous skin fibroblasts. In these experiments, we found an increase in IL-17A mRNA levels by median 11.5-fold as compared to PBMCs cultured alone in the presence of hrIL-2 ($p < 0.01$), thus suggesting that IL-17A is secreted during T cell–fibroblast interactions in early dcSSc. This finding was consistent with the increased expression in the mRNA levels of both the subunit A of IL-17A receptor, IL-17RA, and the subunit C, IL-17RC, in the co-cultured fibroblasts by median 4.3-fold ($p < 0.05$) (**Figure 1B**), and mean 4-fold (**Figure 1C**), respectively, as compared to fibroblasts cultured alone. However, to investigate

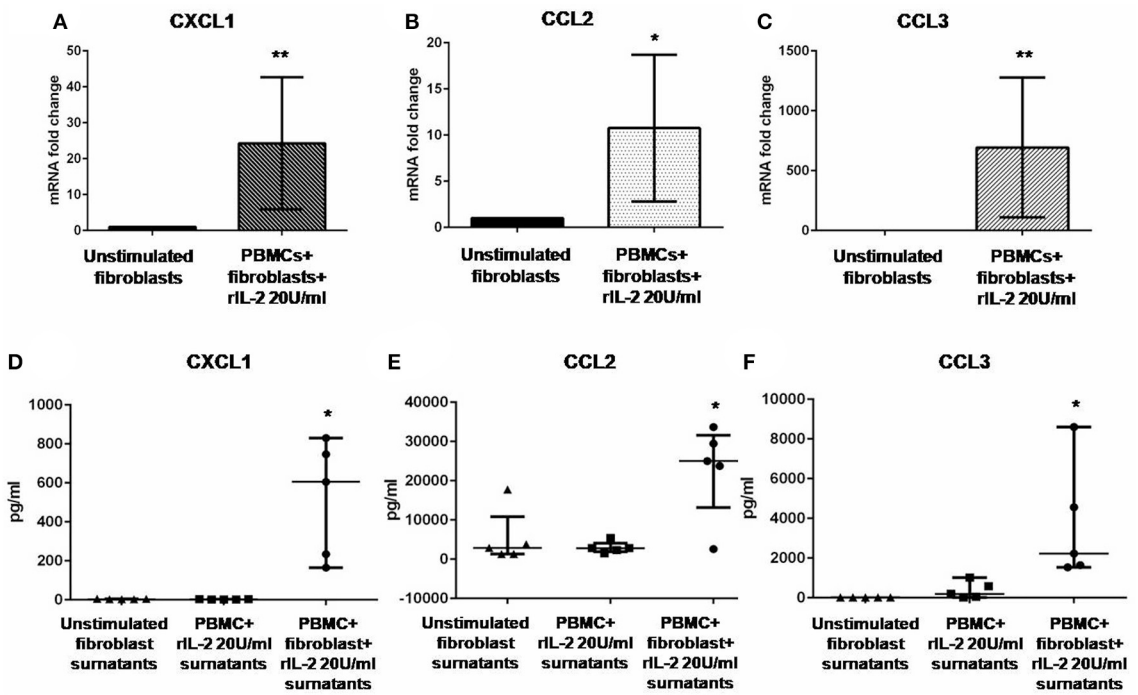

FIGURE 2 | Levels of CXCL1, CCL2, and CCL3 in co-cultured fibroblasts and supernatants from early dcSSc patients. Results in panels **(A–C)** are fold changes in mRNA levels of IL17A target genes in real-time PCR. Results in panels **(D–F)** are concentrations expressed in pg/ml, in multiple suspension immunoassay. **(A–C)** Show the expression of *CXCL1*, *CCL2*, and *CCL3* in fibroblasts co-cultured with autologous PBMCs and hrIL-2 20 U/ml as compared to control fibroblasts. **(D–F)** Show the concentrations of secreted CXCL1, CCL2, and CCL3 in supernatants from co-cocultures and hrIL-2 20 U/ml as compared to supernatants from control fibroblasts after adjusting by concentrations measured in PBMCs cultured with hrIL-2 20 U/ml only. Data are median and IQR ranges, Wilcoxon signed rank test. $^{*}p < 0.05$; $^{**}p < 0.01$; number of samples per group = 5.

whether IL-17 receptor overexpression in co-cultured fibroblasts ensues in the activation of the receptor, a heteromeric structure made of at least one subunit IL-17RA that partners IL-17RC in IL-17A-mediated responses in autoimmune disorders (26), we investigated mRNA levels of several IL-17A target genes in the co-cultured fibroblasts, namely, *CXCL1*, *CCL2*, and *CCL3*, that were found increased by 29-fold, 11.9-fold, and 773.3-fold, respectively ($p < 0.05$) (**Figures 2A–C**). Consistently, the corresponding secreted proteins were increased by 11.2-fold, 8.9-fold, and 252.4-fold, respectively ($p < 0.05$), in supernatants from co-cultures as compared to supernatants from unstimulated fibroblasts (**Figures 2D–F**).

IL-17RA Upregulation and Activation in Skin Fibroblasts Co-cultured With Autologous PBMCs Are Associated With the Downregulation of Pro-Fibrotic Genes in Early dcSSc

Previous reports suggested that IL-17A could negatively regulate type I collagen expression in humans (11, 27, 28) and we found that IL-17A was upregulated in our co-cultured PBMCs. Therefore, we looked at *COL1A1* and other profibrotic genes, namely, *COL3A1* and *CTGF* in SSc fibroblasts co-cultured with the autologous PBMCs overexpressing IL-17A. We found that all these genes were significantly downregulated in co-cultured fibroblasts as compared to control cells to 0.33-fold ($p < 0.001$), to 0.24-fold ($p < 0.01$), and to 0.31-fold ($p < 0.05$) (**Figures 3A–C**), respectively. Furthermore, the expression of two key molecules crucial to the TGF-β signaling pathway, *TGFBR2* and *SMAD3*, was downregulated as well to 0.59-fold and 0.79-fold ($p < 0.05$), respectively (**Figures 3E,F**). Finally, since type I collagen is the most abundant collagen type that accumulates in human skin in SSc (29), we measured concentration of PCI in supernatants from co-cultures as compared to supernatants from unstimulated fibroblasts. Here, we found a decrease of PCI levels in co-cultures from mean 639 ± 109.7 to 486.4 ± 88.16 pg/ml ($p < 0.05$) (**Figure 3D**), thus further confirming a functional effect due to IL-17A.

Hampering IL-17A Signaling in Fibroblasts Co-cultured With Autologous PBMCs Affects Procollagen Type I Secretion and Protects Fibroblasts From Apoptosis in Early dcSSc

Data generated so far prompted us to evaluate if the activation of IL-17A signaling pathway could be implicated in the *in vitro* dynamics between SSc PBMCs and autologous skin fibroblasts from early dcSSc patients. Different T-cell subsets can be present

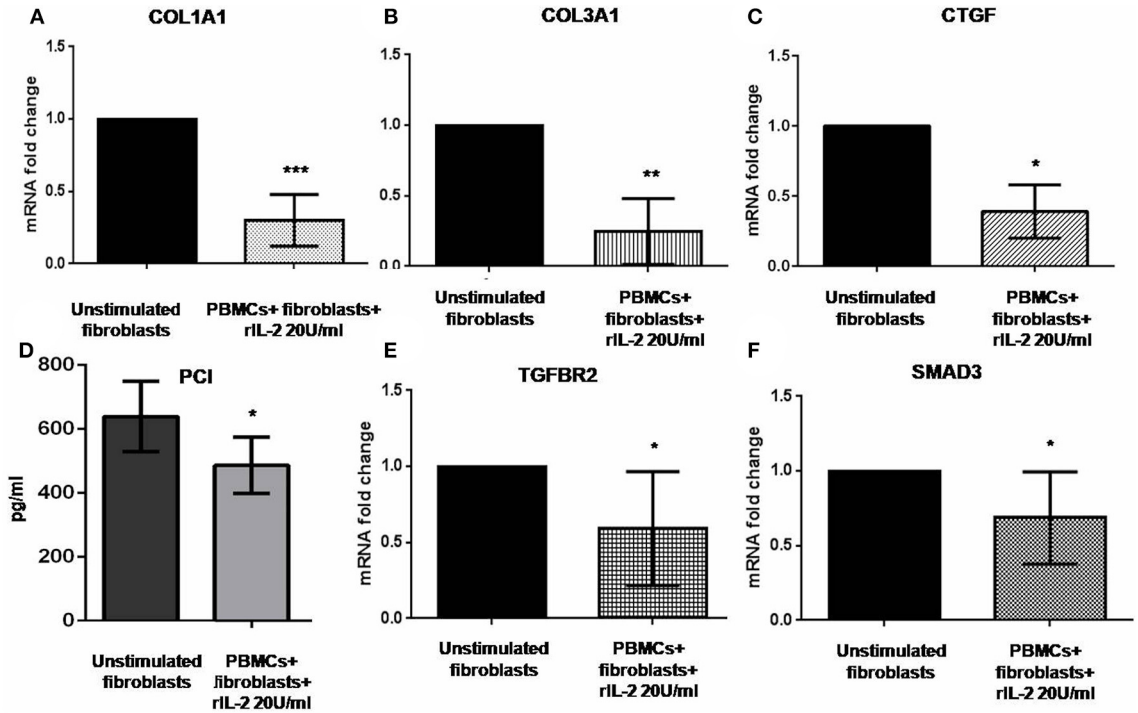

FIGURE 3 | Profibrotic gene levels in co-cultured fibroblasts from early dcSSc patients and PCI in co-culture supernatants. Results in panels **(A–C)** and **(E,F)** are fold changes in mRNA levels of the profibrotic genes *COL1A1*, *COL3A1*, and *CTGF*, and of the two key mediators of the TGF-β signaling *TGFBR2* and *SMAD3* in real-time PCR. All show the expression of the investigated genes in fibroblasts co-cultured with autologous PBMCs and hrIL-2 20 U/ml as compared to control fibroblasts. Data are median and IQR ranges, Wilcoxon signed rank test. Results in panel **(D)** are concentrations as expressed in pg/ml in sandwich ELISA. Data are mean ± SD, paired Student's *t*-test. $^{*}p < 0.05$; $^{**}p < 0.01$; $^{***}p < 0.001$; number of samples per group = 5.

in these co-cultures playing complex interactions with each other and with fibroblasts. Therefore, to link PBMC antifibrotic activity and previously reported proapoptotic effects on co-cultured autologous fibroblasts, we looked at both PCI production and fibroblast apoptosis after stimulation of co-cultured cells, adding a suboptimal dose of ectopic hrIL-17A in order to maximize effects due to this cytokine, given the multiple components that may drive PBMC-induced apoptosis in co-cultured autologous fibroblasts. As further control, in a subset of experiments, we simultaneously administered α-IL-17RA mAb to co-cultures to counteract IL-17A signaling. In these experimental settings, co-cultured fibroblasts showed a reduced PCI production in the presence of hrIL-17A to levels lower than those measured in the presence of PBMCs and BSA 0.1% (354.2 ± 181.2 vs. 486.4 ± 88.16 pg/ml), even though the difference was not statistically significant. In addition, combined treatment with IL-17A and α-IL-17RA mAb allowed the measurement of PCI levels in co-culture supernatants similar to those found in supernatants from fibroblasts cultured alone (623.4 ± 133.6 pg/ml), although the difference with PCI levels from co-cultures with rhIL-17A and isotype control IgG was not statistically significant (**Figure 4A**). Most intriguingly, when we looked at co-cultured fibroblasts stained with annexin V and PI, we found that cells treated with rhIL-17A had an significantly increased expression of Annexin V, that was reduced from mean 44.2 to 32.3% ($p < 0.01$) in presence of α-IL-17RA mAb (**Figure 4B**). **Figures 4C,D** are scatterplot graphs from a representative SSc fibroblast-autologous PBMC co-culture showing the percentage of apoptotic fibroblasts (Annexin V positive) in presence of either rhIL-17A or rhIL-17A *plus* α-IL-17A, respectilvely.

DISCUSSION

We have previously reported that T cells of early SSc patients kill autologous fibroblasts *in vitro*, while we did not observe this phenomenon in the same experimental setting when we used cells from patients affected by different autoimmune diseases, such as systemic lupus erythematosus (5, 6). These data support the hypothesis that T cells undergo an antigen-driven oligoclonal expansion in the skin of SSc patients in the early phases of the disease toward the aberrantly activated fibroblasts (6, 7). Moreover, it is well-known that a T-cell response in SSc tissues is detectable only in the early disease stage, while an extensive fibrosis with a neglectable immune infiltrate is observed in late stages. Factors that drive the failure of such immune response *in vivo* are not known (3). Due to these observations, we wanted to further investigate the dynamics and the function of T cell–fibroblast interaction in SSc, using our experimental co-culture setting that we previously detailed (5, 6).

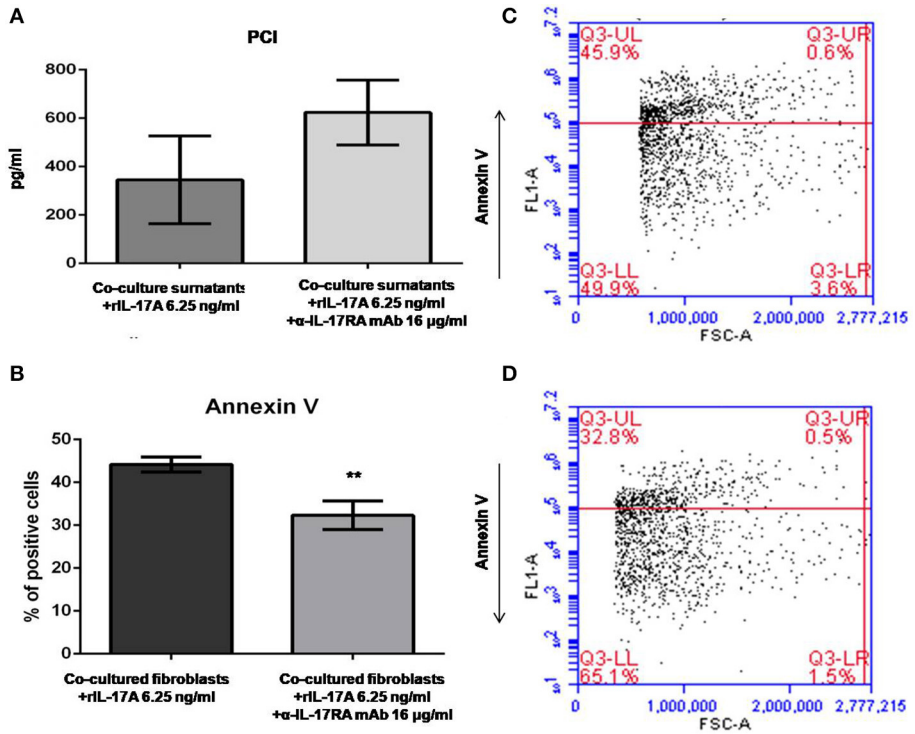

FIGURE 4 | PCI concentration and SSc fibroblast apoptosis in co-cultures exposed to either IL-17A or IL-17A+α-IL-17A mAb. **(A)** Shows that concentrations of PCI in supernatants from SSc PBMC–fibroblast co-cultures treated with ectopic rhIL-17A 6.25 ng/ml are decreased, while simultaneous treatment of these co-cultures with ectopic rhIL-17A and a neutralizing mAb against IL-17RA subunit, α-IL-17A mAb16 µg/ml, increases PCI production (number of samples per group = 3). **(B)** Shows that α-IL-17A mAb at the same concentration is able to reduce significantly the apoptotic rate of co-cultured SSc fibroblasts exposed to rhIL-17A (number of samples per group = 5). Data are mean ± SD, paired Student's *t*-test. $^{**}p < 0.01$. The scatterplot graph in panel **(C)** shows the percentage of apoptotic fibroblasts co-cultured with autologous PBMCs obtained from a representative SSc patient, added with ectopic rhIL-17A 6.25 ng/ml. The scatterplot graph in panel **(D)** shows the percentage of apoptotic fibroblasts co-cultured with autologous PBMCs obtained from the same representative SSc patient, added with both ectopic rhIL-17A 6.25 ng/ml and α-IL-17A mAb16 µg/ml.

IL-17 has been proposed to have a central role in SSc (reviewed in 11). Analysis of our *in vitro* data demonstrated an increased production of IL-17A when T cells and autologous SSc skin fibroblasts were co-cultured. Starting from this finding, we moved to show a role of IL-17A, and its signaling pathway, in profibrotic gene modulation and in proapoptotic effects played by PBMCs co-cultured with autologous skin fibroblasts from early dcSSc patients.

Indeed, we found a downregulation of the mRNA levels of TGFBR2 and SMAD3 in co-cultured fibroblasts that could be, at least in part, associated with modulatory effects exerted by IL-17A on the TGF-β signaling, as recently described in other fibrotic disorders (30). A functional shift of the Th response toward a Th17 profile in SSc patients has been described by us and others (31, 32). Therefore, one possible explanation could be that skin microenvironment in SSc drives a Th17 polarization (10), thus promoting a Th polarization that, in the long term, is not able to eliminate altered SSc fibroblasts but concurs to the fibrosis development through the production of IL-17 (33, 34).

In vitro, data from other groups showed that, in human cells, IL-17A is able to induce a proinflammatory profile (12, 13, 35), including increased expression of CCL2 and CXCL8 chemokines (13, 35), interleukins IL-1β and IL-6 (12, 35), adhesion molecules like ICAM-1 and VCAM-1 (12, 35), and metalloproteinases like MMP-1 (14). Actually, all these factors have been implicated in the pathogenesis of SSc, even though their role seems to be strictly dependent on the phase of the disease (3, 11, 36). Moreover, recent data also indicate that, despite the fact that IL-17A shares high homology with IL-17F and is coordinately expressed, the effects in SSc skin and fibroblasts are restricted to the IL-17A isoform (37).

In a previous paper, we reported that in PBMC–fibroblast co-culture supernatants from early dcSSc patients, TGF-β levels are stably increased over the entire culture period (10 days) (6). In these new sets of experiments, we confirm the stable increase of *TGFB1* and also of *IL4* and *IL1B* mRNAs in PBMCs over the 10 days of co-culture (**Supplementary Figure 2**). This aspect partially explains the impairment of the immune response.

The potential antifibrotic activity of activated T cells has long been known (38, 39). This is the first report that describes such effects in a dynamic system like PBMC–fibroblast co-cultures, highlighting the role of IL-17A. Of note, in previous reports, activated T cell-derived particles specifically induced type I collagen inhibition (40) and, interestingly, also more recent data show that IL-17A antifibrotic effects seem to affect primarily type I collagen (13, 19, 27, 28). In our experiments,

actually, we could demonstrate a downregulation also of the α1 chain of type III collagen at the mRNA level that should be further investigated.

As regards *CTGF* downregulation, data are consistent with the impaired expression of genes encoding for the TGF-β signaling components *TGFBR2* and *SMAD3*, as CTGF is one of the major downstream mediators of TGF-β (41). Consistently with our findings, Nakashima et al. reported that IL-17A is able to induce *COL1A1* and *CTGF* downregulation indirectly *via* the overexpression of miR-129-5p (15). Moreover, Truchetet et al. recently showed that IL-17A is able to prevent TGF-β-dependent myofibroblast differentiation *in vitro* (14).

It has to be underlined, however, that the hypothesized antifibrotic role of IL-17A in SSc is not supported by experimental models of inflammatory/drug-induced fibrosis, in which IL-17A seems to induce fibrosis in both skin and lung disease (16, 17, 42, 43). These discrepancies might depend on the fact that none of the mouse models that have been used to investigate the role of IL-17A in skin and lung fibrosis *in vivo* recapitulate the complete features of SSc. In particular, these animals do not display features of peripheral vasculopathy, nor do they present with circulating autoantibodies.

Lastly, but most intriguingly, the activation of IL-17A axis in our co-cultures was implicated in the modulation of fibroblast apoptosis. Apoptosis of SSc skin fibroblasts induced by co-cultured autologous PBMCs *in vitro* is likely to be influenced by different factors, one of which is the overexpression and activation of the death receptor Fas, as shown by our previous results (6). However, here we demonstrate that the high apoptotic rate of co-cultured fibroblasts added with rhIL-17A was counteracted by the simultaneous treatment with a neutralizing α-IL-17RA mAb, thus demonstrating that IL-17A axis plays a role regardless other possible mechanisms.

To date, little is known about IL-17A implication in programmed cell death. Arif et al. (44) reported that circulating IL-17+ cells autoreactive against several β-islet antigens are detectable in the blood of type I diabetes mellitus patients and induce β-cell death *via* activation of STAT1 and (NF)-kB transcription factors. Moreover, Su et al. (45) demonstrated that IL-17A is crucial in cardiomyocyte apoptosis through STAT3-iNOS pathway activation. On the contrary, other authors described an antiapoptotic activity played by IL-17A in other disease settings (46, 47). In particular, Kim et al. (47) reported that fibroblast-like synoviocytes exposed to IL-17 develop morphological and functional changes in mitochondrial proteins involved in autophagy resulting in resistance to apoptosis.

Our study has some limitations. First, all data come from *in vitro* experiments, as no other options are so far available to explore T cell–fibroblast interactions in SSc. Second, we did not use controls. However, other authors demonstrated that IL-17A stimulation has similar effects in SSc and healthy control fibroblasts (13, 19), thus suggesting that its pro/antifibrotic function is strictly depending on the microenvironment. Moreover, we demonstrated in previous studies (5, 6) that T cell–fibroblast interactions *in vitro* are specific to SSc. Taken together, our data and data from previous studies from independent groups (6, 7) suggest that T cell response in SSc might be also aimed to contrast aberrant TGF-β-dependent myofibroblast activation that is seen in this disease and that IL-17A might play a prominent dual role in this scenario (10–14), bridging a T cell response from a protective role to a profibrotic one in the long term. More studies are needed because of the paucity of data and inconsistent evidences from experimental models of fibrosis. Given so, the lack of clinical trials with IL-17 modulators in SSc is not surprising. Future lines of research are necessary, in particular to explore the proapoptotic potential of IL-17A to be translated in the clinical setting.

DATA AVAILABILITY STATEMENT

The datasets generated during and/or analyzed during the current study are available from the corresponding authors on reasonable request.

ETHICS STATEMENT

The studies involving human participants were reviewed and approved by the Ethics Committee of the Department of Internal and Experimental Medicine F.Magrassi-A. Lanzara of the Second University of Naples. The patients/participants provided their written informed consent to participate in this study.

AUTHOR CONTRIBUTIONS

SV designed the study, planned and performed experiments, analyzed data, and drafted the manuscript. GB performed experiments, analyzed data, and critically revised the manuscript. BR, AB, GP, LP, and LV performed experiments and critically revised the manuscript. RD designed the study, planned experiments, analyzed data, and drafted the manuscript. All authors contributed to manuscript revision, read, and approved the submitted version.

SUPPLEMENTARY MATERIAL

The Supplementary Material for this article can be found online at: https://www.frontiersin.org/articles/10.3389/fimmu.2020.00220/full#supplementary-material

REFERENCES

1. Desbois AC, Cacoub P. Systemic sclerosis: an update in 2016. *Autoimmun Rev.* (2016) 15:417–26. doi: 10.1016/j.autrev.2016.01.007
2. Vettori S, Cuomo G, Abignano G, Iudici M, Valentini G. Survival and death causes in 251 systemic sclerosis patients from a single Italian center. *Reumatismo.* (2010) 62:202–9. doi: 10.4081/reumatismo.2010.202
3. Chizzolini C, Boin F. The role of the acquired immune response in systemic sclerosis. *Semin Immunopathol.* (2015) 37:519–28. doi: 10.1007/s00281-015-0509-1
4. Sakkas LI, Xu B, Artlett CM, Lu S, Jimenez SA, Platsoucas CD. Oligoclonal T cell expansion in the skin of patients with systemic sclerosis. *J Immunol.* (2002) 168:3649–59. doi: 10.4049/jimmunol.168.7.3649

5. De Palma R, Del Galdo F, Lupoli S, Altucci P, Abbate G, Valentini G. Peripheral T lymphocytes from patients with early systemic sclerosis co-cultured with autologous fibroblasts undergo an oligoclonal expansion similar to that occurring in the skin. *Clin Exp Immunol*. (2006) 144:169–76. doi: 10.1111/j.1365-2249.2006.03041.x
6. De Palma R, D'Aiuto E, Vettori S, Cuoppolo P, Abbate G, Valentini G. Peripheral T cells from patients with early systemic sclerosis kill autologous fibroblasts in co-culture: is T-cell response aimed to play a protective role? *Rheumatology*. (2010) 49:1257–66. doi: 10.1093/rheumatology/keq094
7. Bendersky A, Markovits N, Bank I. Vγ9+ γδ T cells in systemic sclerosis patients are numerically and functionally preserved and induce fibroblast apoptosis. *Immunobiology*. (2010) 215:380–94. doi: 10.1016/j.imbio.2009.05.012
8. Workalemahu G, Foerster M, Kroegel C, Braun RK. Human gamma delta-T lymphocytes express and synthesize connective tissue growth factor: effect of IL-15 and TGF-beta 1 and comparison with alpha beta-T lymphocytes. *J Immunol*. (2003) 170:153–7. doi: 10.4049/jimmunol.170.1.153
9. Workalemahu G, Foerster M, Kroegel C. Expression and synthesis of fibroblast growth factor-9 in human gammadelta T-lymphocytes. Response to isopentenyl pyrophosphate and TGF-beta/IL-15. *J Leukoc Biol*. (2004) 75:657–63. doi: 10.1189/jlb.0902471
10. Fenoglio D, Battaglia F, Parodi A, Stringara S, Negrini S, Panico N, et al. Alteration of Th17 and treg cell subpopulations co-exist in patients affected with systemic sclerosis. *Clin Immunol*. (2011) 139:249–57. doi: 10.1016/j.clim.2011.01.013
11. Chizzolini C, Dufour AM, Brembilla CN. Is there a role for IL-17 in the pathogenesis of systemic sclerosis? *Immunol Lett*. (2018) 195:61–7. doi: 10.1016/j.imlet.2017.09.007
12. Kurasawa K, Hirose K, Sano H, Endo H, Shinkai H, Nawata Y, et al. Increased interleukin-17 production in patients with systemic sclerosis. *Arthritis Rheum*. (2000) 43:2455–63. doi: 10.1002/1529-0131(200011)43:11<455::AID-ANR12>3.0.CO;2-K
13. Brembilla NC, Montanari E, Truchetet ME, Raschi E, Meroni P, Chizzolini C. Th17 cells favor inflammatory responses while inhibiting type I collagen deposition by dermal fibroblasts: differential effects in healthy and systemic sclerosis fibroblasts. *Arthritis Res Ther*. (2013) 15:R151. doi: 10.1186/ar4334
14. Truchetet ME, Brembilla NC, Montanari E, Lonati P, Raschi E, Zeni S, et al. Interleukin-17A+ cell counts are increased in systemic sclerosis skin and their number is inversely correlated with the extent of skin involvement. *Arthritis Rheum*. (2013) 65:1347–56. doi: 10.1002/art.37860
15. Nakashima T, Jinnin M, Yamane K, Honda N, Kajihara I, Makino T, et al. Impaired IL-17 signaling pathway contributes to the increased collagen expression in scleroderma fibroblasts. *J Immunol*. (2012) 188:3573–83. doi: 10.4049/jimmunol.1100591
16. Mi S, Li Z, Yang HZ, Liu H, Wang JP, Ma YG, et al. Blocking IL-17A promotes the resolution of pulmonary inflammation and fibrosis via TGF-β1-dependent and –independent mechanisms. *J Immunol*. (2011) 187:3003–14. doi: 10.4049/jimmunol.1004081
17. Gasse P, Riteau N, Vacher R, Michel ML, Fautrel A, di Padova F, et al. IL-1 and IL-23 mediate early IL-17A production in pulmonary inflammation leading to late fibrosis. *PLoS ONE*. (2011) 6:e23185. doi: 10.1371/journal.pone.0023185
18. Okamoto Y, Hasegawa M, Matsushita T, Hamaguchi Y, Huu DL, Iwakura Y, et al. Potential roles of interleukin 17A in the development of skin fibrosis in mice. *Arthritis Rheum*. (2012) 64:3726–35. doi: 10.1002/art.34643
19. Dufour AM, Alvarez M, Russo B, Chizzolini C. Interleukin-6 and collagen type I production by systemic sclerosis fibroblasts are differentially regulated by interleukin-17A in the presence of transforming growth factor-beta 1. *Front Immunol*. (2018) 9:1865. doi: 10.3389/fimmu.2018.01865
20. LeRoy EC, Black C, Fleischmajer R, Jablonska S, Krieg T, Medsger TA Jr, et al. Scleroderma (systemic sclerosis): classification, subsets and pathogenesis. *J Rheumatol*. (1988) 15:202–5.
21. van den Hoogen F, Khanna D, Fransen J, Johnson SR, Baron M, Tyndall A, et al. 2013 classification criteria for systemic sclerosis: an American college of rheumatology/European league against rheumatism collaborative initiative. *Arthritis Rheum*. (2013) 65:2737–47. doi: 10.1002/art.38098
22. Beyer C, Distler JH, Allanore Y, Aringer M, Avouac J, Czirjak L, et al. EUSTAR biobanking: recommendations for the collection, storage and distribution of biospecimens in scleroderma research. *Ann Rheum Dis*. (2011) 70:1178–82. doi: 10.1136/ard.2010.142489
23. Minami Y, Kono T, Miyazaki T, Taniguchi T. The IL-2 receptor complex: structure, function, and target genes. *Annu Rev Immunol*. (1993) 11:245–67. doi: 10.1146/annurev.iy.11.040193.001333
24. Schmittgen TD, Livak KJ. Analyzing real-time PCR data by the comparative C(T) method. *Nat Protoc*. (2008) 36:1101–8. doi: 10.1038/nprot.2008.73
25. Ririe KM, Rasmussen RP, Wittwer CT. Product differentiation by analysis of DNA melting curves during the polymerase chain reaction. *Anal Biochem*. (1997) 245:154–60. doi: 10.1006/abio.1996.9916
26. Gu C, Wu L, Li X. IL-17 family: cytokines, receptors, and signaling. *Cytokine*. (2013) 64:477–85. doi: 10.1016/j.cyto.2013.07.022
27. Chizzolini C, Parel Y, De Luca C, Tyndall A, Akesson A, Scheja A, et al. Systemic sclerosis Th2 cells inhibit collagen production by dermal fibroblasts via membrane-associated tumor necrosis factor alpha. *Arthritis Rheum*. (2003) 48:2593–604. doi: 10.1002/art.11129
28. Chizzolini C, Rezzonico R, Ribbens C, Burger D, Wollheim FA, Dayer JM. Inhibition of type I collagen production by dermal fibroblasts upon contact with activated T cells: different sensitivity to inhibition between systemic sclerosis and control fibroblasts. *Arthritis Rheum*. (1998) 41:2039–47. doi: 10.1002/1529-0131(199811)41:11<2039::AID-ART20>3.0.CO;2-1
29. Busquets J, Del Galdo F, Kissin EY, Jimenez SA. Assessment of tissue fibrosis in skin biopsies from patients with systemic sclerosis employing confocal laser scanning microscopy: an objective outcome measure for clinical trials? *Rheumatology*. (2010) 49:1069–75. doi: 10.1093/rheumatology/keq024
30. Sun B, Wang H, Zhang L, Yang X, Zhang M, Zhu X, et al. Role of interleukin 17 in TGF-β signaling-mediated renal interstitial fibrosis. *Cytokine*. (2018) 106:80–88. doi: 10.1016/j.cyto.2017.10.015
31. Szodoray P, Nakken B, Barath S, Csipo I, Nagy G, El-Hage F, et al. Altered Th17 cells and Th17/regulatory T-cell ratios indicate the subsequent conversion of undifferentiated connective tissue disease to definitive autoimmune systemic disorders. *Human Immunol*. (2013) 74:1510–8. doi: 10.1016/j.humimm.2013.08.003
32. Papp G, Horvath IF, Barath S, Gyimesi E, Sipka S, Szodoray P, et al. Altered T-cell and regulatory cell repertoire in patients with diffuse cutaneous systemic sclerosis. *Scand J Rheumatol*. (2011) 40:205–10. doi: 10.3109/03009742.2010.528021
33. Klemann C, Schröder A, Dreier A, Möhn N, Dippel S, Winterberg T, et al. Interleukin 17, produced by γδ T cells, contributes to hepatic inflammation in a mouse model of biliary atresia and is increased in livers of patients. *Gastroenterology*. (2016) 150:229–241. doi: 10.1053/j.gastro.2015.09.008
34. Park MJ, Moon SJ, Lee EJ, Jung KA, Kim EK, Kim DS, et al. IL-1-IL-17 signaling axis contributes to fibrosis and inflammation in two different murine models of systemic sclerosis. *Front Immunol*. (2018) 9:1611. doi: 10.3389/fimmu.2018.01611
35. Yao Z, Oainter SL, Fanslow WC, Ulrich D, Macduff BM, Spriggs MK, et al. Human IL-17: a novel cytokine derived from T cells. *J Immunol*. (1995) 155:5483–86.
36. Vettori S, Cuomo G, Iudici M, D'Abrosca V, Giacco V, Barra G, et al. Early systemic sclerosis: serum profiling of factors involved in endothelial, T-cell, and fibroblast interplay is marked by elevated interleukin-33 levels. *J Clin Immunol*. (2014) 34:663–8. doi: 10.1007/s10875-014-0037-0
37. Lonati PA, Brembilla NC, Montanari E, Fontao L, Gabrielli A, Vettori S, et al. High IL-17E and low IL-17C dermal expression identifies a fibrosis-specific motif common to morphea and systemic sclerosis. PLoS ONE. (2014) 9:e105008. doi: 10.1371/journal.pone.0105008
38. Kvakan H, Kleinewietfeld M, Qadri F, Park JK, Fischer R, Schwarz I, et al. Regulatory T cells ameliorate angiotensin II-induced cardiac damage. *Circulation*. (2009) 119:2904–12. doi: 10.1161/CIRCULATIONAHA.108.832782
39. Dong Y, Yang M, Zhang J, Peng X, Cheng J, Cui T, et al. Depletion of CD8+ T Cells exacerbates CD4+ T cell-induced monocyte-to-fibroblast transition in renal fibrosis. *J Immunol*. (2016) 196:1874–81. doi: 10.4049/jimmunol.1501232
40. Clemente-Casares X, Blanco J, Ambalavanan P, Yamanouchi J, Singha S, Fandos C, et al. Expanding antigen-specific regulatory networks to treat autoimmunity. *Nature*. (2016) 530:434–440. doi: 10.1038/nature16962

41. Chujo S, Shirasaki F, Kawara S, Inagaki Y, Kinbara T, Inaoki M, et al. Connective tissue growth factor causes persistent Proα2 (I) collagen gene expression induced by Transforming growth factor-β in a mouse fibrosis model. *J Cell Physiol*. (2005) 203:447–56. doi: 10.1002/jcp.20251
42. Wilson MS, Madala SK, Ramalingam TR, Gochuico BR, Rosas IO, Cheever AW, et al. Bleomycin and IL-1beta-mediated pulmonary fibrosis is IL-17A dependent. *J Exp Med*. (2010) 207:535–52. doi: 10.1084/jem.20092121
43. Lei L, Zhao C, Qin F, He ZY, Wang X, Zhong XN. Th17 cells and IL-17 promote the skin and lung inflammation and fibrosis process in a bleomycin-induced murine model of systemic sclerosis. *Clin Exp Med*. (2016) 34(Suppl.100):14–22.
44. Arif S, Moore F, Marks K, Bouckenooghe T, Dayan CM, Planas R, et al. Peripheral and islet interleukin-17 pathway activation characterizes human autoimmune diabetes and promotes cytokine-mediated β-cell death. *Diabetes*. (2011) 60:2112–19. doi: 10.2337/db10-1643
45. Su SA, Yang D, Zhu W, Cai Z, Zhang N, Zhao L, et al. Interleukin-17A mediates cardiomyocyte apoptosis through Stat3-iNOS pathway. *BiochimBiophysActa*. (2016) 1863:2784–94. doi: 10.1016/j.bbamcr.2016.08.013
46. Wang J, Zhang Y, Yin K, Xu P, Tian J, Ma J, et al. IL-17A weakens the antitumor immunity by inhibiting apoptosis of MDSCs in lewis lung carcinoma bearing mice. *Oncotarget*. (2017) 8:4814–25. doi: 10.18632/oncotarget.13978
47. Kim EK, Kwon JE, Lee SY, Lee EJ, Kim DS, Moon SJ, et al. IL-17-mediated mitochondrial dysfunction impairsapoptosis in rheumatoid arthritis synovial fibroblaststhrough activation of autophagy. *Cell Death Dis*. (2017) 8:e2565. doi: 10.1038/cddis.2016.490

Conflict of Interest: SV received consultancy fees from Boehringer-Ingelheim and Thermo-Fischer, speaking fees and/or educational support from Abbvie, Roche, Pfizer, and BMS. However, no specific funding was received to carry out the work described in this manuscript.

The remaining authors declare that the research was conducted in the absence of any commercial or financial relationships that could be construed as a potential conflict of interest.

Advantages of publishing in Frontiers

OPEN ACCESS
Articles are free to read for greatest visibility and readership

FAST PUBLICATION
Around 90 days from submission to decision

HIGH QUALITY PEER-REVIEW
Rigorous, collaborative, and constructive peer-review

TRANSPARENT PEER-REVIEW
Editors and reviewers acknowledged by name on published articles

Frontiers
Avenue du Tribunal-Fédéral 34
1005 Lausanne | Switzerland

Visit us: www.frontiersin.org
Contact us: frontiersin.org/about/contact

REPRODUCIBILITY OF RESEARCH
Support open data and methods to enhance research reproducibility

DIGITAL PUBLISHING
Articles designed for optimal readership across devices

FOLLOW US
@frontiersin

IMPACT METRICS
Advanced article metrics track visibility across digital media

EXTENSIVE PROMOTION
Marketing and promotion of impactful research

LOOP RESEARCH NETWORK
Our network increases your article's readership